HumanAir

Final Report

AE3200 Design Synthesis Exercise

Group 15

Alex van der Lugt	5324564	Mihai Cristian Petria	5559081
Eunkyung Cho	5497558	Diogo S.C. Fernandes	5446538
David-Nicholas Cantar-Gogitidze	5504627	Matthias Van Mechelen	5483220
Mika Ruyssenaars	5460530	Niels Ruijten	5239990
Rashmi Siriwardane Arachchilage	5572959	Tom Gleeson	5050502

Delft University of Technology

TU Delft

HumanAir

[This page is intentionally left blank.]

HumanAir

Final Report

by

Group 15

Alex van der Lugt	5324564	Mihai Cristian Petria	5559081
Eunkyung Cho	5497558	Diogo S.C. Fernandes	5446538
David-Nicholas Cantar-Gogitidze	5504627	Matthias Van Mechelen	5483220
Mika Ruyssenaars	5460530	Niels Ruijten	5239990
Rashmi Siriwardane Arachchilage	5572959	Tom Gleeson	5050502

Instructor:	Dr.ir. R.C. Alderliesten
Coaches:	W. Wu and H. Li
Institution:	Delft University of Technology
Place:	Faculty of Aerospace Engineering, Delft
Project Duration:	6 May 2024 - 28 June 2024
Version:	2.0 (25th June 2024)

Cover Image: Own Work

Preface

This report builds on the conceptual design developed in the Midterm Report, as well as the project strategy and design ambition outlined in the Project Plan and the Baseline Report. It represents the culmination of ten weeks of dedicated effort by a design team composed of ten Bachelor students in Aerospace Engineering at Delft University of Technology.

The successful completion of this project would not have been possible without the exceptional support from the Aerospace Engineering faculty staff. We extend our heartfelt thanks to the AE3220 teaching assistants, particularly Katharina-Inés Janisch, and the members of the OSCC, who played a crucial role in organizing this year's spring Design Synthesis Exercise. Special gratitude is owed to our tutor, Dr.ir. R.C. Alderliesten, and our project coaches, Wencan Wu and Haonan Li. Additionally, we are deeply appreciative of Dr. Roeland De Breuker for his insightful lectures on aircraft aeroelasticity. Their professional insights were invaluable at every stage of the project and essential to its success.

Lastly we are very grateful for the support we have received from Mission Aviation Fellowship International. Maarten Temminck and Peter Fryatt have made this project possible by donating their time and providing technical information and feedback throughout the project duration. We hope our project, in one way or another, has helped or will help MAF International in its mission to provide "help, hope, and healing through aviation" to those in need.

DSE Group 15
19 May 2024

Executive Overview

Mission Aviation Fellowship (MAF) is the largest humanitarian air operator in the world. Using light aircraft, the organisation aims to reach remote communities hindered by geographical obstacles like jungles, mountains, swamps, and deserts, or separated due to conflict to deliver much-needed help. MAF wishes to reduce its current environmental footprint while maintaining the economic sustainability of its operations. This report aims to make an argument decision on the design option that has been developed to facilitate their needs. This executive overview will provide insight into the means introduced in this report to achieve its aim.

Project Definition

To define a clear goal for the end product of this project, a mission need statement is set up. All choices made throughout this project will aim to adhere to this statement.

HumanAir Mission Need Statement

Provide a small aircraft that outperforms current Cessna 206 humanitarian operations in terms of CO_2 emissions and economic viability.

With the mission need statement that defines the goal for the product, it is also important to establish a goal for the project itself. This is what is reflected by the project objective statement.

HumanAir Project Objective Statement

With ten students in ten weeks, develop and design a small-sized aircraft with corresponding ground facilities, able to reduce the MAF fleet's environmental footprint by 50%.

Market Analysis

Before the design and development of a product, conducting a market analysis is crucial. This analysis includes several key components. First, the current market is explored to understand the existing market landscape and provide insights into current dynamics. Next, future trends in the general aviation industry are investigated, with a positive growth trend expected from 2024 to 2033.

To achieve economies of scale, multiple target segments within the general aviation industry were identified: the humanitarian sector, tourism/sightseeing sector, and medical evacuation sector. Additionally, stakeholders are analysed, focusing on competitors, potential competitors, potential collaborators, and customers, with MAF being our primary customer.

The number of aircraft expected to be sold annually is calculated based on those aligned with the mission characteristics. Finally, a thorough SWOT analysis evaluates the strengths, weaknesses, opportunities, and threats within the market. HumanAir's unique selling point is its low CO_2 emissions, distinguishing it from competitors. However, this approach may require significant investments in new infrastructure. To secure a more competitive position in the market, it is important to minimise the need for new construction during the design phase.

Based on the trends studied throughout the last five years for similar aircraft, it was concluded that around 30 aircraft can be sold each year. It is important to mention that this expected introduction of a new aircraft to the market requires ongoing monitoring of trends and demand dynamics. With respect to manufacturing, the concept of a learning curve applies. In the initial stages of the production, the average time of production per unit is relatively high but as the cumulative volume of production increases, the time decreases, thereby increasing the number of outputs converging to the estimated 30 aircraft.

User Requirements

Table 1 shows an overview of the user requirements driving the design.

Table 1: Overview of user requirements for the HumanAir HA-1 aircraft

ID	Statement	Check
	User Requirements	
HA-UR-01	The aircraft shall have a range of 600 nm	✓
HA-UR-02	The aircraft shall carry 6 passengers excluding pilot or 540 kg of freight	✓
HA-UR-03	Take-off shall be operable from unpaved airstrips with a Take-off Run Available (TORA) of less than 500 m	✓
HA-UR-04	The aircraft shall comply with CS-23 safety and reliability requirements at sea-level atmospheric conditions with still air	UN
HA-UR-05	The aircraft shall comply with requirements for IFR operations	UN
HA-UR-06	The operational CO_2 emissions of the aircraft shall be reduced by at least 50% compared to current C206 operations	✓
HA-UR-07	The aircraft shall be operable at all MAF airports currently in use	✓
HA-UR-08	The direct operating costs (fuel, maintenance & overhaul) shall remain below US $300/hour for current operations	✓
HA-UR-09	The maximum unit cost shall not exceed US $1.5 million	✓
HA-UR-10	The aircraft shall have a cruise speed of at least 50 m/s	✓
HA-UR-11	The aircraft shall be capable of adhering to a flight profile that enables current operational practice	✓
HA-UR-12	The aircraft shall be capable of operating in all of the operating conditions encountered by MAF	UN
HA-UR-13	The aircraft shall be able to be reconfigured for different missions within 30 minutes	UN
HA-UR-14	The aircraft shall be able to transport a stretcher	✓
HA-UR-15	The aircraft shall have a maximum development time until operational of 5 years	UN
HA-UR-16	The aircraft shall have the possibility to carry live animals and/or dangerous goods at the same time as passengers	✓
HA-UR-17	The aircraft shall be able to accommodate stopovers as part of the mission	✓
HA-UR-18	The aircraft shall be able to be refueled and recharged within 60 minutes	✓
HA-UR-19	The aircraft shall have fuel reserves equal to 15% of trip fuel and 75 minutes of loiter flight at 450 m above airfield elevation before the final landing	✓

The Aircraft

For a better visualisation, a 3 view engineering drawing is provided below with the most relevant dimensions.

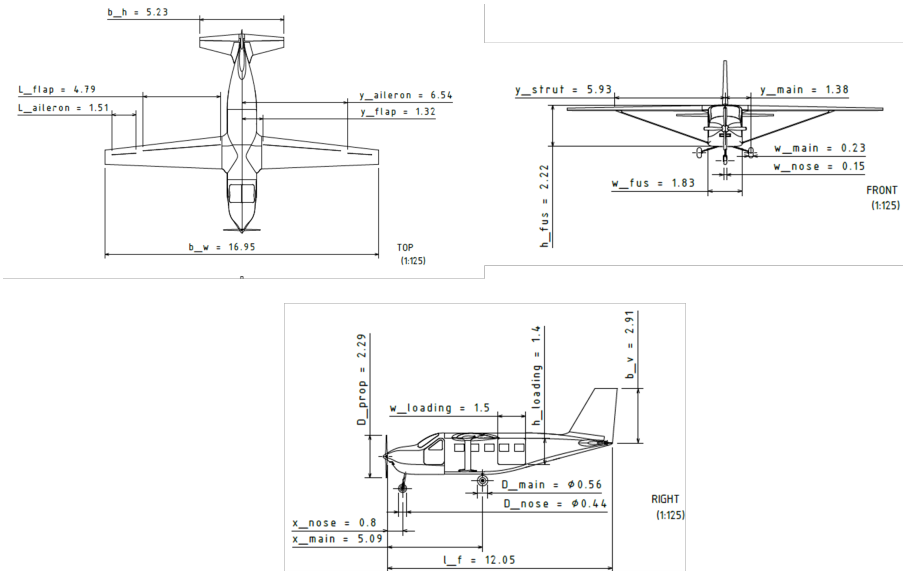

Figure 1: 3-view engineering drawing

The proposed design can be summarised by the parameters presented in Table 2:

Table 2: Overview of Design Parameters for the **HA-1** Aircraft

Parameter	Value	Unit	Parameter	Value	Unit
Fuselage			Vertical Stabiliser		
Fuselage Length	12.05	[m]	Surface Area	5.62	[m^2]
Seats Abreast	2	[-]	Leading Edge Sweep	36	[°]
Top Width	1.83	[m]	Span	2.9	[m]
Bottom Width	1.83	[m]	Root Chord Length	2.67	[m]
Height	1.2	[m]	Tip Chord Length	0.88	[m]
Wing Mounting Method	High Wing Strut-braced	[-]	x_{cg}	0.9	[MAC]
Main Wing			Stability		
Surface Area	26.13	[m^2]	Stability Margin	0.05	[-]
Quarter Chord Sweep	0	[°]	Undercarriage		
Span	16.95	[m]	Strut Height Main Nose	0.82	[m]
Root Chord Length	2.2	[m]	CoG offset Nose Gear	5.09	[m]
Tip Chord Length	0.88	[m]	CoG offset Main Gear	0.8	[m]
Aerofoil	FX 63-137	[-]	Wheel Diameter Nose	0.435	[m]
x_{LEMAC}	3.8	[m]	Wheel Diameter Main	0.556	[m]
Horizontal Stabiliser			Propulsion		
Surface Area	5.47	[m^2]	Number of Engines	1	[-]
Quarter Chord Sweep	9.72	[°]	Engine Type	Reciprocating	[-]
Span	5.22	[m]	Engine Length	1.114	[m]
Root Chord Length	1.49	[m]	Engine Width	0.85	[m]
Tip Chord Length	0.6	[m]	Engine Height	0.75	[m]
Aerofoil	NACA0012	[-]	Engine Mass	363	[kg]
x_{cg}	3.57	[MAC]	Motor Mass	35	[kg]
Aileron			Flaps		
Start Position	0.77	[%span]	c'/c	1.075	[-]
End Position	0.95	[%span]	Surface	15.62	[m^2]
Roll Rate	9.89	[°/s]	Deflection Landing	45	[°]
$C_{L_{\delta_a}}$	6.24	[1/°]	Deflection Take-off	45	[°]
C_{L_P}	-0.03	[1/°]	Flap Start	0.16	[%span]
Turn Time	6.06	[s]	Flap End	0.72	[%span]
Hinge Position	0.35	[% chord]	$\alpha_{Landing}$	10.15	[°]
Stick Arm	0.35	[m]	$\alpha_{Take-Off}$	13.14	[°]
Overall					
Maximum Take-off Weight		3585		[kg]	
Operating Empty Weight		2696		[kg]	
CO_2 Reduction Old Technology		37		[%]	
CO_2 Reduction New Technology		70		[%]	

Subsystems

Retractable Landing Gear

In order to meet the emissions reduction target, drag needs to be drastically reduced compared to aircraft of similar size. For that reason, a retractable landing gear has been chosen. The retraction mechanism for the main landing gear is shown in Figure 2.

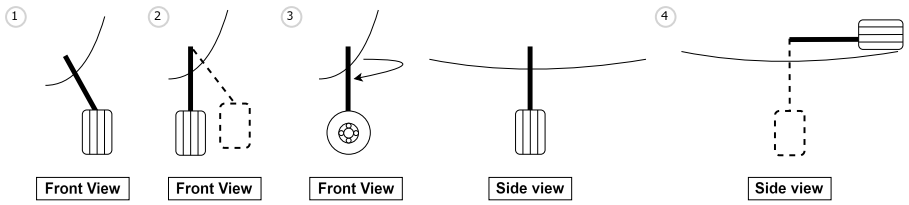

Figure 2: Main Landing Gear Retraction Motion

The chosen landing gear retraction system is electric due to its high reliability, efficiency and ease of maintenance.

Hybrid Propulsion System

In order to meet emissions requirements, the HA-1 aircraft uses a hybrid propulsion system to drastically reduce emissions for short flights, while longer ranges can still be achieved using traditional internal combustion. The hybrid system is laid out in a parallel configuration, meaning that both the electric motor and combustion engine can supply full design power on their own. Due to the weight of the aircraft and short take-off requirements, a powerful, yet efficient, engine was needed. For this reason, the Red A03 was selected as the internal combustion engine for the aircraft. The specifications of the engine are tabulated in Table 3 and the engine is shown in Figure 3. Furthermore, a layout of the full propulsion system is shown in Figure 4, with the battery being placed further aft in the aircraft, under the floor.

Table 3: Specifications of the RED A03-003 Engine

Fuel Type	Jet A-1
Take-Off Power (5 min)	368 kW
Maximum Continuous Power	338 kW
Dry Mass (inc. gearbox)	363 kg
Maximum Efficiency (at 223 kW)	40%
Unit Cost (inflation adjusted)	US$232 220

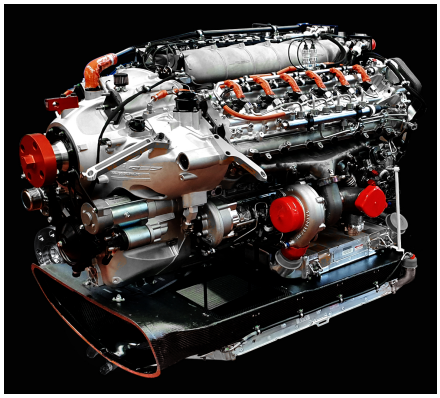

Figure 3: Red A03-003 V12 engine

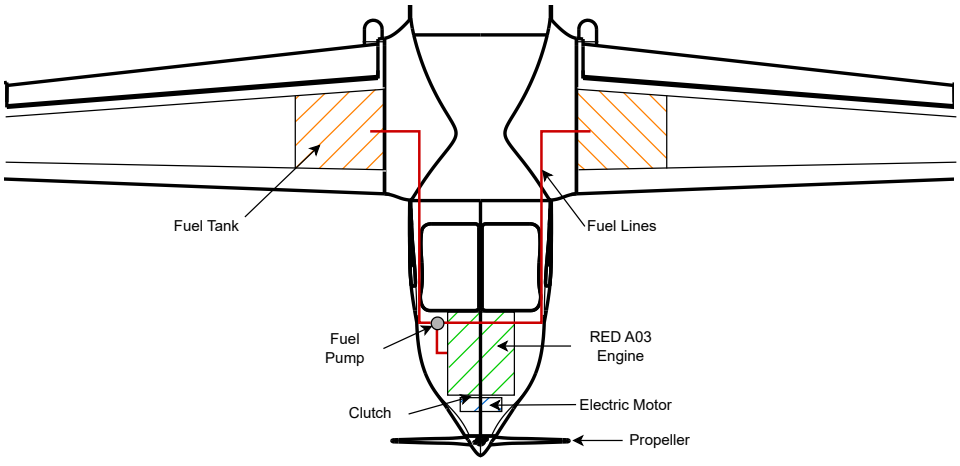

Figure 4: Layout of the Propulsion System

A clear understanding of when to use each type of energy: fuel or battery during the flight phases of the aircraft is needed. An optimisation strategy was analysed and can be visualised in Figure 5.

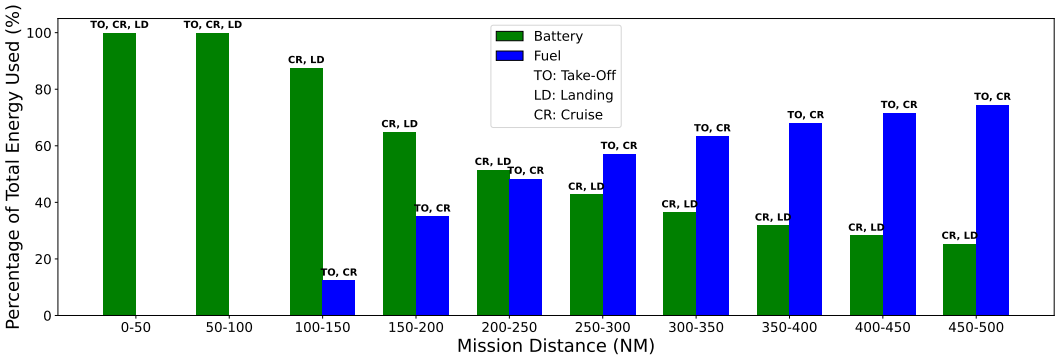

Figure 5: Battery Deployment Optimisation Strategy for Different Leg Distances

The strategy varies depending on the flight length. It is preferred to use the batteries during cruise and landing, and the fuel during heavy operating conditions such as take-off. In case the batteries cannot be used for the entire cruise phase, fuel will be used to compensate for the remaining distance.

Operations and Logistics Concept

Operations and logistics are intended to be similar to MAF's current operations. The primary differences will be related to the hybrid-electric powertrain.

First of all, the aircraft's batteries will need to be charged whilst on the ground at the base between flights. The supporting infrastructure and procedures are designed to allow the batteries to be charged to full within 1 hour. The most significant additional infrastructure required at bases will include solar panels and battery packs. It is envisioned that the solar panels will charge the battery packs, which in turn will then charge the aircraft at a higher rate than what would be possible with solar panels alone.

Flight Performance

The flight performance of the aircraft was analysed and it was determined that the design meets the requirements on stall speed, climb gradient, take-off performance, landing performance, cruise and range. It falls somewhat short of extra performance targets set by the team, though the performance is considered sufficient for the mission. Note that the flight performance analysis still requires verification and validation, though the results match earlier estimations well, giving confidence in the results. The most important figures are presented in Table 4 and the payload-range performance is shown in Figure 6.

Table 4: Flight Performance Evaluation Results. "SL" means sea level, i.e. 0m ISA+0. The plusminus signs for the climb gradient results indicate that these figures are estimates only.

Item	Value	Requirement	Target
Landing stall speed, SL, MTOW	26.8 m/s	≤31 m/s	≤25 m/s
Max. clean climb rate, SL, MTOW	4.3 m/s	-	≥5 m/s
Max. take-off climb gradient, SL, MTOW	±6.8%	≥4%	-
Max. landing climb gradient, SL, MTOW	±6.0%	≥3%	-
Min. TORA for take-off, 750m ISA+18, MTOW, grass	450 m	≤500 m	-
Min. TORA for landing, 750m ISA+18, MTOW, grass	345 m	≤500 m	-
Cruise speed	60 m/s	≥50 m/s	-
Max. cruise altitude	4900 m	≥3700 m	-

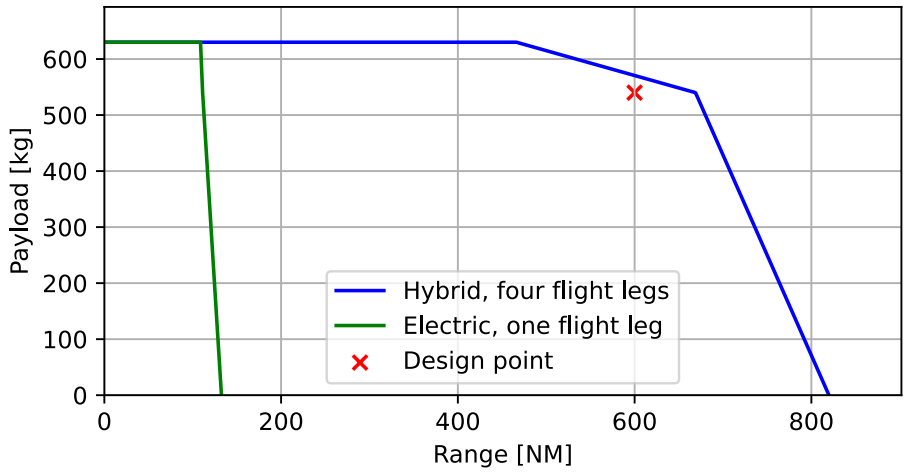

Figure 6: Payload-range diagram, indicating that all requirements regarding range are met by the current design. Take-offs and landings as well as mandatory reserves are included

Cost Breakdown

Requirement **HA-UR-09** states that for MAF, the maximum unit price should not exceed $1.5m. While the unit cost for a single aircraft (**$1.28m**) is below this threshold, allowing for a modest profit when selling at $1.5m, this does not cover the cost of the ground infrastructure, which must be factored in for MAF.

Taking a ground infrastructure cost of **$285 000** gives a total system cost (aircraft and ground infrastructure) for MAF of $1.565M. In order to meet MAF's price requirement, it has been decided to sell the aircraft to them at a price of $1.5M (i.e., a loss of $65 000 per aircraft). Assuming 20 aircraft are sold to MAF, this gives a total loss of $1.3M. Assuming a sale price of $1.5M is maintained for other customers, the profit from the sale of six aircraft will compensate for the loss made on sales to MAF.

Given a total aircraft development and manufacturing cost of $640M, plus the ground infrastructure cost for 20 aircraft (20 x $285 000), the total cost is $645M. Taking a sale price of $1.5M, this means that roughly **430** aircraft will need to be sold to break even. Assuming a rate of 30 sales per year, this means the programme will break even after about 14 years, and eventually achieve a total programme **profit of ca. $100M** after the entire production run of **500 aircraft**. The sales number might increase over the course of time since the GA market values is increasing. However, 30 aircraft sold per year is deemed a conservative value that will decrease the risk in further phases of the development process.

To make the outlook more favourable, the sale price for **non-MAF customers** could be increased to **$2M**. In this event, about 330 aircraft will need to be sold to break even (including the aircraft sold at a loss to MAF). This would take roughly 11 years.

HA-1 vs Competition

A comparison of how HA-1 performs compared to similar aircraft, **when being charged via conventional power grid** instead of ground charge station, is given in Table 5.

Table 5: HA-1 vs Competition

Parameter	HumanAir HA-1	Cessna 206	Cessna 208
Unit cost	$1 500 000	$550 000 – 1 200 000	$2 164 000
Operational cost / hour	$322	$650	$842
Aircraft currently flying	-	N/A in Europe Aprox. 3000 in US	150 in Europe Aprox. 400 in US
CO_2 reduction of the HA-1	-	23%	48%

From the table it is clear that HA-1 performs better in almost all categories with respect to the two selected aircraft. It is worth mentioning however that the hourly cost for the Cessna 206 assumes only 200 hours of flight per year while for the other two aircraft, the cost is calculated for 600 flight hours. Thus, that price is expected to be lower than $650 per hour. However, the price can be still approximated at $400 which is around 25% more than what the HA-1 concept proposes. This will account for the difference in prices since the $300 000 paid extra will be distributed by operating the aircraft for less than 5 years.

Furthermore, it can also be seen that the unit cost for HA-1 is higher than the previously mentioned **$244 per hour**, and that the CO_2 emissions reduction is reduced from 70% to around 23% w.r.t. Cessna 206 and 48% w.r.t. Cessna 208. This is due to the fact that the ground charging station is not included in the unit cost of HA-1 for any other customers than MAF. This is done as the cost approximated for it will not be relevant for other customers as it is based on the data specific to MAF airbases - temperature profile, wind profile, surface available, etc. The other customers may still be satisfied by the achieved reduction without charging with fully renewable energy, or might opt for other renewable energy sources like hydropower, wind power, or nuclear power.

Given all the aspects mentioned above, the hourly cost and the emission reduction level were updated based on average European levels of 0.22 kgeCO_2/kWh by 2030 and a price of 0.2847 €/kWh (equal to $0.31/kWh) as the charging price from the conventional electrical grid. Further analysis can be performed by the customer to determine if the advantage that building a new charging facility will bring to their operations.

Technical Risk Assessment

To ensure the project will not encounter any unexpected problems during future design phases, a risk assessment has been performed. This assessment aims to identify all risks, after which corresponding mitigation and contingency strategies are thought out. An overview of the risks before mitigation is presented in Table 6.

Table 6: Pre-mitigation Risk Map

	Very Low RIsk	Low Risk	Medium Risk	High Risk	Very High Risk
	Risk Assessment				
Consequence: Catastrophic (=0.9)	PR-MIS-01		PR-FIN-03, PR-LDG-01	PR-FIN-05	PR-POW-01
Consequence: Critical (=0.7)		PR-POW-04, PR-REQ-01, RP-PRO-01	PR-POW-02, PR-DES-01, PR-LIF-01	PR-DES-03, PR-FIN-01, PR-RIS-01	PR-POW-05, PR-DES-02
Consequence: Marginal (=0.5)		PR-POW-03, PR-FIN-04	PR-DES-04, PR-DEL-03	PR-FIN-02, PR-DEL-01, PR-DEL-02	
Consequence: Minimal (=0.3)			PR-EOL-01		
Consequence: Negligible (=0.1)					
	Very Unlikely (=0.1)	Unlikely (=0.3)	Probable (=0.5)	Very Probable (=0.7)	Frequent (=0.9)
	Likelihood				

The meaning of all identifiers is irrelevant here, but one should pay special attention to PR-POW-01, PR-FIN-05, PR-POW-05 and PR-DES-02 which have to do with for example the risk of a battery not being available, the retractable landing gear concept not working or the project not being attractive enough for potential customers. To counter these risks, the set-out mitigation strategies are applied which results in Table 7.

As can be noted, the magnitude of all risk has been reduced to at least medium risk. This provides an acceptable risk, but it should be closely monitored during the remainder of the project. An example here is PR-POW-01, the risk of the required more efficient battery technology not being available as expected. As HumanAir is entering a market where such big emission reductions have never been achieved, it is deemed necessary to take the risk in pursuit of innovation.

Table 7: Post-mitigation Risk Map

	Very Low RIsk	Low Risk	Medium Risk	High Risk	Very High Risk
	Risk Assessment				
Consequence: Catastrophic (=0.9)	PR-POW-04, PR-MIS-01, RP-PRO-01	PR-FIN-03, PR-LDG-01	PR-POW-01		
Consequence: Critical (=0.7)		PR-DES-02, PR-RIS-01	PR-POW-02		
Consequence: Marginal (=0.5)		PR-DES-01, R-DES-04, PR-DEL-01, PR-DEL-01, PR-REQ-01, PR-LIF-01			
Consequence: Minimal (=0.3)	PR-FIN-02	PR-POW-03, PR-FIN-04, PR-DEL-03, PR-EOL-02	PR-POW-05	PR-DES-03, PR-FIN-01, PR-FIN-05	
Consequence: Negligible (=0.1)					
	Very Unlikely (=0.1)	Unlikely (=0.3)	Probable (=0.5)	Very Probable (=0.7)	Frequent (=0.9)
	Likelihood				

Contents

Nomenclature

Abbreviations

Abbreviation	Definition
ATC	Air Traffic Control
CFRP	Carbon Fibre-Reinforced Polymers
CG	Centre of Gravity
CFD	Computational Fluid Dynamics
DOC	Direct Operating Cost
DOT	Design Option Tree
DSE	Design Synthesis Exercise
ELCA	Environmental Life Cycle Analysis
EOL	End-of-life
GFRP	Glass Fibre-Reinforced Polymers
ICE	Internal Combustion Engine
IFR	Instrument Flight Rules
ISA	International Standard Atmosphere
KE	Kinetic Energy
LE	Leading edge
MAC	Mean Aerodynamic Chord
MAF	Mission Aviation Fellowship
MSL	Mean Sea Level
SOC	State of Charge
TE	Trailing edge
TORA	Take-Off Run Available
V&V	Verification and Validation
WBS	Work Breakdown Structure
WFD	Work Flow Diagram
HM	Hinge moment

Symbols

Symbol	Definition	Unit
a	Distance from the typical section half chord to the elastic axis, non-dimensionalised with the half chord B	[-]
$A_{caliper}$	Caliper area	[m^2]
A_{prop}	Propeller effective surface area	[m^2]
AR	Aspect Ratio	[-]
b	Main wing wingspan	[m]
B	half chord of the typical section	[m]
b_c	Canard wingspan	[m]
b_f	Width of fuselage	[m]
b_h	Horizontal tailplane wingspan	[m]
b_v	Vertical tailplane wingspan	[m]
C_D	Total aircraft drag coefficient	[-]
C_{d_0}	Airfoil zero-lift drag coefficient	[-]
C_{D0}	Total aircraft zero-lift drag coefficient	[-]
$\Delta C_{D0_{propeller}}$	Increase in zero-lift drag due to rotating propeller	[-]
$\Delta C_{D0_{surface}}$	Increase in zero-lift drag due to surface inaccuracies	[-]
C_F	Coefficient of skin friction drag	[-]
C_L	Total aircraft lift coefficient	[-]
$C_{L_{ground}}$	Lift coefficient when aircraft is on ground	[-]
C_{L_α}	Lift curve slope of the typical section airfoil	[1/rad]
$C_{L_{\alpha_{clean}}}$	Lift curve slope of wing	[1/rad]
$C_{L_{\alpha_{flapped}}}$	Lift curve slope of wing when flaps are deployed	[1/rad]
$C_{L_{\dot{\alpha}}}$	Change in typical section C_L for a varying rate of change in angle of attack	[1/rad]
$C_{L_{\alpha_{A-h}}}$	Tailless aircraft lift coefficient slope	[-]
$C_{L_{\alpha_h}}$	Horizontal tailplane lift coefficient slope	[-]
C_{L_c}	Lift coefficient of 3D canard	[-]
C_{L_h}	Lift coefficient of the 3D horizontal tailplane	[-]
$C_{L_{MAX,Clean}}$	Aircraft maximum lift coefficient in clean configuration	[-]
$C_{L_{MAX,Landing}}$	Aircraft maximum lift coefficient during landing	[-]
$C_{L_{MAX,Take-off}}$	Aircraft maximum lift coefficient during take-off	[-]
$C_{L_{Wing}}$	Lift coefficient of 3D wing	[-]
C_l	Airfoil lift coefficient	[-]

Symbol	Definition	Unit
$C_{l_{MAX,Clean}}$	Airfoil maximum lift coefficient in clean configuration	[-]
$C_{l_{MAX,Landing}}$	Airfoil maximum lift coefficient during landing	[-]
$C_{l_{MAX,Take-off}}$	Airfoil maximum lift coefficient during take-off	[-]
C_h	Hinge moment coefficient	[-]
C_{h_0}	Hinge moment coefficient at 0 deg angle of attack	[-]
C_{h_α}	Hinge moment coefficient derivative w.r.t. angle of attack	[-]
C_{h_δ}	Hinge moment coefficient derivative w.r.t. aileron deflection	[-]
$C_{M_{AC_\beta}}$	change in $C_{M_{AC}}$ for a change in flap deflection β	[1/rad]
C_m	Longitudinal moment coefficient	[-]
$C_{m_{ac}}$	Longitudinal moment coefficient around aerodynamic centre	[-]
C_{m_α}	Longitudinal moment coefficient	[-]
C_{n_β}	Weathercock stability derivative	[-]
$C_{n_{\beta_f}}$	fuselage contribution to the weathercock stability derivative	[-]
$C_{n_{\beta_i}}$	Wing contribution to the weathercock stability derivative	[-]
$C_{n_{\beta_p}}$	Nacelle contribution to the weathercock stability derivative	[-]
c_{tip}	Wing tip chord	[m]
c_{tip_c}	Canard tip chord	[m]
c_{tip_h}	Horizontal tailplane tip chord	[m]
c_{tip_v}	Vertical tailplane tip chord	[m]
c_{root}	Horizontal tailplane root chord	[m]
c_{root_c}	Canard root chord	[m]
c_{root_h}	Horizontal tailplane root chord	[m]
c_{root_v}	Vertical tailplane root chord	[m]
$\overline{c}$	Mean aerodynamic chord length	[m]
d	Distance between the typical section aerodynamic center and center of gravity of the typical section aileronless airfoil, non-dimensionalised with the half chord B	[-]
D_e	Diameter of engine	[m]
D_{gt}	Diameter of gas turbine	[m]
D_p	Propeller blade diameter	[m]
D_{w_m}	Diameter of main landing gear wheel	[m]
D_{w_n}	Diameter of nose landing gear wheel	[m]
d_{ground}	Ground distance	[m]
E_{Al}	Young's Modulus of Al-6061	[MPa]
E	Endurance	[h]
e	Oswald efficiency factor	[m/s]
e_{bat}	Battery specific energy	[Wh/kg]
e_{fuel}	Fuel specific energy	[Wh/kg]
$F_{retarded}$	Retarded force	[N]
$F_{caliper}$	Caliper force	[N]
g	Sea-level gravitational acceleration	[m/s^2]
$H_{cg_{gr}}$	Height of CG location w.r.t ground	[m]
$H_{CG_{OEW}}$	Height of OEW CG w.r.t. bottom of the fuselage	[m]
H_s	Height of landing gear strut	[m]
h	Altitude	[m]
H	Distance from the typical section centerline to the aileron hinge, non-dimentionalized with the half chord B	[-]
h_e	Height of engine	[m]
h_f	Fuselage height	[m]
h_{fr}	Front spar height	[m]
h_r	Rear spar height	[m]
h_{re}	Height of reciprocating engine	[m]
I_{xx}	Second moment of area about x-axis	[m^4]
I_θ	Second moment of area of the typical section	[m^4]
K_h	Heave stiffness of the typical section	[N/m]
K_θ	torsional stiffness of the typical section	[Nm/rad]
l_e	Length of engine	[m]
l_f	Fuselage length	[m]
l_{fn}	Distance from fuselage nose to exposed root leading edge	[m]
l_{gt}	Length of gas turbine	[m]
l_h	Distance between wing and horizontal stabiliser quarter chord MAC	[m]
l_m	Distance between CG location and the main landing gear	[m]
l_n	Distance between CG location and the nose landing gear	[m]
l_{re}	Length of reciprocating engine	[m]
MTOW	Maximum take-off weight	[kg]
M_{cruise}	Cruise Mach number	[-]
m_e	Mass of engine	[m]
m_{motor}	Mass of electric motor	[m]
n	Load factor	[-]
N_e	Number of engines	[-]

Symbol	Definition	Unit
Nf	Number of cycles until fatigue failure; fatigue life	[-]
n_p	Number of propeller blades	[-]
OEW	Operating empty weight	[kg]
P_{bl}	Blade power loading	[hp/ft^2]
P_{mw}	Load on main landing gear wheel	[N]
P_{nw}	Load on nose landing gear wheel	[N]
P_{TO}	Take-off power	[W]
p_{ptr}	Powertrain specific power	[kW/kg]
q	Dynamic pressure	[Pa]
q_{div}	Divergence boundary	[Pa]
q_{rev}	Reversal boundary	[Pa]
q_{flut}	Flutter boundary	[Pa]
RoC	Rate of climb	[m/s]
S	Main wing surface area	[m^2]
S_h	Horizontal tailplane surface area	[m^2]
S_{wf}	Flapped area	[m^2]
S_{prime}	Wing area including the flaps area	[m^2]
S_i	Surface area influenced by propeller wake	[m^2]
S_{net}	Wing surface outside of the fuselage	[m^2]
S_{max}	Maximum axial stress experienced in a component	[N/m^2]
S_{ult}	Ultimate strength of a material	[N/m^2]
S_θ	first moment of area of the typical section	[m^3]
SFC	Specific fuel consumption	[kg/kWh]
T_{cruise}	Cruise thrust	[N]
ToP	Take-off parameter	[-]
t_{spar}	Spar thickness	[m]
t_{skin}	Skin thickness	[m]
t/c	Thickness-to-chord ratio	[m]
V_D	Dive speed of the aircraft	[m/s]
V_{climb}	Climb speed	[m/s]
V_{cruise}	Cruise speed	[m/s]
V_{stall}	Stall speed	[m/s]
V_∞	Airspeed of the typical section	[m/s]
W_{bat}	Battery weight	[kg]
W_{fuel}	Fuel Weight	[kg]
$W_{payload}$	Payload weight	[kg]
W_{ptr}	Powertrain weight	[kg]
W_w	Wing weight	[kg]
W/P	Power loading	[N/W]
W/S	Wing loading	[N/m^2]
w_e	Width of engine	[m]
w_{re}	Width of reciprocating engine	[m]
x_{cgc}	CG location of canard	[%MAC]
x_{cgh}	CG location of horizontal tailplane	[%MAC]
x_{cgv}	CG location of vertical tailplane	[%MAC]
x_{cgWing}	CG location of main wing	[%MAC]
x_{LEMAC}	Position of leading edge of the MAC w.r.t fuselage nose	[m]
$\overline{x}_{ac}$	AC loaction	[m]
$\overline{x}_{cg}$	most aft CG location	[m]
δ_a	Aileron deflection	[deg]
τ	Aileron effectivness	[deg]
η_{EM}	Electric motor efficiency	[-]
η_{GB}	Gear box efficiency	[-]
η_{th}	Thermal efficiency	[-]
η_{bat}	Battery efficiency	[-]
$\Lambda_{hingleine}$	Sweep angle at hinge line	[deg]
$\Lambda_{c/4}$	Quarter chord wing sweep angle	[deg]
$\Lambda_{c/4_h}$	Quarter chord horizontal tailplane sweep angle	[deg]
$\Lambda_{c/4_c}$	Quarter chord canard sweep angle	[deg]
$\Lambda_{c/4_v}$	Quarter chord vertical tailplane sweep angle	[deg]
λ	Wing taper ratio	[-]
ν	Poisson Ratio	[-]
ρ_{cruise}	Cruise density	[kg/m^3]
σ_y	Yield Strength of Al-6061	[MPa]
$\dot{\theta}$	Rate of twist of the typical section	[rad/s]
Ψ	Overturn angle	[deg]
$\frac{d\epsilon}{d\alpha}$	Downwash gradient	[-]

1 | Introduction

HumanAir is a project currently being developed by a team of ten students dedicated to designing and developing a small-sized aircraft, along with the necessary ground facilities, within a ten-week timeframe. This project was initiated by Mission Aviation Fellowship (MAF). MAF is an organisation that operates in the humanitarian aviation sector providing support to isolated communities in the world. Recently, MAF recognised the need to renew some of its fleets and the organisation aims to replace older aircraft with more environmentally friendly and economically sustainable models. With this mission in mind, the HumanAir team aims to design an aircraft that outperforms current Cessna 206 humanitarian operations in terms of CO_2 emissions and economic viability.

This report intends to provide a complete overview of all activities conducted by the HumanAir team to arrive at a final design proposal. Starting with a set of requirements that follow from a thorough mission analysis, the concept is worked out in detail to arrive at a proposal aircraft, the HumanAir HA-1, designed to facilitate MAF's operational needs. The HA-1 will enable MAF to reduce their emissions by at least 50%, while also reducing their operating costs compared to their current Cessna 206.

The report is structured as follows. First, Chapter 2 defines the objectives of the HumanAir project. Using the market analysis of Chapter 3 and the functional analysis as described in Chapter 4, an aircraft concept trade-off is worked out in Chapter 5, aiming to select the optimal concept to meet MAF's needs. To limit the design space, requirements are then set up in Chapter 6. After analysing the mission in Chapter 7, the first design step can be taken by estimating the weight of the aircraft in Chapter 8. With this, the subsystems of aerodynamics, stability & control and propulsion & power can be designed, which are discussed in Chapter 9, Chapter 11 and Chapter 12 respectively. Synthesising all different subsystem designs, a final overview of the proposed aircraft system is shown in Chapter 13, and compliance with all flight performance requirements is assessed in Chapter 14. To see the relation between all internal components of the aircraft, Chapter 15 works out the system architecture. To ensure the aircraft remains functional, necessary ground systems are designed in Chapter 16, after which user requirements on cost and sustainability are shown to be complied with Chapter 17 and Chapter 18 respectively. In order to make sure the project does not face any unexpected issues in later phases, a thorough risk analysis and an analysis on reliability, availability, maintenance and safety is then be conducted in Chapter 19 and Chapter 21 respectively. To increase the confidence in the used design tools, and the HA-1 system, verification and validation are performed in Chapter 22 after which finally, Chapter 23 provides a future outlook for the HumanAir project.

2 | Project Definition

Before initialising any development phase, it is important to clearly define the project objectives. This ensures everyone is on the same page from the start and works effectively towards the same goals. Defining this well in the early stages of the project increases the chances of the project succeeding in a later phase [1]. To facilitate this, Section 2.1 will first introduce some context on the mission by describing the system and introducing the mission need statement and project objective statement which shall be discussed in Section 2.2 and Section 2.3.

2.1. System Description

As briefly mentioned in the introduction already, HumanAir's mission is to provide an alternative to the current operational fleet of MAF. Current aircraft need to operate in remote areas where they need to be able to land on airstrips characterized by difficult terrain that only provide very minimal resources. The current aircraft are run on jet fuel, as this is a cheap fuel available at all these MAF airports. The need for a new fleet originates from the fact that the current operational schedule, using a fleet of Cessnas, has a relatively large environmental impact. MAF aims to reduce this.

The HumanAir system can be divided into two distinct elements: the aircraft and the ground facilities & operations.

- **Aircraft:**
  The aircraft element is comprised of all design work on the actual flying aircraft. As the type of aircraft is unknown at this stage of the project, it is still unclear what the aircraft element will entail, but components like an engine/motor or a wing are common components in this element.

- **Ground Facilities & Operations:**
  The aircraft is supported by a range of ground facilities. If, for example, the type of fuel needed for the aircraft element would change during the design phase, this needs to be supported by corresponding ground facilities. Changes in the aircraft element can also lead to changes in ground operations.

2.2. Mission Need Statement

To define a clear goal for the end product of this project, a mission need statement is set up. All choices made throughout this project will aim to adhere to this statement.

HumanAir Mission Need Statement

Provide a small aircraft that outperforms current Cessna 206 humanitarian operations in terms of CO_2 emissions and economic viability.

2.3. Project Objective Statement

With the mission need statement that defines the goal for the product, it is also important to establish a goal for the project itself. This is what is reflected by the project objective statement.

HumanAir Project Objective Statement

With ten students in ten weeks, develop and design a small-sized aircraft with corresponding ground facilities, able to reduce the MAF fleet's environmental footprint by 50%.

3 | Market Analysis

Prior to the design and development of a product, it is crucial to evaluate the need for the solution that will be developed. Section 3.1 explores the existing and future market landscape, providing insights into its current and future dynamics. Section 3.2 outlines the specific target market segments that the product aims to serve. Additionally, Section 3.3 identifies and discusses the relevant stakeholders involved in the market, including competitors and customers. After that, the expected number of aircraft that would be sold is presented in Section 3.4. Finally, Section 3.5 presents a strength, weakness, opportunity and threat (SWOT) analysis.

3.1. Current and Future Market

Market segmentation is an approach to classify the markets into distinct groups of customers that share similar characteristics. Segmentation can be done via function (commercial, military, general aviation, etc.), geographical region, demographic or aircraft type. With respect to the top-level requirements, the market of concern is general aviation air transport which focuses on civil aviation that is outside of commercial and military purposes. General aviation includes corporate aviation, fractional ownership operations, business aviation, personal/private travel, air tourism, recreational flying, air sports and training & education.

The market includes helicopters, business jets, gliders, piston fixed-wing aircraft and turboprops as the standard aircraft. The number of general aviation (GA) in the International Area as a function of time is shown in Figure 3.1. Currently, the largest and one of the fastest-growing markets is the piston fixed-wing aircraft. This was mostly in 2019 but due to the COVID-19 outbreak, the sector came to a halt and caused a reduction in the market value. Figure 3.1 below showcases the past trends in the active number of general aviation aircraft from 1995 to 2020 per geographical region.

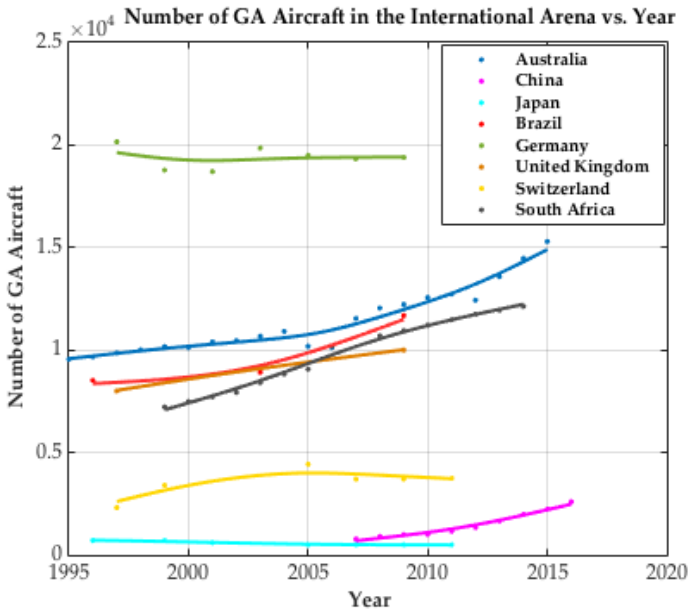

Figure 3.1: Number of GA Aircraft in Different Countries per Year [2, p.12]

As illustrated in Figure 3.1, there has been a positive growth trend in most countries. This historical growth not only proves the market's viability but also provides a basis for anticipating future trends. Before entering a new market, a business must evaluate future trends to identify potential opportunities or threats and ensure the market's growth prospects. The expected trend is given in Figure 3.2

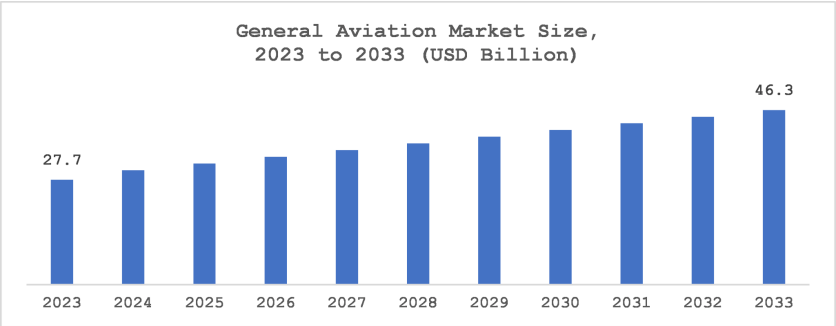

Figure 3.2: Global General Aviation Market Growth Forecast, 2023–2033 [3]

The general aviation market was valued at USD 27.7 billion in 2023 and is projected to reach USD 46.3 billion by 2033, with an expected growth rate of 4.8% from 2024 to 2033 [3]. This expected positive growth trend presents an opportunity to expand its customer base in the general aviation market. Additionally, the positive growth may attract potential investors since it demonstrates the potential for profitability. This is particularly beneficial given HumanAir's status as a new business, which often faces challenges in securing initial capital.

3.2. Target Market

One of the strategies for a business to provide competitive prices is to benefit from economies of scale. By producing at a high volume, fixed costs such as equipment and rent can be spread across a larger number of units, resulting in lower unit costs, which allows businesses to provide their product at a more attractive price. To achieve such economies of scale, HumanAir has strategically chosen to target multiple segments within the general aviation market. This strategic decision not only enhances HumanAir's revenue potential but also reduces the risk of failure through diversification.

The first market that HumanAir aims to target is the humanitarian aviation sector, where organisations such as Mission Aviation Fellowship (MAF) and Jungle Aviation and Radio Services (JAARS) operate. Within the humanitarian aviation sector, small-sized aircraft are mostly used due to their adaptability, cost-effectiveness and ability to reach remote areas. Unlike the commercial aviation sector, organisations involved in this market do not aim to maximise market share or profit. Instead, their primary focus lies in providing air transformation services for humanitarian aid purposes. For the product to be competitive within this market, it is crucial not only for it to offer competitive prices but also to prioritise sustainability and adaptability to the unique challenges of the operations. Noteworthy competitors in this domain include Cessna and Beechcraft [4]. These manufacturers' aircraft are already operational within organisations such as MAF and the UN Humanitarian Air Service (UNHAS).

Another target market segment is medical evacuation. Air ambulance services are essential in transporting injured individuals or rescuing patients from remote or inaccessible locations. It is a viable market with sufficient customer demand. The global air ambulance service market was valued at USD 6.2 billion in 2022 and is projected to reach USD 19.2 billion by 2032, showing substantial growth potential[(a)]. Competitive pricing is crucial in this sector, as excessively high operating costs could restrict the number of patients who can be rescued. Additionally, the air vehicle must be able to be operated in a wide range of environments and conditions, as air ambulances are frequently deployed due to limitations in ground transportation options.

The last target market is the tourism/sightseeing sector, where small aircraft are often employed to offer aerial views over cities or mountains. According to a report from Insight Partners, the helicopter tourism market, a significant component of sightseeing is projected to expand from US$745 million in 2020 to US$1.015 billion by 2028[(b)]. This underscores the positive market potential within the sector.

[(a)] URL: `https://www.futuremarketinsights.com/reports/air-ambulance-services-market` [accessed 8 May 2024]
[(b)] URL: `https://www.theinsightpartners.com/reports/helicopter-tourism-market` [accessed 8 May 2024]

In addition to competitive pricing, consideration for durability is essential when designing an aircraft for this market segment. The aircraft used for tourism purposes are subjected to frequent take-off and landing and thus, aircraft components such as landing gear would wear or tear faster. This is disadvantageous for tourism companies since the maintenance cost would be higher.

3.3. Stakeholders

Stakeholders are individuals or organisations who are affected by and/or can affect the mission. In HumanAir's mission, there are various stakeholders involved. These people are identified and their interests are explained briefly in Table 3.1. Furthermore, the assessment of their influence and interest is conducted, categorising them as either high or low. To reduce subjectivity, multiple individuals independently evaluate these factors and the assessment was finalised only after individual evaluation. Moreover, in cases where both influence and interest are deemed high, the stakeholder is identified as a key stakeholder.

Table 3.1: Stakeholder Interest

Stakeholder	Example	Description	Influence (high/low)	Interest (high/low)	Key/non-key
Customer	UNHAS, MAF	Customers are interested in purchasing aircraft at a reasonable price with high product quality. Not only that, they often set design requirements according to their operational needs. For example, MAF requires a short airstrip.	High	High	Key
Competitors	Cessna, Beechcraft, Cirrus	Competitors constantly monitor market trends and new developments to adapt to new trends or changes. Thereby, they can maintain or increase their market share and presence.	Low	Low	Non-key
HumanAir Project Team Members	Diogo, Matthias, Nicholas	Project team members are interested in creating an aircraft design that complies with all the top-level requirements. The aircraft design can be altered based on their decisions.	High	High	Key
Environmental groups and communities	Greenpeace	Environmental groups and communities are concerned about the positive/negative impact that the HumanAir's design would bring to the environment	Low	High	Non-key
Regulatory Agencies	EASA, FAA	These agencies set the standards and rules that the designed aircraft has to comply with. Non-compliance with regulations can lead to fines or other legal penalties.	High	High	Key
Government	Dutch government	Governments are interested in an increase in job opportunities, gross domestic product (GDP) and environmental sustainability. The government may be a source of finance if they are willing to support sustainable aviation	High	Low	Non-key

Different stakeholder groups have different interests and objectives. This inherent variability often leads to stakeholder conflicts. Designing an aircraft that satisfies all stakeholder's expectations is highly challenging, necessitating businesses to prioritise stakeholders based on their importance. The stakeholder map, shown in Figure 3.3, effectively illustrates the groups in which HumanAir should prioritise. The key stakeholders are in the top right quadrant of the diagram. Therefore, customers, project team members and regulatory agencies shall be considered first when designing the aircraft.

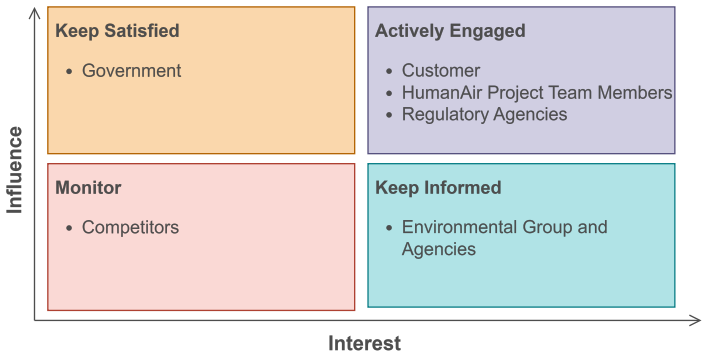

Figure 3.3: Stakeholder Map

Competitors

Within the general aviation market, there are various existing aircraft manufacturers. These include Cessna – known for its wide range of single- and multi-engine piston aircraft, as well as business jets, Beechcraft – specialising in turboprop and piston-engine aircraft, Cirrus – the biggest piston-powered aircraft producer in recent years, and Piper – which has manufactured various single-engine aircraft with broadly similar specifications to the Cessna 206 and HumanAir's planned aircraft [5]. An overview of aircraft from the aforementioned companies that align with the mission characteristics (e.g. range, maximum occupants, take-off distance) is available in Table 3.2.

Table 3.2: Selected Aircraft

Manufacturer	Type	Range [km]	Cruise Speed [km/h]	Maximum Occupants	Payload [kg]	Take-Off Distance [m]	Unit Price [US$]	Operations Cost [US$/h]
Cessna	206[c],[d],[e],[f]	1350	262.1	6	400	600	745 000	215.9
	208[c],[e],[f],[g]	1982	321.8	10–14	2145	354	2 320 000	714
	182[c],[f],[h]	1720	287	4	270	461	800 000	182.75
Beech	Bonanza G36[f],[i],[j]	1704	321.8	6	544	664	925 000	238.25
	Baron G58[f],[i],[k]	2054	370.1	6	651	714.8	1 500 000	392.5
Cirrus	SR20[f] [6, 7]	1313	287	4	352	596.8	634 900	156
Piper	M350[l],[m] [8]	2487	395	6	593	637	2 100 000	411
	Archer LX[f],[n] [9]	967	237	4	266	612	389 000	165.75

[c] URL: https://www.maf.nl/over-ons/vliegtuigen [accessed 1 May 2024]
[d] URL: https://www.aopa.org/go-fly/aircraft-and-ownership/aircraft-guide/aircraft/cessna-206 [accessed 1 May 2024]
[e] URL: https://cessna.txtav.com/ [accessed 1 May 2024]
[f] URL: https://www.aircraftcostcalculator.com/AircraftOperatingCosts/ [accessed 1 May 2024]
[g] URL: https://infogram.com/bca-table-2023-turboprops-1ho16vorwrxm84n [accessed 1 May 2024]
[h] URL: https://www.trade-a-plane.com/search?category_level1=Single+Engine+Piston&make=CESSNA&model=T182T+SKYLANE&listing_id=2429425&s-type=aircraft [accesssed 1 May 2024]
[i] URL: https://beechcraft.txtav.com/ [accessed 1 May 2024]
[j] URL: https://pilotpassion.com/beechcraft-g36-bonanza-cost/ [accessed 1 May 2024]
[k] URL: https://www.aircharterservice.com/aircraft-guide/private/hawkerbeechcraftcorp-usa/beechcraftbaron58 [accessed 1 May 2024]
[l] URL: https://www.controller.com/listing/for-sale/229875193/2022-piper-m350-piston-single-aircraft [accessed 1 May 2024]
[m] URL: https://europeanaircraftsales.com/piper-dealer/piper-m350/ [accessed 1 May 2024]
[n] URL: https://www.aviationunlimited.com/piper_archer_dxtxlx.htm [accessed 1 May 2024]

Customers

Customers are individuals, businesses, government agencies and nonprofit organisations that have an interest in purchasing these general aviation air transport. The customers are segmented based on their purpose; humanitarian, tourism/sightseeing purposes and medical evacuations. For each segment, potential customers are identified and their top potential user requirements are presented below.

Humanitarian Aviation Sector

Potential Customers: Mission Aviation Fellowship (MAF), Special Representative of the UN Secretary-general (SRSG), Office for the Coordination of Humanitarian Affairs (OCHA), United Nations High Commissioner for Refugees (UNHCR), European Community of Humanitarian Organisation (ECHO)

Potential User Requirements:

- The aircraft shall be operable from short, unpaved and rough airstrips
- The aircraft shall be operable in challenging weather conditions, including extreme heat and cold
- The aircraft operations shall have a low environmental impact

Medical Evacuation Sector

Potential Customers: Air Ambulance, Medical Air Service, Skyservice Air Ambulance, Amref Health Africa, LifeFlight, AirLink

Potential User Requirements:

- The aircraft shall be able to deploy in a short time span for rapid response to emergencies
- The aircraft shall have sufficient space to carry medical equipment for the initial treatment of evacuees
- The aircraft shall have reliable communication and navigation systems for the seamless transfer of patients

Tourism/sightseeing Sector

Potential Customers: British Airtours, Papillon, Tessel Air, Red Eagle Aviation

Potential User Requirements:

- The aircraft shall be designed with a focus on passenger comfort.
- The aircraft shall have low direct operating costs
- The aircraft shall be capable of doing short take-off and landing to access various scenic locations

It is thus clear that different target customer groups have distinct needs. Consequently, the aircraft design would need to be slightly modified to accommodate these requirements. For instance, aircraft intended for the tourism sector may necessitate additional legroom or larger windows. However, it is important to note that all three sectors share a reasonable amount of similar requirements. Therefore, the aircraft designed for the humanitarian aviation sector can be sold to another target market with minimal modification.

Potential collaborators

HumanAir had a precious opportunity to meet with an MAF representative, obtaining crucial insights into the market. One of the important findings was that they are willing to have an aircraft that is

operational in the market within five years. Considering the new aircraft certification process usually takes around five to nine years[o], it would be highly challenging for HumanAir to accomplish the task independently. To expedite market entry, collaboration with established manufacturers or companies may be necessary.

The advantage of forming a joint venture or strategic partnership lies in its ability to shorten the time required to penetrate the market. Existing manufacturers would already have extensive knowledge within the industry and, through collaboration, HumanAir could leverage them. Additionally, the partner business may have an existing production facility. Utilising pre-existing infrastructure would allow HumanAir to enter the market quicker.

On the other hand, collaborating with larger entities carries the risk of dependence. HumanAir's status as a small business entails inherent limitations in financial and resource capabilities. Relying heavily on the partner's capital, expertise or market access may limit HumanAir's long-term growth prospects or establish its brand identity within the market. Therefore, collaboration would have both pros and cons. The following is the list of potential collaborators:

- Textron Aviation
- Bombardier
- Cirrus Aircraft
- Dassault Aviation

The list of stakeholders shown in Table 3.1 was refined to ensure a better understanding of the following steps of the mission analysis phase. Thus, a reorganisation was made incorporating more specific stakeholders that are part of the already identified ones. All of this can be seen in Table 3.3 with their respective IDs which will be used for further references to them.

Table 3.3: Reorganised Stakeholders

Stakeholder	**ID**	**Stakeholder**	**ID**
MAF Maintenance Crew	TC	Airworthiness Authorities	AA
MAF Ground Operations Crew	GOC	Aircraft Manufacturers	AM
MAF Administrative Staff	MAS	Communities	COM
MAF Donors	DON	TU Delft	TUD
MAF Air Crew	MAC	Humanitarian Organisations	HO

3.4. Sales Forecast

One of the predominant user requirements focuses on the reduction of CO_2 emissions by 50% which helps outperform current humanitarian, medical evacuation and tourism/sightseeing operations. This allows the replacement of current aircraft with a more sustainable option. The size of the demand for the target market thereby relies on the average shipment of these aircraft annually. Table 3.4 shows the average shipment of aircraft that align with the mission characteristics from Cirrus, Piper, Cessna and Beechcraft within the years 2019 - 2023[p].

[o] URL: https://www.spiritaero.com/pages/article/digital-thread-for-next-gen-aircraft/ [accessed 6 May 2024]

[p] URL: https://gama.aero/facts-and-statistics/statistical-databook-and-industry-outlook/annual-data/

Table 3.4: Average Shipment of Selected Aircraft Within 2019 - 2023

Manufacturer	2019	2020	2021	2022	2023	Average
Cessna						
CE-182T Skylane	33	27	38	48	39	37
CE-T182T Turbo Skylane	-	-	-	-	27	27
CE-T206H Turbo Stationair	37	26	50	42	41	39
Beechcraft						
Beechcraft Bonanza A/G36	7	12	0	3	5	5
Beechcraft Baron B/G58	15	8	0	0	5	6
Cirrus						
Cirrus SR20	53	56	81	100	115	81
Piper						
PA-46-350P Malibu Mirage / M350	21	15	19	19	22	19

The Table 3.4 shows a great variation in average sales over five years across different aircraft brands. For instance, Beechcraft averages only five or six sales, whereas Cirrus sells approximately 81 aircraft. This disparity can be attributed to factors such as market presence, unit pricing, and differences in customer base. By including both high and low sales figures, it reflects the diversity within the market.

The sales forecast can be made based on Table 3.4. Taking the mean value of the average shipments of selected aircraft between 2019 and 2023, the purchase of approximately *30 aircraft* is expected per year. It is important to mention that this expected introduction of a new aircraft to the market requires ongoing monitoring of trends and demand dynamics. With respect to manufacturing, the concept of a learning curve applies. In the initial stages of the production, the average time of production per unit is relatively high but as the cumulative volume of production increases, the time decreases, thereby increasing the number of outputs converging to a shipment range similar to what is listed on Table 3.4.

3.5. Mission SWOT Analysis

SWOT analysis is a tool used to evaluate strengths, weaknesses, opportunities and threats involved in a mission. Strengths and weaknesses are the internal factors and opportunities and threats are the external factors that affect the success of a project. Identifying these four factors allows HumanAir to distinguish its business position in a market. The mission SWOT analysis can be found in Figure 3.4.

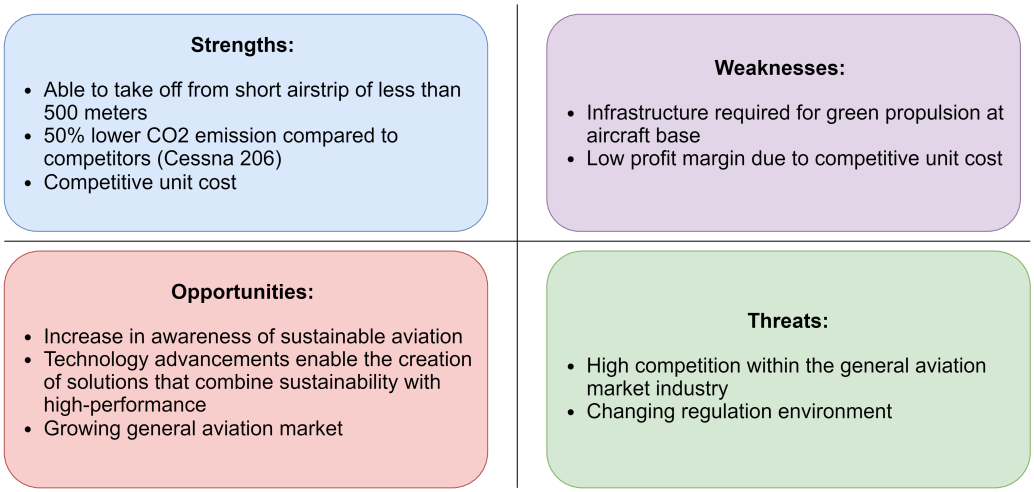

Figure 3.4: Mission SWOT Analysis

Strength

HumanAir distinguishes itself in the market with its aircraft design, emitting 50% less CO_2 than its competitors. This unique selling point is especially effective as the awareness of sustainable aviation

has been increasing over time. Within the aviation industry, continuous efforts have been made to reduce carbon emissions. For instance, the United Kingdom aims to achieve a net zero carbon emissions commitment by 2050 through improvements in aircraft and engine efficiency, the use of more sustainable fuel and more efficient operation of airspace[q]. Capitalising on this prevailing trend alongside its unique selling point, HumanAir would be able to penetrate the existing general aviation industry successfully.

HumanAir stands out with its ability to take off and land on short airstrips and its competitive unit cost. This capability enables the HA-1 to serve multiple markets within the general aviation sector, including humanitarian aviation, emergency evacuation, and tourism, all of which require short-takeoff capabilities. Consequently, this broadens the potential customer base and reduces the risk of business failure. Maintaining a competitive unit cost enhances HumanAir's potential for revenue growth and profitability by targeting a broader market segment.

Weakness

However, designing a new aircraft always involves significant research and development costs. Since HumanAir aims for a significant reduction in CO_2 emissions, some novel technology has to be used. For instance, a new propulsion system must be designed. While these initiatives align with sustainability goals, they entail additional expenses. Consequently, the break-even point itself is high because of all of the costs involved and the competitive pricing strategy further increases the number of aircraft that have to be sold in order to break even.

Another weakness of HumanAir is that the construction of new infrastructure may be necessitated because of its approach to reducing carbon dioxide emissions. While the aircraft itself has a competitive unit price, the additional investment and logistical considerations associated with establishing infrastructure could deter potential customers. Such limitations might result in a reduced customer base and subsequently lower potential revenues for the company. However, careful consideration during the aircraft design phase may limit the need for the construction of new infrastructure. By prioritising minimising infrastructure requirements, HumanAir would be able to be in a more competitive position within a market.

Opportunity

The opportunities include the increasing awareness of sustainable aviation, advancements in technology, and a growing general aviation market. The expanding market increases the likelihood of higher product sales. Additionally, the rising awareness of sustainability is particularly beneficial for HA-1, as the primary unique selling point is low CO_2 emissions. Achieving these low emissions has been made possible by new battery technology, which is a direct result of technological advancements.

Threat

The primary threat HumanAir faces is the high level of competition within the general aviation market. As a new business, HumanAir may find it challenging to survive or enter the market independently. This risk, however, can be significantly reduced through collaboration with established manufacturing companies such as Textron Aviation. Additionally, the changing regulatory environment poses a common threat. This can be mitigated by carefully monitoring and staying informed about relevant regulations and their changes.

[q] URL: https://www.sustainableaviation.co.uk/ [accessed 2 May 2024]

4 | Functional Analysis

When initialising the development of any product, it is essential to create an overview of all the functions the final product must perform to fulfil its assigned mission, and how they relate to each other. Later in the design process, this overview can be used as a starting point for the development of various subsystems, and as a reference during the validation stage. The first step in this analysis is to establish the mission architecture – the various components of the mission – as done in Section 4.1. Then, one can start identifying the various functions that the product must perform, which can be visualised in a Functional Breakdown Structure (FBS), as created in Section 4.2. Finally, it is possible to analyse the flow between the functions, that is, how they all relate to each other during the mission, which can be visualised in a Functional Flow Diagram (FFD). This is done in Section 4.3.

4.1. Mission Architecture

Before the functions of the product can be determined, it is important to first establish the mission architecture, that is, what elements, systems and subsystems are part of the mission, and how they interact with each other and the environment. For HumanAir, there are two main segments to the mission: The aircraft and the ground operations. Within both segments, several subsystems can be identified. A full overview of the architecture is available in Figure 4.1.

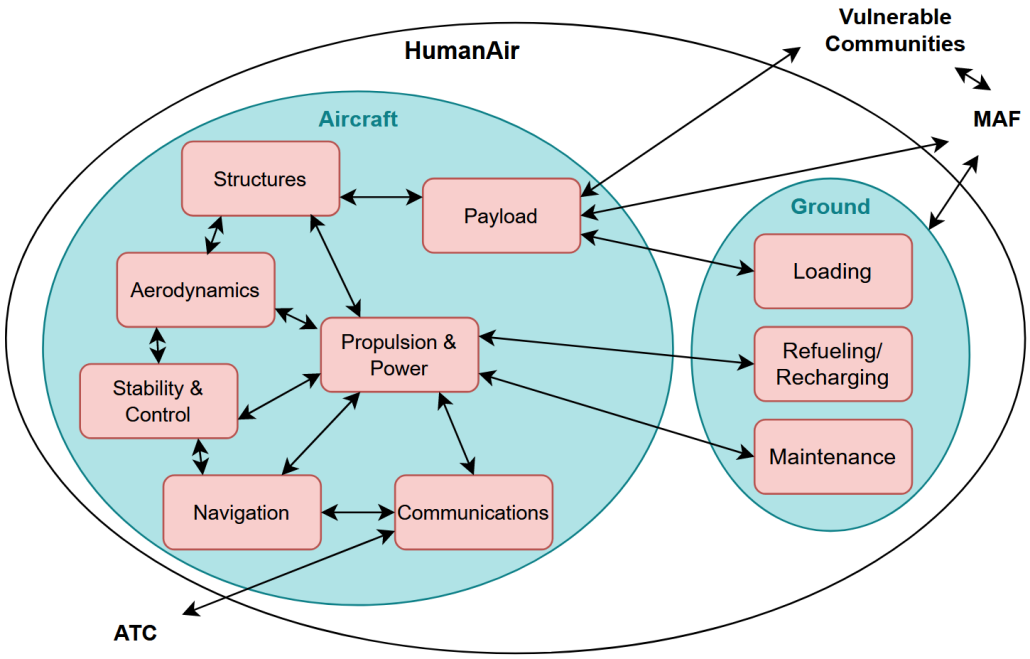

Figure 4.1: Mission Architecture

4.2. Function Identification

The first step in the functional analysis is scoping out all possible functions the system needs to perform. For this, the mission was divided into six phases.

- **Design the aircraft:**
  During this phase, the design of the aircraft is established. This includes all steps ranging from the project setup to the final test performed.
- **Manufacture the aircraft:**
  In this phase, the result of the design phase is manufactured. All parts should be produced and

assembled into subsystems and systems.

- **Certify the aircraft:**
  After, but also during the aforementioned phases, the product should be certified. This includes various tests and deliverables that confirm compliance with aircraft regulations.
- **Deploy the aircraft:**
  Then, the fully certified product needs to be distributed to the locations where it will be used in the operational phase. This phase entails different aspects like transportation, training of personnel, implementing set-up procedures etc.
- **Operate the aircraft:**
  In the operation phase, the product is operated by the customer. This means it is implemented in their day-to-day operations, but it also includes support activities such as maintenance and servicing.
- **Retire the aircraft:**
  At the end of the aircraft's operational life, it must be retired. It should be transported to a location where it can be either stored or dismantled, depending on the End Of Life (EOL) policy. The EOL policy of the HumanAir project can be found in Section 18.5.

With the mission phases identified, an important distinction can be made. The only mission phase where the aircraft itself has to perform functions is the operating phase. All other phases exclusively contain actions from third parties like manufacturing personnel or certification authorities.

The objective of a functional breakdown structure (FBS) is to scope out all possible functions the system needs to perform, and to identify what has to be designed for. However, it is evident that the aircraft should also be designed for easy manufacturing and retirement, even though the aircraft itself is not performing any function during these phases. Hence, to stay within the scope of this chapter, only a preliminary overview of what each of these phases requires from the third parties will still be presented. In future chapters, more attention will be allocated to them, and the requirements they impose on the design.

The final FBS is presented in Figure 4.2. It was made with the help of sources [10, 11]. The ground segment is only indirectly considered in this diagram, as it is seen as a supporting segment to the aircraft segment. In case some functions are only to be performed in certain situations, these functions are marked with an **IF:** statement.

4.3. Flow Analysis

Once the various functions have been identified, it is possible to analyse how they relate to each other. This allows for a more complete understanding of when the product needs to perform each function. This process may also aid in identifying additional functions. Once again sources [10, 11] were used. Since only the operational phase contains actual functions of the aircraft, only this phase will be considered, to avoid convolution of the diagram. The result of the analysis is presented in Figure 4.3.

Mission Need Statement

Provide a small aircraft that outperforms current Cessna 206 humanitarian operations in terms of CO_2 emissions and economic viability.

- Design Aircraft — FUN-1
- Manufacture Aircraft — FUN-2
  - Plan Manufacturing — FUN-2.1
  - Create Manufacturing and Assembly Facility (if required) — FUN-2.2
  - Create Storage Warehouse (if required) — FUN-2.3
  - Purchase or Create Tooling (if required) — FUN-2.4
  - Hire and Train Personnel (if required) — FUN-2.5
  - Manufacture Parts & Subassemblies — FUN-2.6
  - Assemble Aircraft — FUN-2.8
  - Store Aircraft — FUN-2.9
- Certify Aircraft — FUN-3
  - Familiarise with Certification Specifications — FUN-3.1
  - Define Certification Rules — FUN-3.2
  - Demonstrate Means of Compliance — FUN-3.3
- Deploy Aircraft — FUN-4
  - Transport Aircraft and Personnel to Deployment Zone — FUN-4.1
  - Train Personnel — FUN-4.2
- Operate Aircraft — FUN-5
- Retire Aircraft — FUN-6
  - Park and Store Aircraft — FUN-6.1
  - Disassemble Equipment and Parts — FUN-6.2
  - Recycle — FUN-6.3
  - Dispose — FUN-6.4

AND

General Aircraft Functions (performed at every stage)

- Provide Structural Integrity — FUN-5.1
  - Carry Static Loads — FUN-5.1.1
  - Carry Dynamic Loads — FUN-5.1.2
  - Carry Vibrational Loads — FUN-5.1.3
- Provide Static Control Stability — FUN-5.2
  - Provide Static Longitudinal Control Stability — FUN-5.2.1
  - Provide Static Lateral Control Stability — FUN-5.2.2
- Provide Dynamic Control Stability — FUN-5.3
  - Provide Dynamic Lateral Control Stability — FUN-5.3.1
  - Provide Static Lateral Control Stability — FUN-5.3.2
- Provide Ground Control & Stability — FUN-5.4
  - Provide Ground Stability — FUN-5.4.1
  - Provide Steering Capability — FUN-5.4.2
- Provide In-Flight Control — FUN-5.5
  - Provide Longitudinal Control — FUN-5.5.1
  - Provide Lateral Control — FUN-5.5.2
  - Provide Vertical Control — FUN-5.5.3
  - Provide Autopilot — FUN-5.5.4
- Provide Visual Aids — FUN-5.6
  - Provide Visual Aids for Other Airspace Users — FUN-5.6.1
  - Provide Visual Aids for Individuals on Ground — FUN-5.6.2
- Provide Essential Information to ATC — FUN-5.7
  - Provide Location — FUN-5.7.1
  - Provide Identification — FUN-5.7.2
- Provide Realtime Information on Aircraft Parameters to Control System — FUN-5.8
  - Determine Energy Level — FUN-5.8.1
  - Determine Location — FUN-5.8.2
  - Determine Heading — FUN-5.8.3
  - Determine Airspeed — FUN-5.8.4
  - Determine Altitude — FUN-5.8.5
  - Determine Attitude — FUN-5.8.6
  - Determine Atmospheric Conditions — FUN-5.8.7
- Provide Suitable Environment to Passengers — FUN-5.9
  - Control Temperature of Cabin — FUN-5.9.1
  - Provide Adequate Oxygen Levels — FUN-5.9.2
  - Provide Appropriate Cabin Pressure — FUN-5.9.3
  - Provide Cabin Lightning — FUN-5.9.4
  - Provide Life-Support Equipment — FUN-5.9.5
  - Provide Ability to Look Outside — FUN-5.9.6
- Withstand Adverse Environmental Conditions — FUN-5.10
  - Keep Structures Clear of Ice — FUN-5.10.1
  - Withstand Turbulence — FUN-5.10.2
  - Withstand Lightning Strike — FUN-5.10.3
  - Withstand Precipitation — FUN-5.10.4
- Perform Emergency Operations — FUN-5.11
  - Land on Water — FUN-5.11.1
  - Operate Under Engine Failure — FUN-5.11.2
  - Re-start Engine In-Flight — FUN-5.11.3
  - Protect Against Fire — FUN-5.11.4
- Provide Internal Configuration Changes — FUN-5.12
  - Allow for Seat to be Removed — FUN-5.12.1
  - Allow Cargo Hold Wall to be Removed — FUN-5.12.2
- Provide CS23 Specified Performance — FUN-5.13
- Provide Maintenance Capabilities — FUN-5.14
  - Provide Access to Aircraft Structural Components — FUN-5.14.1
  - Provide Essential Spare Equipment — FUN-5.14.2
  - Provide Cleaning Capability — FUN-5.14.3
- Load Energy Soource — FUN-5.16
  - Provide Energy Source Storage Space — FUN-5.16.1
  - Provide Access to Energy Source Storage — FUN-5.16.2
- Provide Avionics — FUN-5.17
  - Provide Electronic Power — FUN-5.17.1
  - Provide Internal Communications — FUN-5.17.2
  - Provide External Communications — FUN-5.17.3

Phase-Specific Operations

- Perform Pre-Flight Ground Operations — FUN-5.18
  - Plan Flight — FUN-5.18.1
  - Load Payload — FUN-5.18.2
  - IF: Main Base Take-Off
    - Charge Battery — FUN-5.18.3
    - Refuel — FUN-5.18.4
  - IF: Refuelling Required
    - Refuel at Remote Base — FUN-5.18.5
- Switch on Aircraft — FUN-5.19
  - Turn on Avionics — FUN-5.19.1
  - Turn on Propulsion System — FUN-5.19.2
- Perform Ground Maneuvring — FUN-5.20
  - Provide Longitudinal Ground Control (any surface) — FUN-5.20.1
  - Provide Lateral Ground Control (any surface) — FUN-5.20.2
- Take-Off — FUN-5.21
  - Deploy High-Lift Devices — FUN-5.21.1
  - Provide Take-Off Lift — FUN-5.21.2
  - Provide Take-Off Thrust — FUN-5.21.3
  - Lift-Off — FUN-5.21.4
- Climb — FUN-5.22
  - Retract Landing Gear — FUN-5.22.1
  - Switch Flaps to Climb Configuration — FUN-5.22.2
  - Provide Climb Lift — FUN-5.22.3
  - Provide Climb Thrust — FUN-5.22.4
- Load / Unload Payload — FUN-5.15
  - Provide Payload Space — FUN-5.15.1
  - Provide Access to Payload Space — FUN-5.15.2
  - Provide Seating — FUN-5.15.3
  - Provide Space for a Stretcher — FUN-5.15.4
- Brake on Ground — FUN-5.15
  - Provide Reverse Propeller Thrust — FUN-5.15.1
  - Provide Wheel Breaking — FUN-5.15.2
- Cruise — FUN-5.23
  - Switch Flaps to Cruise Configuration — FUN-5.23.1
  - Provide Cruise Lift — FUN-5.23.2
  - Provide Cruise Thrust — FUN-5.23.3
  - Maintain Heading, Altitude & Airspeed — FUN-5.23.4
  - Change Heading, Altitude & Airspeed — FUN-5.23.5
- Descend — FUN-5.24
  - Switch Flaps to Descent Configuration — FUN-5.24.1
  - Provide Descent Lift — FUN-5.24.2
  - Provide Descent Thrust — FUN-5.24.3
  - IF: Divert
    - Divert — FUN-5.24.4
- IF: Loiter — Loiter — FUN-5.25
  - Switch Flaps to Loiter Configuration — FUN-5.25.1
  - Provide Loiter Lift — FUN-5.25.2
  - Provide Loiter Thrust — FUN-5.25.3
- Land — FUN-5.26
  - Perform Approach — FUN-5.26.1
  - Extend Landing Gear — FUN-5.26.2
  - Go around — FUN-5.26.3
  - Touch-Down and Absorb Loads — FUN-5.26.4
- Perform post-landing operations — FUN-5.27
  - Manoeuvre on Ground — FUN-5.27.1
  - Shut Down Systems — FUN-5.27.2
  - Unload Payload — FUN-5.27.3
- Inspect & Maintain — FUN-5.28
  - Inspect Aircraft — FUN-5.28.1
  - Maintain Aircraft if required — FUN-5.28.2
  - Service Aircraft if required — FUN-5.28.3

Legend

- Origin
- Level 1
- Level 2
- Level 3
- Aircraft Function — ID
- IF: Condition

Figure 4.2: Functional Breakdown Structure

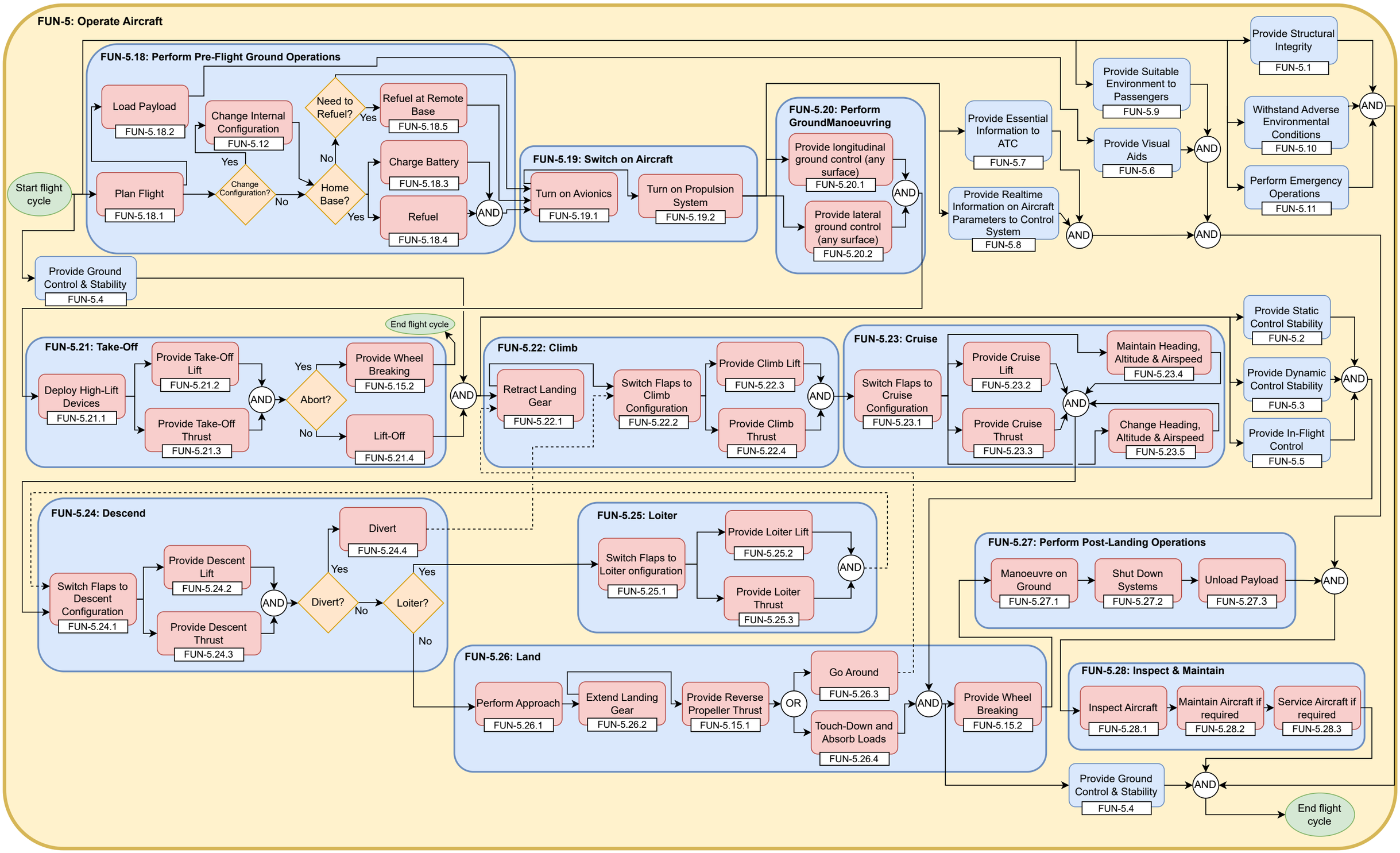

Figure 4.3: Functional Flow Diagram - Operations (Lower Level)

5 | Concept Selection

This chapter describes the conceptual design chosen for the preliminary design process. Initially, the three analysed concepts are presented, followed by an explanation of the trade-off method used to decide which one is the best. The same trad-off procedure was also used for the other trade-offs performed throughout the design process. The overall specifications were decided in detail in the midterm report and will be briefly summarised [12].

5.1. Design Options

Many design options were generated and subsequently discarded in previous project phases, with only 3 final concepts left to be analysed in more detail to perform a good trade-off process [12]. A summary of the top-level Design Option Tree (DOT) was made in the baseline report and mentioned in the midterm report, where the non-concepts, non-feasible concepts and concepts too difficult to analyse were discarded [12, 13].

New concepts were made by combining the remaining subsystems. For the energy system, only a hybrid fuel electric powertrain is left as a configuration option. For now, three concepts using this hybrid powertrain with propeller propulsion have been made such that they cover the remaining subsystem options. They were shown in a broad design option tree (DOT) in the baseline report [13].

The first design option is a blended wing body concept without a horizontal stabiliser, such that it will roughly have the shape of a flying wing. To retain ground visibility from the cockpit, a transparent panel could be installed on the floor of the cockpit. Furthermore, to provide propeller ground clearance, it will be placed on top of the fuselage so that the wing shields the engine from any debris. The location of the vertical stabiliser is left to the preliminary design stage (if this concept was chosen).

The second design option is a conventional aircraft configuration with a canard and a low wing. This concept will use multiple engines, placed on the wings, although the exact location is to be determined in a later design stage. Despite the low-wing configuration, acceptable pilot ground visibility is possible, thanks to the use of a canard, with the main wing thus placed far aft.

The third and last design option is a purely conventional configuration with the aforementioned hybrid propeller powertrain. The concept thus has a high wing and the engine shall be placed at the front of the fuselage. The exact type of tail is to be determined later in the design. This concept offers excellent ground visibility as the wing is located above the pilots, thus enabling them to look down all around the aircraft. Examples of the aircraft are shown in Figure 5.1.

(a) Example of concept 1[(a)] **(b)** Example of concept 2[(b)] **(c)** Example of concept 3[(c)]

Figure 5.1: Examples of the Selected Concepts

[(a)] URL: https://commons.wikimedia.org/wiki/File:HX-2_Image.jpg [accessed 1 May 2024]
[(b)] URL: https://commons.wikimedia.org/wiki/File:Piaggio_P-180_Avanti_Rennes_2010_(cropped).jpg [accessed 1 May 2024]
[(c)] URL: https://en.wikipedia.org/wiki/GippsAero_GA8_Airvan [accessed 1 May 2024]

After roughly analysing the subsystems of all three concepts selected, a trade-off was performed to decide the winner that will be developed more in the next design phases of the project. Besides the subsystem design, the financial analysis and emissions calculator had a crucial part in deciding on the numbers' ranking. Thus, Table 5.3 shows the steps and the winner concepts.

5.2. Trade-off Method

First, the reader shall have a clear understanding of the numbers and colours in the trade-off table from which the score is calculated. The colour and number strategy is included in Table 5.1.

Table 5.1: Colour and Number Strategy for Trade-Off Tables

	Unacceptable	Bad	Correctable Deficiencies	Good	Excellent
Score	1	2	3	4	5

The colours and their meaning are kept consistent throughout the whole report. The tables also contain each criterion's weight with column widths scaled to the relative value of the weights. The weights always add up to 1.

Secondly, the steps required to find the winner of a trade-off process are explained: first, the candidates are listed. Then, a table of **criteria**, **justification**, what it **accounts for**, **ranking strategy**, **weight** and **weight's justification** is included to explain where the numbers come from. Furthermore, the trade-off table covers all the required numbers as well as the score of each candidate following Equation 5.1.

$$score = \sum(weight \cdot assigned\ value) \tag{5.1}$$

For example, Table 5.2 shows how a possible candidate's score is set during the process for which candidate 2 is the winner.

Table 5.2: Example of Trade-off Table

	Criterion 1	Criterion 2	Criterion 3	Criterion 4	Criterion 5	
Weight	0.2	0.15	0.3	0.2	0.15	**Score**
Candidate 1	4	2	5	1	4	3.40
Candidate 2	5	3	4	1	5	3.60

5.3. Trade-Off Process

The section provides the rationale for the criteria chosen for the concept trade-off as well as which candidate is the winner highlighted in a yellow cell.

Firstly, the weights, criteria and their reasoning are shown in Table 5.3. The design team considers that these are the most important aspects that shall be taken into account. Most of them are closely related to the requirements such as **HA-UR-06**, **HA-UR-07**, **HA-UR-08**, **HA-UR-09**, and **HA-UR-15**.

Table 5.3: Trade-off Criteria for Three Concepts Selected

Criterion	Justification	Accounts for	Ranking Strategy	Weight	Weight Justification
Ground Clearance	MAF mission operations on landing strips with a lot of stones and dust. The lower the ground clearance, the more damage can be done	Scrape angle limit, roll angle limit, and lateral ground clearance	Assess the distance of the wing and propulsion system to the ground and how they are potentially shielded by other components	0.10	Ground clearance issues are easier to work around (adjust landing gear/engine position, add reinforcements, etc.)

Emission reduction	One of the driving project requirements is reaching a 50% emission reduction but a bigger reduction is always welcomed	CO_2 emissions during aircraft operations. This includes the full life cycle of the energy source, emissions during ground operations and maintenance	Calculations have been made on the emissions for each aircraft concept at its maximum range and preliminary optimisation of the legs' combinations	0.30	Reducing emissions is the main goal of this design project
Development Risk	Some concepts are technologically significantly less developed than others, so they would require more development time and cost	Meeting the 5-year-to-market deadline, the possibility of collaboration with existing manufacturers, the difficulty of certification, and the possibility of cost overruns.	Assess the novelty of the design concept and the ease with which it could be certified.	0.20	While it is important to quickly get the aircraft to market to fulfil the objective, some delay may be acceptable if it leads to improved performance.
Cost	Since MAF is funded by donations, costs in all respects are desired to be as low as possible.	Operating cost (aircraft maintenance, service, and energy), ground station development cost, insurance, overhaul, and aircraft unit cost	Assess the cost of each aircraft concept based on the cost estimate previously calculated.	0.30	Generally, cheaper aircraft will be deployed faster, thus more easily achieving the project goal. And MAF will be able to fund more aircraft more quickly.
Operability	Harsh and poorly developed conditions for the pilots and aircraft of MAF	Pilot visibility, pilot workload, ease of control, and the ability to load and change configuration in a short time	Asses the operability parameters based on the sizing performed for all three design concepts treated.	0.10	Since the main objectives of this are a reduction of emissions and cost, decreased operability could be accepted if it means the aircraft performs significantly better in the other areas

Following the detailed assignment process for the weights and criteria, the final trade-off table was made as shown in Table 5.4.

Table 5.4: Trade-off Table for the Three Concepts

	Ground Clearance	Emission Reduction	Development Risk	Cost	Operability	
Weight	0.1	0.3	0.2	0.3	0.1	**Score**
Flying Wing	3	1	1	2	1	1.5
Canard	3	4	4	4	3	3.8
Conventional	4	3	5	5	5	4.3

It was thus concluded that the **Conventional Aircraft** is the winner of the trade-off process. For the next sections of the report, it is referenced as the **HumanAir HA-1 Aircraft**. To increase the confidence in the result of the trade-off, a sensitivity analysis was made by slightly changing the weights for each criterion and the importance of some criteria. The detailed procedure was explained and showed in the midterm report, where it was concluded that the conventional concept remains the winner [12].

6 | Requirement & Compliance

Following the functional analysis, the requirements could be set up and analysed for compliance. The requirements are a key part of the aircraft design as they constrain the design space itself. At the end of a design cycle, they are revisited to check whether the designed system fits into this constrained design space. The full list of requirements used to constrain the HumanAir HA-1 design is given in Section 6.1. Additionally, the compliance matrix for these requirements is given in Section 6.2.

6.1. Requirements

The requirements can be divided into user, stakeholder, system, and subsystem requirements, with each level being more detailed than the previous. Generally, requirements also flow down between the levels, meaning that a lower-level requirement is the result of one from a higher level. Therefore, the following notation is used for the unique identifiers of requirements:

- *User requirement*: HA-UR-XX, where HA represents HumanAir, UR stands for user requirement and XX is the sequential number assigned.
- *Stakeholder requirement*: HA-STK-[stakeholder]-XX, where STK represent stakeholders, [stakeholder] indicates from which stakeholder the requirement was derived and XX is the sequential number.
- *System requirement*: HA-SYS-XX, where SYS refers to the system and XXX is the sequential number.
- *Subsystem requirement*: HA-[Subsystem]-XX, Where [subsystem] indicates to what subsystem the requirement is applicable and XX is the sequential number.
- *Related requirements*: HA-[Top-Level]-[Requirement ID], where [Top-Level] refers to the ID of the top-level requirement and [Requirement ID] refers to the original ID of the requirement. For the top-level requirement the lowest level is always chosen, e.g. in case a user requirement flows down into a system- and then a subsystem requirement, the requirement would be HA-SYS-XX-[Subsystem]-XX.

Table 6.1 lists all the requirements created, where specific requirements on avionics have not been expanded yet since they will be designed later. Each requirement can be classified under driving, killer or key requirements. **Driving** requirements (*purple*) dominate the overall mission envelope, **killer** requirements (*red*) influence the design to an unacceptable level, and **key** requirements (*blue*) are of primary importance to the l customer.

Table 6.1: Full List of Requirements for the HumanAir HA-1 Aircraft

ID	Statement
	User Requirements
HA-UR-01	The aircraft shall have a range of 600 nm
HA-UR-02	The aircraft shall carry 6 passengers excluding pilot or 540 kg of freight
HA-UR-03	Take-off shall be operable from unpaved airstrips with a Take-off Run Available (TORA) of less than 500 m
HA-UR-04	The aircraft shall comply with CS-23 safety and reliability requirements at sea-level atmospheric conditions with still air
HA-UR-05	The aircraft shall comply with requirements for IFR operations
HA-UR-06	The operational CO_2 emissions of the aircraft shall be reduced by at least 50% compared to current C206 operations
HA-UR-07	The aircraft shall be operable at all MAF airports currently in use
HA-UR-08	The direct operating costs (fuel, maintenance & overhaul) shall remain below US $300/hour for current operations
HA-UR-09	The maximum unit cost shall not exceed US $1.5 million
HA-UR-10	The aircraft shall have a cruise speed of at least 50 m/s

HA-UR-11	The aircraft shall be capable of adhering to a flight profile that enables current operational practice
HA-UR-12	The aircraft shall be capable of operating in all of the operating conditions encountered by MAF
HA-UR-13	The aircraft shall be able to be reconfigured for different missions within 30 minutes
HA-UR-14	The aircraft shall be able to transport a stretcher
HA-UR-15	The aircraft shall have a maximum development time until operational of 5 years
HA-UR-16	The aircraft shall have the possibility to carry live animals and/or dangerous goods at the same time as passengers
HA-UR-17	The aircraft shall be able to accommodate stopovers as part of the mission
HA-UR-18	The aircraft shall be able to be refueled and recharged within 60 minutes
HA-UR-19	The aircraft shall have fuel reserves equal to 15% of trip fuel and 75 minutes of loiter flight at 450 m above airfield elevation before the final landing
Stakeholder Requirements	
HA-STK-GOC-01	The aircraft shall adhere to refuelling safety regulations
HA-STK-MAC-01	The aircraft shall include designated seats for passengers
HA-STK-MAC-02	The aircraft shall include a designated seat for each pilot in the cockpit
HA-STK-MAC-03	The aircraft shall provide the pilots with visibility of the airstrip and surrounding area at all times during take-off, descent, and landing
HA-STK-HO-01	The aircraft shall provide occupants with oxygen equal to a pressure altitude of less than 12500 ft MSL[(a)]
HA-STK-HO-02	The aircraft shall provide transportation for medical equipment, food, water, and shelter materials
HA-STK-TUD-01	The aircraft preliminary design process shall be completed in less than 10 weeks
HA-STK-TC-01	The aircraft shall not be damaged by the airstrips in a way that would require additional maintenance
System Requirements	
HA-UR-12-SYS-01	The maximum operating temperature shall be at least 55 °C
HA-UR-12-SYS-02	The minimum ground operations temperature shall be at most −10 °C
HA-UR-12-SYS-03	The aircraft shall be able to be operated for extended periods in a temperature and humidity of 30 °C and 0-100% relative humidity
HA-UR-12-SYS-04	The aircraft shall be able to withstand lighting strikes
HA-UR-12-SYS-05	The aircraft shall be able to operate in heavy rain
HA-UR-12-SYS-06	The aircraft shall be able to operate in hail
HA-UR-12-SYS-07	The aircraft shall be able to operate under intense sunlight for prolonged periods
HA-UR-12-SYS-08	The aircraft shall be resistant to corrosion due to salt water
HA-UR-12-SYS-09	The aircraft shall be resistant to the growth of fungi
HA-UR-07-SYS-10	The takeoff and landing requirements shall be met at 750 m ISA +18 °C
HA-UR-07-SYS-11	The aircraft shall be able to operate from sandy and/or dusty landing strips
HA-UR-07-SYS-12	The aircraft shall be able to operate from airstrips with debris on the ground
HA-UR-07-SYS-13	The aircraft's sensitive systems shall have ground clearance of at least 30 cm
HA-UR-07-SYS-14	The aircraft shall be able to land on airstrips sloped upwards by 11%
HA-UR-11-SYS-15	The aircraft shall be able to land with a glideslope of 3°
HA-UR-16-SYS-16	Must have a cargo hold separate from passenger cabin capable of holding dangerous goods according to ICAO regulations
HA-UR-16-SYS-17	The aircraft shall be able to be loaded without damaging the airframe
HA-SYS-18	The aircraft shall have a disposal of waste parts program
HA-SYS-19	The aircraft shall have an end-of-life design phase
HA-UR-04-SYS-20	The aircraft shall be able to determine its position with respect to ground bases
HA-UR-04-SYS-21	The aircraft shall be able to communicate with Air Traffic Control
HA-UR-04-SYS-22	The aircraft shall include means to provide internal communications
HA-UR-04-SYS-23	The aircraft shall be able to determine its airspeed
HA-UR-04-SYS-24	The aircraft shall be able to determine its altitude
HA-UR-04-SYS-25	The aircraft shall be able to determine its heading
HA-UR-04-SYS-26	The aircraft shall be able to determine the external atmospheric conditions
HA-UR-04-SYS-27	The aircraft shall have means to visually communicate its position
HA-UR-04-SYS-28	The aircraft shall be able to climb, in initial climb configuration, with a gradient of at least 4%
HA-UR-04-SYS-29	The aircraft shall be able to climb, in landing configuration during a go-around, with a gradient of at least 3%

[(a)] URL: `https://www.ecfr.gov/current/title-14/chapter-I/subchapter-F/part-91/subpart-C/section-91.211` [accessed 1 May 2024]

HA-UR-04-SYS-30	The aircraft shall not vibrate to the extent of interfering with control or causing excessive fatigue to the pilots
HA-UR-04-SYS-31	The aircraft shall have a stall speed in landing configuration at maximum take-off weight of no more than 31.4 m/s
HA-UR-04-SYS-32	The aircraft shall have a clear stall warning with sufficient margin to prevent accidental stalling
HA-UR-04-SYS-33	The aircraft shall include a flight recorder to register flight data throughout the flight
HA-UR-04-SYS-34	The aircraft shall include emergency lighting and emergency exits
HA-UR-04-SYS-35	The aircraft shall include fire extinguisher placed in positions defined by CS-23 regulations
HA-UR-04-SYS-36	The aircraft shall provide protection for all occupants against injury, accounting for flight, ground and emergency landing conditions defined by CS-23 regulations
HA-UR-16-SYS-37	The aircraft shall enable the loading of 540 kg of freight aft in the cabin
HA-UR-16-SYS-38	The aircraft shall accommodate all possible combinations of cargo and passenger loading
HA-UR-04-SYS-39	The aircraft shall have controllable longitudinal handling during ground operations
HA-UR-04-SYS-40	The aircraft shall have controllable directional handling during ground operations
HA-UR-06-SYS-41	The landing gear shall be retractable
HA-SYS-42	The aircraft shall have a mass of less than 4000 kg when no contingencies are applied
HA-SYS-43	No aircraft component shall succumb to fatigue within 30 years of its production date
HA-SYS-44	The aircraft shall display no signs of aeroelastic effects at airspeeds ranging from 0 m/s to $1.15 \cdot V_D$ for all operational altitudes
Power System Requirements	
HA-POW-01	The battery shall be able to discharge at sufficient power to provide take-off power, without reducing the rated number of cycles
HA-UR-04-POW-02	The aircraft shall provide power to all systems on board for the entire mission duration
Propulsion System Requirements	
HA-UR-04-PRO-01	The propulsion system shall provide continued safe operation without a hazardous loss of power or thrust while being operated in rain for at least 3 minutes with the rate of water ingestion being not less than 4% by weight, of the engine induction airflow rate at the maximum installed power or thrust approved for take-off and at flight idle
HA-UR-04-PRO-02	Each propeller shall be shown to have vibration stresses, in normal operating conditions, that do not exceed values that have been shown by the propeller manufacturer to be safe for continuous operation
HA-UR-04-PRO-03	Propellers and other components of complete engine installations shall be protected against the accumulation of ice as necessary to enable satisfactory functioning without appreciable loss of thrust when operated in the icing conditions
HA-UR-04-PRO-04	The total usable capacity of the fuel tanks must be enough for at least 30 min of operation at maximum continuous power
HA-UR-04-PRO-05	Each tank compartment must be ventilated and drained to prevent the accumulation of flammable fluids or vapours
HA-UR-04-PRO-06	All parts of the fuel system up to the tank which are subjected to fuelling pressures shall have a proof pressure of 1.33× and an ultimate pressure of at least 2.0×, the surge pressure likely to occur during fuelling
HA-UR-03-PRO-07	The propulsion system shall produce at least 292 kW of power during take-off
HA-UR-10-PRO-08	The propulsion system shall produce at least 234 kW of power continuously
HA-SYS-13-PRO-09	The propeller shall have a ground clearance of at least 0.32 m
HA-UR-06-PRO-10	The electric motor shall be able to provide the required take-off power without assistance from the combustion engine
HA-UR-05-PRO-11	The combustion engine shall be able to provide the required take-off power without assistance from the battery
HA-UR-07-PRO-12	The combustion engine shall be powered by Jet A-1 fuel
Structural Requirements	
HA-SYS-01-STR-01	The structure shall accommodate a battery
HA-SYS-01-STR-02	The aircraft shall be manufactured using materials able to withstand temperatures between −10 °C to 50 °C
HA-UR-04-STR-03	The aircraft's structural design loads shall be determined based on all critical combinations of anticipated external or internal pressures, forces, or moments that could arise during flight, ground operations, or water manoeuvres
HA-UR-04-STR-05	The aircraft's critical flight loads shall be established from all combinations of airspeed and load factor at and within the boundaries of the manoeuvre and gust envelope
HA-UR-04-STR-06	The aircraft shall withstand the limit loads (equal to the structural design loads) without interference with the safe operation of the aircraft and detrimental permanent deformation
HA-UR-04-STR-07	The aircraft shall withstand ultimate loads equal to the limit loads multiplied by 1.5× safety factor for 3 seconds
HA-UR-04-STR-08	Each fuel tank must be supported so that tank loads are not concentrated

HA-UR-04-STR-09	There shall be at least 13 mm of clearance between the fuel tank and the firewall
HA-UR-04-STR-10	The passenger and the pilot cabin shall be manufactured of materials that respect the safety regulations imposed by CS-23 regulations
HA-UR-04-STR-11	The aircraft shall uphold its designed structural integrity even in the event of system failure
HA-UR-04-STR-14	The aircraft's structural design loads shall account for loads resulting from taxi, take-off, landing, and handling conditions on the applicable surface in normal and adverse attitudes and configurations
HA-UR-04-STR-15	The aircraft shall be designed to minimise hazards due to structural damage caused by high-energy fragments from an uncontained engine or rotating-machinery failure
HA-UR-04-STR-16	The aircraft shall be free from flutter at all speeds within and sufficiently beyond the structural design envelope, for any configuration and condition of operation, accounting for critical degrees of freedom; and accounting for any critical failures or malfunctions
HA-UR-04-STR-17	The aircraft shall be free from divergence at all speeds within and sufficiently beyond the structural design envelope, for any configuration and condition of operation, accounting for critical degrees of freedom; and accounting for any critical failures or malfunctions
HA-UR-12-STR-18	The aircraft parts shall be protected against loss of strength due to any cause likely to occur in the expected operational environment according to CS-23 regulations
HA-UR-12-STR-19	The aircraft parts shall be protected against deterioration due to any cause likely to occur in the expected operational environment
HA-UR-04-STR-20	The aircraft shall have adequate provisions for ventilation and drainage
HA-UR-04-STR-21	The aircraft design shall be designed taking into account measures to allow maintenance, preventive maintenance and/or servicing
HA-UR-04-STR-22	The aircraft shall be designed to withstand thermal loads
HA-UR-04-STR-23	The aircraft shall implement factor of safety of 1.2 for each part, article or assembly likely to deteriorate in service before normal replacement
HA-UR-04-STR-24	The aircraft shall implement factor of safety of 1.2 for each part, article or assembly subject to appreciable variability because of uncertainties in manufacturing processes or inspection methods
HA-UR-04-STR-25	The cargo compartment shall be designed for its maximum loading and for the critical load distributions at the maximum load factors
HA-UR-04-STR-26	The baggage compartment shall be designed for its maximum loading and for the critical load distributions at the maximum load factors defined by CS-23 regulations
Stability and Controllability Requirements	
HA-UR-04-STB-01	The aircraft shall provide static longitudinal stability at all combinations of mass and centre of gravity in the aircraft's defined range
HA-UR-04-STB-02	The aircraft shall provide static lateral stability at all combinations of mass and centre of gravity in the aircraft's defined range
HA-UR-04-STB-03	The aircraft shall provide static directional stability at all combinations of mass and centre of gravity in the aircraft's defined range
HA-UR-04-STB-04	The aircraft shall be dynamically stable in the short period oscillation mode at all combinations of mass and centre of gravity in the aircraft's defined range
HA-UR-04-STB-05	The aircraft shall be dynamically stable in the Dutch roll oscillation mode at all combinations of mass and centre of gravity in the aircraft's defined range
HA-UR-04-STB-06	The aircraft shall not have divergent dynamic longitudinal stability so unstable as to increase pilot workload or endanger occupants
HA-UR-04-STB-07	The empennage shall provide controllability in the event of wing stall
HA-UR-04-STB-08	The aircraft shall not have a tendency to hazardously depart from controlled flight inadvertently, including after a critical loss of thrust
HA-UR-04-STB-09	The elevator control forces for temporary application shall not exceed 334 N
HA-UR-04-STB-10	The elevator control forces for prolonged application shall not exceed 44.5 N
HA-UR-04-STB-11	The aileron control forces for temporary application shall not exceed 222 N
HA-UR-04-STB-12	The aileron control forces for prolonged application shall not exceed 22 N
HA-UR-04-STB-13	The rudder control forces for temporary application shall not exceed 667 N
HA-UR-04-STB-14	The rudder control forces for prolonged application shall not exceed 89 N
HA-UR-04-STB-15	The aircraft shall have a minimum control speed that does not exceed $1.2V_{S1}$
HA-UR-04-STB-16	Using a favorable combination of controls, the aircraft shall be able to be rolled from a steady 30° banked turn through an angle of 60°, so as to reverse the direction of the turn within (MTOW / 9.81 + 200) / 590 seconds during take-off
HA-UR-04-STB-17	Using a favorable combination of controls, the aircraft shall be able to be rolled from a steady 30° banked turn through an angle of 60°, so as to reverse the direction of the turn within (MTOW / 9.81 + 200) / 590 seconds during approach
HA-UR-04-STB-18	The aircraft shall be able to maintain lateral and directional trim during cruise
HA-UR-04-STB-19	The aircraft shall be able to maintain longitudinal trim during climb, level flight, descent and approach

HA-UR-04-STB-20	Residual control forces shall not fatigue or distract the pilot of the aircraft during normal operations and likely abnormal and emergency operations
HA-STB-21	The elevator shall be able to provide the required down force to enable rotation at 30 m/s in take-off configuration at all combinations of mass and centre of gravity in the aircraft's defined range
Landing Gear Requirements	
HA-UR-04-LDG-01	The aircraft landing gear shall be able to sustain the loads during an emergency landing defined by CS-23 regulations
HA-UR-04-LDG-02	The landing gear shall provide ground stability
HA-LDG-03	The tail scrape angle shall be at least 15°
HA-LDG-04	The tip-back angle shall be larger than the scrape angle at all combinations of mass and centre of gravity in the aircraft's defined range
HA-LDG-05	The overturn angle shall be less than 55° at all combinations of mass and centre of gravity in the aircraft's defined range
HA-UR-07-LDG-06	The tyres shall have an inflation pressure of at most 60 psi
HA-SYS-41-LDG-07	The landing gear shall allow for take-off rotation at all combinations of mass and centre of gravity in the aircraft's defined range
HA-SYS-42-LDG-08	The load on the nose wheel shall at least be 8% of the aircraft weight at all combinations of mass and centre of gravity in the aircraft's defined range
HA-SYS-43-LDG-09	The undercarriage shall allow for retraction
Aerodynamic Requirements	
HA-SYS-10-AER-01	The wing shall be able to produce a lift coefficient of 2.9 during landing using a proper flap setting.
HA-SYS-10-AER-02	The wing shall be able to produce a lift coefficient of 2.9 during take-off using a proper flap setting.
HA-AER-03	The flapped area shall not exceed 80% of the total wing surface area.
HA-UR-06-AER-04	The complete aircraft shall have a C_{D0} that does not exceed 0.028.
HA-AER-05	The aircraft shall generate adequate lift to counter the MTOW in cruise configuration.
Operational Requirements	
HA-UR-04-OPE-01	The aircraft shall not produce more than 80dBA of noise at 2500m from the aircraft.
HA-UR-18-OPE-02	The ground power infrastructure shall be able to generate 500 kWh per day per aircraft
HA-UR-18-OPE-03	The ground power infrastructure shall include a battery with the capacity to store the energy required to fully charge an aircraft
HA-UR-18-OPE-04	The battery charger shall be able to deliver 250 kW of power to the aircraft
Avionics Requirements	
HA-UR-04-AVS-01	The minimum required flight and navigational instruments shall be in accordance with the CS-23 regulations

6.2. Compliance Matrix

To check whether the designed system complies with the requirements, a compliance matrix has been made. In this matrix it is noted whether the requirement has been met (✓), it is as of yet unknown whether it has been met (**?**), or whether it has not been met (**X**). A short explanation is also included, often referring to the specific section in the report where compliance with the requirement is discussed or verified. The compliance matrix is tabulated in Table 6.2.

Table 6.2: Compliance Matrix for the HA-1 Aircraft

ID	Check	Justification
User Requirements		
HA-UR-01	✓	Verified by analysis in Chapter 14
HA-UR-02	✓	Verified by analysis in Chapter 14 and Chapter 10
HA-UR-03	✓	Verified by analysis in Chapter 14
HA-UR-04	?	Can only be fully verified once detail design is complete
HA-UR-05	?	Aircraft is designed for this, but has to be confirmed with regulators
HA-UR-06	✓	Aircraft is sized for this; verified by analysis in Section 18.4
HA-UR-07	✓	Aircraft is sized for this, see Chapter 16; verified by analysis in Chapter 14
HA-UR-08	✓	Verified by analysis in Chapter 17
HA-UR-09	✓	Verified by analysis in Chapter 17
HA-UR-10	✓	Verified by analysis in Chapter 14

HA-UR-11	✓	Verified by analysis in Chapter 14
HA-UR-12	?	Aircraft is designed for this, but not every aspect is covered yet
HA-UR-13	?	Aircraft is designed for this, but needs to be verified by testing
HA-UR-14	✓	Verified by inspection of cabin layout[12]
HA-UR-15	?	Complied with according to Chapter 23, but development time is highly volatile
HA-UR-16	✓	Verified by inspection, this is designed for in Chapter 16
HA-UR-17	✓	Verified by analysis in Chapter 14
HA-UR-18	✓	Complied with as part of design in Chapter 16
HA-UR-19	✓	Verified by analysis in Chapter 14
Stakeholder Requirements		
HA-STK-GOC-01	?	Can only be fully verified once detail design is complete
HA-STK-MAC-01	✓	Verified by inspection of cabin layout[12]
HA-STK-MAC-02	✓	Verified by inspection of cabin layout[12]
HA-STK-MAC-03	✓	Achieved by high wing layout and cockpit window layout
HA-STK-HO-01	✓	The flight ceiling limit of CS-23 is below this altitude
HA-STK-HO-02	✓	Complied with since the aircraft has a configurable cabin
HA-STK-TUD-01	✓	A preliminary aircraft design is described in this report
HA-STK-TC-01	?	Aircraft has been designed with this in mind, but detailed analysis is needed to verify
System Requirements		
HA-UR-12-SYS-01	?	Materials are selected for compliance, but operating conditions analysis is yet to be done
HA-UR-12-SYS-02	?	Materials are selected for compliance, but operating conditions analysis is yet to be done
HA-UR-12-SYS-03	?	Materials are selected for compliance, but operating conditions analysis is yet to be done
HA-UR-12-SYS-04	?	Design for lightning and verification are to be done in the detail design stage
HA-UR-12-SYS-05	?	Design for rain and verification are to be done in the detail design stage
HA-UR-12-SYS-06	?	Design for hail and verification are to be done in the detail design stage
HA-UR-12-SYS-07	?	Materials are selected for compliance, but operating conditions analysis is yet to be done
HA-UR-12-SYS-08	?	Materials are selected for compliance, but operating conditions analysis is yet to be done
HA-UR-12-SYS-09	?	Design for fungal growth and verification are to be done in the detail design stage
HA-UR-07-SYS-10	✓	Verified by analysis in Chapter 14
HA-UR-07-SYS-11	✓	Performance on unpaved runways is verified by analysis in Chapter 14
HA-UR-07-SYS-12	✓	Performance on unpaved runways is verified by analysis in Chapter 14
HA-UR-07-SYS-13	✓	Verified by inspection of engine intake, propeller, and empennage
HA-UR-07-SYS-14	✓	Verified by analysis in Chapter 14
HA-UR-11-SYS-15	✓	Verified by analysis in Chapter 14
HA-UR-16-SYS-16	✓	Described in Chapter 16
HA-UR-16-SYS-17	✓	Verified by inspection; a large cargo door is present
HA-SYS-18	✓	Disposal of waste parts is described in Section 18.5
HA-SYS-19	✓	The end-of-life phase is described in Section 18.5
HA-UR-04-SYS-20	?	Avionics design is left for detail design; It is included in fixed equipment mass budget
HA-UR-04-SYS-21	✓	Communication architecture is analysed in Section 15.3
HA-UR-04-SYS-22	?	Avionics design is left for detail design; It is included in fixed equipment mass budget
HA-UR-04-SYS-23	?	Avionics design is left for detail design; It is included in fixed equipment mass budget
HA-UR-04-SYS-24	?	Avionics design is left for detail design; It is included in fixed equipment mass budget
HA-UR-04-SYS-25	?	Avionics design is left for detail design; It is included in fixed equipment mass budget
HA-UR-04-SYS-26	?	Avionics design is left for detail design; It is included in fixed equipment mass budget
HA-UR-04-SYS-27	?	Avionics design is left for detail design; It is included in fixed equipment mass budget
HA-UR-04-SYS-28	✓	Verified by analysis in Chapter 14
HA-UR-04-SYS-29	✓	Verified by analysis in Chapter 14
HA-UR-04-SYS-30	✓	Aerodynamic vibrations are analysed in Section 10.8.4
HA-UR-04-SYS-31	✓	Verified by analysis in Chapter 14
HA-UR-04-SYS-32	?	Stall indication is left for detail design
HA-UR-04-SYS-33	?	Avionics design is left for detail design; It is included in fixed equipment mass budget
HA-UR-04-SYS-34	?	Avionics design is left for detail design; It is included in fixed equipment mass budget
HA-UR-04-SYS-35	?	Placement of fire extinguishers is left for detail design
HA-UR-04-SYS-36	?	Can only be analysed when aircraft detail design is complete

HA-UR-16-SYS-37	✓	Aircraft is sized for this in Section 11.1
HA-UR-16-SYS-38	✓	Aircraft is sized for this in Section 11.1
HA-UR-04-SYS-39	✓	Aircraft is sized for this in Section 11.2.2
HA-UR-04-SYS-40	✓	Aircraft is sized for this in Section 11.2.2
HA-UR-06-SYS-41	✓	Aircraft is designed for this in Section 11.2.1 and Section 11.3.4
HA-SYS-42	✓	Weight is well within this limit with contingencies
HA-SYS-43	✓	This is verified by fatigue analysis in Section 10.7
HA-SYS-44	✓	Verified by aeroelastic analysis in Section 10.8
Power System Requirements		
HA-POW-01	✓	Selected battery pack is certified for the required discharge power
HA-UR-04-POW-02	✓	The electrical system is designed for this in Section 12.6
Propulsion System Requirements		
HA-UR-04-PRO-01	✓	The chosen engine is already certified
HA-UR-04-PRO-02	?	Vibrational analysis is left for the detail design
HA-UR-04-PRO-03	?	Design for ice and verification are to be done in the detail design stage
HA-UR-04-PRO-04	✓	The fuel tanks are sized for this in Section 12.5
HA-UR-04-PRO-05	✓	The fuel tanks are sized for this in Section 12.5
HA-UR-04-PRO-06	?	Detailed design of the fuel tanks is yet to be done
HA-UR-03-PRO-07	✓	The chosen engine is certified for a higher take-off power
HA-UR-10-PRO-08	✓	The chosen engine is certified for a higher continuous power
HA-UR-07-PRO-09	✓	Verified by inspection
HA-UR-06-PRO-10	✓	The selected electric motor is certified for a higher take-off power than required
HA-UR-05-PRO-11	✓	The selected engine does not need external power to run
HA-UR-07-PRO-12	✓	The selected engine is certified for Jet-A1 operation
Structural Requirements		
HA-SYS-01-STR-01	✓	Aircraft is sized for this in Section 11.3.4[12]
HA-SYS-01-STR-02	?	Materials are selected for compliance, but operating conditions analysis is yet to be done
HA-UR-04-STR-03	✓	The wing is analysed for these loads in Chapter 10
HA-UR-04-STR-04	✓	The wing is analysed for these loads in Chapter 10
HA-UR-04-STR-05	✓	The wing is analysed for these loads in Chapter 10
HA-UR-04-STR-06	✓	Wing structural integrity is analysed for limit loads in Chapter 10
HA-UR-04-STR-07	?	Ultimate loads are yet to be analysed in the detail design phase
HA-UR-04-STR-08	✓	The wing is analysed including fuel tanks in Chapter 10
HA-UR-04-STR-09	✓	The fuel tanks are not located near the firewall
HA-UR-04-STR-10	✓	The selected materials are certified for use in CS-23
HA-UR-04-STR-11	?	This is yet to be analysed in the detail design phase
HA-UR-04-STR-14	✓	The wing is analysed for these loads in Chapter 10
HA-UR-04-STR-15	?	Engine failure containment is left for detail design
HA-UR-04-STR-16	✓	Verified by analysis in Section 10.8.4
HA-UR-04-STR-17	✓	Verified by analysis in Section 10.8.2
HA-UR-12-STR-18	?	Analysis of the effect of all environmental conditions is left for detail design
HA-UR-12-STR-19	?	Analysis of the effect of all environmental conditions is left for detail design
HA-UR-04-STR-20	?	Ventilation and drainage are left for detail design
HA-UR-04-STR-21	✓	Verified by analysis in Chapter 21
HA-UR-04-STR-22	?	Analysis of thermal loads is yet to be done in the detail design phase
HA-UR-04-STR-23	✓	The wing is analysed with this safety factor in Chapter 10
HA-UR-04-STR-24	✓	The wing is analysed with this safety factor in Chapter 10
HA-UR-04-STR-25	?	Detail design of the cargo compartment is yet to be done
HA-UR-04-STR-26	?	Detail design of the baggage compartment is yet to be done
Stability and Controllability Requirements		
HA-UR-04-STB-01	✓	Aircraft is sized for this using moment analysis in Section 11.3.2
HA-UR-04-STB-02	✓	Verified by analysis of stability derivatives
HA-UR-04-STB-03	✓	Aircraft is sized for this in Section 11.3.5
HA-UR-04-STB-04	?	Detailed dynamic stability analysis is yet to be done
HA-UR-04-STB-05	?	Detailed dynamic stability analysis is yet to be done
HA-UR-04-STB-06	?	Detailed dynamic stability analysis is yet to be done
HA-UR-04-STB-07	✓	Empennage configuration is chosen to stay clear of deep stall in Section 11.3.1

HA-UR-04-STB-08	?	Detailed dynamic stability analysis is yet to be done
HA-UR-04-STB-09	?	Elevator control layout design is left for detail design
HA-UR-04-STB-10	?	Elevator control layout design is left for detail design
HA-UR-04-STB-11	✓	Verification by analysis in Section 11.3.6
HA-UR-04-STB-12	✓	Verification by analysis in Section 11.3.6
HA-UR-04-STB-13	?	Rudder control layout design is left for detail design
HA-UR-04-STB-14	?	Rudder control layout design is left for detail design
HA-UR-04-STB-15	✓	Control surfaces are sized for this in Chapter 11
HA-UR-04-STB-16	✓	Verification by analysis in Section 11.3.6
HA-UR-04-STB-17	✓	Verification by analysis in Section 11.3.6
HA-UR-04-STB-18	✓	The elevator is sized for a more limiting condition in Section 11.3.3
HA-UR-04-STB-19	✓	The elevator is sized for this in Section 11.3.3
HA-UR-04-STB-20	?	Detailed analysis of control forces is yet to be performed
HA-STB-21	✓	The elevator is sized for this in Section 11.3.3
Landing Gear Requirements		
HA-UR-04-LDG-01	?	Detailed structural design of the undercarriage is yet to be performed
HA-UR-04-LDG-02	✓	Undercarriage is sized for this in Section 11.2.2
HA-LDG-03	✓	Undercarriage is sized for this in Section 11.2.2
HA-LDG-04	✓	Undercarriage is sized for this in Section 11.2.2
HA-LDG-05	✓	Undercarriage is sized for this in Section 11.2.2
HA-UR-07-LDG-06	✓	Undercarriage is sized for this in Section 11.2.2
HA-SYS-41-LDG-07	✓	Undercarriage is sized for this in Section 11.3.4
HA-SYS-42-LDG-08	✓	Undercarriage is sized for this in Section 11.3.4
HA-SYS-43-LDG-09	✓	Undercarriage is designed for this in Section 11.2.1
Aerodynamic Requirements		
HA-SYS-10-AER-01	✓	Flaps are designed for this in Section 9.1
HA-SYS-10-AER-02	✓	Flaps are designed for this in Section 9.1
HA-AER-03	✓	Verified by inspection
HA-UR-06-AER-04	✓	Verified by analysis in Section 9.2
HA-AER-05	✓	Verified by analysis in Chapter 14
Operational Requirements		
HA-UR-04-OPE-01	✓	Verified by analysis in Section 12.7
HA-UR-18-OPE-02	✓	Ground station is designed for this in Chapter 16
HA-UR-18-OPE-03	✓	Ground station is designed for this in Chapter 16
HA-UR-18-OPE-04	✓	Ground station is designed for this in Chapter 16
Avionics Requirements		
HA-UR-04-AVS-01	?	Avionics design is left for detail design; It is included in fixed equipment mass budget

7 | Mission Analysis

In all parts of the design, operating conditions play a vital role. By analysing the mission, important requirements for flight performance can be derived to be used in the design process. First, Section 7.1 will introduce several operating parameters, like temperature and elevation. After that, Section 7.2 will provide an overview of possible missions to be performed by the aircraft. Then, Section 7.3 will introduce the target flight profile, after which Section 7.4 will impose more constraints that follow from flight performance. Finally, Section 7.5 will introduce how the battery will be deployed during flight.

7.1. Operating Conditions

MAF operates mainly in countries with desert or tropical climates[a]. The high temperatures are often combined with high ground elevations, resulting in significantly lower air densities at airfield level, lowering lift and thus reducing take-off and landing performance. Extremely high humidity levels, intense sunlight, frequent heavy precipitation and thunderstorms cause challenges such as corrosion, fungi growth, lightning strikes and degradation by UV exposure. Additionally, during cruise, the aircraft may be exposed to temperatures below the freezing point.

The lowered air density at airfields has to be taken into account in the design of the aircraft, otherwise, performance requirements will not be met in the deployment zone. On the other hand, if the aircraft is designed for the most limiting conditions, it will be oversized (specifically, the wings will be too large) for all other conditions, resulting in reduced efficiency. As a compromise, it was decided to design for average conditions. Airfield conditions for the main MAF bases are displayed in Table 7.1 with the calculated air density according to the 1976 International Standard Atmosphere (ISA). The averages given in the last row were used to compute standard airfield conditions that will be used going forward in the design, displayed in Table 7.2. Note the significant reduction of 12.5% in air density compared to ISA sea level conditions, resulting in an equal reduction in lift.

Table 7.1: Conditions at MAF Main Operating Bases

Country	**Place**	**Elevation** [m]	**Avg. max. temperature** [°C]	**ISA air density** [kg/m^3]
Australia	Nhulunbuy[b]	20	30.8	1.1586
Chad	N'Djamena[c]	295	35.8	1.1031
Guinea	Conakry[d]	26	31.9	1.1536
Kenya	Nairobi[c]	1798	24.5	0.9540
Liberia	Monrovia[c]	8	29.8	1.1641
Madagascar	Antananarivo[c]	1276	24.3	1.0178
Papua New Guina	Mt Hagen[e]	1728	21.8	0.9711
South Sudan	Juba[c]	457	34.5	1.0865
Tanzania	Arusha[e]	1415	25.2	0.9977
Timor-Leste	Dili[c]	4	30.9	1.1604
Uganda	Kampala[e]	1223	26.0	1.0186
	Average	**750**	**28.7**	**1.0714**

MAF services most often short unpaved airstrips without airport facilities present. One of the main

[a] URL: `https://mafint.org/programmes/programmes-overview` [accessed 25 June 24]
[b] URL: `http://www.bom.gov.au/climate/averages/tables/cw_014512_All.shtml` [accessed 20 May 24]
[c] URL: `https://www.dwd.de/DE/leistungen/klimadatenwelt/klimadatenwelt_node.html` [accessed 20 May 24]
[d] URL: `https://www.ncei.noaa.gov/pub/data/normals/WMO/1961-1990/` [accessed 20 May 24]
[e] URL: `https://weatherspark.com/` [accessed 20 May 24]

Table 7.2: Standard Airfield Conditions

Variable	Value
ISA temperature offset	+18 °C
Elevation of airfield	750 m
Temperature at airfield	28.1 °C
Density at airfield	1.071 kg/m^3

requirements for the HumanAir aircraft is that it has to be capable of operating from runways with a take-off run available (TORA) of 500 m or less with reasonable payload and fuel level. The runway may be uneven and sloped, and debris and dust may be present. Sufficient ground clearance for the propeller is therefore important.

7.2. Example Missions

A variety of missions are performed by MAF with its fleet of aircraft. The most important categories are passenger transport to remote areas, medical evacuations, transportation of the deceased, transport of freight and ground inspection missions.

The aircraft therefore must be re-configurable to carry passengers, a stretcher or freight. Ideally, the reconfiguration must be able to be performed within 30 minutes. Additionally, a clear view of the ground must be provided to pilot and passengers for inspection missions. Some of the freight may be considered dangerous goods, such as fuel, chemicals or live animals. These may not be transported in the same cabin space as passengers.

7.3. Design Flight Profile

The design flight profile is the most limiting flight the aircraft should be able to perform in terms of required fuel and battery capacity. It is displayed in Figure 7.1 and explained further below.

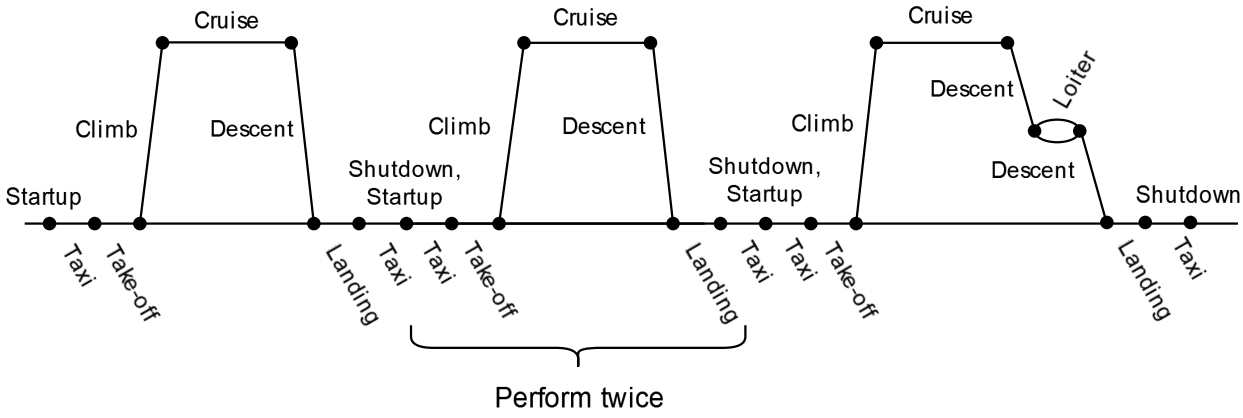

Figure 7.1: Design Flight Profile for the HA-1 Aircraft

Since MAF often services multiple airstrips in a single flight, three intermediate landings are included before the return to the initial airfield. No refuelling is possible at these airstrips. The total ground distance covered is 150 NM per leg for a total of 600 NM. The aircraft flies with design payload (540 kg) for the entirety of the flight.

Standard conditions apply to all airstrips (Table 7.2). The climb phases are performed with a climb rate of 2.5 m/s. Cruise is performed at 3000 m MSL at 60 m/s. Descent is performed at −2.5 m/s. The

main operating base is often a medium to large airport where other aircraft operate as well. Hence before the final landing, the aircraft loiters for 30 minutes as it waits for permission to land.

Requirements for fuel reserves may vary per deployment zone. For the design of this aircraft, the reserve policy of MAF Kenya was used [14]. There the aircraft is required to carry fuel for an additional 45 minutes of loiter and 15% of the total trip fuel (excluding loiter). The loiter altitude is required to be 1500 ft (about 450 m) above airfield elevation. Hence the loiter altitude is taken as 1200 m.

7.4. Flight Performance Requirements

Flight performance requirements are determined by the CS23 certification specifications [15, 16] as well as MAF. Additional performance targets are set by the design team to provide performance similar to aircraft presently operated by MAF, however these are not hard requirements. The requirements are displayed in Table 7.3.

Table 7.3: Flight Performance Requirements (req.) and Targets for the HA-1 Aircraft

Item	Type	Value	Notes
Design payload	MAF req.	540 kg	Or 6 passengers excl. pilot with 90 kg per passenger (same for pilot)
Maximum payload	Target	630 kg	Or 7 passengers excl. pilot, with reduced range
Take-off run available (TORA) for takeoff and landing	MAF req.	<500 m	With reasonable payload and fuel
Cimb gradient in initial climb	CS23 req.	≥4%	At MTOW, sea level
Climb gradient after aborted landing	CS23 req.	≥3%	At MTOW, sea level
Climb rate	Target	≥5 m/s	At MTOW, sea level, similar to Cessna 206 [17]
Maximum cruise altitude	MAF req.	≥3700 m	From email correspondence
Stall speed in landing configuration	CS23 req.	≤31.4 m/s	
Stall speed in landing configuration	Target	≤25 m/s	Similar to Cessna 206 [17] with Horton STOL kit used by MAF[f]
Cruise speed	MAF req.	≥50 m/s	From email correspondence

7.5. Battery Deployment Optimisation Strategy

To maximise the emissions reduction potential of the aircraft, it is essential to determine when each type of energy (fuel or battery) should be used. An optimisation strategy based on flight phases was devised, and is explained in this section.

An example of one leg of various distances in nautical miles is shown in Figure 7.2. Fuel is used during take-off as it can decrease the mass of the aircraft, which leads to a decrease in drag and power required. Less power required means less battery or fuel used. This is an improvement as it saves time and valuable resources. A conservative approach is used where the power required stays constant even though the weight of the aircraft decreases to have a margin for unforeseen situations or flight conditions. The aircraft will always be loaded with the required fuel and the 15% margin for loiter. The preferred type of energy is fuel because there could be multiple legs during a mission and this is

[f] URL: `https://www.curryaviationparts.com/` [accessed 19-6-2024]

taken as a safety measure. The emissions will still remain the same as they were calculated using a conservative approach. During the cruise, the battery is preferred to be used first as the cost of the resource is significantly lower than the cost of the fuel. A margin will always be left for landing, though this can be low thanks to the exchange of the potential energy for kinetic energy during descent. If during cruise the margin for landing is reached, the aircraft will switch to fuel. Of course, if there are more legs for a single mission, there could be a case when just fuel is the only type of energy left to be used. Thus, the aircraft will fly exclusively on fuel. Otherwise, the aforementioned procedure will be tried to be maintained. If the leg can be a fully electric one, fuel will still be loaded for loiter as mentioned. If multiple legs are needed, fuel will be loaded as needed in order to have a reserve for loiter and also for the other procedures already discussed.

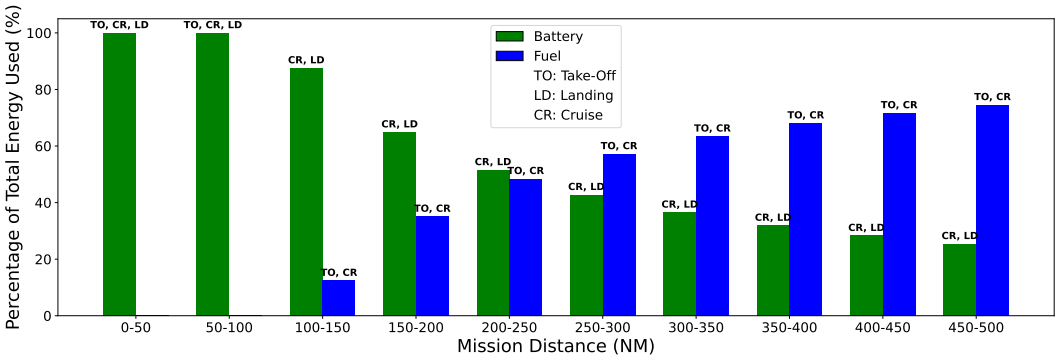

Figure 7.2: Battery Deployment Optimisation Strategy for Different Leg Distances

It can be observed that for small distances such as 50 NM and 100 NM, a full electric flight will be performed. Even for a 150 NM distance, the percentage of fuel used is less than 20% of the energy required. One needs to take into account that this battery deployment can be modified depending on special cases and that the switch between fuel and battery is almost instantaneous so no inconvenience will occur. There will also be always enough fuel or battery to support a missed approach or go-around.

8 | Weight Estimation

This chapter describes the methods used to estimate the weight of the HA-1 aircraft together with the distribution of weight among the different subsystems. Firstly, a reminder of the weights obtained using class I Weight estimation will be presented followed by the method used for the Class II Weight estimation. The changes performed to the Class II Weight method to take into account the introduction of a hybrid system will be highlighted and explained.

8.1. Class I Weight Estimation

The Class I Weight Estimation is based on the method described in detail in [12]. An iteration procedure was performed by varying design parameters mentioned in Section 20.1. The obtained design points were input to the class I method and the battery percentage was optimised such that the CO_2 reduction is maximised. The results for the selected concepts can be visualised in Table 8.1:

Table 8.1: Result of Class I Weight Estimation

Weight component	HA-1
OEW	21260
W_{ptr}	1593
W_{bat}	6329
W_{fuel}	2511
W_w	2973
$W_{payload}$	7725
$MTOW$	31188

The best design was characterised by a CO_2 emission reduction of 39% with current battery technology and a battery percentage usage of 13% during the flight duration.

8.2. Class II Weight Estimation

The Class II method uses the method described in Roskam Part V [18]. The weight groups included in the OEW calculated are wing weight, empennage weight, fuselage weight, nacelle weight - equal to 0 since there is no nacelle- , landing gear weight, powerplant weight, flight control system weight, hydraulics and pneumatic system weight, instruments avionics and electronics weight, electrical system weight, air conditioning pressurisation and anti deicing system weight, oxygen system weight, APU weight - equal to 0 in the case of the HA-1 aircraft-, furnishing weight, auxiliary gear weight, and paint weight.

All the weight components mentioned above were grouped in 3 main groups: **structures weight** - wing weight, empennage weight, fuselage weight, nacelle weight, landing gear weight -, **powerplant weight** - fuel system weight, electric motor weight, IC engine -, and **fixed equipment weight** - rest of them.

For each weight group, multiple methods were used and the average of them was used in the optimisation loop. This approach was also recommended by Roskam [18].

To the aforementioned weight groups, the fuel and battery weights are added which are calculated using the same procedure as explained in the Class I Weight estimation presented in [12]. The battery weight is included in the OEW group. However, some of the components of the aircraft do not depend on the inclusion of a battery in the aircraft. Thus, the weight will be overestimated especially since the method presented in Roskam [18] does not take into account the hybrid system weight. The decision

was made to subtract the battery weight from the OEW in the calculation of the following groups: flight control systems, hydraulics and pneumatic systems, instruments avionics and electronics, air conditioning pressurisation and anti-deicing system weight, furnishings, and auxiliary gear.

Once the powerplant was chosen and the weight of it was fully known, the weight of the powerplant was no longer calculated using statistical formula and was directly replaced with the newly found weight of the powerplant. The same procedure was applied to the wing group once the structural analysis was completed. The final results obtained after running the optimisation loop can be visualised in Table 8.2

Table 8.2: Class 2 Weight Estimation with Components

Item	**Weight [N]**
MTOW	35192
Total Powerplant	5490
Total Structures	8990
Wing	3786
Empennage	651
Fuselage	3448
Nacelle	0
Landing Gear	1086
Total Fixed Equipment	3960
Flight Control Systems	722
Hydraulics and/or Pneumatics	0
Instruments, Avionics and Electronics	423
Electrical System	843
Air conditioning, Pressurization and Anti or Deicing	464
Oxygen System	117
APU	0
Furnishings	1074
Auxiliary Gear Weight	193
Paint	126
OEW	26471
Battery	7079
Fuel	2784
Payload w/o pilot	5933
Pilot	989
Engine	3989
Propeller	989
Electric Motor	385
Passenger	824
Luggage	165

It can be seen that the MTOW increased after class II weight. This is mainly due to the higher weight of the wing than for usual aircraft due to the higher lift required as a result of the addition of batteries. The weight was still kept under the 40000N as stipulated in the requirements. The CO_2 emission reduction decreased due to the increase in wing weight being only 37% with the current battery technology and 70% with the expected battery technology.

The contingency applied for the Class II Weight estimation method was set at 12% as previously stated in the TPM section of the midterm report [12]. However, as stated before, some of the weights are already fixed such as powerplant weight, wing weight, and payload+pilot weight. Contingency was applied also to these values to make computations easier. Additionally, the oxygen system will be required only if the service ceiling is moved above 3048m. Thus, all the additional calculated kilograms from the aforementioned groups can be distributed later to other subsystems while making sure no major c.g. shifts occur. This will allow for more growth moving the available contingency to 17.5% if the oxygen system is kept, and 20.5% if the oxygen system is no longer incorporated.

9 | Aerodynamic Design

Due to the stringent requirements on the take-off and drag performance, it is important to perform a detailed aerodynamic analysis. This analysis will also provide inputs to all other departments, as for example, the lift can have a great influence on the structural and stability design. To analyse aerodynamics, Section 9.1 will trade-off and size the high-lift devices. Finally, Section 9.2 will implement computational fluid dynamics to get accurate data on the aircraft's aerodynamic characteristics.

9.1. High Lift Devices

High Lift Devices (HLD) are used to enhance the aerodynamic performance during the landing and take-off procedures during which more lift is required than the clean wing configuration can produce. Thus a sizing procedure had to be developed based on the requirements **HA-SYS-10-AER-01** and **HA-SYS-10-AER-02**. In order to use the proper sizing procedure, the flap type had to be chosen. Thus, a trade-off had to be performed between multiple possibilities.

Table 9.1: Trade-off Criteria for HLD

Criterion	Justification	Accounts for	Ranking Strategy	Weight	Weight Justification
Manufac-turing complexity and cost (MCC)	To minimise the cost of the manufacturing and installation of the HLD. Additionally, increasing the complexity will have a negative impact on the reliability of the system.	Manufactuign cost and reliability	Based on literature [19]	0.35	It represents the most significant criteria due to the fact that an increased cost will have a direct impact on 2 of the top-level user requirements: HA-UR-08 and HA-UR-09.
C_L increase (CLI)	To make sure that the HLD can provide sufficient lift such that aircraft doesn't stall.	Safety during operations	Based on literature [19]	0.3	A highly important criteria that makes sure the aircraft is safely operated under the conditions defined by take-off and landing requirements.
Drag (DRG)	To minimise the drag generated by the HLD during take-off and landing.	Aerodynamic drag	Based on literature [19]	0.25	Drag impacts negatively the performance of the aircraft during take-off and landing. If drag is increased, more power will need to be delivered by the engine, which will lead to an increase in the CO_2 emissions.
Deflection range (DFR)	A higher deflection range allows for more optimal flap setting giving more possibilities to the pilot.	Flap setting possibilities.	Based on literature [19]	0.15	Less important criteria, however it is still important to provide the pilot with better tools to work with while flying the aircraft.

A visualisation of the flap types that are going to be analysed in the trade-off is provided in Figure 9.1

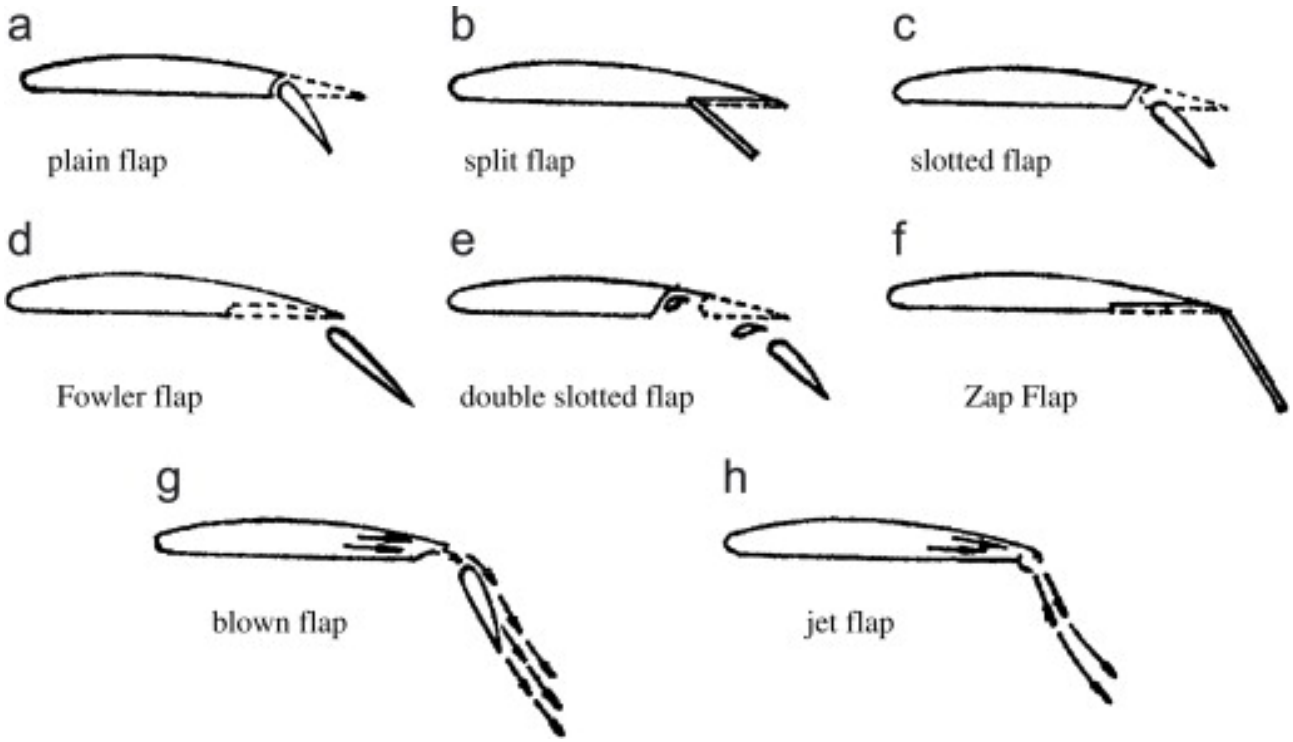

Figure 9.1: Types of Flaps[(a)]

Table 9.2: Trade-off Table for TE HLD (flap)

	MCC	CLI	DRG	DFR	
	0.35	0.30	0.20	0.15	**Score**
Plain	5	1	3	5	3.4
Split	5	1	1	5	3.0
Single slotted	4	3	4	4	**3.7**
Double slotted	1	4	5	5	3.3
Triple slotted	1	5	5	5	3.6

As can be seen, the best option in terms of HLD is given by the single-slotted flap. Thus, the following design procedure was implemented. Firstly, the increase in maximum lift coefficient was calculated to be 0.7 for both the take-off and landing conditions. Therefore the following formula was used to calculate the flapped are [19]:

$$S_{wf} = S\frac{\Delta C_{L,max}}{\Delta C_{l,max}}\frac{1}{0.9\cos\Lambda_{hingeline}}, \tag{9.1}$$

where S is the wing surface expressed in m^2, $\Delta C_{l,max}$ is the maximum increase in lift coefficient of the 2D wing which for a single slotted flap is equal to 1.3 [19], and $\Lambda_{hingeline}$ is the sweep angle of the hinge line. The hinge line is situated at 0.25 of the chord length [19] which results in the sweep angle at that location to be always lower than 5°. Thus, a small angle approximation can be made which results in a value of 1 for the cosine.

The flapped area should not represent more than 80% of the surface area of the wing since space is required also for the placement of the ailerons. The flaps start on each side of the wing at 10cm from the fuselage of the aircraft and they end at a position such that the calculated flapped surface area is achieved.

Due to the deployment of the HLD, the lift curve slope shifts to the left with 15° [19] and the slope

increases. The new lift curve slope can be determined using Equation 9.2.

$$C_{L_{\alpha_{flapped}}} = C_{L_{\alpha_{clean}}} \frac{S'}{S} \tag{9.2}$$

The ratio between the new wing surface area when flaps are deployed and the wing surface area in clean configuration can be obtained using the following formula:

$$S' = 1 + \frac{S_{wf}}{S} \frac{c_f}{c} \frac{\Delta c}{c_f}, \tag{9.3}$$

where the ratio between the increased chord length and the flap chord can be taken from Figure 9.2 at the 45° deflection angle set for both take-off and landing.

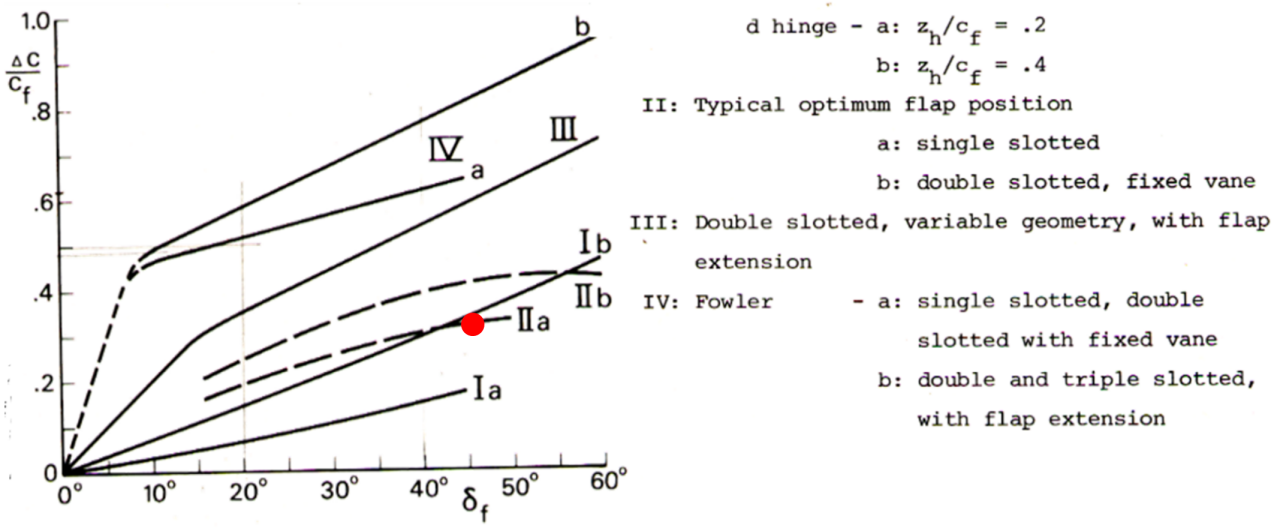

Figure 9.2: Chord Variation for Different Flaps[19]

Using the calculated $C_{L_{\alpha_{flapped}}}$, the lift coefficient when the aircraft is on the ground during take-off and the angle of attack during take-off and landing can be calculated using Equation 9.4 and Equation 9.5.

$$C_{L_{ground}} = (15° + \alpha_{L=0} + 5°) C_{L_{\alpha_{flapped}}} \tag{9.4}$$

$$AoA = \frac{C_{L_{max_{clean}}} + \Delta C_{L_{max}}}{C_{L_{\alpha_{flapped}}}} - (15° + \alpha_{L=0}) - 5° \tag{9.5}$$

The 5° that appear in the two aforementioned equations come from the landing gear which is settled such that the aircraft is tilted with 5° while resting on ground. This facilitates the rotation of the aircraft as mentioned in Chapter 11. The calculated parameters can visualised in Chapter 13.

9.2. Computational Fluid Dynamics Analysis

As the XFLR5 panel method analysis as used in [12] is limited in both accuracy and range of applications (it is limited to the analysis of wings only), it was opted to implement the use of computational fluid dynamics (CFD) in the detailed design of this project. This section will elaborate on its implementation and the design iterations performed with it.

9.2.1. Model Setup

For this project, Siemens STAR-CCM+ has been used. This software offers a lot of automated operations, enabling the CFD simulation to be used in the design process as the preparation time for the analysis of multiple design options is reduced drastically.

The model itself is a Reynolds Averaged Navier-Stokes (RANS) model. This solver averages the solution of the Navier-Stokes equations over time. This provides fast solutions that are numerically accurate for engineering purposes. However, as the solution is averaged over time, the turbulent behaviour cannot be analysed in detail, as the turbulence also gets averaged over time.

To still have an insight into the influence of turbulence on the final numerical output, a turbulence model is used. For the purpose of this project, the Spalart-Allmaras model was chosen, as this was specifically developed for aerospace engineering applications [20]. Also, as follows from Table 22.3, this model performs the closest to average compared to the $\kappa - \omega$ and $\kappa - \epsilon$ turbulence models. To model the correct flow behaviour close to the wall, one should implement a corresponding y+ value. For this, a y+ $<= 1$ is desired [(b)]. The wall distances in the model have been adapted to approximate this value for y+ using an online calculator [(c)]. Finally, the computational mesh was adjusted to provide an accurate representation of the aeroplane geometry at an acceptable computational cost. Roughly 2500000 were used. This makes the model sufficiently accurate, as will be proven in Section 22.2.2, while still having acceptable computational times.

9.2.2. Design Iterations

To start the aerodynamic design, the outcomes of the previous design phase as reported in the midterm report [12] were converted into a complete CAD model. This served as a baseline to perform iterations on. The first step here is to generate an aerodynamically shaped fuselage.

For this, the final bounding boxes of the fuselage design of the midterm were used as a starting point. Using a minimum clearance of 10cm to provide enough room for structural thickness, the following shape was generated.

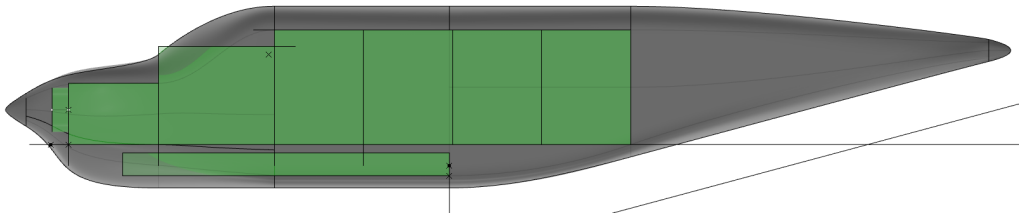

Figure 9.3: Fuselage Design Based on Bounding Boxes of Fuselage Sizing of [12].

As can be seen in Figure 9.3, a bounding box intersects the fuselage shape in the front of the aircraft. This is acceptable, however, as the intersecting bounding box is the one for the pilot. They will be positioned towards the back of the cockpit and a window can thus intersect the front of the cockpit bounding box. This also ensures the pilot is close enough to the window to provide enough over-nose visibility. Moreover, the bottom box intersects the fuselage shape in the lateral direction, but this is acceptable as the nose landing gear is positioned in the middle and will thus not take up the full box width.

After also adding the wing, horizontal stabiliser, vertical stabiliser and the wing strut, an initial simulation could be run. This provides a C_L of 0.896 and a C_D of 0.056. To get a C_{D0} out of this, one should estimate the Oswald efficiency factor. To do this, a method from Nita and Scholz [21] has been used.

[(b)] URL: https://www.linkedin.com/pulse/understanding-y-cfd-simulation-sijal-ahmed/ [accessed 17 June 2024]
[(c)] URL: https://www.cfd-online.com/Tools/yplus.php [accessed 17 June 2024]

This results in an Oswald efficiency factor of 0.74. Implementing this gives a C_{D0} of 0.024.

Looking at the results after post-processing, one can note regions where improvements can be made.

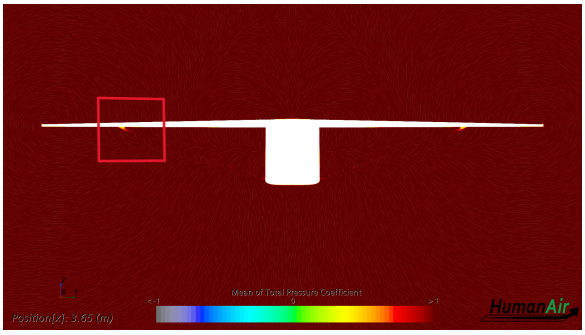

(a) Total Pressure Coefficient, indicating energy level in the flow, right after the Wing Strut.

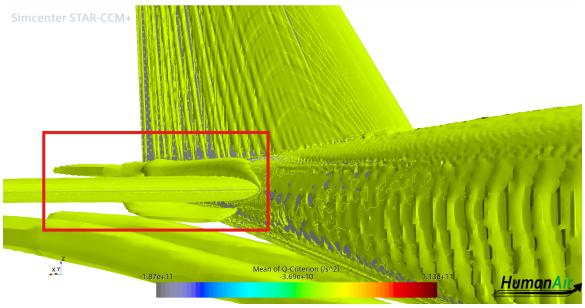

(b) Q-criterion, indicating regions with high vorticity, at the Horizontal and Vertical Stabiliser.

Figure 9.4: Post-processing of Baseline CFD-simulation, indicating low flow energy behind the strut and high vorticity at the empennage.

The total pressure coefficient of Figure 9.4a shows a region with a very low energy after the connection point between the strut and the wing. Also, the Q-criterion of Figure 9.4b, which aims to visualise regions with high vorticity, shows an increased vorticity at the root of the horizontal tail.

To solve this behaviour, fairings have been implemented, as is seen in Figure 9.5.

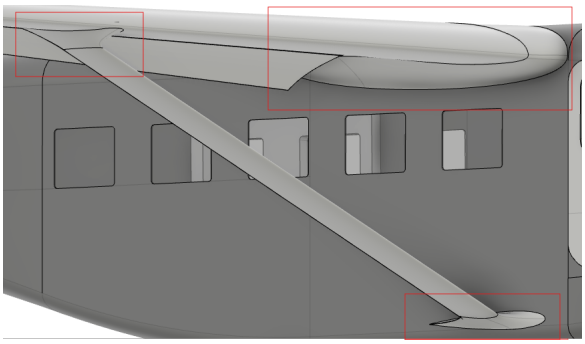

(a) Fairings Implemented at the Top and Bottom of the Wing Strut and at the Root of the Main Wing.

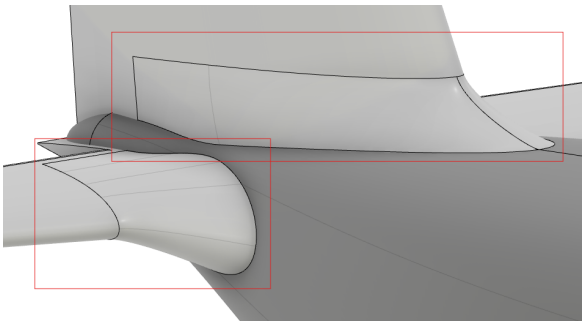

(b) Fairings Implemented at the Root of Both the Horizontal and Vertical Stabiliser

Figure 9.5: Implemented Aerodynamic Design Changes.

After implementing these fairings, as well as small iterations on the fuselage shape and wing planform design, the model was run in CFD again. One should note that these changes to the configuration are the result of multiple design iterations, but only the final results will be reported for the purpose of this report. This resulted in a C_L of 0.873 and a C_D of 0.046. Calculating the C_{D0} from this with the earlier mentioned method gives a value of 0.016. Hence, the design changes provide a reduction in zero-lift drag of 33.85% compared to the baseline design. Looking at the value for C_L, a lift value of $36\,954$ N is obtained, enough to counter the MTOW calculated in Chapter 8.

9.2.3. Correction for Propeller Drag

As the propeller substantially influences the flow behind the nose of the aircraft, the impact of it on the aerodynamic characteristics of the aircraft cannot be neglected. However, modelling it in CFD would need the implementation of a moving reference frame, something that is hard to model accurately and is also computationally expensive. Also, as there is no accurate CAD data available on the chosen

propeller, the results of the simulation would still be inaccurate. Therefore, instead of modelling the propeller, it was decided to run the analysis without one and correct the data afterwards.

To do this, a method from Biber [22] was used. This method uses Equation 9.6 and Equation 9.7 to estimate the difference in C_{D0} caused by the rotation of the propeller in-flight. Only the difference in C_{D0} was analysed as this was the only design input parameter used in the iterative design process and gives insight into emission reduction.

$$\Delta C_{D0} = C_F \frac{S_i}{S} \frac{\Delta q_s}{q} \tag{9.6}$$

$$\frac{\Delta q_s}{q} = \left(\frac{V_s}{V_{cruise}} \right)^2 - 1 = \left(\frac{V_{cruise} + \Delta V}{V_{cruise}} \right)^2 - 1 = \left(1 + \frac{T_{cruise}}{\rho_{cruise} A_{prop} V_{cruise}^2} \right)^2 - 1 \tag{9.7}$$

Using a method from Introduction to Aerospace Engineering [23], the skin friction coefficient for a turbulent flow was estimated to be 0.00343. This is a conservative estimate since the flow is partly laminar as well. The ratio of $\frac{S_i}{S}$ was taken as 0.96. Taking the other parameters from the aeroplane's geometrical layout and the cruise condition's flow parameters, this results in a $\Delta C_{D0_{Propeller}}$ of 0.00112.

9.2.4. Correction for Surface Inaccuracy

A final correction to be made is for roughness or inaccuracy in the surfaces exposed to the airflow. The CFD models the aeroplane as a fully smooth surface. However, this is rather inaccurate as any aeroplane will have all sorts of surface errors, like rivets or panel gaps for doors and windows. To correct for this, Proesmans and Vos [24] suggest adding an extra 1.5% to the zero-lift drag coefficient. This gives a $\Delta C_{D0_{Surface}}$ of 0.00024.

9.2.5. Comparison with Cessna 206

Earlier reports mentioned the need to drastically decrease the aerodynamic drag compared to a Cessna 206 [12]. To confirm this, the C_{D0} resulting from this section will be compared to the C_{D0} of this Cessna, being 0.0326 [25].

Adding all contributions from previous sections, the final C_{D0} for the HumainAir HA-1 is **0.0174** Comparing this to the Cessna C_{D0}, one can observe a **decrease of 46.5%**.

10 | Structural Design

Design under structural considerations is essential for every engineering project to ensure the structure's ability to endure flight conditions. Section 10.1 determines the type of structure which kick-starts the journey of structural design. Starting off with the trade-off of materials in Section 10.2. Thereafter, the load distributions are discussed in Section 10.3. Section 10.4, Section 10.5, Section 10.6 explores the structural design of the wing, strut and fuselage, respectively. Finally, the structural decisions are evaluated against fatigue and aeroelasticity, in Figure 10.16 and Section 10.8.

10.1. Airframe Structure Trade-off

One of the initial considerations to discuss is the airframe structural type. The four main relevant airframe types are monocoque, semi-monocoque, truss structure and geodesic structure. A monocoque structure carries the structural integrity and shape of the aircraft where the skin bears all the loads without needing an internal framework. A semi-monocoque incorporates an external skin bearing most of the load but is also reinforced with some internal framework (e.g. stringers, bulkheads, etc.). A truss structure incorporates longerons and diagonal bracing creating triangular elements. A geodesic structure consists of a space frame spiralling load-bearing members and creating a lattice framework, producing the required aerodynamic shape[(a)]. The type of structure can be determined with a trade-off against the five criteria presented in Table 10.1.

Table 10.1: Trade-off Criteria and Justification for Airframe Structure

Criterion	Justification	Accounts for	Ranking Strategy	Weight	Weight Justification
Structure Weight (WGH)	A lightweight structure enhances payload capacity, fuel economy, and operational range, and reduces airframe stress.	Weight of the airframe	Based on Literature [26]	0.25	Significantly impacts overall aircraft weight, affecting fuel efficiency and payload.
Subsystem integration (SSI)	Facilitates the ease of integrating other subsystems, reducing unnecessary weight and easing maintenance.	Ease of integrating other subsystems	Based on Literature [26]	0.15	Minor contribution to satisfying requirements
Manufacturing Complexity and Cost (MCC)	Affects production time and scalability; less complex structures reduce time and costs, aiding economic viability.	Ease of manufacturing processes, the number of manufacturing steps, the precision required	Based on Literature [26]	0.25	Influences meeting project deadlines (REQ HA-UR-15) and cost requirements (REQ HA-UR-08 and REQ HA-UR-09), justifying a higher weight.
Structural Integrity (SIG)	Ensures the structure can handle operational loads; all concepts meet minimum requirements with varying performance.	Design of the structure, the loads it encounters	Based on Literature [26]	0.15	Less critical for general aviation compared to military aircraft. Given lower operational stresses, thus lower weight.
Aerodynamics (AER)	Impacts fuel consumption, range, speed, operational costs, and CO_2 emissions through drag minimisation and lift.	Minimise drag, sufficient lift generation, ensure stability and control	Based on Literature [26]	0.20	Directly affects CO_2 emissions, supporting the emission requirement (REQ HA-UR-06).

The trade-off for these four concepts against these five criteria is given in Table 10.2.

[(a)]URL: `https://eaglepubs.erau.edu/introductiontoaerospaceflightvehicles/chapter/aerospace-structures/` [accessed 22 May 2024]

Table 10.2: Trade-off Table for Airframe Structure

	WGH	SSI	MCC	SIG	AER	
	0.25	0.15	0.25	0.15	0.2	**Score**
Monocoque	5	3	2	3	5	3.65
Semi-monocoque	4	5	3	4	5	**4.1**
Truss	3	1	5	2	3	3.05
Geodesic	3	3	1	5	4	3

- *Monocoque:* In terms of structural weight, monocoque does not incorporate the weight through attachment points that would have been prevalent for the other three choices. This increases manufacturing complexity to ensure the skin carries the load and maintains the aerodynamic shape. The monocoque also excels in its aerodynamic efficiency due to reduced parasite drag.
- *Semi-monocoque:* The semi-monocoque's combination of internal space and easy accessibility scores highly on subsystem integration. It optimises the space and maintains strength with the combined use of stringers, longerons and bulkheads. In addition, it helps with inspection and maintenance. It is easier to manufacture than monocoque because the subsequent attachment of stringers and bulkheads allows for some leeway with manufacturing, and requires less assembly in comparison to truss and geodesic. The semi-monocoque and monocoque both provide great structural integrity but due to the load distribution redundancy and greater tolerance to damage, the semi-monocoque scores higher.
- *Truss:* Truss is one of the most common classical airframe structures. It is easy to manufacture since it does not incorporate complex interlocking of load-carrying members, or incorporate the skin within the load-carrying members. The truss structure's open nature results in a higher drag. It is disadvantageous for subsystem integration due to its crowded interior.
- *Geodesic:* The geodesic has high manufacturing complexity, and therefore a higher cost, due to their intricate detail and high precision as its nature allows to cancel out torsional loads, thereby creating a much stronger and more durable structure, which is more advantageous to military aircraft. Thereby, scoring the highest in the structural integrity criteria.

In conclusion, the semi-monocoque structure wins the trade-off due to its strength in structural weight, subsystem integration, structural integrity and aerodynamic efficiency. In most general aviation aircraft including the current Cessna fleet owned by MAF, the airframe is constructed using the semi-monocoque structure as well [27].

10.2. Material Selection

Material selection will be conducted for the wingbox, as it is the primary load-bearing component of the aircraft. The material's strength ensures that the wings can support those loads. Therefore, the wing box material has to be chosen carefully. The typical material groups used in the aerospace industry are aluminium alloys, titanium alloys, steel, carbon fibre-reinforced plastic (CFRP) and glass fibre-reinforced plastic (GFRP) [28]. Since GFRP is mostly used for secondary structure, it was not included in the trade-off.

Aluminium is one of the most used aerospace materials by quantity. About 60% to 80% of aircraft are made with aluminium alloys and it is popular due to its desirable properties [28]. Aluminium alloys are low cost, easy to fabricate, lightweight, have high specific stiffness and strength, and have high fatigue resistance. However, it is susceptible to stress corrosion cracking and low mechanical properties at elevated temperatures.

Titanium alloys are known for their excellent resistance to corrosion and oxidation, high strength, long fatigue life, fracture toughness and creep strength. However, it has a relatively high density of

4500 kg/m^3 and a major disadvantage of high cost. Additionally, it is difficult to machine and requires special material removal processes as well [28].

Steel is widely employed across various sectors due to its remarkable properties. The properties that make steel popular are its high Young's modulus, yield stress, fatigue resistance and fracture toughness [28]. However, it has a relatively high density of 7200 kg/m^3 which is 2.5 times greater than that of aluminium and 1.5 times higher than that of aluminium. Moreover, the majority of steels are highly prone to corrosion, which is undesirable.

CFRP is widely utilised as a structural material in aircraft due to its exceptional properties such as lightweight, high stiffness, strength, and fatigue performance [28]. However, it has a relatively high cost and susceptibility to delamination. Moreover, the recycling process for composites is not straightforward, and the production of CFRP emits significant amounts of greenhouse gases. Before selecting the material, criteria were first set, and the weight was assigned. The chosen criteria are given in Table 10.3.

Table 10.3: Trade-off Criteria and Justification for Wing Box Material Selection

Criterion	Justification	Accounts for	Ranking Strategy	Weight	Weight Justification
Strength-to-weight ratio (STW)	High strength-to-weight ratio are essential for the wing box to efficiently bear aerodynamic loads, ensuring optimal performance and fuel efficiency.	Specific strengths which is the ratio between the material's yield strength	Based on literature [29]	0.25	Influences weight of the wing structure, impacting fuel efficiency and payload accuracy.
Fatigue Resistance (FTR)	Critical for preventing sudden catastrophic failures due to cyclic loading during flight.	Fatigue resistance of materials	Based on literature [28]	0.20	Effective maintenance and inspection protocols can mitigate fatigue-related concerns.
Environmental Durability (EDR)	Material must resist corrosion, oxidation, and wear in harsh aviation environments, ensuring long-term reliability and safety.	Corrosion resistance, oxidation resistance, wear	Based on literature [28]	0.15	Assigned considering its indirect impact compared to direct structural loads.
Cost (CST)	Keeping material costs low is important to maintain overall aircraft cost and increase profitability.	Cost of material	Based on literature [28]	0.25	Aligned with unit cost user requirement (REQ-HA-UR-08) and HumanAir's status as a new business.
Environmental Sustainability (SST)	Utilise sustainable materials to reduce overall pollution and environmental impact, distinguishing HumanAir's aircraft in the market.	Recyclability of material	Based on literature [28]	0.15	Relatively less immediate impact compared to other criteria.

The trade-off for the four materials against the above five criteria is given in Table 10.4.

Table 10.4: Trade-off for Wing Box Material

	STW	FTR	EDR	CST	SST	Score
	0.25	0.2	0.15	0.25	0.15	
Aluminium alloys	4	3	3	5	4	3.9
Titanium alloys	4	4	5	1	3	3.25
Steel	3	3	2	3	4	3
CFRP	5	4	4	1	2	3.2

Aluminium alloys, particularly Al-6061, will be employed in the structural design. This alloy offers a versatile combination of mechanical strength and corrosion resistance due to the presence of silicon and magnesium, making it a preferred choice for numerous aerospace applications [(b)].

10.2.1. Fire Safety

To comply with **HA-UR-04**, the aircraft needs to have a fire-resistant firewall in between the combustion engine and passenger cabin, as well as a fire-resistant casing around the battery. MAF occasionally also transports ICAO-regulated dangerous goods like fuel, chlorine, paint, engines, and refrigerant. These are currently transported in the cargo pod beneath the floor of the aircraft, thus letting the aircraft fuselage be the separator between passengers and dangerous goods. However, for the HumanAir HA-1 aircraft, the space of the pod is now taken up by the battery and retractable undercarriage, leaving no more room for cargo stowage. Therefore, the HA-1 aircraft has been equipped with a removable bulkhead that separates the passengers from the dangerous goods aft in the cabin. To keep manufacturing and maintenance costs low, it has been decided to choose the same material for all three applications. The material chosen is a ceramic composite laminate, which has been proven to outperform conventional metallic firewall materials in thermal tests. It consists of 3M Nextel AF-10 ceramic oxide fabric, co-cured with a composite laminate to provide sufficient strength[30]. Before curing, the Nextel AF-10 fabric needs to be heat treated to ensure it does not quickly degrade in humid conditions[(c)]. The material complies with the requirement of being able to withstand 1200 °C for 5 minutes to contain a battery fire in the event of a thermal runaway[(d)].

According to ICAO regulations, this bulkhead also needs to prevent the spreading of smoke and fumes, thus being airtight, and provide a barrier of heat between the cargo and passengers [31]. Therefore, the bulkhead fills the entire cabin cross-section to effectively cut the cabin in two.

10.3. Loading Analysis

To begin sizing the structural components, an analysis of the loads is essential. The aircraft is subjected to heavy non-linear aerodynamic forces, inertial forces and propulsive forces where the wing carries most of these loads. The fuselage is subjected to inertial loads and torques' caused by gust loads which are all relatively small in comparison to the wing loads. Therefore, the external and internal load distribution is analyzed for the wing. This is done under critical load factors positioned at the boundaries of the flight envelope Figure 10.2. The coordinate system used to illustrate the loading distributions is shown in Figure 10.1.

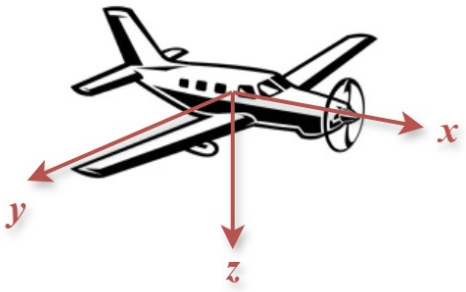

Figure 10.1: Coordinate System

10.3.1. Load Factor Diagrams

Regulations define the limit load factors n (the ratio of lift to weight) for which the aircraft must be able to withstand loads without any permanent deformation. The calculation of these limit load factors is done by creating V-n diagrams according to the procedure described by CS-23 regulations [15]. The diagrams for the HA-1 aircraft are presented in Figure 10.2. From the plots, it is clear that the manoeuvring loads are the limiting ones, with a maximum load factor of 3.51, and a minimum load factor of -1.40. These are therefore the load factors used to size the structure.

[(b)] URL: `https://www.aircraftmaterials.com/data/aluminium/6061.html` [accessed 01 June 2024]
[(c)] URL: `https://www.3m.com/3M/en_US/p/d/b40066347/` [Accessed 25 June 2024]
[(d)] URL: `https://pieaeronefs.ch/en/news/syteme-de-protection-feu/` [Accessed 19 June 2024]

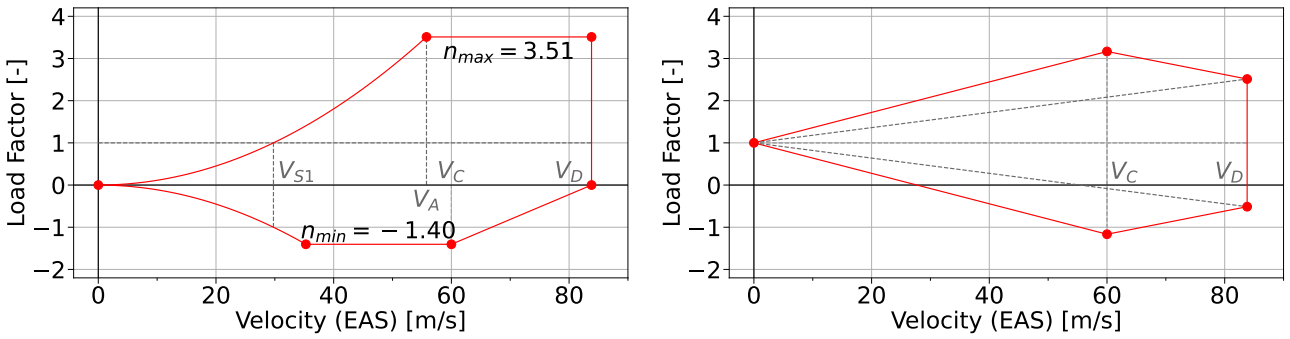

(a) Manoeuvre Diagram

(b) Gust Diagram

Figure 10.2: Plots of the Limit Load Factor Required by Regulations [15] with Airspeed (V-n diagram), for Manoeuvre and Gust Loading

10.3.2. Influence of Struts

As much as the struts help with the bending relief and allow for extra structural support, they give a statically indeterminate problem due to the built-in end of the fuselage giving three constrained degrees of freedom (translation in y, translation in z and rotation about x) and extra support from the strut - meaning four unknowns to solve with only three static equilibrium equations.

In usual cases, this is counteracted with the use of a compatibility equation. A compatibility equation is a mathematical expression that quantitatively describes the extra constraint and exactly how it restricts the deformation of the system at that extra support. However, conventional compatibility equations are not applicable in this scenario due to the absence of specific constraints. As a result, an alternative method was necessary.

The influence of the strut is determined through an iterative process. Equating the deflection at the position of the strut to the vertical component of the strut elongation gives a quantification of the internal force felt by the strut. However, this is only possible if the properties of the strut are known.

$$v = \delta_y = \frac{PL}{AE_{Al}} \cdot sin\theta \tag{10.1}$$

where v is the deflection bending deflection at the strut position, δ_y is the vertical component of the elongation of the strut, P is the strut force, L is the length of the strut, A is the cross-sectional area of the strut and θ is the angle between the wing and the strut.

During cruise, the upward deflection of the wing suggests that the strut is under tension. However, during landing, with just inertial loads present, it causes a downward deflection which loads the strut in compression - this means susceptibility to buckling. In addition to inertial loads, there are also impact loads from landing which induce higher axial loads, but in addition, residual stresses emerge from landing impacts thereby increasing the likelihood of buckling. Therefore, a material with high axial strength for tensile strength and high elastic modulus to resist buckling is required. In addition, the aerodynamics department requires an airfoil cross-section to comply to the drag requirements. This means the material should also have high formability for manufacturing purposes. Therefore, Al 6061 is chosen for the strut. In addition, the airfoil's area needs to be initially estimated to enable an iterative procedure. First, an initial area is assumed to calculate the corresponding strut force. This force is then used to recalculate the deflection at that point. The updated deflection results in a new strut force, and this process is repeated iteratively until the values converge.

10.3.3. External Loads

The external loads such as the distribution of lift and weight are plotted in Figure 10.3. The lift distribution is extracted from the preliminary wing modelled on XFLR5 - which gives the C_L distribution. The velocity and the air density can be determined for the scenario - thereby getting the lift distribution.

$$L = C_L \frac{1}{2} \rho V^2 S \tag{10.2}$$

where L is the lift force, ρ is the air density at that specified altitude and V is speed. The weight distribution is determined by superposing the weight due to the structural wing (from Class II Weight Estimation) and the fuel weight - which is assumed to be placed between the root and the strut position. The code computes the area enclosed by the wing within this region and ensure that the fuel is averaged and linearly distributed along this region.

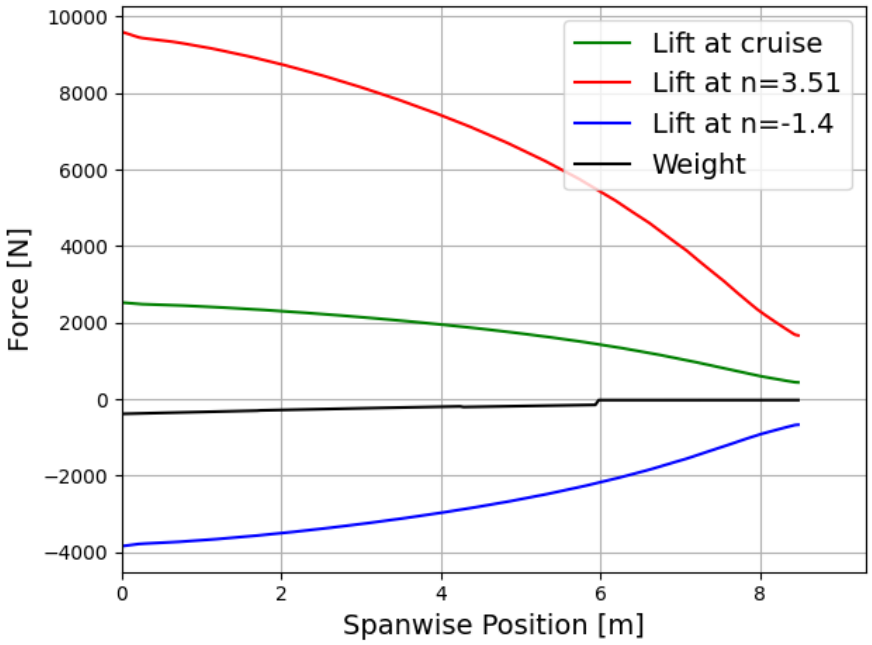

Figure 10.3: External Load Distribution Along y-axis

10.3.4. Internal Loads

As the wing structure is subjected to loads, it experiences varying levels of axial and shear stresses from the root to the tip. The resultant forces and moments generated by the stress distribution within a cross-section translate into an internal shear force, an internal moment, an internal axial force and an internal torque for that specific cross-section at a given spanwise location. These stress distributions are the main point of interest for the sizing of the wing and therefore require the internal load distribution. The following mathematical expressions for the internal loads are from statics [32].

The shear force along the span is calculated with the use of the resultant distributed force w which is equal to $-(L-W)$ as y is pointed downward. A positive internal shear means a shear deformation that give a positive slope on the y-z axis. Discontinuous changes in the shear force is directly proportional to the negative of the change in point force - in this case, the vertical strut force component.

$$V_z(y) = -\int_{b/2}^{y} w_z(y')\, dy' \qquad \Delta V_z = -P_z \tag{10.3}$$

The bending moment about the x along the span is calculated by integrating the shear force. A positive

bending moment causes a bending deformation that results in tensile stress in the positive quadrant of the y-z plane.

$$M_x(y) = \int_{b/2}^{y} V_z(y') \cdot dy' \tag{10.4}$$

The torque (moment about the y-axis) along the span is calculated using the aerodynamic moment. In addition, in usual cases, there is torque due to the sweep of the wing but since the design incorporates a straight wing (zero sweep at quarter chord length), this torque contribution is negligible.

$$M_y(y) = \int_{b/2}^{y} M_{aero}(y') \cdot dy' \tag{10.5}$$

$$M_{aero}(y') = C_{m,aero}(y') \cdot \frac{1}{2}\rho V^2 Sc \tag{10.6}$$

The axial load along the half-span is calculated using the influence of the strut force along the y-axis. Discontinuous changes in the axial force are directly proportional to the negative of the change in point force - in this case, the horizontal strut force component.

$$\Delta V_y = -P_y \tag{10.7}$$

The internal axial load along the half-span, internal shear load along the half-span, the internal moment along the half-span and the internal torque are plotted in Figure 10.4.

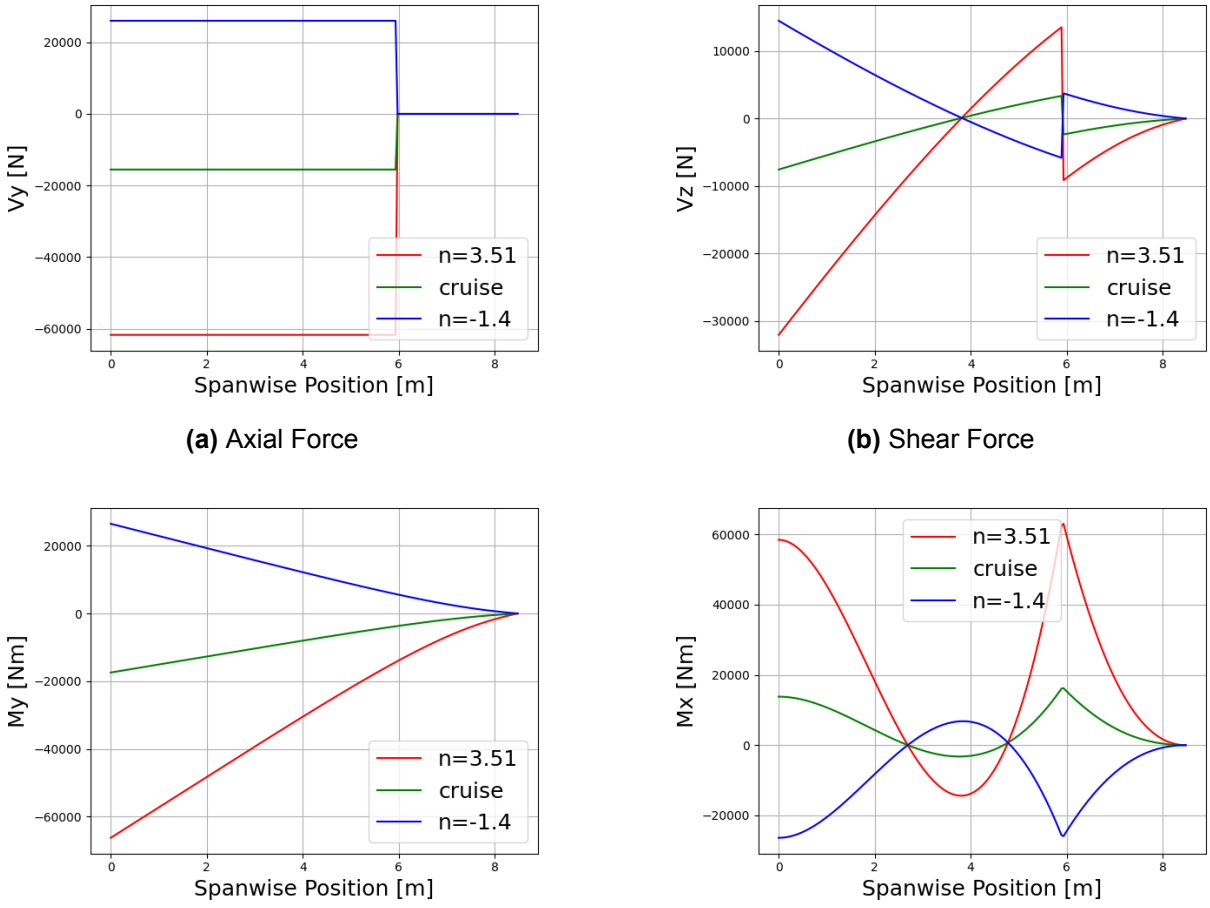

(a) Axial Force

(b) Shear Force

(c) Torque

(d) Bending Moment

Figure 10.4: Internal Load Diagrams Along the Half-span y

The axial load felt by the structure is due to the influence of the strut. During flight, the upward deflection of the wing requires a tensile support from the strut which means the y-component of the force causes

compression on the wing between the root and the strut position. During landing and on-ground operations where only inertial loads are present, the wing is bending downward causing the strut to provide a compressive force onto the wing which results in a tensile force along the region between the root and the strut positioning.

In Figure 10.4b, a negative initial shear force can be seen (for load factors n = 3.51 and cruise) and this is logical as the support from the built-in fuselage junction creates a negative slope on the y-z plane. Along the span, this shear becomes less negative and eventually positive until the strut position. The z-component of the strut force causes a negative discontinuous jump and continues to gradually become less negative till zero shear force at the end. For the load factor of -1.4, the same behaviour can be seen but with the opposite sign. The true bending relief provided by the strut can be seen in Figure 10.4d. It is logical that at most regions, a positive internal moment is experienced which implies that the wing is deflected upwards causing a tensile stress on the bottom half of the wing. However, around 2 to 3.5 metres, there is a negative internal bending moment. This is reflected in the bending deflection, analysed at a later stage. In Figure 10.4c, it shows the highest internal torque at the built-in end. This is logical as the built-in end is the only support supporting torque so all the loads are transferred to this support which results in the support experiencing the biggest internal torque.

10.4. Wingbox Sizing

With the loading distributions now determined, we can proceed to size the wingbox. The wingbox, a critical load-bearing section of the wing, consists of two spars, upper and lower wing skin panels, and stiffeners, all joined to form a box-like structure. This configuration is aptly named due to its shape. Each component of the wingbox plays a unique role in withstanding internal loads. The spars primarily resist shear forces, and their separation enables effective torsional shear resistance. Meanwhile, the skin and stiffeners work together to handle axial loads, mainly resulting from bending moments.

Given the internal load dynamics, the wingbox must be capable of withstanding lateral shear loads, bending moments, torques, and axial forces from the struts. The design of a wingbox involves various adjustable features. The sizing strategy focuses on selecting a few key variables that drive the design while constraining the other parameters, and thereby optimizing for weight. In other words, three variables are optimized for minimum weight, while ensuring all potential failure modes are addressed.

The variables are presented as follows:

- **Thickness of spar:** The spar thickness is assumed to linearly vary along the half-span, in proportion to the wing's taper. This approach prevents overdesign in certain regions, ensuring an efficient and optimized structure.
- **Thickness of skin:** The skin thickness is assumed to be constant along the half-span. The stringers will dominate when carrying the axial stresses, so a constant skin thickness is an acceptable assumption. It also allows for an easier manufacturing process, reducing complexity and cost.
- **Number of stringers:** The number of stringers vary discontinuously over five different regions along the span; 20%, 20%, 10%, 20%, 30% of the half-span. Contrary to the spars which predominantly carry shear, the stringers carry the axial stresses (due to bending and strut axial loads) which do not vary proportionally along the span, mainly due to the presence of the strut. Therefore, different regions experience different axial stresses so optimizing for different regions prevents over-designing.

The constant variables are just as crucial as the varying ones. These variables are as follows:

- **Stringer type:** The chosen stringer is the 20x30x5 mm L-stringer, which results in the highest strength-to-weight ratio. The use of L-stringers, in contrast to square and omega stringers, offers higher maintenance and repair, therefore lowering maintenance costs.

- **Number and position of spars:** Two spars are used for the wing sizing [e]. The front spar is located at 15% of the chord and the rear spar is located at 65% of the chord, sufficiently separated to ensure torsional shear stiffness.
- **Material:** The material of the wingbox is Al-6061, as decided in Section 10.2.
- **Strut position:** Initially, 40% of the half-span was assumed, but design iterations showed the need for more bending relief, leading to a new position of 70% of the half-span.
- **Rib placement:** The placement of the ribs becomes crucial for buckling analysis - the effective length of panels/stringers. As will be seen in upcoming chapters, the stiffened buckling analysis is only concerned with the ratio of the distance between the ribs a against the distance between stringers b, for the effective "panel" subjected to buckling. So a conservative approach is taken where a/b is assumed to be above a certain value such that the most critical constant C can be used for the buckling analysis.

In order to proceed to the optimisation of these parameters under various constraints, some simplifications were made.

STR-ASSU-01: The wing box consists of two spars with the skin modelled as a straight line connected from the ends of each spar. This is **conservative** assumption as the skin - and therefore the stringers - are placed closer to the neutral axis and therefore underestimates the second moment of area. Due to the inverse proportionality between stress and the second moment of area, a lower second moment of area will overestimate the stress and thereby create a conservative approach for design.

STR-ASSU-02: The cross-section is assumed to be symmetric about the neutral axis. This is a valid assumption as the level of asymmetry is relatively small due to the airfoil chosen - this implies a small product moment of inertia. Therefore, the bending formulas for a symmetric cross-section are assumed.

STR-ASSU-03: The strut is hinged on both ends. This is a **conservative** assumption as this makes the strut more vulnerable to buckling so buckling critical stresses are underestimated.

STR-ASSU-04: The stringers and the skin are sufficiently far from the neutral axis such that their individual inertia about their own centroidal axis is negligible relative to the parallel axis term.

The *scipy.optimize* library was used to optimize for these three variables for minimum mass, constraining it under various failure modes. This requires an expression for the mass of the wing box in terms of the parameters that are varying.

$$M_{spar} = \rho \cdot t_{spar} \cdot (h_f + h_r) \cdot l \tag{10.8}$$

where ρ is the density of Al-6061 and l is the length of the half-span.

$$M_{stringer} = \rho \cdot A_{str} \cdot no_{str} \cdot l \tag{10.9}$$

where A_{str} is the area of the stringer and no_{str} is the number of the stringers.

$$M_{skin} = \rho \cdot t_{skin} \cdot p \cdot l \tag{10.10}$$

where p is the perimeter of the airfoil. The total mass expression is the summation of these three contributions.

This expression is then optimized for the three key variables under tensile failure, deflection constraint, shear buckling of spar webs and buckling of stiffened panels.

[e] URL: `ttps://janes.migavia.com/usa/cessna/cessna-208-caravan.html` [accessed 5 June 2024]

10.4.1. Axial Failure

The yielding - permanent deformation - on the structural component should always be accounted for when designing. This occurs when there are elongations and shortenings due to axial stresses felt along the span, predominantly due to the bending loads. For this constraint, the critical parameter is the yield strength of Al-6061. Due to the isotropic nature of aluminium, yielding under tension and compression are of the same rate. In other words, the elongation and the shortening of the structure only depend on the type of loading under that section. For the most critical load factor of n = 3.51, the upward deflection causes a tensile stress on the bottom half of the wingbox and a compressive stress on the top half of the wingbox. Due to the influence of the strut, it causes a compressive strut in the region between the fuselage junction and the strut - which increases the compressive stress on the top half but eases the tensile forces on the bottom half. So the critical section is the top half of the wingbox in the region between the fuselage junction and the strut position.

In order to size the wingbox such that it is constrained by its yield strength, the axial stress along the span should be quantified.

$$\text{FoS} = \frac{\text{Failure Strength}}{\text{Applied Stress}} = 1.2 \tag{10.11}$$

where FoS is the factor of safety, failure strength is the yield strength and the applied stress can be expressed as follows

$$\sigma(y) = \sigma_{axial}(y) + \sigma_{bending}(y) \tag{10.12}$$

where

$$\sigma_{axial}(y) = \frac{F}{A(y)} \qquad \sigma_{bending} = \frac{M(y)h_{max}(y)}{I_{xx}(y)} \tag{10.13}$$

where F is a constant compressive value of the strut force's horizontal component, A(y) is the area variation along the span, M(y) is the bending moment about the x-axis along the span and $h_{max}(y)$ is the variation of the distance between the neutral axis (assumed to be along the centroidal axis) and the highest point of the wing box - this is where the maximum stress occurs.
So the variables (spar thickness, skin thickness and the number of stringers) define the variation of the second moment of area parameter. This is then sized to meet the yield strength constraint. The bending moment of inertia can be calculated as follows

$$I_{xx} = \frac{1}{12}t_{\text{spar}}h_f^3 + \frac{1}{12}t_{\text{spar}}h_r^3 + no_{\text{str}}A_{\text{str}}h_{\text{str}}^2 \tag{10.14}$$

where no_{str} is the number of stringers, A_{str} is the area of the stringers and h_{str} is the average y-distance from the neutral axis to the centroid of the skin panel [33].

10.4.2. Deflection Constraint

Deflection is the form of deformation that occurs under bending. The degree to which a structural element displaces impacts the structural integrity of the component, especially when deflection is the biggest when it comes to deformation. For this constraint, the critical parameter constraining the deflection is the maximum allowable deflection. This is assumed to be 10% of the wingspan [34]. The deflection along the span can be calculated as such:

$$v''(y) = -\frac{M(y)}{E_{Al} \cdot I_{xx}(y)} \tag{10.15}$$

where v"(y) is the second derivative of deflection against y and M(y) is the bending moment about the x-axis distribution. Integrating this once gives the following equation

$$v'(y) - v'(0) = \int_0^y -\frac{M(y')}{E_{Al} \cdot I_{xx}(y')} \cdot dy' \tag{10.16}$$

where v'(y) represents the first derivative of the deflection along the span - in other words, the slope along the span. Due to the clamped built-in end at the fuselage-wing junction, the slope at the root is 0 and therefore v'(0) is zero. Thereafter, integrating this again gives the following equation

$$v(y) - v(0) = \int_0^y \int_0^{y'} -\frac{M(y'')}{E_{Al} \cdot I_{xx}(y)''} \cdot dy'' \cdot dy' \tag{10.17}$$

where v(y) represents the deflection along the span. Similarly to the slope at the root, the deflection at the root is also zero due to the clamped nature of the built-in end. So finally, the deflection equation is as follows

$$\therefore \quad v(y) = \int_0^y \int_0^{y'} -\frac{M(y'')}{E_{Al} \cdot I_{xx}(y)''} \cdot dy'' \cdot dy' \tag{10.18}$$

The variables (spar thickness, skin thickness and number of stringers) shape the second moment of area which drives the sizing to meet the deflection constraint because M(y) and E are not dependent on these variables [33].

For reference, the deflection along the span can be found in Figure 10.5. The maximum deflection is around 0.12 which is sufficiently below the maximum deflection of approximately 1.7 metres - so deflection is not the driving constraint. The central region of the half-span shows unconventional bending behaviour - which is due to the strut. Figure 10.4d shows positive internal moments in that region which implies tension on the top half of the wingbox and compression on the bottom half of the wingbox.

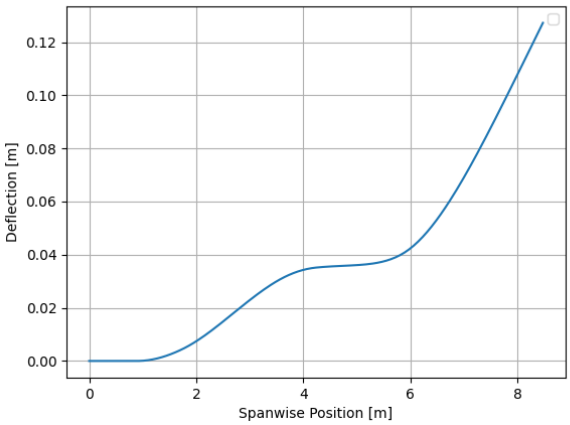

Figure 10.5: Deflection Along y-axis

10.4.3. Shear Buckling of Spar Webs

Shear buckling is a failure mode where a panel - in this case, the spar webs - is subjected to sudden wave-like deformation due to shear stresses. The webs - which are primarily responsible for carrying shear - are thin-walled and therefore susceptible to shear buckling under severe loads so it is crucial to size for this. For this constraint, the critical parameter is the critical shear stress [35] where shear buckling occurs. It is a parameter dependent on the geometry of the "panel" subjected to shear - shown in Figure 10.6.

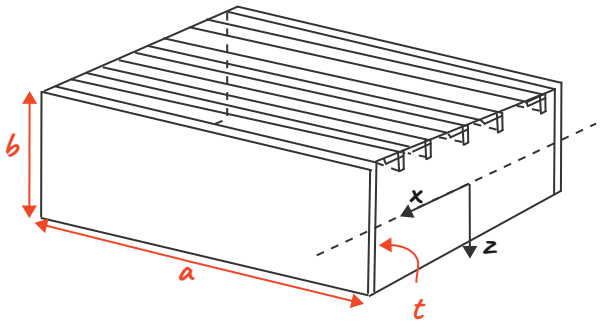

Figure 10.6: Spar web, where b is the smallest length of the panel and t is thickness

$$\tau_{cr} = \frac{\pi^2 k_s E_{Al}}{12\,(1-\nu^2)} \cdot \left(\frac{t}{b}\right)^2 \tag{10.19}$$

where τ_{cr} is the critical shear buckling shear stress, k_s is the shear buckling coefficient that is empirically determined through Figure 10.7, t is the thickness of the panel - the thickness of the spar - and b is the height of the spar. The shear buckling coefficient k_s is based on the aspect ratio a/b of the panel. For conservative design, an a/b of 5 is assumed so that the more critical C can be used for the design, and the placement of the ribs can be more freely designed in later design stages according to these constraints. In addition, hinged attachment is assumed which is also a conservative approach. This results in the k_s being 5.8.

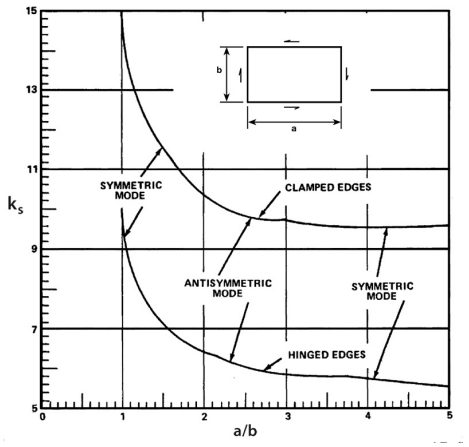

Figure 10.7: Web Shear Buckling Coefficient [35]

The actual shear experienced by the wingbox is made up of the shear due to the lateral shear in the z-axis and shear due to torsion (Figure 10.8).

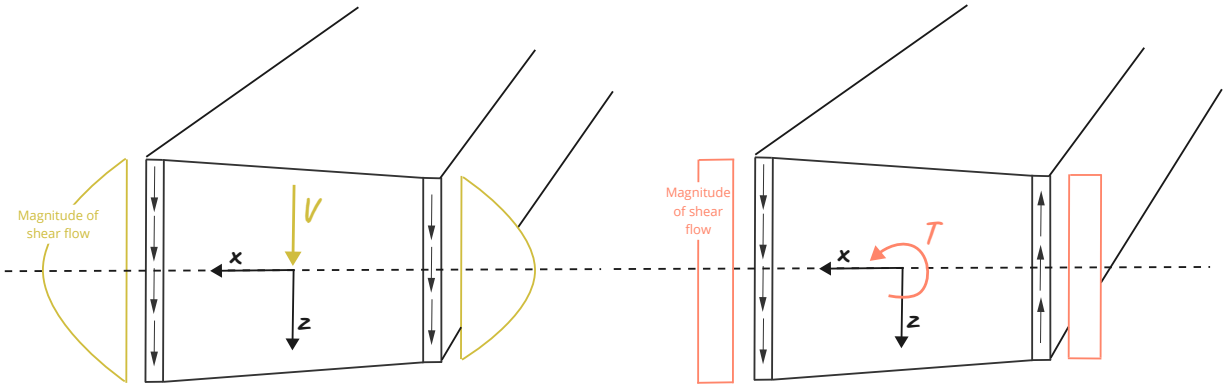

Figure 10.8: Shear Stress as a Result of Lateral Shear (left) and Torsion (right)

$$\tau_{max}(y) = \frac{V(y) \cdot Q(y)}{I_{xx}(y) \cdot t_{spar}(y)} + \frac{T(y)}{2 \cdot t_{spar}(y) \cdot A_m(y)} \tag{10.20}$$

where $V(y)$ is the lateral shear in the z-axis varied along the span, Q(y) is the first moment of area varied along the span, T(y) is the moment about the y-axis - the torque- varied along the span and $A_m(y)$ is the enclosed area of the wing box varied along the span. The first moment of area is another geometrical property quantifying the distribution of area about the x-axis - similar to I, but derived from shear stress. The first moment of area should be found about the neutral axis - where maximum shear occurs.

$$Q = \int_{A'} y \cdot dA' = \overline{y}' \cdot A' = \frac{h_f}{4} \cdot \frac{h_f}{2} \cdot t_{spar} + \frac{h_r}{4} \cdot \frac{h_r}{2} \cdot t_{spar} \tag{10.21}$$

The enclosed area is also expressed in terms of the variables.

$$A_m = \frac{h_f + h_r}{2} \cdot (0.65c - 0.15c) \tag{10.22}$$

As previously mentioned, the second moment of area is expressed in terms of the 3 variables [33].

10.4.4. Buckling of Stiffened Panels

The top and bottom skin panels are also subjected and vulnerable to buckling. However, the presence of stiffeners attached to the skin requires a different approach from pure skin buckling [33]. The critical stress at which the skin buckles can be calculated using the following expression.

$$\sigma_{cr} = C \cdot \frac{\pi^2 E_{Al}}{12\,(1-\nu^2)} \cdot \left(\frac{t}{b}\right)^2 \tag{10.23}$$

where C is another buckling constant that is acquired empirically, t is the thickness of the skin and b is the smallest width of the respective “panel” under consideration, as can be seen in Figure 10.9. The C depends on the aspect ratio and the boundary condition of the skin panel. For a conservative approach, a hinged boundary condition is assumed and an a/b above 3 is assumed where C platous to 4.0.

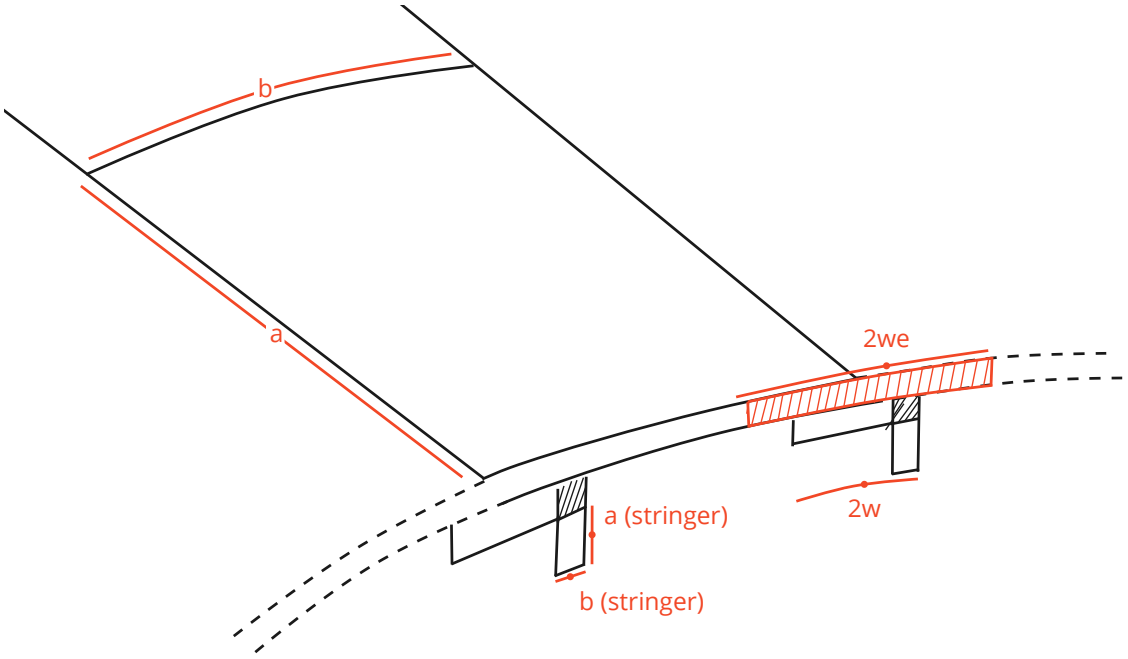

Figure 10.9: Stiffened Panel Consisting of the “Panel” of Interest, the Analysed Stringers and the Effective Width

The buckling nature of the stringers should also be accounted for. This is done by quantifying the critical crippling stress. When considering the synchronised buckling of the stiffened panel, the local buckling of the stringer is of importance - rather than the global instability regarding column buckling. The crippling stress of the stringer can be found by doing a weighted summation of the skin buckling of each individual flange of the stringer as can be seen in Figure 10.9.

$$\frac{\sigma_{cc}^i}{\sigma_y} = \alpha \cdot \left(\frac{C}{\sigma_y} \cdot \frac{\pi^2 E_{Al}}{12\,(1-\nu^2)} \cdot \left(\frac{t}{b}\right)^2\right)^{1-\eta} \tag{10.24}$$

$$\sigma_{cc} = \frac{\sum \sigma_{cc}^i \cdot A^i}{\sum A^i} \tag{10.25}$$

where t is the thickness of each stringer flange and b is the length of each flange of the stringer. In addition, α and ν are empirical constants and they are 0.8 and 0.6, respectively.

However, the fact that they are rigidly attached into one component allows a higher structural resistance under buckling that is not quantitatively accounted for. This is done with the use of the effective width of the stringer as can be seen in Figure 10.9.

$$w_e = \frac{t}{2} \cdot \sqrt{\frac{C\pi^2}{12(1-\nu^2)}} \cdot \sqrt{\frac{E_{Al}}{\sigma_{cc,stringer}}} \tag{10.26}$$

where w_e is the effective width, t is the thickness of the skin, and σ_{cc} is the crippling stress of one stringer. In addition, C is another empirically determined buckling coefficient that is quantified based on the b/t ratio and its torsional resistance Figure 10.10.

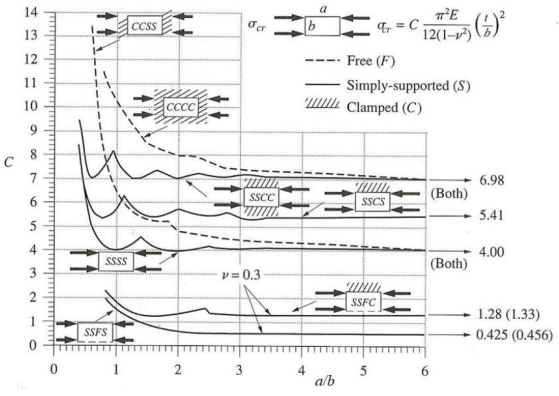

Figure 10.10: Buckling Constant C [36]

Now, the previous skin buckling critical stress should account for the reduction in the width b.

$$\frac{\sigma_{cc}^i}{\sigma_y} = \alpha \cdot \left(\frac{C}{\sigma_y} \cdot \frac{\pi^2 E_{Al}}{12\,(1-\nu^2)} \cdot \left(\frac{t}{b-2w_e} \right)^2 \right)^{1-\eta} \tag{10.27}$$

Subsequently, the overall critical buckling stress of the entire stiffened panel can be expressed as follows.

$$\sigma_{cr} = C \cdot \frac{\pi^2 E}{12\,(1-\nu^2)} \cdot \left(\frac{t}{b-2w_e} \right)^2 \tag{10.28}$$

10.4.5. Maximum Stress Constraint

The stresses along the span (axial and shear) can be found in Figure 10.11, along with the maximum allowed stress to avoid permanent deformation. The stiffened skin buckling constrained the axial stresses and the shear buckling of spar webs constrained the shear stresses. In other words, the stiffened skin buckling primarily sized the number of stringers and the shear buckling of the spar webs sized the spar thickness.

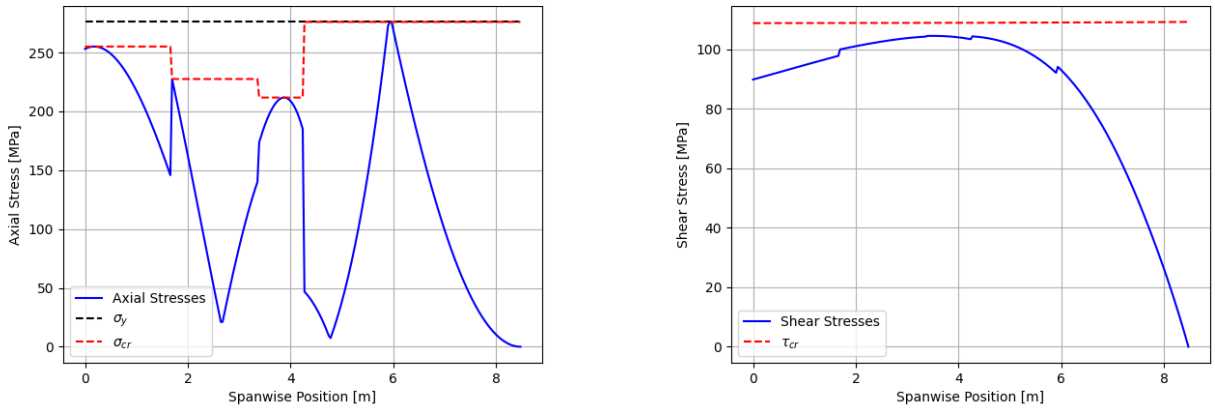

(a) Axial

(b) Shear

Figure 10.11: Axial and Shear Stress Along the Span in Relation to the Critical Stresses

10.4.6. Final Wingbox

Once the three variables were optimized for minimum weight under deflection, axial failure, stiffened panel buckling and shear web buckling, the specifications of the final wingbox can be seen in Table 10.5 and Figure 10.12.

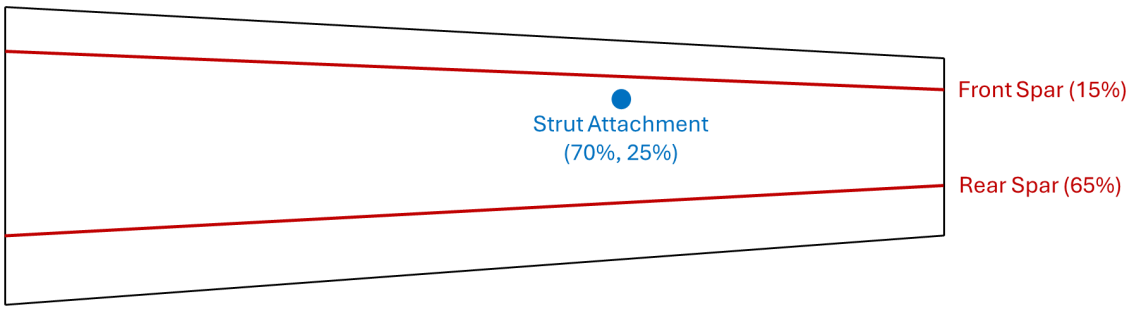

Figure 10.12: Wing Top View

Table 10.5: Specifications for Spar Thickness, Skin Thickness, and Stringer Number

Spar Thickness [mm]		
Root		1.5
Tip		0.6
Skin Thickness [mm]		0.5
Stringer Number	0%-20%	18
	20%-40%	10
	40%-50%	8
	50%-70%	36
	70%-100%	34

10.5. Strut Sizing

The influence of the strut was analysed in Section 10.3.2 where the strut force was calculated in an iterative manner. In order to meet the C_{d_0} requirement, the struts are to be produced in the shape of airfoils - implying the sizing should be done similarly to the wingbox. Due to the statically indeterminate nature, an initial cross-sectional area was assumed and was optimized to be 0.001 square meters. This was analysed when the wing was analysed under the most critical load factor of 3.51, where the strut was in tension. However, under load factors of n=-1.4 and on-ground operations, the strut is under compression and, therefore, vulnerable to buckling. This section will briefly cover a conceptual sizing of the structural cross-section of the strut ensuring its compressive competency.

Due to the airfoil cross-section, the sizing can be done similarly to the wing - however there are significant differences.

- The strut is loaded axially - contrary to the wing experiencing heavy non-linear spanwise forces.
- The strut has a constant cross-section - contrary to the tapered wing.
- The assumed hinged boundary conditions - contrary to the wing under four supports.

Due to the strut being sufficiently smaller than the wing, only one spar is needed to support the loads - especially when it is not subjected to torsion. The two design concepts for the strut sizing can be found in Figure 10.13. In order to maintain a set second moment of area to resist buckling, there should be sufficient area distributed sufficiently far from the neutral axis - this can be done with either local thickening or the use of stringers. In later stages in the design, the two concepts should be traded off with regard to their strength/weight ratio.

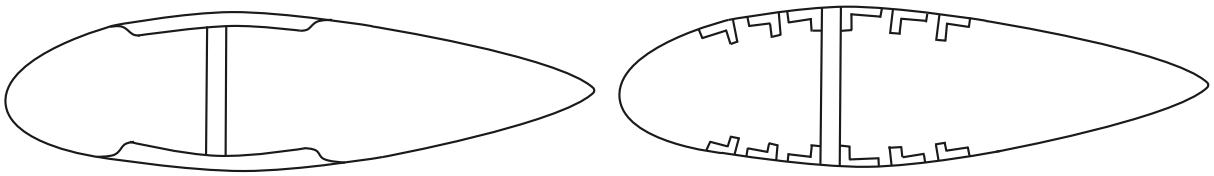

Figure 10.13: Two Strut Design Concepts: Local Thickening of Skin (left) or Use of Stringers (right)

10.6. Revised Fuselage Sizing

The fuselage sizing for the selected conventional aircraft concept was determined using methodologies outlined in Roskam [37], Raymer [38], and Jenkinson's [39] methods. Furthermore, statistical data from similar aircraft was incorporated into the analysis. The preliminary sizing and the relative positioning of the conventional aircraft can be found in the mid-term report [12].

The main changes between the preliminary fuselage sizing and the final design involved the additional power components (motor, gearbox, etc.). Initially, the motor was not positioned next to the engine during the preliminary sizing phase. However, it became necessary to place them together due to the determination of the parallel architecture system. This prompted changes in the positioning. The motor, which is 0.18 meters in length, required all components located behind it, including the engine, cockpit, and passenger area, to be shifted backwards accordingly.

Additionally, the battery configuration was revised. The centre of gravity of batteries needed to be positioned at a precise location - due to their high mass and therefore significant influence on stability. Initially, a single bulk of the batteries did not achieve the desired balance, so the battery setup was modified into two separate locations to achieve the necessary stability. Consequently, the centre of gravity for the first battery is at 2.7 meters with a length of 0.9 meters, and for the second battery, it is at 5.6 meters with a length of 0.95 meters.

Once the fuselage's internal layout is determined, the weight distribution is of use to calculate the inertial loads along the fuselage. However, due to the non-pressurised nature of the fuselage, the fuselage is relatively not loaded in comparison to other structural components like the wing. This implies that cut-out analysis of pilot, passenger, cargo doors and windows is easier to perform since the skin does not carry much shear.

10.7. Fatigue Analysis

Any structural component of the aircraft carries a certain load that varies over the flight profile. For the wing of an aircraft, a loading profile as illustrated in Figure 10.14 can be expected [40]. In the figure, S_max refers to the maximum axial stress experienced by the wing, and S_min to the minimum axial stress. For different aircraft components, different load limits will be experienced. However, the cyclic nature of the loads applied on the components prevails.

This cyclic load variation will eventually lead to crack nucleation and propagation within the structural

components, resulting in material failure, a phenomenon otherwise known as material fatigue [40]. It is thus not only important to verify whether the aircraft structure *can* carry the loads subjected to it, but also *how often* it is able to carry these loads.

As visible in Figure 10.15, the cyclic load experienced can be conservatively approximated by a sinusoidal loading with amplitude the regular maximum stress experienced by the component, period the duration of a flight, and a mean load of 0.

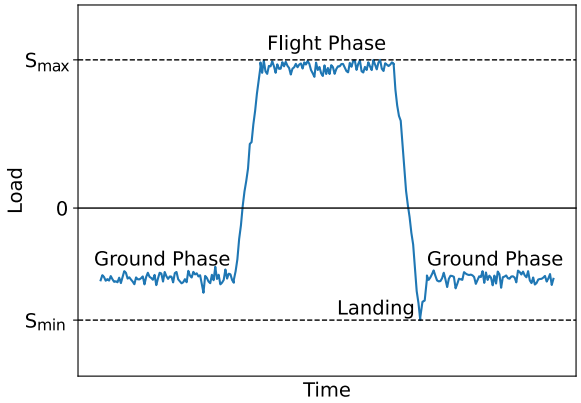

Figure 10.14: Wing Loading Variation over Generalised Flight Profile

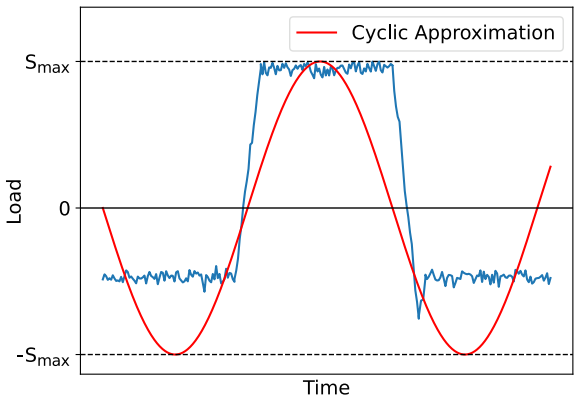

Figure 10.15: Cyclic Load Approximation of Wing Loading

Through experimental research, it has been proven that the stress amplitude of the applied cyclic load (S) is exponentially proportional to the lifetime of a component, expressed in the number of loading cycles (Nf). The relationship between these two variables is often illustrated by so-called S-N curves. The coefficient of proportionality not only varies with component material characteristics but is also highly dependent on the mechanical nature of the components (normal, notched, bent, etc.), which introduce stress concentrations. One can acquire the S-N curve for various materials and component mechanical natures from research. However, for normal samples exposed to a cyclic load with mean stress of 0, a good preliminary approximation of the curve can be obtained by assuming:

$$S = \begin{cases} S_{ult} & 0 \leq Nf \leq 100 \\ e^{ln(S_{ult}) + \frac{ln(\alpha \cdot S_{ult}) - ln(S_{ult})}{ln(10^6) - ln(100)} \cdot (Nf - ln(100))} & 100 < Nf \leq 10^6 \\ \alpha \cdot S_{ult} & 10^6 < Nf \leq \infty \end{cases} \tag{10.29}$$

Where S_{ult} is the ultimate stress of the component material and α = 0.3 for aluminium alloys [40]. The relationship for $100 \leq Nf \leq 10^6$ is also referred to as Basquin's law [40]. In order to account for the fact that most components do contain stress concentrations, and to account for the approximate nature of Basquin law analysis, the Nf obtained is often divided by 4 as a contingency measure.

Hence, in order to estimate how often a component of the HA-1 can carry the applied cyclic load, the following methodology can be applied:

1. Identify the maximum stress S_{max} acting on the component and assume cyclic loading as presented in Figure 10.15.
2. Identify the material of the component and the material properties α and S_{ult}.
3. Construct the approximate S-N curve and read the Nf corresponding to the applied S_{max}.
4. Divide the obtained fatigue life (Nf) by 4.

In the current report, only a fatigue analysis for the wings will be presented, as the loading on other components remains largely unknown. However, once the loading on the other components is known, a similar preliminary analysis can be performed using the aforementioned methodology.

As mentioned in Section 10.2, the wing is made out of AA 6061-T6, which has an S_{ult} of 310 MPa. From the load analysis presented in Section 10.3, the maximum axial stress experienced by the aircraft is 116 MPa, assuming a cruise altitude of 3000 m and a load factor of 1.5, which is far greater than the load factors experienced during regular flight[(f)], again ensuring a conservative estimate is obtained. Applying the aforementioned methodology, the results presented in Figure 10.16 were obtained.

To validate the results, an S-N curve for a normal AA6061-T6 specimen was retrieved from the FAA's "Metallic Materials Properties Development and Standardization (MMPDS)" handbook [41, p. 3-289]. As the experimental curve lies on the right of the Basquin law approximation, this further ensures the estimated lifetime of 44700 flights is conservative. Furthermore, since the wing often carries the largest stresses within an unpressurised structure, and since the rest of the structural components should be designed to avoid large stress concentrations, this value may also serve as an approximation for the fatigue life of the entire aircraft.

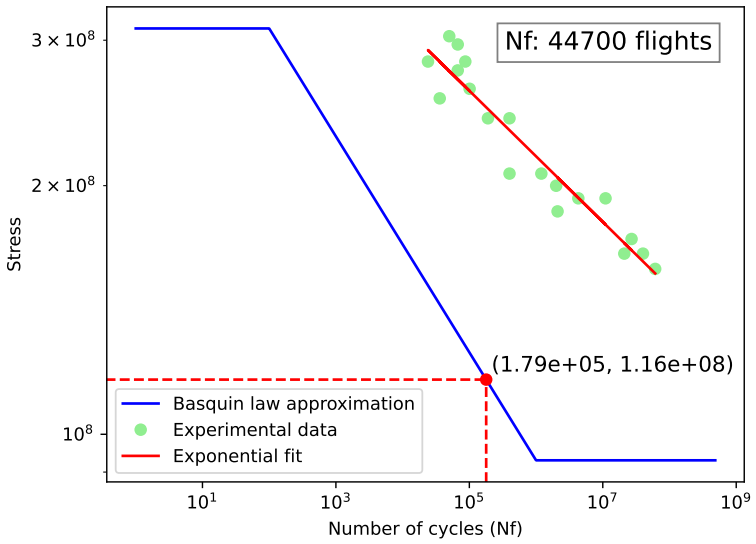

Figure 10.16: Estimation of the HA-1's Fatigue Life

With the aircraft having to endure an expected 600 flights per year over the course of its operational lifetime, according to the preliminary estimate, the aircraft should not succumb to fatigue within 78 years. However, this estimate is preliminary and should be refined by considering the entire structure, stress concentrations, variations in material properties (e.g., due to welding), and the effects of corrosion in the future.

10.8. Aeroelastic Analysis

When an aircraft wing is subjected to an aerodynamic load, the elastic structure deforms either vertically (heave motion), torsionally (pitch motion), or both simultaneously. This structural deformation, however, implies a change in the aerodynamic loads acting on the wing, which in turn implies a different structural deflection.

This phenomenon of interdependence between the elastic properties of the aircraft structure and applied aerodynamic loads is studied in the field of aeroelasticity, which aims to accurately predict the structure's response by considering the complete fluid-structure system simultaneously.

There are three dangerous categories of aeroelastic responses: Divergence, Aileron Reversal, and Flutter. The aeroelastic characteristics of the HA-1 wing with respect to each of these responses will be discussed in Section 10.8.2, Section 10.8.3 and Section 10.8.4 respectively. Aeroelastic analysis of other aircraft components like the strut shall be performed in the future when they have been further developed.

10.8.1. Assumptions

Due to the complex nature of fluid-structure interactions, a number of simplifying assumptions are often made to reduce the computational expense [42]. An overview of all assumptions made for the

[(f)] URL: https://aviation.stackexchange.com/questions/21902/what-level-of-g-force-does-our-body-experience-when-we [accessed 15/06/2024]

current analysis is listed below:

AE-ASSU-01: The typical section of the aircraft wing exhibits a similar aeroelastic response to that of the full 3D wing.

AE-ASSU-02: The effect of high Mach and Reynolds numbers on the aerodynamic forces experienced by the aircraft are neglected.

AE-ASSU-03: Slender, high aspect ratio wings are assumed.

AE-ASSU-04: Quasi-steady flow is assumed. Only slow variations in the flow prevail.

AE-ASSU-05: Aerodynamic center of the typical section is located at the quarterchord point.

AE-ASSU-06: Structural damping matrix is neglected for the classical flutter analysis.

AE-ASSU-07: Only aerodynamic forces that are an instantaneous function of the typical section angle of attack are considered. The time history effects of the flow are neglected.

AE-ASSU-08: The influence of the strut is neglected.

AE-ASSU-09: Typical section angle of attack is assumed to be small.

AE-ASSU-10: The wing carries a sweep angle of 0 [rad]

One of the most notable assumptions in the list is **AE-ASSU-01**. The typical section of an aircraft wing refers to the airfoil placed at 70% along the half wingspan of the aircraft. This simplification argues that the typical section of the aircraft wing exhibits a similar aeroelastic response to that of the full 3D wing. Therefore, when the typical section is aeroelastically stable, so will the full 3D wing.

Despite the severity of some assumptions when compared to real-world conditions, using them during analysis still ensures surprisingly accurate results for the subsonic flight regimes at which the HA-1 operates [42]. It should also be noted that, for the HA-1, typical section analysis of the wing is conservative in nature. As illustrated in Section 10.4, the HA-1 features a strut extending to 70% of the wing, which aids in carrying the wing loads. In the typical section analysis, the influence of this strut is ignored, although, in reality, it would significantly counteract any heave motion of the wing. For these reasons, performing a typical section analysis to evaluate each of the three aeroelastic responses is expected to yield accurate and conservative results.

An overview of the necessary typical section parameters for the simplified aeroelastic analysis is illustrated in Figure 10.17, where AC represents the wing aerodynamic centre, EA the typical section elastic axis, COG_{main} the centre of gravity of the aileronless airfoil, and $COG_{aileron}$ the centre of gravity of the aileron.

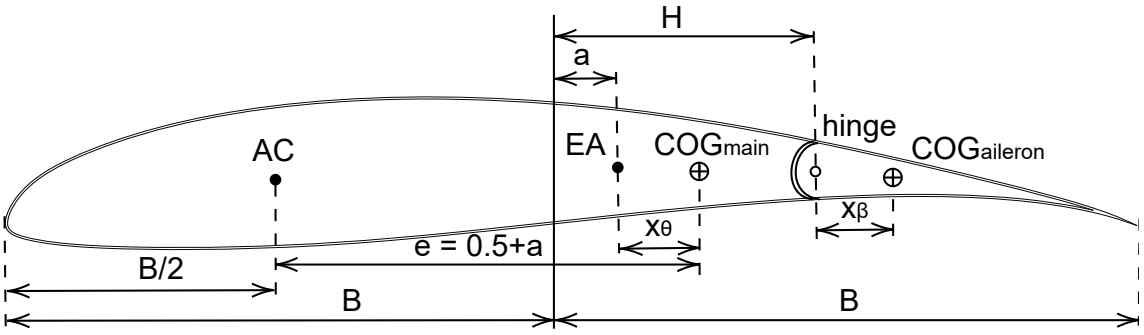

Figure 10.17: Parameters of a Generalized Typical Section [42]

10.8.2. Divergence

Divergence is a static aeroelastic phenomenon where the elastic twist of the wing becomes theoretically infinite. When an aircraft reaches its divergence speed, the aerodynamic load exceeds that which the elastic structure can carry in equilibrium. This results in the structure deforming in such a way, that

the newly resulting aerodynamic load further increases the wing deformation in the same direction. This way, a positive feedback loop is created, eventually leading to the failure of the wing. From a mathematical perspective, this means divergence occurs when there exists an imbalance between structural and aerodynamic stiffness parameters.

The divergence boundary is the value of dynamic pressure which separates the regions of dynamic pressure where the aircraft does and does not experience divergence. The reason it is called a boundary is because the airspeed at which this dynamic pressure is achieved changes with altitude. Hence, when plotting the divergence speed against altitude, a boundary curve will be observed.

As divergence occurs upon instability between stiffness parameters, the divergence *boundary* can thus be obtained by *balancing* the structural and aerodynamic stiffness matrices. Rearranging the equality for dynamic pressure results in the closed-form solution presented in Equation 10.30 [42].

$$q_{div} = \frac{K_\theta}{S \cdot C_{L_\alpha} \cdot (\frac{1}{2} + a) \cdot B} \tag{10.30}$$

In Equation 10.30, q_{div} represents the divergence boundary in $\mathrm{N/m^2}$, K_θ the torsional stiffness of the typical section in $\mathrm{Nm/rad}$, C_{L_α} the lift curve slope of the typical section airfoil in $1/\mathrm{rad}$, S the wing surface area per unit span of the total aircraft in $\mathrm{m^2}$, B the half chord of the typical section in m, and a the distance as stipulated by Figure 10.17, non-dimensionalised with the half chord B.

If the dynamic pressure experienced by the aircraft wing is lower than this boundary value, the typical section will not undergo divergence, and the wing is predicted to remain intact. For the HA-1, the divergence boundary lies at $q_{div} = -54\,086\,\mathrm{N/m^2}$. Assuming sea-level altitude, this translates into divergence occurring at an airspeed of −297 m/s.

Clearly, this divergence speed far exceeds the subsonic flow regimes for which the typical section analysis approach is accurate. However, since the typical section analysis is accurate for subsonic flow regimes and indicates no divergence for these regimes, it can be argued that **no divergence will occur at the subsonic cruise speeds at which the HA-1 operates**.

Furthermore, K_θ for the HA-1 was obtained by analyzing a simplified wing which extrapolates the typical section toward the aircraft centerline. By doing so, the original positive taper of the wing toward the root chord is ignored, resulting in aeroelastic analysis of a weaker, more slender wing than is actually present. This further adds to the certainty that no divergence will occur for the HA-1.

Since the boundary indicates a negative dynamic pressure, the aircraft would have to fly backwards for divergence to occur. This result might be surprising but can be explained by the HA-1 wing's elastic axis being located in front of the aerodynamic centre, ensuring torsional stability in all low-speed, forward flight regimes.

Note that, in general, the lowest airspeed at which the dynamic pressure boundary is exceeded always occurs at sea-level altitude, where air density is highest. However, the HA-1 will only reach its highest airspeeds at its cruise altitude of 3000 m, where a larger airspeed is required to reach the same dynamic pressure, further increasing the certainty that the HA-1 will not experience divergence over its flight regime.

10.8.3. Control Reversal

Control- or aileron reversal is a phenomenon where the usual functionality of wing control surfaces is reversed. That is, the resulting roll motion associated with a given roll input is reversed. Similar to divergence, it is a static aeroelastic phenomenon. However, contrary to divergence, the aircraft remains operable after the control reversal dynamic pressure boundary is exceeded. Nevertheless, control reversal is not allowed to occur within the flight envelope as per CS23 regulations [15].

Similar to divergence, a closed-form solution can be found for the reversal boundary, which is presented

in Equation 10.31 [42].

$$q_{rev} = \frac{2 \cdot [\sqrt{1 - H^2} + \arccos(H)] \cdot K_\theta}{C_{L_\alpha} \cdot C_{M_{AC_\beta}} \cdot 2 \cdot B \cdot S} \tag{10.31}$$

In Equation 10.31, q_{rev} represents the reversal boundary in $\mathrm{N/m^2}$, K_θ the torsional stiffness of the typical section in $\mathrm{Nm/rad}$, C_{L_α} the lift curve slope of the typical section airfoil in $1/\mathrm{rad}$, S the wing surface area per unit span of the total aircraft in [m^2], B the half chord of the typical section in m, $C_{M_{AC_\beta}}$ the change in $C_{M_{AC}}$ for a change in flap deflection β (defined positive clockwise) in $1/\mathrm{rad}$, and a and H the distances as stipulated by Figure 10.17, non-dimensionalised with the half chord B.

If the dynamic pressure experienced by the aircraft wing is lower than this boundary value, the typical section will not undergo control reversal, and the aileron control inputs are predicted to yield a desired aircraft response. For the HA-1, the reversal boundary lies at $q_{rev} = 27\,800\,\mathrm{N/m^2}$. Assuming sea-level altitude, this translates into control reversal occurring at an airspeed of 210 m/s.

Similar to divergence, the control reversal speed far exceeds the subsonic flow regimes for which the typical section analysis approach is accurate. However, following a similar logic, **no control reversal will occur at the subsonic cruise speeds at which the HA-1 operates**.

Furthermore, again due to the conservative nature of the K_θ estimate, and the assumption of sea-level altitude, the certainty that the HA-1 will not encounter control reversal over it's flight regime is increased.

10.8.4. Flutter

Flutter is a dynamic aeroelastic phenomenon whereby the fluid flow allows for self-sustained oscillations within the aircraft wing structure. Depending on the flow parameters, these oscillations can be damped or diverging. The flutter boundary is the dynamic pressure at which the wing oscillation transitions between the two regimes. At the flutter boundary itself, the oscillations are simple harmonic.

Many types of flutter exist, varying in their origin and resulting response. Due to the assumptions made, typical section analysis only allows for accurate analysis of classical flutter, whereby the wing oscillations are constrained to heave and pitch motion. Other types of flutter, like propeller whirl flutter and buffeting, will be analyzed in the future, once the propulsion system and turbulent flow characteristics of the aircraft are better understood.

To derive an expression for the classical flutter boundary, the equation of motion for the typical section must be solved for various airspeeds (V_∞). This equation assumes quasi-steady flow and is presented in Equation 10.32. Contrary to the derivation of the divergence and reversal boundaries, it is clearer to determine the flutter boundary by first assuming a value for air density (sea-level assumed), solving for the velocity at which flutter occurs, and then reformulating this to find the flutter boundary.

$$\begin{bmatrix} m & S_\theta \\ S_\theta & I_\theta \end{bmatrix} \ddot{\underline{x}} - \begin{bmatrix} -qSC_{L_\alpha}\frac{1}{V_\infty} & -qSC_{L_{\dot\alpha}}\frac{B}{V_\infty} \\ qSC_{L_\alpha}\frac{d\cdot B}{V_\infty} & qS\frac{B\dot\theta}{V_\infty}(C_{L_{\dot\alpha}}(d\cdot B) + C_{L_\alpha}a(0.5-a)B \end{bmatrix} \dot{\underline{x}} + \begin{bmatrix} K_h & qSC_{L_\alpha} \\ 0 & K_\theta - qSC_{L_\alpha}(e\cdot B) \end{bmatrix} \underline{x} = 0 \tag{10.32}$$

In Equation 10.32, m represents the mass of the typical section (which is equivalent to the mass per unit span of the 3D wing) in kg, S_θ the first moment of area of the typical section $\mathrm{m^3}$, I_θ the second moment of area of the typical section $\mathrm{m^4}$, q the dynamic pressure experienced by the typical section in $\mathrm{N/m^2}$, S the wing surface area per unit span of the total aircraft in $\mathrm{m^2}$, C_{L_α} the lift curve slope of the typical section airfoil in $1/\mathrm{rad}$, V_∞ the airspeed of the typical section in $\mathrm{m/s}$, K_h the heave stiffness of the typical section in $\mathrm{N/m}$, K_θ the torsional stiffness of the typical section in $\mathrm{Nm/rad}$, $C_{L_{\dot\alpha}}$ the change in typical section C_L for a varying rate of change in angle of attack in [1/rad], B the half chord of the typical section in m, $\dot\theta$ the rate of twist of the typical section in [rad/s], and a and d the distances as stipulated in Figure 10.17, non-dimensionalised with the half chord B.

To solve Equation 10.32, the solution $\underline{x} = \hat{\underline{x}} \cdot e^{p \cdot t}$ is substituted into the equation, and the resulting characteristic equation is solved for the eigenvalues p. When approaching the problem computationally, however, often an iterative approach is taken, where the value of p is guessed and updated based on how well the guessed solution solves the differential equation.

Assuming sea-level altitude, Equation 10.32 can then be solved for the eigenvalues p for all flight speeds within the range [0; $5 \cdot V_D$], where V_D represents the aircraft dive speed and 5 was chosen arbitrarily to have sufficient range of analysis. It is then argued that the airspeed for which Re(p) > 0 for any of the eigenvalues represents the flutter speed of the aircraft at sea-level altitude. By squaring this value, and multiplying it by 1.225/2, the flutter boundary can be found.

If the dynamic pressure experienced by the aircraft wing is lower than this boundary value, the typical section will not experience flutter, and the wing is predicted to remain intact. For the HA-1, classical flutter occurs at a sea-level airspeed of 287 m/s, as indicated in Figure 10.18. This means the classical flutter boundary lies at $q_{flut} = 50\,451\,\mathrm{N/m^2}$. Similar to divergence and control reversal, the flutter speed far exceeds the subsonic flow regimes for which the typical section analysis approach is accurate. However, following a similar logic, **no flutter will occur at the subsonic cruise speeds at which the HA-1 operates**.

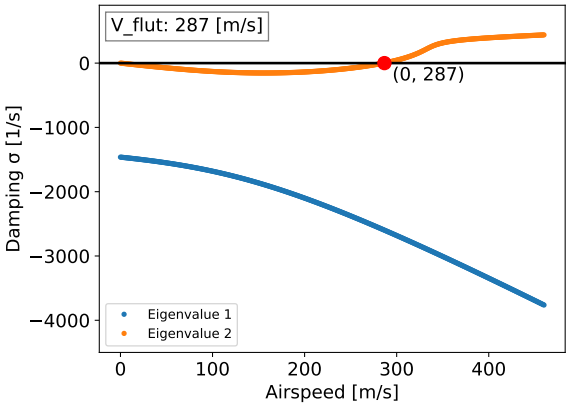

Figure 10.18: Estimation of the HA-1's Minimum Flutter Speed

Furthermore, again due to the conservative nature of the K_θ and K_h estimate (which follows the same logic), and the assumption of sea-level altitude, the certainty that the HA-1 will not encounter flutter over its flight regime is increased.

10.8.5. Certification

To be aeroelastically certified according to CS23 requirements, the aircraft must display no signs of aeroelastic effects at airspeeds ranging from 0 to $1.15V_D$ for all operational altitudes [15].

For the HA-1, $1.15V_D = 96\,\mathrm{m/s}$ which is still below the subsonic airspeeds for which the typical section analysis is accurate. Hence, based on the results of Section 10.8.2, Section 10.8.3, and Section 10.8.4, the HA-1 aircraft will not undergo any adverse aeroelastic phenomena.

11 | Stability & Control Design

Design of aircraft stability and controllability for all stages of flight and ground handling is paramount to guarantee the safety of occupants and the longevity of the aircraft. This design is highly dependent on the placement of every other subsystem in the aircraft, due to its sensitivity to changes in centre of gravity (CG). Therefore, a number of subsystems have been iteratively sized together to ensure the aircraft is stable at all times. Firstly, the centre of gravity range for which stability was sized was determined in Section 11.1. Secondly, the undercarriage was sized for ground stability in Section 11.2. Lastly, the empennage and control surfaces were designed in Section 11.3.

11.1. Centre of Gravity Excursion

In order to size for stability and analyse it, the CG excursion encountered during operation must be known. First, the empty weight CG was determined using the component weights found in the Class II weight estimation and the known component locations. This CG is shifted from the empty weight position by the pilot, passengers, luggage, and potential cargo. These can be loaded into the aircraft in numerous different ways, and with the inclusion of random cargo, one could come up with near-infinite combinations. Therefore, seven loading sequences have been chosen to represent the CG excursion the aircraft will encounter, thus setting the acceptable limits for most forward and aft CG.

The first six of these sequences are made up of all possible combinations of passenger transport loading. Passengers are assumed to weigh 75 kg with 15 kg of luggage excluding contingency. These passengers are seated at 75% the first three boxes of the cabin mentioned in Section 10.6, with the last box being reserved for luggage at 50%. The pilot is assumed to be a passenger, but their entire mass of 90 kg is placed in the cockpit box. Next, the passengers can be loaded either front-to-back or back-to-front, causing a different CG excursion. Therefore, both situations have been analysed, where the passengers are assumed to load in adjacent seats first as this is most limiting. Lastly, the fuel CG is assumed to be fixed and located at 40% of the MAC, with all of it placed in the wing.

The remaining sequence accounts for the limiting situation where dangerous goods are to be transported, which is stored in the rear of the cabin in accordance with HA-UR-16-SYS-39. This means 540 kg is placed at 6.5 m from the nose, with one pilot seated in the cockpit.

Once the full CG range of these seven sequences had been obtained, the most forward and aft CG locations could be found. A safety factor of 2% MAC was then applied to these limiting CGs to account for mass inaccuracies and movement of people within the aircraft. The two most limiting loading sequences can be found in Figure 11.1, where the grey lines represent the CG limit with a safety margin.

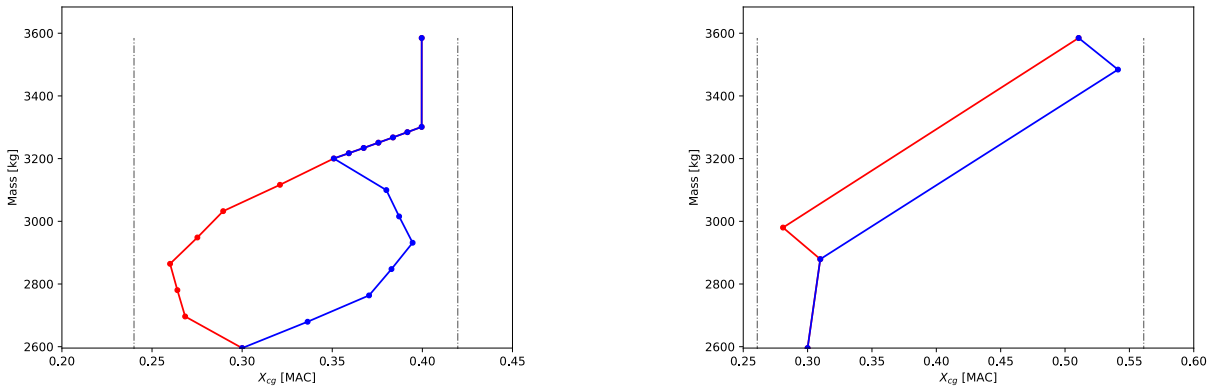

(a) Most forward CG: Passengers/luggage/fuel

(b) Most aft CG: fuel/cargo/pilot

Figure 11.1: Design CG excursion of the HA-1 Aircraft

11.2. Undercarriage Design

The undercarriage provides ground stability and controllability in the form of steering and braking capabilities. To reduce drag it was also designed to be retractable in, for which the retraction system is traded off in Section 11.2.1. Secondly, the undercarriage was sized to comply with requirements on ground stability and manoeuvrability in Section 11.2.2. Lastly, the braking performance was analysed and commercially available brakes were chosen for the aircraft, as is described in Section 11.2.3.

11.2.1. Retraction System

The landing gear retraction system is a critical part of the aircraft design as the ability to retract the undercarriage greatly reduces drag. However, a retractable landing gear also poses extra risks and costs in terms of maintenance, reliability, and operational viability. Therefore, a retraction mechanism had to be designed that is as simple as possible to limit the number of moving parts, while also being easy to control for the pilots in case of emergency. Additionally, the aircraft shall be equipped with a warning system to make sure pilots do not attempt to land without the landing gear being extended.

Figure 11.2 illustrates the retraction motion that the main gear has to execute. This retraction mechanism is based on the mechanism Cessna uses on several of their aircraft, with the addition of the rotation of the wheel (step 3) to limit the vertical space needed in the fuselage. This system makes use of a single pivot assembly which is mounted to the actuator and gear strut in such a way that only one actuator and rotation is needed for the entire retraction[(a)].

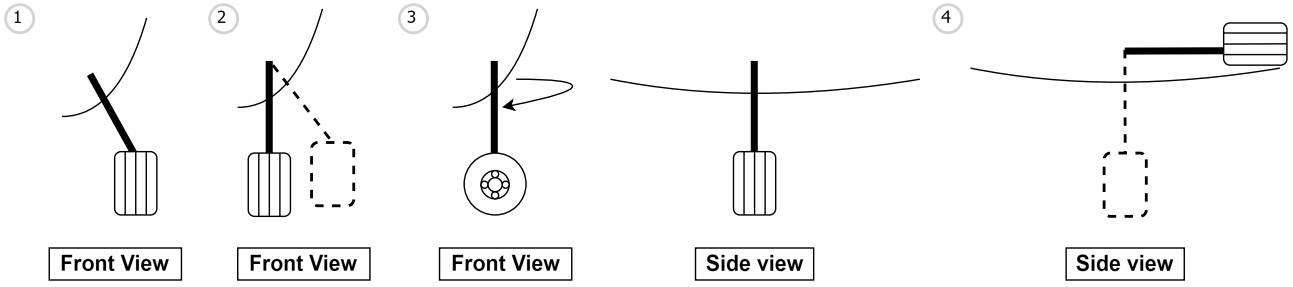

Figure 11.2: Landing Gear Retraction Motion

The retraction of the nose gear is much simpler as it is not positioned outboard of the fuselage. It is simply pulled up and stowed underneath the engine, although the wheel is still rotated using an

[(a)]URL: https://www.cessnaflyer.org/magazine/article-archives/maintenance-technical/cessna-s-retractables-the-system-demystified.html [Accessed 25 June 2024]

additional actuator to limit its footprint in the fuselage. Three types of actuators are available, which are hydraulic, pneumatic and electric retraction systems. Among these actuators, the electric system has been chosen for implementation.

Hydraulic systems are most commonly used because of their excellent reliability and small actuator sizes while still delivering high working pressures [43]. However, due to the complexity of the system, requiring multiple actuators and many hydraulic lines, it is costly and time-intensive to inspect and maintain. This made it an unfavourable option for MAF and thus it was excluded from the trade-off.

Pneumatic actuation systems operate on compressed air to raise and lower the landing gear. Despite their robustness and lower initial cost, only a few aircraft implement this system due to its issues with ice formation within the system [43]. Additionally, it is bulkier and requires more frequent maintenance compared to other systems.

Electric systems retract and extend the landing gear through the use of electric motors which convert electricity from the battery into mechanical power. These motors provide precise control, high reliability, high efficiency, and easier maintenance. However, they require a significant amount of power and are costly, although this is not a large drawback for the HA-1 since a powerful battery is already included on the aircraft[44]. To choose the retraction system mechanism, a trade-off was performed and Table 11.1 shows the trade-off criteria that were selected with their justification.

Table 11.1: Trade-off Criteria and Justification for Landing Gear System Selection

Criterion	Justification	Accounts for	Ranking Strategy	Weight	Weight Justification
Maintenance (MTN)	Ease of maintenance procedures reduces downtime and labour costs, lowering long-term operational expenses.	Accessibility and frequency of inspection	Based on literature [43, 44]	0.25	Given that the MAF operates in a remote region where the supply of specific parts may be challenging, easy maintenance is critical.
Cost (CST)	Essential to keep costs low to maintain the aircraft unit price below USD 1.5 million and enhance Human-Air's market competitiveness.	Manufacturing and long-term operational expenses	Based on literature [43, 44]	0.20	Cost is important but less so than passenger safety, which is directly linked to maintenance and reliability.
Reliability (RLB)	Ensures safe operation during takeoff and landing, the most critical phases of flight where most accidents occur.	Consistent performance under various conditions without failure	Based on literature [43, 44]	0.25	Reliability is directly linked to passenger and pilot safety, which is of paramount importance.
Weight (WGH)	Additional weight reduces fuel efficiency; minimising landing gear weight increases payload capacity.	Weight of the landing gear	Based on literature [43, 44]	0.15	While weight is significant, the total mass of the aircraft includes various components, with the landing gear being just one part.
Size (SZE)	Limited internal aircraft space necessitate a compact retraction system for efficient use of space.	Physical dimensions of the landing gear	Based on literature [43, 44]	0.15	Compared to other criteria linked to safety or market competitiveness, size is less important.

Based on the criteria determined, the two concepts were given scores through a quantitative process. These scores were then compiled and they are presented along with an indication of the chosen system in Table 11.2.

Table 11.2: Trade-off for Retractable Landing Gear System

	MTN	CST	RLB	WGH	SZE	
	0.25	0.2	0.25	0.15	0.15	**Score**
Pneumatic	2	4	3	3	3	2.95
Electric	4	3	5	2	4	3.75

Following the trade-off analysis, the electric system was selected for the retractable landing gear system. Despite its higher cost and weight compared to pneumatic systems, it offers superior reliability, a smaller size, and ease of maintenance. To ensure safe operation, an inspection of the landing gear will be conducted. Visual checks and assessments for obvious damage will be routinely performed on wheels, shock struts, and fork assemblies. Additionally, other components such as shock absorbers and overheating of brake units will be inspected every 100 flight hours and/or annually. This plan was devised based on the Bonanza, an aircraft similar to HumanAir's, operating under an electric motor.

11.2.2. Undercarriage Sizing

With the retraction system now being finalised, the undercarriage had to be sized to provide ground stability and controllability. This was done by placing the points of contact of the tyres in the required locations to provide, tip-back, scrape, and turnover angle stability. These tyres were then connected to the fuselage to determine the strut geometry. The tyre locations were sized for the limit angles defined by HA-LDG-03, HA-LDG-04, and HA-LDG-05 to limit strut length, which reduced the required stiffness of the struts and made them easier to fit in the fuselage.

First and foremost, the tyres were picked from a catalogue of available aircraft tyres. To be able to land on hard sand, hard grass, and gravel, the maximum inflation pressure was found to be 60 psi. This already eliminated most tyres as an option, in the end leaving ten tyres to be compiled in ascending order of maximum load. Naturally, these tyres also increase in size as the maximum allowable load increases.

Next, the main landing gear was placed to allow for stability during manoeuvring and clearance during take-off. Due to the way the aforementioned angles affect each other, this is an iterative process. First, a minimum of 8% of the most aft CG weight was placed on the nose wheel to provide enough traction to steer[45]. From this, an initial set of tyres was chosen for all three points of contact. Then using the initial guess $H_s = 1.5 \cdot D_{w_m}$ the main gear could be placed with Equation 11.1 to account for the tip back angle β from the aft CG. Using this preliminary location, the strut height required to account for the scrape angle θ could be found with Equation 11.2.

$$l_{m_{aft}} = \tan(\beta)(H_{CG_{OEW}} + H_s + 0.5 \cdot D_{w_m}) \quad (11.1)$$

$$H_{s_{scrape}} = l_{gt} \tan\theta - 0.5 \cdot D_{w_m} \quad (11.2)$$

Where l_{gt} is the longitudinal distance between the point of contact of the main gear and the start of the tail cone. Since Equation 11.2 provides a revised strut height, these equations had to be iterated until they converged to account for both angles at the same time.

Once the main wheels had been placed, the nose wheel location could readily be found using moment equilibrium around the CG. In close to all analysed configurations this led to a nose wheel that was placed in front of the fuselage. Therefore, it was chosen to place the nose gear at 0.80 m from the nose, at which point the new loading of the nose could be found for all combinations of mass and CG from the CG excursion diagrams. Thus a new set of tyres could was chosen so that the iteration for the main wheel placement could also be redone.

Lastly, with the longitudinal stability now managed, the width of the main gear needed to be sized to account for the turnover angle. The most forward CG is limiting for turnover performance, leading to Equation 11.3 for a turnover angle ψ [45].

$$y_{min} = \frac{l_{m_{fwd}} + l_{n_{fwd}}}{\sqrt{\frac{l_{n_{fwd}}^2 \tan^2 \psi}{(H_{CG_{OEW}} + H_s + 0.5 \cdot D_{w_m})^2} - 1}} \tag{11.3}$$

With y_{min} now also known, the location of all three wheels of the undercarriage was known. The connection struts could then be sized later such that they are easily retractable and are placed at the correct angles to resist the loads of landing and manoeuvring on the ground. For the last iteration of the HA-1 aircraft, it was also decided to extend the nose gear such that the ground angle of attack equals 5°. This aids in take-off performance as more lift is available during the ground roll.

11.2.3. Braking Performance

In order to calculate the breaking performance several conservative assumptions had to be made. Firstly, it was assumed that only the friction force between the calliper and the brake disk is going to slow down the aircraft. Secondly, a conservative value was taken for the friction coefficient between the calliper of the disk as can be visualised in Figure 11.3.

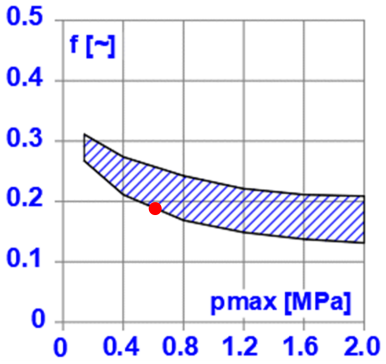

Figure 11.3: Friction Coefficient vs Pressure Applied

As can be seen, the lower value of 0.185 for the friction coefficient was chosen as stated before. Using conservation of energy, the kinetic energy absorbed by the brake system is equal to the work done by the retarded force:

$$F_{retarded} = \frac{KE}{d_{ground}}, \tag{11.4}$$

where KE is the kinetic energy and d_{ground} is the distance that the aircraft travelled on the ground before reaching the stopping point. The relation between the retarded force and the force that needs to be applied on the calliper is obtained as follows:

$$F_{caliper,req} = F_{retarded} \frac{0.5 D_{wm}}{0.5(r_{in} + r_{out})}, \tag{11.5}$$

where r_{in} and r_{out} are the inner and outer radius of the caliper. The force that the caliper produces by applying a pressure differential in the hydraulic system can be calculated using the following formula:

$$F_{caliper,apl} = 2 \cdot p_{max} \cdot A_{caliper} \tag{11.6}$$

where p_{max} is the maximum pressure differential applied expressed in Pa, and $A_{calliper}$ is the area on the calliper which needs to be multiplied by two since the force is applied on both sides of the breaking disk.

As long as $F_{calliper,req}$ is smaller than $F_{calliper,apl}$ for a specific breaking system, the requirement is

met. The braking system was chosen to be **030-05213 Cleveland brake assembly**[(b)] which is able to produce 2405N of force when a 100psi pressure differential is applied. The value is greater than the 2391N required to stop the aircraft and it is known that the chosen breaking system can sustain pressure differentials up to 600psi[(c)].

11.3. Stability, Controllability, and Empennage Design

The in-flight stability and controllability of the aircraft are influenced by numerous systems, which also influence each other. The most important of these systems is the empennage, for which the configuration was chosen in Section 11.3.1. Next, the longitudinal stability was designed as described in Section 11.3.2, Section 11.3.3, and Section 11.3.4. Lastly, the design process of the vertical stabiliser for directional stability is described in Section 11.3.5, after which lateral stability was sized in Section 11.3.6.

11.3.1. Empennage Configuration Trade-Off

As one of the lifting surfaces of the aircraft, the empennage has a significant effect on the aerodynamic and, most importantly, stability characteristics of the aircraft. Previously, a conventional tail was chosen for the development of the conceptual conventional design, which then won the full system trade-off. However, due to the significant influence the empennage has on the design of the rest of the aircraft, it was decided that a full trade-off of the possible empennage configurations has to be performed. these configurations for the empennage have been listed previously, and the V-tail, twin-boom tail, T-tail, and conventional tail have been chosen to enter the trade-off. Next, the criteria and weights were determined, which are listed in Table 11.3 along with justifications.

Table 11.3: Trade-off Criteria for the Empennage Configuration Selection, Along with Respective Weights

Criterion	Justification	Accounts for	Ranking Strategy	Weight	Weight Justification
Weight (WGH)	The tail configuration has a significant effect on the structural weight of the aircraft, as it also influences other subsystems	Weight of the empennage and structural support necessary	Quantitative: estimate overall weight and influence on the rest of the aircraft	0.25	Structural weight varies significantly between tail configurations. Saving weight is of importance since the aircraft design is already heavy
Drag (DRG)	Tail drag affects fuel burn and power required	Wetted area and related drag. Also includes drag associated with changes of aircraft shape and interference drag	Comparative: drag estimation of different configurations is known with respect to the conventional	0.35	To reach the proposed emissions reduction, power required/drag need to be as small as possible
Cost (CST)	Cost should be as low as possible, and configurations differ in maintenance required	Manufacturing cost of tail configurations and maintenance cost of control mechanisms due to complexity	Comparative: cost estimation is known with respect to conventional	0.10	The empennage is not a large part of the aircraft cost
Stability & controllability (SCO)	The aircraft should be inherently stable and easy to control	Static/dynamic stability, responsiveness of controls, control coupling	Qualitative: past experience on ease of control and stability of a configuration	0.20	providing stability & controllability is the main function of the empennage

[(b)]URL: https://www.univair.com/tires-wheels-brakes/cleveland/brake-parts-assemblies/030-05213-cleveland-brake-assembly/ [accessed on 18 June 2024]

[(c)]URL: https://www.skyshop.com.au/landing.pdf [accessed on 18 June 2024]

Oper-ability (OPE)	operability is of importance to MAF as they operate in challenging conditions	Ease of loading/unloading the aircraft, Pilot visibility, Ground clearance during take-off and landing	Qualitative: rough scoring for each component of operability, then combine	0.10	Ease of operation is not the main function of the empennage and can be traded off for more emissions reduction

Now the four concepts could be scored in accordance with the ranking strategy described in Table 11.3. Beginning with the weight, it was found that the conventional configuration is the lightest due to its limited surface size and direct mounting to the fuselage. The T-tail was found to be slightly heavier due to the more complex mounting of the tail, although surface area could be reduced further due to the end plate effect of the horizontal stabiliser. The V-tail is slightly heavier due to the longer fuselage necessary to prevent its characteristic snaking motion. Lastly, the twin-boom tail is the heaviest due to the required structural rigidity of the booms due to their small cross-sectional area [37]. Next, both the V-tail and T-tail have reduced drag compared to the conventional empennage due to less interference drag and a smaller required tail surface respectively [38]. The twin-boom tail increases drag due to the blunt shape of the aft fuselage. Cost is mainly linked to complexity and the maturity of the configuration. Therefore, conventional is clearly the cheapest option with the T-tail being a close second. The V-tail and twin-boom tail are both less technologically mature and would also require more maintenance. Stability and controllability is optimal for all options except the V-tail, which is more temperamental and has the tendency to start snaking [37]. Lastly, operability is worst for the conventional configuration, with both the T-tail and V-tail providing more ground clearance at take-off rotation, whereas the twin-boom tail significantly improves loading capabilities. A summary of the given scores is given in Table 11.4.

Table 11.4: Summary of Empennage Configuration Trade-off

	WGH	DRG	CST	SCO	OPE	
	0.25	0.35	0.10	0.20	0.10	**Score**
V-tail	4	5	3	3	4	4.05
Twin boom	3	3	3	5	4	3.5
T-tail	4	5	4	5	4	4.55
Conventional	5	4	5	5	3	4.45

The best empennage configuration thus seems to be the T-tail, with it barely winning over the conventional configuration. However, when a conceptual sizing of this tail configuration was done, it was quickly found that the horizontal tailplane is at risk of deep stall. Due to the length of the fuselage and height of the vertical stabiliser, the horizontal stabiliser would be right in the middle of the detached, turbulent wake of the wing at stall conditions, making a recovery near impossible. Since the dimensions of the aircraft and placement of the wing and stabiliser would likely not change drastically anymore, it was decided to continue the design process with the conventional empennage configuration to prevent the occurrence of deep stall.

11.3.2. Horizontal Stabiliser Sizing

Now that the conventional configuration has been chosen for the empennage, the horizontal stabiliser needs to be sized. To start off with, a number of design decisions were made; Firstly, to maximise aerodynamic efficiency, the aspect- and taper ratio have been chosen to be 5 and 0.4 respectively [12]. Next, the hinge line of the elevator has been chosen to have no sweep, making the control system easier to incorporate and manufacture. Lastly, the trailing edge of the root chord has been placed at the most aft point of the fuselage, maximising the distance between the wing and stabiliser.

With these initial parameters in place, a scissor plot could be constructed to find the required tail surface area. This plot consists of two lines, the stability and controllability lines, assessed at cruise

and landing conditions respectively. The equations used to construct the stability and controllability lines are shown in Equation 11.7 and Equation 11.8 respectively [46, 47].

$$\frac{S_h}{S} = \frac{\bar{x}_{cg} - \bar{x}_{ac} + S.M.}{\left[\frac{C_{L_{\alpha_H}}}{C_{L_{\alpha_{A-H}}}}\left(1 - \frac{d\epsilon}{d\alpha}\right)\frac{l_h}{\bar{c}}\left(\frac{V_h}{V}\right)^2\right]} \quad (11.7) \qquad \frac{S_h}{S} = \frac{\bar{x}_{cg} - \bar{x}_{ac} + \frac{C_{m_{ac}}}{C_{L_{A-H}}}}{\left[\frac{C_{L_H}}{C_{L_{A-H}}}\frac{l_h}{\bar{c}}\left(\frac{V_h}{V}\right)^2\right]} \quad (11.8)$$

Equations 11.7 and 11.8 neglect the effect of drag and propulsive forces as they are often complicated to quantify at this stage of the design. Drag is a stabilising force and equal to, or larger than thrust, making this a conservative assumption.

Now before Equations 11.7 and 11.8 can be used to find the required tail size, a number of parameters had to be explored that influence this sizing. Firstly, the horizontal stabiliser lift rate $C_{L_{\alpha_H}}$ and and aircraft-less-tail lift rate $C_{L_{\alpha_{A-H}}}$ needed to be found. Since the airfoil and geometry of both the wing and stabiliser were already known, these could readily be imported from flow5 [12]. However, for the aircraft-less-tail lift rate, a correction factor for the effect of the wing area inside the fuselage had to be applied to the known wing lift rate. This correction factor is given in Equation 11.9.

Secondly, the location of the aircraft-less-tail aerodynamic centre $\bar{x}_{ac}$ had to be found. This term consists of the wing aerodynamic centre location and correction factors for the fuselage. For an unswept wing flying in the incompressible regime, the wing AC could be found with $\bar{x}_{ac_w} = 0.205 + 0.005 \cdot AR$ [46]. The correction factor for the fuselage is given by Equation 11.10.

$$C_{L_{\alpha_{A-H}}} = C_{L_{\alpha_w}}\left(1 + 2.15\frac{b_f}{b}\right)\frac{S_{net}}{S} + \frac{\pi}{2}\frac{b_f^2}{S} \quad (11.9) \qquad \Delta\bar{x}_{ac_f} = -\frac{1.8}{C_{L_{\alpha_{A-H}}}}\frac{l_f h_f l_{fn}}{S\bar{c}} \quad (11.10)$$

Thirdly, the horizontal stabiliser effectiveness or tail/wing speed ratio $\left(\frac{V_h}{V}\right)$ had to be determined. From statistical data, this is given to be 0.92 for a conventional tail placed directly behind the main wing[46]. However, this does not take into account the effect of the propeller on the horizontal stabiliser as it increases its effectiveness. Therefore, Equation 11.11 was used to estimate the increased effectiveness of the horizontal stabiliser due to the propeller [48]. $S_{h,slip}$ is the stabiliser area affected by the slipstream, taken as the area directly behind the propeller disc. P_{av} is the maximum continuous power available after efficiencies in shaft horsepower (shp). The remaining parameters are also expressed in imperial units. However, since η_h is dimensionless, it could be directly multiplied with the aforementioned 0.92 to find the new horizontal stabiliser effectiveness.

Next, the downwash on the horizontal tailplane had to be considered. It was quickly found that small variations in the vertical location of the horizontal stabiliser had no meaningful effect on the tail downwash in the high-wing conventional empennage configuration, due to its proximity to the wing vortex shed plane. Therefore, any positive effects from this contribution have been neglected, leaving the statistical relation of Equation 11.12 to determine the downwash on the tail [46].

$$\eta_h = 1 + \left(\frac{S_{h,slip}}{S_h}\right)\frac{2200 \cdot P_{av}}{q_{cruise}V_{cruise}\pi D_p^2} \quad (11.11) \qquad \frac{d\epsilon}{d\alpha} = \frac{C_{L_{\alpha_w}}}{\pi AR}\left(\frac{0.4876}{\sqrt{r^2 + 0.6319}}\right) \quad (11.12)$$

Where r is defined as $r = l_h \cdot \frac{2}{b}$, with l_h being the distance between the wing and horizontal stabiliser aerodynamic centre. This means that logically, the tail distance from the wing determines the magnitude of the downwash on the stabiliser.

Lastly, the aircraft pitching moment about its aerodynamic centre $C_{m_{ac}}$ had to be found. This coefficient once again consists of multiple contributions. Namely, the wing, fuselage, and landing flaps contribution. Of these, the wing and flaps both have a large negative contribution to this moment, with the fuselage only having a small contribution. The wing, fuselage, and flaps contributions are given by Equation 11.13, Equation 11.14, and Equation 11.15 respectively[47].

$$C_{m_{ac_w}} = C_{m_{0,airfoil}} \left(\frac{AR}{AR+2} \right) \quad (11.13) \qquad C_{m_{ac_{fus}}} = -1.8 \left(1 - 2.5 \cdot \frac{b_f}{b} \right) \frac{\pi b_f h_f l_f}{4 \cdot S\bar{c}} \frac{C_{L_0}}{C_{L_{\alpha_{A-H}}}} \quad (11.14)$$

$$C_{m_{ac_{flap}}} = \mu_2 \left\{ -\mu_1 \Delta C_{l_{max}} \frac{c'}{c} - \left[C_{L_{A-H}} + \Delta C_{l_{max}} \left(1 - \frac{S_{wf}}{S} \right) \right] \frac{1}{8} \frac{c'}{c} \left(\frac{c'}{c} - 1 \right) \right\} - C_{L_{land}} (0.25 - \bar{x}_{ac}) \quad (11.15)$$

Where $C_{m_{0,airfoil}}$ could be readily imported from the flow5 analysis of the wing airfoil, and μ_1 and μ_2 are statistical parameters depending on the flap span and deflection[47]. The remaining flap parameters have been defined previously in Section 9.1. The difference between $C_{L_{land}}$ and $C_{L_{A-H}}$ is defined by the fact that the former concerns full aircraft lift, while the latter only concerns the lift without the downforce of the horizontal stabiliser during landing. Since $C_{L_{land}}$ was know, the lift coefficient with tail could be found using Equation 11.16. Where C_{L_h} is the maximum downforce the tail can provide during landing, found from the elevator sizing.

$$C_{L_{A-H}} = C_{L_{land}} - C_{L_h} \left(\frac{V_h}{V} \right)^2 \frac{S_h}{S} \quad (11.16)$$

With all parameters now defined, the scissor plot could be constructed for any configuration considered during this part of the design process. Figure 11.4 shows the scissor plot for the final iteration of the HA-1 aircraft. A neutral stability margin of 5% MAC has been used to make sure the CG is always in front of the neutral point. Furthermore, the CG range found using Figure 11.1 has been included. It should be noted that the CG range does not precisely fit between the lines of the plot, with a small gap being left at the stability side. This is a result of the iterative process, as the plot is very sensitive to changes in tail size due to the effects of propwash. After all, out of all the iterations, this configuration produced the smallest stabiliser surface area.

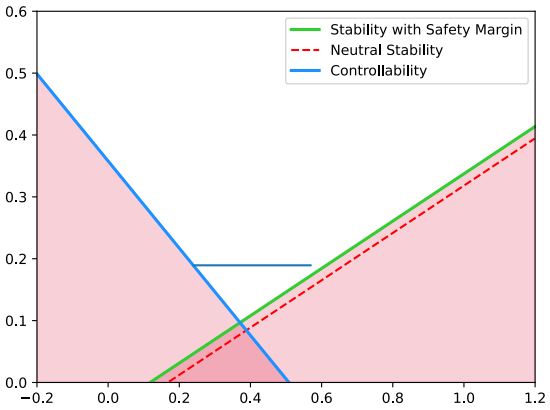

Figure 11.4: Scissor Plot of the HA-1 Aircraft, including CG excursion

11.3.3. Elevator Sizing

An integral part of the horizontal stabiliser is the elevator, used to provide longitudinal (pitch) control. Since the sizing of the elevator is usually left to the detailed design phase, in which more detailed aircraft characteristics are known than they were at this stage of the design, the preliminary sizing method of Al-shamma has been used and adapted to the existing stability design[49]. As the method describes, an elevator-to-stabiliser span ratio $\frac{b_e}{b_h}$ and elevator deflection δ_e were chosen first to be 1.0 and $\pm 25^\circ$ respectively.

Next, the required tail lift was calculated for the limiting situation of take-off rotation for all combinations

of mass and CG. Once again drag was neglected as a conservative estimation since precise data on the drag in take-off configuration was not readily available. In return, the moment of rotation was taken as the static equilibrium since the full aircraft moment of inertia is difficult to determine at this time. These assumptions lead to Equation 11.17.

$$L_h = \frac{1}{(l_h - l_w)} \left(C_{L_{TO}} \frac{1}{2} \rho_{TO} V_{TO}^2 S \cdot l_w - T_{TO} Z_{ptr} - W \cdot l_{cg} + C_{m_{w_{fl}}} \frac{1}{2} \rho_{TO} V_{TO}^2 S \bar{c} \right) \tag{11.17}$$

Where l_w is the distance of the wing AC to the main gear point of contact, $C_{L_{TO}}$ is the lift coefficient during the take-off ground roll, l_{cg} is the distance of the CG to the main gear point of contact, and $C_{m_{w_{fl}}}$ is the moment coefficient of the flapped wing. With the absolute tail lift known, the required lift coefficient could easily be found using Equation 11.18. This lift coefficient is achieved at the stabiliser angle of attack given by Equation 11.19.

$$C_{L_h} = \frac{2 \cdot L_h}{\rho_{TO} S_h \left(\frac{V_h}{V} V_{TO} \right)^2} \tag{11.18}$$

$$\alpha_h = \alpha_{TO} \left(1 - \frac{d\epsilon}{d\alpha} \right) + i_h - \epsilon_0 \tag{11.19}$$

Where i_h is the installation angle of the horizontal stabiliser, and ϵ_0 is the tail downwash at zero angle of attack. Using the values from Equations 11.18 and 11.19, the elevator chord ratio could be found using the elevator effectiveness of Equation 11.20 and then by solving Equation 11.21 for $\frac{c_e}{c}$.

$$\tau_e = \left| \frac{C_{L_h} + C_{L_{\alpha_h}} \alpha_h}{C_{L_{\alpha_h}} \delta_e} \right| \tag{11.20}$$

$$\tau_e = -6.624 \left(\frac{c_e}{c} \right)^4 + 12.07 \left(\frac{c_e}{c} \right)^3 - 8.292 \left(\frac{c_e}{c} \right)^2 + 3.295 \left(\frac{c_e}{c} \right) + 0.004942 \tag{11.21}$$

For the final design iteration the value for $\frac{c_e}{c}$ was found to be 0.3, meaning that 30% of the horizontal stabiliser is the elevator. This also means the hinge line, used to determine the stabiliser size, is placed at 70% of the chord. During the design process, the limit for the chord ratio has been placed at 40% where the method recommends 50% [49]. This was done to apply an extra margin of safety necessary due to the assumptions made for the moment equilibrium.

11.3.4. Longitudinal Stability Design Iteration

Now that all the separate components of longitudinal stability were found, they needed to be combined and optimised. This optimisation is a highly iterative process, with multiple iteration loops needing to be performed at the same time to come to a converged design. The main parameters that were iterated upon are the wing and undercarriage placement, stabiliser size and accordingly l_h and η_h, and the battery location in the fuselage. Below a brief overview of the iteration process is given:

1. A value of the OEW CG location on the wing $OEW_{\bar{c}}$ was chosen between -0.2 to 0.5. Then a value for the battery CG location was chosen between 0.2 and 0.8 of the fuselage length.
2. Using initial guesses, the wing was placed on the fuselage using Equation 11.22. A lower limit of $x_{LEMAC} > 3.2$ m was used to make sure the wing did not move outside of the fuselage.
3. The preliminary CG excursion was determined without the weight of the undercarriage, and undercarriage sizing was performed using this CG excursion. Additionally, the battery was split to allow for gear retraction.
4. Iteration of wing position: The new OEW CG was now calculated including the undercarriage. Then, the revised undercarriage position was calculated, before updating the wing position. This was iterated until the wing position converged.
5. The elevators were sized with the current horizontal stabiliser dimensions to check whether take-off rotation was possible with the previously found wing and undercarriage placement. If it was found that the elevator would exceed the maximum size, the loop was broken and the next

battery CG position was chosen for a new attempt.

6. Iteration of stabiliser size: A value for $\frac{S_h}{S}$ was chosen and l_h was calculated. Then the scissor plot was constructed and the required CG excursion was checked against the plot for the stabiliser size. In case the CG excursion did not fit in between the lines, a larger $\frac{S_h}{S}$ was chosen as the next iteration
7. End of iteration: After the entire range of $OEW_{\bar{c}}$ and battery CG location had been iterated over, the smallest value for $\frac{S_h}{S}$ was chosen and corresponding parameters were saved.

$$x_{LEMAC} = x_{fuselage} + \bar{c}\left[\left(\frac{x}{\bar{c}}\right)_{wing}\frac{M_{wing}}{M_{fuselage}} - \left(\frac{x}{\bar{c}}\right)_{OEW_{\bar{c}}}\left(1+\frac{M_{wing}}{M_{fuselage}}\right)\right] \tag{11.22}$$

11.3.5. Vertical Stabiliser Sizing

The vertical stabilizer plays a crucial role in the lateral stability of the aircraft. During this phase of the design process, the weathercock stability was chosen as the condition to be used to size the vertical tail. A fast procedure can be implemented to make sure the C_{n_β} is always positive by using the graph in Figure 11.5.

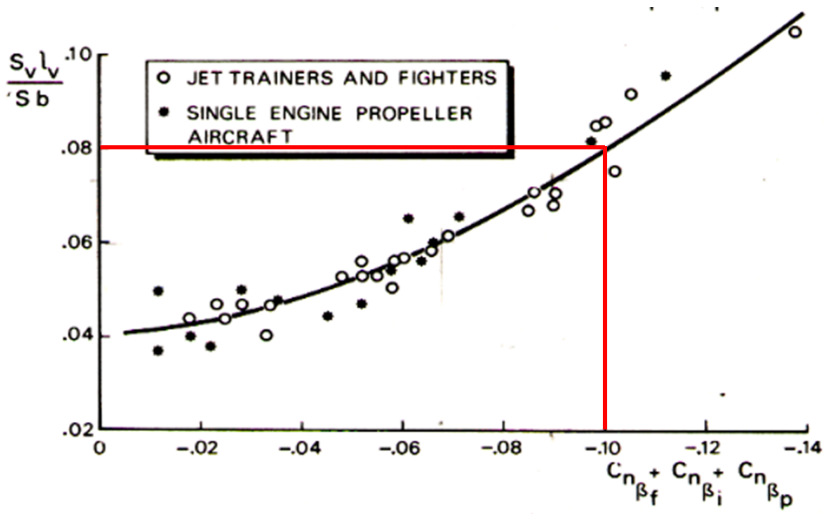

Figure 11.5: Weathercock Stability Derivatives [45]

In order to be able to use the aforementioned graph, the contribution to the weathercock stability derivative of the fuselage, wing and propeller has to be calculated. Since the aircraft uses a high-wing configuration the contribution of the wing is already known to be -0.017 [45]. Secondly, the propeller contribution can be calculated using Equation 11.23:

where B_p is the number of blades per propeller, l_p is the distance from the propeller to the aircraft c.g., D_p is the propeller diameter, S is the wing surface area, and b is the wingspan. By using the calculated aircraft parameters, the propeller contribution was calculated to be equal to -0.005.

Finally, the fuselage contribution can be calculated using the following formula with the parameters described in Figure 11.6:

$$C_{n_{\beta_p}} = -0.053 B_p \sum \frac{l_p D_p^2}{Sb} \quad (11.23)$$

$$C_{n_{\beta_f}} = -k_\beta \frac{S_{fs} l_f}{Sb} \frac{h_{f_1}}{h_{f_2}}^{0.5} \frac{b_{f_2}}{b_{f_1}}^{0.5} \quad (11.24)$$

$$k_\beta = 0.3 \frac{l_{cg}}{l_f} + 0.75 \frac{h_{f_{max}}}{l_f} - 0.105 \quad (11.25)$$

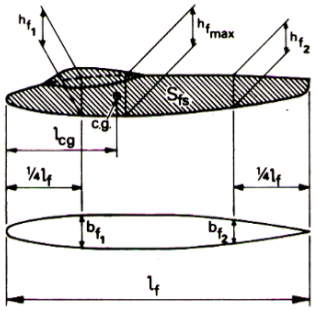

Figure 11.6: Fuselage Dimensions

Plugging the aircraft parameters obtained from the CATIA model and the previous subsystems that were sized, the contribution of the fuselage was calculated to be -0.081. Thus, the sum of the three contributions is equal to -0.103. Looking at the graph in Figure 11.5, the tail volume is equal to 0.08. By using the statistically determined dimensions of the vertical tailplane presented in [12], and ensuring the tailplane fits on the fuselage, the final dimensions were established, and the values are tabulated in Chapter 13.

11.3.6. Aileron Sizing

The ailerons represent control surfaces that are used for the roll motion of the aircraft. CS-23 defines specific turn times that the aircraft has to achieve in certain conditions **HA-UR-04-STB-17**, **HA-UR-04-STB-18**. Thus, a sizing procedure had to be implemented to make sure that the designed ailerons meet the aforementioned requirements.

The turn rate can be calculated using the formula from [19]:

$$P = -\frac{C_{l_{\delta_a}}}{C_{l_P}} \delta_a \frac{2V}{b}, \quad (11.26)$$

where $C_{l_{\delta_a}}$ and C_{l_P} can be found using Equation 11.27 and Equation 11.28 from [19]:

$$C_{l_{\delta_a}} = \frac{2 c_{l_\alpha} \tau}{Sb} \int c(y) y dy, \quad (11.27) \qquad C_{l_P} = -\frac{4(c_{l_\alpha} + c_{d_0})}{Sb^2} \int y^2 c(y) dy, \quad (11.28)$$

where the integrals are evaluated in the first case between the start and end point of the aileron, and in the second case over the entire wingspan. τ represents the aileron effectiveness which is a function of the hinge line position and can be chosen based on Figure 11.7. The maximum effective deflection of the aileron was chosen to be set at 14° based on aircraft statistics [19], while the other geometric parameters are defined in Figure 11.8.

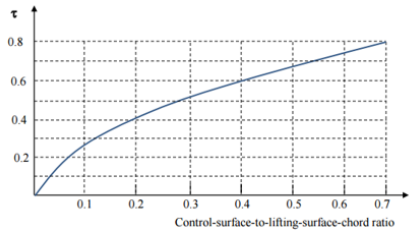

Figure 11.7: Aileron Effectiveness [19]

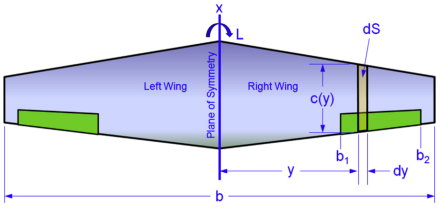

Figure 11.8: Aileron Dimensions Scheme [19]

Plugging in the parameters in the aforementioned formulas results in some final values that are tabulated in Chapter 13.

Additionally, the aileron had to be sized such that the control forces applied to turn the aircraft did not exceed the values stipulated in CS-23 regulations **HA-UR-04-STB-12**. To be able to calculate the required stick arm length such that the required force will not exceed the value stipulated in the requirement, the following formula was used:

$$arm_{stick} = \frac{abs(HM)}{222}, \tag{11.29}$$

where HM is the hinge moment that can be calculated by multiplying the hinge moment coefficient C_h with the dynamics pressure at certain conditions, the hinge arm, and the surface of the aileron. The hinge moment coefficient is given by Equation 11.30:

$$C_h = C_{h_0} + C_{h_\alpha}\alpha + C_{h_\delta}\delta, \tag{11.30}$$

where C_{h_0} is the hinge moment at 0° angle of attack taken from XFLR5, C_{h_α} is the variation of hinge moment with the angle of attack for the 3D wing, C_{h_δ} is the variation of hinge moment with the aileron deflection for the 3D wing. Roskam method was used to size the last two stability derivatives which is described in [48] pages 467-485.

After following the sizing procedure presented in the literature, a value of -0.38 per rad was obtained for C_{h_α}, while C_{h_δ} was found to be equal to -0.73 per rad. Using the value of 0.035 of C_{h_0}, and the chosen maximum deflection of 14°, the following values were found for cruise, take-off, and landing conditions for the stick arm length: 0.21m, 0.12m, and 0.09m respectively. Thus, the most critical case is given by the cruise conditions which require a stick length of at least **21cm** to keep the force below 222N.

12 | Propulsion & Power Design

The design of the propulsion and power subsystem is key to to achieve the targeted 50% emissions reduction, as the burning of fuel in the engine is responsible for the vast majority of CO_2 emissions. In previous design phases, it was determined that a hybrid-electric propulsion system was best to achieve the goals of this project, and this chapter focuses on designing that system. Focusing first on the propulsion part of the design, in Section 12.1, a trade-off is performed to decide which type of hybrid-electric architecture is used. With that decided, various commercially available components can be selected: the combustion engine in Section 12.2, the electric motor in Section 12.3 and the propeller in Section 12.4. The general layout of the propulsion system, including the fuel system, is then in Section 12.5, while the layout of the electrical system is determined in Section 12.6. Finally, as the propulsion system generates the most noise in the aircraft, a noise analysis is presented in Section 12.7.

12.1. Hybrid Architecture Trade-Off

There are 3 main architecture options for a hybrid-electric powerplant: serial, parallel, or series-parallel. In a serial hybrid powerplant, the combustion engine drives an alternator which feeds into an electric system also connected to a battery, and an electric motor which provides the mechanical power (in an aircraft, by driving the propeller). Meanwhile, in a parallel hybrid system, the combustion engine and electric motor (connected to the battery) both directly drive a shaft connected to the propeller, linked to each other via a gearbox or clutch. Finally, a series-parallel system combines both approaches, with the combustion engine driving both the shaft and an alternator, allowing it to directly provide mechanical power, and power the electric system.

Each option has its own merits and downsides, and a trade-off was therefore performed to establish the one most suited for the HA-1 aircraft. This trade-off was performed in accordance with the procedure defined in Section 5.2. Accordingly, a set of scoring criteria and corresponding weights were first defined, as presented in Table 12.1.

With the criteria defined, the various design options can be scored according to the defined ranking strategy.

In terms of efficiency, the parallel and series-parallel configurations have roughly the same efficiency, as both the motor and engine directly drive the shaft with the propeller. The serial configuration has lower efficiency, however, as mechanical energy is converted to electrical energy and back, introducing losses. These losses are not too great, however (only in the order of 10-20%) [50, 51], so the parallel and series-parallel options get the highest score (5), while the serial one gets one mark lower (4).

When it comes to reliability, the parallel and series-parallel options are fail-safe, as either power source (motor or engine) can provide full power. The series-parallel does have more components, however, leading to more maintenance and a higher likelihood of failure. For the series option, the motor can provide power if the engine fails, but the reverse is not possible, so it is not fail-safe. Nevertheless, modern components are very reliable, and this setup is still more reliable than for conventional aircraft. The parallel option therefore receives the highest score (5), and the two others get one mark lower (4).

In terms of geometric layout, both the parallel and series-parallel options force a restricted layout, as the combustion engine must be in the same location as the propeller (unless a long and heavy shaft is used), while the series option allows for more freedom. The series option therefore receives the highest score (5), while the other two get the worst possible (1).

As for cost, the difference between the options lies in the ‘linkage’ components, notably a clutch for the parallel option, an alternator for the series option, and both for the series-parallel option. Alternators

are significantly more expensive than clutches[(a)] [52], so the parallel option gets the highest score (5), the serial gets a mid-range score (3), and the series-parallel, needing both, gets the worst one (1).

Finally, with regards to weight, the analysis is similar to cost, as clutches are much lighter than alternators[(a)] [52]. The scores are therefore also the same as for cost.

A summary of these scores, along with the weighted results, is presented in Table 12.2. It can be clearly seen that the parallel hybrid architecture is the superior architecture, scoring highly in efficiency, reliability, cost and weight.

Table 12.1: Trade-off Criteria for the Hybrid Architecture Selection, Along with Respective Weights

Criterion	Justification	Accounts for	Ranking Strategy	Weight	Weight Justification
Efficiency (EFF)	To achieve the desired emissions reduction, the energy usage should be as low as possible.	Fuel burn (and therefore emissions), energy cost, effect on fuel and battery weight	Quantitative: efficiency estimate based on literature	0.35	This will have a big impact on operating costs and emissions.
Reliability (RLB)	The aircraft must be rated for IFR, and as it is single-engine, the propulsion system must be highly reliable.	Reliability of components, whether the layout is fail-safe, and also safety and availability	Quantitative: how many parts does each architecture have, how complex/reliable is each component	0.25	This will play a big role in maintenance/ overhaul cost, overall aircraft reliability/availability, and (IFR) certification cost.
Geometric Layout (GLY)	Some configurations may force certain layouts of components, negatively affecting stability and structural considerations	Effect on structures and stability (ground and airborne)	Qualitative: does the architecture allow for choice of layout?	0.10	While it has an effect on stability and structures, the layout is not expected to be an insurmountable problem
Cost (CST)	Since MAF is funded by donations, costs in all respects are desired to be as low as possible.	Effect on unit cost of the aircraft (unit cost of components, development cost, development risk)	Quantitative: component cost estimation (of components that differ)	0.10	Cost is a major factor for this aircraft, but the operating costs are already accounted for in other criteria.
Weight (WGH)	Affects overall aircraft weight and therefore cost, both directly and indirectly (snowball effect).	'Linkage' components (i.e. those that differ): gearbox, alternator, wiring. Also accounts for the expected snowball effect	Quantitative: component weight estimation (of components that differ)	0.20	The snowball effect can be very significant and thus this criteria can have a major impact. Nevertheless, the difference lies in the smaller components of the subsystem.

Table 12.2: Summary of Hybrid Architecture Trade-off

	EFF	RLB	GLY	CST	WGH	
	0.35	0.25	0.10	0.10	0.20	**Score**
Serial	4	4	5	3	3	3.8
Parallel	5	5	1	5	5	4.6
Series-Parallel	5	4	1	1	1	3.15

12.2. Combustion Engine Selection

With the architecture of the propulsion system decided upon, its various components could be selected based on commercially available options. The first to be selected was the combustion engine.

[(a)] URL: `https://aerospace.honeywell.com/us/en/products-and-services/product/hardware-and-systems/electric-power/250kw-generator` [accessed 5 June 2024]

It had been previously determined that a reciprocating engine is the best engine type for the mission thanks to its low cost and high efficiency [12]. Given the requirements that the engine run on jet fuel (**HA-UR-07-PRO-13**), and the power requirement of 292 kW (**HA-UR-03-PRO-08**, **HA-UR-05-PRO-12**), few options were commercially available. In fact, when considering that the engine should already be certified for aircraft use, only one choice was possible: the RED A03 family, by Raikhlin aircraft Engine Developments (RED)[(b)]. All engines meet the requirements, so the cheapest and lightest option was selected: the RED A03-003 [53].

The RED A03-003 is highly efficient twin-turbo V12 engine, delivering up to 500 hp (368 kW). The full specifications of the engine are presented in Table 12.3, while a two-view drawing along with dimensions is presented in Figure 12.2. While the engine produces significantly more power than required, its high power-to-weight ratio of 1.01 kW/kg means it is only around 30% heavier than a Continental CD-300 (the next most powerful jet fuel aircraft piston engine), while producing 67% more power [54]. The additional power also means that the aircraft can take off in shorter distances (see Chapter 14). The engine design requires an air intake to be placed on its underside, so an intake is placed in the bottom part of the nose, as seen in Figure 12.1.

Table 12.3: Specifications of the RED A03-003 Engine[(b)]

Fuel Type	Jet A-1
Take-Off Power (5 min)	368 kW
Maximum Continuous Power	338 kW
Dry Mass (inc. gearbox)	363 kg
P/W engine	1.01kW/kg
Maximum Efficiency (at 223 kW)	40%
Unit Cost (inflation adjusted)	US$232 220[(c)]

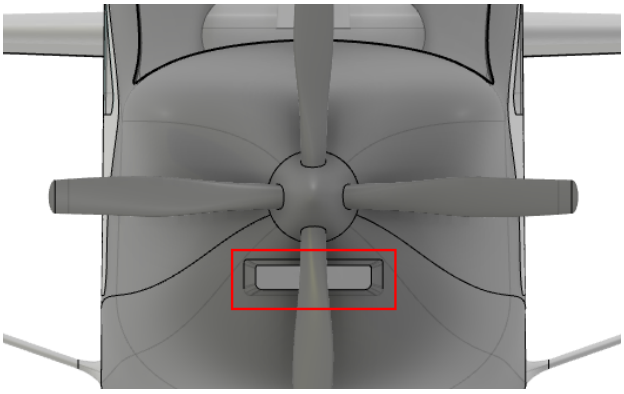

Figure 12.1: View of the Engine's Air Intake in the Aircraft's 3D Model

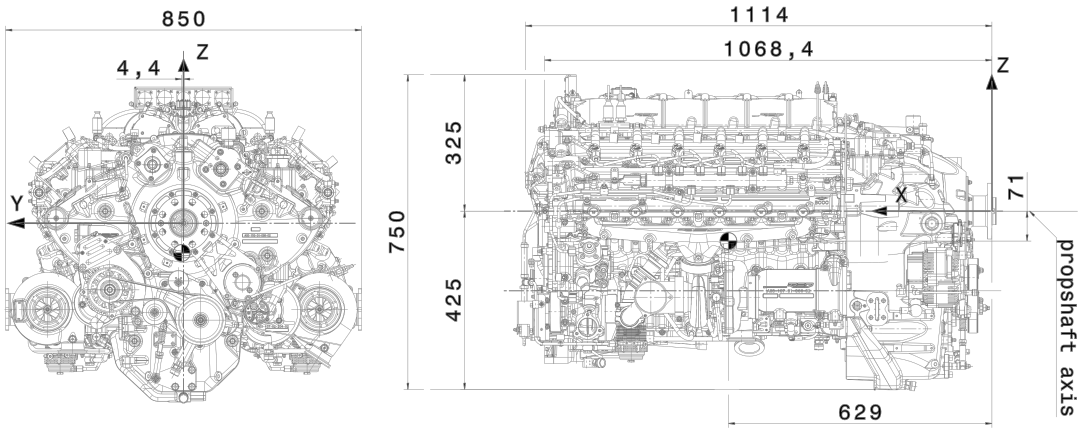

Figure 12.2: Front- and Side-view Drawings of the RED A03-003 Engine[(b)]. (All dimensions are in mm.)

[(b)]URL: `https://red-aircraft.de/red-a03-003/` [accessed 3 June 2024]

[(c)]URL: `https://www.avweb.com/news/500-horsepower-v-12-turbo-diesel-engine-from-germany/` [accessed 10 June 2024]

12.3. Electric Motor Selection

The other main component of a hybrid-electric propulsion system is the electric motor. Given the power requirement of 292 kW (**HA-UR-03-PRO-08**, **HA-UR-05-PRO-11**), and the fact that electric propulsion is not yet common in aircraft, few electric motors are commercially available and certified for use in aircraft. In fact, the only motor that does meet these requirements, and isn't too overpowered and therefore heavy, is H3X Technologies' HPDM-350 [55].

The H3X HPDM-350 is an integrated motor drive (i.e. an inverter is included, and DC power can be provided directly from the battery), with a high power-to-weight ratio of 10.8 kW/kg. A full list of specifications is available in Table 12.4. The motor has a built-in liquid cooling system, with the radiators placed on the outside of the motor[(d)]. Some of the air from the engine air intake will be passed through these radiators.

Table 12.4: Specifications of the H3X HPDM-350 Electric Motor [55]

Take-Off Power	380 kW	Length	0.176 m
Maximum Continuous Power	350 kW	Diameter	0.540 m
Mass	35 kg	Unit Cost	US$100 000[(e)]

12.4. Propeller Selection

The mechanical energy produced by the engine and/or electric motor must be transformed into kinetic energy by means of a propeller. Propellers are often specifically designed for each type of aircraft, but given the limited time before delivery of the aircraft, it was decided to use a commercially available one.

Only two commercially available and certified propellers were able to meet the power required and were not overpowered and thus too heavy and costly. These were the 4HFR34C763 propeller by McCauley (initially intended for the Cessna 208EX) [56], and the HC-B3TN-2 propeller by Hartzell (initially intended for the Cessna 206) [57]. While the Hartzell propeller is around 10% lighter, it is almost twice as expensive[(f)], and can only transmit powers marginally above the maximum power of the combustion engine (368 kW, while the propeller's maximum power is 372 kW). Furthermore, the Hartzell propeller cannot transmit the full power of the electric motor (380 kW), which could for example be useful in case of a shorter runway. It was therefore decided to use the McCauley 4HFR34C763 propeller, the specifications of which are given in Table 12.5.

Table 12.5: Specifications of the McCauley 4HFR34C763 Propeller [56].

Maximum Continuous Power	410.1 kW	Diameter	2.286 m
Number of Blades	4	Material	Aluminium
Mass	60.3 kg	Unit Cost	US$50 000[(f)]

12.5. Propulsion System Lay-Out

The choice of a parallel hybrid architecture implies a constrained geometric layout, with both the engine and the electric motor needing to be in the nose of the aircraft, close to where the propeller is. The HPDM-350 electric motor can have a shaft pass entirely through it, so the chosen layout is to have a single shaft connecting the combustion engine to the propeller, with the electric motor mounted in between. An overrunning clutch [52] is placed at the connection of the engine to the shaft, to allow the

[(d)] URL: `https://h3x.tech/` [accessed 17 June 2024]
[(e)] Information provided by email by H3X Technologies.
[(f)] URL: `https://ottosenprop.com/products/` [accessed 5 June 2024]

shaft to automatically disconnect from the engine when the electric motor is providing power. This layout can be seen in detail in Figure 12.3. When the engine is providing power, the motor does not need to be disconnected as its resistance to spinning is minimal. The motor can be disconnected from the rest of the electric circuit to avoid it acting as an alternator. The electrical system is expanded upon in Section 12.6.

During all stages of flight and operation, the RED A03 engine needs to be supplied with enough fuel to allow for the desired power output. With a required fuel flow of 85 kg/h[g] and a design safety margin of 1.5 [58], this leads to a fuel flow of 127.5 kg/h or 160 L/h for which the fuel system shall be designed. The fuel is stored in the inboard section of the wing, between the strut and the fuselage, where more than enough space is available to store the previously found 365 L of fuel. Since the aircraft is configured with a high wing, a gravity-fed single-pump fuel system is used to deliver the fuel to the engine. A cross-feed valve or pump is not necessary since the fuel tanks are located close to the centre-line of the aircraft and will thus not have a large effect on lateral stability. Each tank is fitted with a ram-air vent and fuel sump system to ensure correct pressurisation and to enable inspection of the fuel [58]. A schematic of the fuel system layout is also available in Figure 12.3.

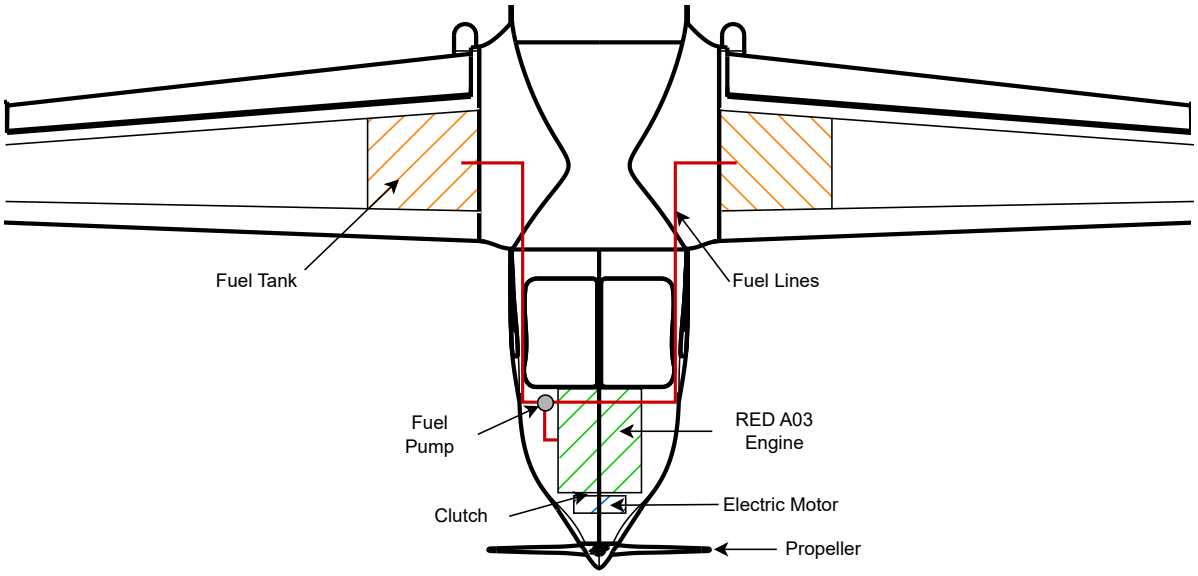

Figure 12.3: Layout of the Propulsion System

12.6. Electric Block Diagram

The electric block diagram can be visualised in Figure 12.4. The engine circuit and the battery circuit run in parallel. They are activated using a contactor placed in the cockpit of the aircraft. Since none of them is delivering the required voltage directly to the other subsystems, a converter is used to make sure the 28V is delivered at the two separate busses. Protection is added on the circuit between the two power sources and the two respective busses such that the subsystems or the busses will not be affected in case of a malfunction. Additionally, inverters are added such that in case AC current is required by other subsystems, the 28V DC current can be transformed accordingly. All the instruments in the cockpit will run directly on 28V DC current such that no change is required. The primary inverter is equipped on the engine side, while a secondary inverter is mounted on the battery side of the electric circuit. In case a malfunction is detected in one of the two branches, the pilot can decide to switch to the other branch and rely solely on it. Two ground plugs are present: one for charging the batteries from the ground charging system, and one mounted on the engine branch that can be used to power the instruments and other subsystems without running the engine or the batteries. Finally, an internal

[g] URL: `https://red-aircraft.de/red-a03-003/` [accessed 3 June 2024]

switch is used to make sure the battery and engine are not engaged at the same time to prevent charging of batteries during the flight.

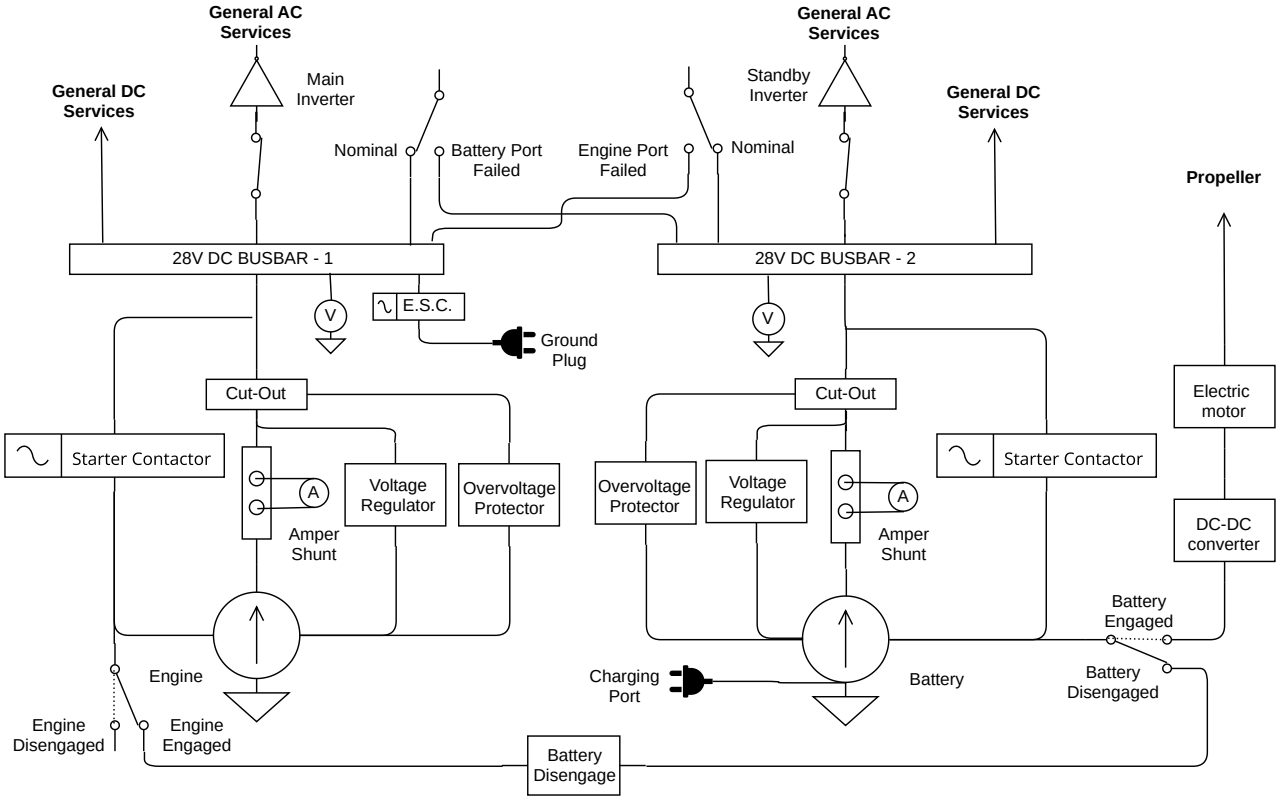

Figure 12.4: Electric Block Diagram of the HA-1 aircraft showcasing the two parallel circuits used to power the aircraft subsystems

12.7. Noise

The noise generated by the aircraft needs to comply with the threshold imposed by the regulators. According to **HA-UR-04-OPE-01** the aircraft shall not produce more than 80dBA of sound at 2500m from the aircraft. The main sources of noise at that distance are the V12 engine used and the propeller. In the following paragraphs, the procedure used to size the noise from the identified sources will be presented for both cruise and take-off conditions - landing is disregarded since during this flight phase only the batteries are used to drive the propeller making the noise significantly lower than in the other two cases.

Firstly, for the propeller, the procedure used to measure the noise produced was taken from [59]. The A-weighted noise level can be calculated using Equation 12.1:

$$SNL_{weighted,prop} = SNL_{prop} - 14dB = FL_1 + FL_2 + FL_3 + DI + NC + PNL - 14dB, \quad (12.1)$$

where FL_1 is a partial level based on the power delivered to the propeller and its rotation tip speed, FL_2 is an adjustment that takes into account the diameter and the number of blades of the propeller, FL_3 accounts for atmospheric absorption and spherical spreading of the sound to the observation point, DI is the correction for the directivity pattern, PNL represents the perceived noise level that can be computed based on statistical data, and NC accounts for the number of propellers - in the case of the HA-1 aircraft that is equipped with only one propeller, NC is equal to **0dB**.

Using Figure 1 and Figure 2 from [59] and the propeller's geometrical data, the blade tip Mach number was computed to be equal to 0.78 during cruise and 0.75 during take-off. Based on the previously calculated tip Mach number, the delivered power, and Figure 3 from [59], FL_1 was computed to be

78dB for cruise and **84dB** for take-off.

FL_2 was found based on Figure 4 from [59]. The number of propeller blades is equal to 4, the diameter of the propeller is also known, so a value of **7dB** was deducted from the aforementioned graph [59] - the value is the same for both take-off and cruise condition.

FL_3 is deduced from Figure 5 in [59], and taking into account that the noise has to be measured at 2500 m from the aircraft. A value of **-26dB** is found for both cruise and take-off flight phases. A similar procedure is used also for the directivity index DI. The worst value from the graph in Figure 6 [59] was chosen for both cases, resulting in a value of **1dB**.

Lastly, the PNL can be computed using Figure 9 from [59] and is found to be equal to 4.5dB for cruise and 4dB for take-off. Thus, by using Equation 12.1, the non-weighted sound-noise level is equal to **64.5dB** for cruise and **70dB** for take-off.

Now, that the propeller noise has been computed, the engine noise needs to be calculated and added to the aforementioned values. For the measurement of its noise level, Equation 12.2 presented in [60] combined with the available data from [61] is used.

$$SNL_{engine} = L_w + 10 \log \frac{P_{engine}}{P_{exp}} - 20 \log \frac{2500}{914} + DI, \tag{12.2}$$

Here, L_w is the reference engine power level which is calculated as the average noise level of the engines 17-30 in Table 1 from [61], P_{engine} is the engine power in cruise/take-off conditions, P_{exp} is the average power of the engines 17-30 in Table 1 from [61], and third term refers to the distance correction factor due to the fact that experimental data from [61] is measure at 914 m, and DI is the same directivity index as previously calculated for the propeller. Given this, the engine noise level is measured at **71dB** during cruise and **73.5dB** during take-off.

To obtain the total weighted noise level of the two sources, the calculated values are transformed from dB to W/m^2, added together, and then converted back to dB - subtract 14dB to obtain the weighted sound level in dBA. The final values are **58dBA** for cruise and **61dBA** for take-off.

13 | Aircraft Parameters

With sufficient details for each subsystem's procedures now made in the previous chapters, the preliminary design of the HA-1 aircraft can be finished. This chapter contains all of the parameters derived from both the design tool created but also hand calculations. A compressive overview can be found in Table 13.1. Also, a visual representation of the design including all of the sized subsystems can be seen in Table 13. This synthesis marks the end of the preliminary design phase of the aircraft and sets the starting point of a possible detailed design analysis process.

Table 13.1: Overview of Design Parameters for the **HA-1** Aircraft

Parameter	Value	Unit	Parameter	Value	Unit
Fuselage			Vertical Stabiliser		
Fuselage Length	12.05	[m]	Surface Area	5.62	[m^2]
Seats Abreast	2	[-]	Leading Edge Sweep	36	[°]
Top Width	1.83	[m]	Span	2.9	[m]
Bottom Width	1.83	[m]	Root Chord Length	2.67	[m]
Height	1.2	[m]	Tip Chord Length	0.88	[m]
Wing Mounting Method	High Wing Strut-braced	[-]	x_{cg}	0.9	[MAC]
Main Wing			Stability		
Surface Area	26.13	[m^2]	Stability Margin	0.05	[-]
Quarter Chord Sweep	0	[°]	Undercarriage		
Span	16.95	[m]	Strut Height Main Nose	0.82	[m]
Root Chord Length	2.2	[m]	CoG offset Nose Gear	5.09	[m]
Tip Chord Length	0.88	[m]	CoG offset Main Gear	0.8	[m]
Aerofoil	FX 63-137	[-]	Wheel Diameter Nose	0.435	[m]
x_{LEMAC}	3.8	[m]	Wheel Diameter Main	0.556	[m]
Horizontal Stabiliser			Propulsion		
Surface Area	5.47	[m^2]	Number of Engines	1	[-]
Quarter Chord Sweep	9.72	[°]	Engine Type	Reciprocating	[-]
Span	5.22	[m]	Engine Length	1.114	[m]
Root Chord Length	1.49	[m]	Engine Width	0.85	[m]
Tip Chord Length	0.6	[m]	Engine Height	0.75	[m]
Aerofoil	NACA0012	[-]	Engine Mass	363	[kg]
x_{cg}	3.57	[MAC]	Motor Mass	35	[kg]
Aileron			Flaps		
Start Position	0.77	[%span]	c'/c	1.075	[-]
End Position	0.95	[%span]	Surface	15.62	[m^2]
Roll Rate	9.89	[°/s]	Deflection Landing	45	[°]
$C_{L_{\delta_a}}$	6.24	[1/°]	Deflection Take-off	45	[°]
C_{L_P}	-0.03	[1/°]	Flap Start	0.16	[%span]
Turn Time	6.06	[s]	Flap End	0.72	[%span]
Hinge Position	0.35	[% chord]	$\alpha_{Landing}$	10.15	[°]
Stick Arm	0.35	[m]	$\alpha_{Take-Off}$	13.14	[°]
Overall					
Maximum Take-off Weight		3584		[kg]	
Operating Empty Weight		2696		[kg]	
CO_2 Reduction Old Technology		37		[%]	
CO_2 Reduction New Technology		70		[%]	

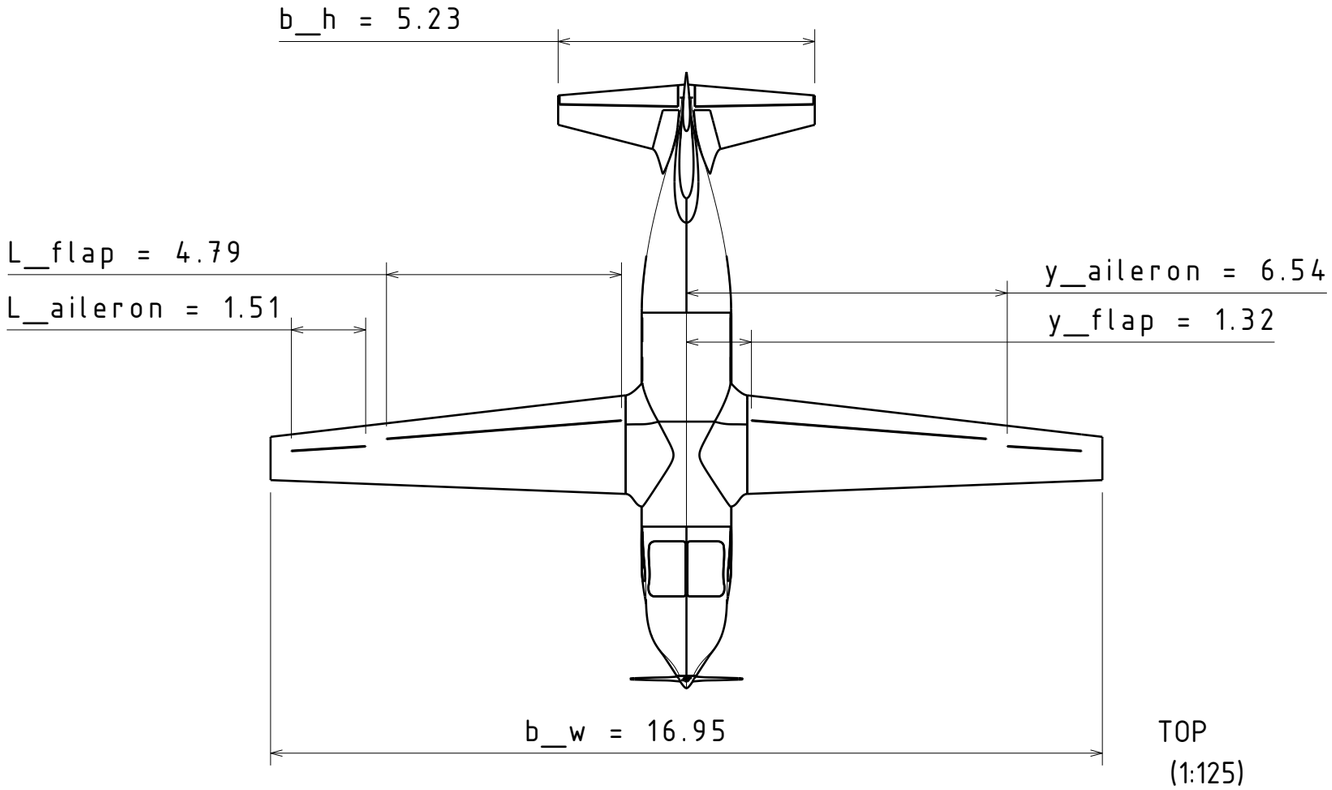

TOP
(1:125)

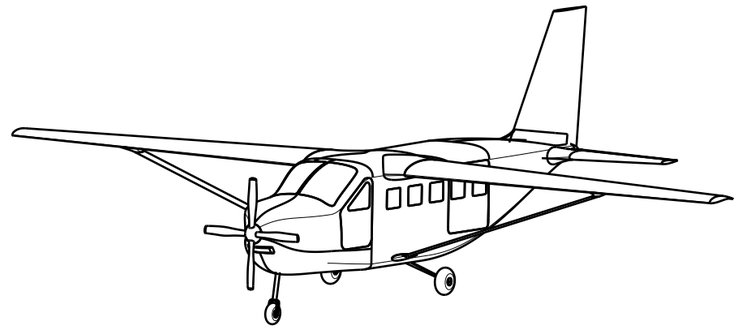

ISOMETRIC
(1:125)

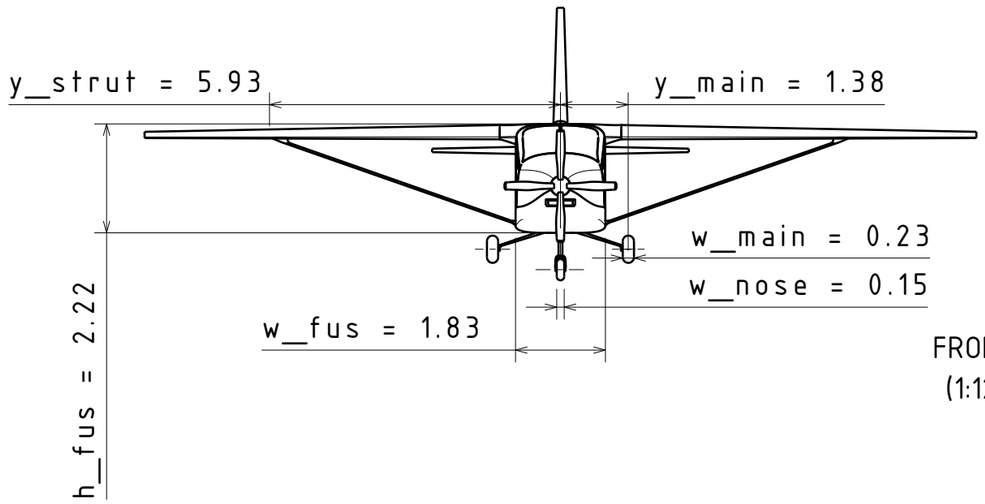

FRONT
(1:125)

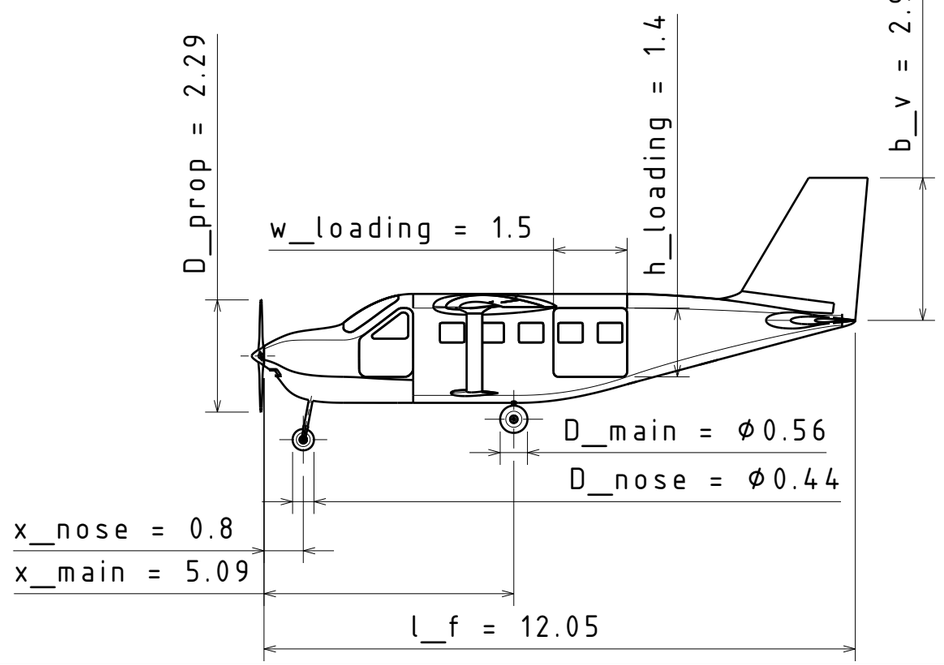

RIGHT
(1:125)

All dimensions are provided in [m].

HumanAir			HumanAir		
DRAWN BY: Mika Ruyssenaars	DATE: 18/06/2024		DRAWING TITLE: HumanAir HA-1 Geometrical Overview		
CHECKED BY: Nicholas Cantar	DATE: 18/06/2024	SIZE: A3	DRAWING NUMBER: 001	REV: A.1	
DESIGNED BY: HumanAir	DATE: 19/06/2024	SCALE: 1:125	MTOW(kg): 3179.13		SHEET: 1/1

14 | Flight Performance Analysis

To see whether the aircraft meets all requirements on flight performance, this chapter will introduce a worked-out analysis of all important flight performance parameters. To do this, first, the model that was used to analyse the aircraft is presented in Section 14.1, after which the results are presented and discussed in Section 14.2.

14.1. Method for Performance Analysis

In this section, the methods behind the various flight performance calculations are discussed. First, the underlying drag and thrust model is explained, and then the methods for determining the stall speed, maximum climb rate, maximum climb gradient, required runway length for take-off and landing, and the mission performance are given.

Drag Prediction

Theoretical aircraft drag prediction is a complex subject and the results can vary greatly in accuracy [62]. For the flight performance evaluation of the HA-1 aircraft the simplified parabolic drag formula was used [62]:

$$C_D = C_{D0} + \frac{C_L^2}{\pi \cdot AR \cdot e}.$$

This formula is only accurate up to values of C_L of about 1 [63]. This means low-speed and high-altitude performance cannot be predicted accurately.

Additionally, it assumes that minimum drag occurs at zero lift while the airfoil used has a $C_{L_{C_{Dmin}}}$ of 0.866, as the result of chamber. However, the simplified formula gives a maximum lift-over-drag ratio of 15.9, which is relatively high for this type of aircraft [64]. If any offset is applied to the lift coefficient the maximum lift over drag increases further resulting in possibly unrealistic high performance figures. Though the CFD analysis suggests an $(L/D)_{max}$ of 19, at this point there is not enough confidence in this analysis to assume such high performance. Following from the same reasoning the initial estimate of 0.028 for C_{D0} was used, instead of 0.016 as derived from the CFD analysis.

The effect of ground effect on drag during takeoff and landing is taken into account using the method by Nicolai [65]. The effect on lift is not taken into account, which is conservative for take-off and non-conservative for landing. However as will be seen, landing performance requirements are met with a large margin, so the non-conservative effect is not problematic.

An increase of 0.011 for C_{D0} is used for the extended landing gear, the value of the Cessna Cardinal RG which has a similar landing gear configuration [65]. The increase in drag due to flap deployment is modelled using the method of Roskam [48].

Thrust and Propeller Efficiency

For piston engines the engine power can be assumed constant with velocity and decreasing with altitude according to the Gagg and Ferrar model [62]:

$$P_{engine} = P_{engine,sealevel} \cdot (1.132 \cdot \sigma - 0.132)\,.$$

Here σ is the density ratio ρ/ρ_0 with ρ accounting for both altitude and temperature changes. ρ_0 is the

standard sea-level density of 1.225 kg/m^3.

A clutch mechanism is included that can connect either the electric or fuel engine to the propeller shaft. For this a powertrain efficiency η_{pt} of 0.9216 is included. The shaft power is thus given by

$$P_{shaft} = \eta_{pt} \cdot P_{engine}.$$

The propeller converts shaft power to propulsive power. With a propeller efficiency η_p of 0.85, the propulsive power available is now given by

$$P_a = \eta_p \cdot P_{shaft}.$$

However, for constant-speed propellers, the propeller efficiency can only be assumed constant for higher air speeds. At lower speeds, η_p will decrease down to $\eta_p = 0$ at standstill. For take-off and low-speed performance, this effect needs to be accounted for to derive accurate results. Here it is done using the third model proposed in Gudmundsson section 14.4.2 [62]. The thrust is estimated by cubic interpolation between the static thrust at zero airspeed,

$$T_{static} = 0.85 \cdot P_{shaft}^{2/3} \cdot (2 \cdot \rho \cdot A_2)^{1/3} \cdot \left(1 - \frac{A_{spinner}}{A_2}\right)$$

(derived from momentum theory and adjusted for various losses, with the propeller area A_2 equaling 4.1 m^2 and the spinner area $A_{spinner}$ equaling 0.13 m^2), the thrust at cruise speed,

$$T_{cruise} = \eta_p \cdot P_{shaft}/V_{cruise},$$

and the thrust at maximum speed,

$$T_{Vmax} = \eta_p \cdot P_{shaft}/V_{max}.$$

At V_{cruise} an additional constraint is set by requiring $d\eta_p/dV = 0$. Because unpredictable behaviour was observed in this interpolation for $V > V_{cruise}$, the thrust is calculated using

$$T(V) = \eta_p \cdot P_{shaft}/V$$

beyond cruise speed. Propeller efficiency for velocities below cruise speed is now calculated using

$$\eta_p(V) = T(V) \cdot V/P_{shaft}$$

Stall Speed

Calculating the stall speed is straightforward and only requires the formula [63]:

$$V_S = \sqrt{\frac{W}{0.5 \cdot \rho \cdot S \cdot C_{L_{max}}}} \tag{14.1}$$

where $C_{L_{max}}$ is the maximum lift coefficient for the required flight configuration and W is the gross weight of the aircraft. It should be noted that the wing surface area S is adjusted when the flaps are deployed, here and everywhere where the variable is used.

Maximum Climb Rate

Assuming a small flight path angle ($L = W$) the rate of climb of the aircraft is given by [63]:

$$RoC = \frac{P_a - P_r}{W} \tag{14.2}$$

Where P_a is the available propulsive power and P_r is the power required for steady, level flight, and W is the gross aircraft weight in Newtons. If power available is assumed constant with speed RoC_{max} occurs at $V_{P_{r_{min}}}$, however as this assumption is not made a numeric solver is used to maximise Equation 14.2. Then $P_a = \eta_p \cdot P_{shaft}$ and $P_r = V \cdot D = V \cdot 0.5 \cdot \rho \cdot V^2 \cdot S \cdot C_D$ for a given velocity and altitude and C_D given by Equation 14.1.

Maximum Climb Gradient

The maximum climb gradient occurs for propeller aircraft at velocities close to stall speed [66]. Because the drag model is limited to low C_L values no accurate climb gradient figures can be provided. Still, to get an estimate of whether CS23 requirements are met, the maximum climb gradient is calculated by maximising Equation 14.3 [63] with drag multiplied by 1.5 to account for low-speed drag increase. Note that here W is in Newtons as well.

$$Gradient = \frac{T - 1.5 \cdot D}{W} \cdot 100\% \tag{14.3}$$

Take-Off Performance

The take-off ground run is calculated using the method by Ruijgrok [63]:

$$s_g = \int_0^{V_{LOF}} \frac{V}{\frac{g}{W} \cdot (T - D - \mu_r(W \cdot \cos\xi - L) - W \cdot \sin\xi)} \tag{14.4}$$

Here W is the gross aircraft weight in Newtons, T is the speed-adjusted engine thrust at full take-off power, L the lift force, D the drag force adjusted for ground effect, μ_r the rolling resistance (0.02 for paved runways and 0.05 for grass runways), and ξ the runway slope angle (positive corresponds to an upwards slope). V_{LOF} equals 1.1 times the stall speed in take-off configuration, the value assumed by Gudmundsson [62], with a minimum of 30 m/s required for achieving the control authority to rotate. Since it is undesirable to lift off at the very end of the runway, one second of flight at V_{LOF} is added to the ground distance calculated by Equation 14.4 to derive the minimum runway length.

Landing Performance

For the landing ground distance, the method by Gudmundsson is used [62]. The aircraft is assumed to touch down at $V_T = 1.1 \cdot V_{S0}$. The deceleration at the average speed $V_{avg} = V_T/\sqrt{2}$ is calculated and assumed constant for the entire ground run. This results in the following formula to calculate the ground distance:

$$s_g = \frac{-V_T^2 \cdot W}{2 \cdot g \cdot (T - D - D_g - W \cdot \sin\xi)}$$

Where W is the gross aircraft weight in Newtons, T equals $-0.4 \cdot T_{static}$ as reverse thrust is applied, D is the aerodynamic drag, and ξ is the runway slope (positive is upwards). D_g is the landing gear drag given by $D_g = \mu \dot{f} \cdot (W \cdot \cos\xi - L)$ with μ equaling 0.4 for paved runways and 0.2 for grass runways

(since Gudmundsson provides no estimate for dry grass the factor for wet grass is used) and f equals the fraction of the weight that is carried by the main landing gear (as only the main landing gear is assumed to have brakes).

As suggested by Gudmundsson, one second of free rolling at touchdown speed is added since braking is not applied immediately at touchdown. Additionally, since it is not desirable to touch down at the very start of the runway, two seconds of flight at touchdown speed are added to derive the minimum runway length.

Mission Performance

To determine whether the aircraft is able to perform the design mission of Chapter 7 the flight is analysed through step-wise integration of the flight time t, ground distance s, true airspeed V, altitude h, fuel consumption and battery usage.

The fuel consumption rate of the piston engine is calculated by:

$$\dot{W}_F = -\frac{P}{\eta_p \eta_{pt}} \cdot SFC$$

where P is the propulsive power and SFC is the power-specific fuel consumption, calculated from the engine specifications[(a)] and certification document [53] to be 0.5841 × 10^{-7} N/(W s) for flight conditions or 0.621 × 10^{-7} N/(W s) when delivering maximum take-off power.

The rate at which the battery capacity BC (in Wh) is depleted when electric power is used is calculated through:

$$\dot{BC} = -\frac{P}{3600 \cdot \eta_p \cdot \eta_{pt} \cdot \eta_{em} \cdot \eta_{bat}}$$

where η_{em} is the electric motor efficiency (0.925) and η_{bat} is the battery efficiency (0.97). The battery is only discharged up to a depth-of-discharge of 80%.

The flight phases are described below. The entirety of the flight is performed in an ISA atmosphere with a constant temperature offset of +18 °C. Furthermore, startup, warm-up and idle fuel consumption are ignored. The drag caused by the propeller at idle thrust is neglected as well. Though currently the

- **Take-off:** The aircraft takes off from an airfield at 750 m MSL. The duration of the take-off is multiplied by the maximum take-off power of the engine to derive the energy consumed. The altitude and distance covered are taken as 0 m and the final velocity is the lift-off velocity.
- **Acceleration:** The aircraft accelerates with maximum continuous thrust at constant altitude up to 50 m/s.
- **Climb:** The aircraft climbs at a constant climb rate of 2.5 m/s and constant speed until the cruise altitude of 3000 m is reached. Now the propulsive power equals $P = RoC \cdot W + V \cdot D$, derived by rewriting Equation 14.2.
- **Cruise:** The aircraft first accelerates to cruise speed, 60 m/s. Then the aircraft maintains a constant velocity and altitude for the duration of the cruise such that the total ground distance covered equals 150 nm per flight leg.
- **Descent:** The aircraft descents at a constant −2.5 m/s and thrust is applied such that the aircraft does not decelerate.
- **Landing:** The aircraft lands at an airfield at 750 m MSL. Since reverse thrust is used, the engine is set at 0.4 times the maximum continuous power for the duration of the braking phase. This is

[(a)] URL: `https://red-aircraft.de/red-a03-003/` [accessed 19-6-2024]

an approximation, based on that $0.4 \cdot T_{static}$ was used for reverse thrust.

The above is performed for a total of four times such that the final ground distance covered is 600 nm. During the final descent, the aircraft loiters at 1200 m altitude for 75 minutes, conforming to the reserve fuel policy outlined in Chapter 7. The loiter phase is performed at constant C_L, with the aircraft first decelerating to obtain the C_L corresponding to maximum C_L^3/C_D^2 to minimize fuel consumption [63].

The first two legs are performed with the piston engine. Burning fuel in the beginning of the flight lowers weight and thus fuel consumption for the rest of the flight. But if one waits until the last leg to switch to electric, usable battery capacity may be left over at the final landing (as would be the case if 685 kW h/kg batteries are used). The aircraft will not be able to take off a second time with electric power though, so any residual usable battery capacity is used during the last cruise phase. Hence the battery is always discharged up to the maximum depth of discharge, minimizing fuel use. The 15% trip fuel reserve requirement is conformed to by carrying extra fuel. By calculating the equivalent fuel use for the electrically-flown flight phases the battery usage is accounted for in the reserves as well.

14.2. Performance Analysis Results and Discussion

The analysis results are displayed in Table 14.1, Figure 14.1 and Figure 14.2. Before the results are discussed, it is important to mention that the performance models still need to be verified and validated. However, the results correspond well with the initial estimations used earlier in the design.

As can be seen in Table 14.1, while the CS23 requirements are met, the targets for stall speed and maximum rate of climb are not. However the difference is not too great to be considered unacceptable. The take-off and landing runway length requirements are met, even at the standard airfield conditions. In Figure 14.1 it can be seen that the fuel and payload weight may need to be reduced for airfields at higher elevations. But note that high-altitude mountain airstrips are often sloped, greatly reducing the take-off and landing distances. Figure 14.1 assumes no slope, no wind, and grass runways.

As seen in Figure 14.2, the aircraft exceeds the 600 NM range requirement. With 540 kg payload up to 670 NM ground distance can be covered with four flight legs, at 630 kg up to 470 NM, and with no payload up to 820 NM. Using only electric power and flying only a single leg, the aircraft can cover up to 110 NM with 540 kg payload.

Table 14.1: Flight Performance Evaluation Results. “SL” means sea level, i.e. 0m ISA+0. The plusminus signs for the climb gradient results indicate that these figures are estimates only, see Section 14.1

Item	Value	Requirement	Target
Landing stall speed, SL, MTOW	26.8 m/s	≤31 m/s	≤25 m/s
Max. clean climb rate, SL, MTOW	4.3 m/s	-	≥5 m/s
Max. take-off climb gradient, SL, MTOW	±6.8%	≥4%	-
Max. landing climb gradient, SL, MTOW	±6.0%	≥3%	-
Min. TORA for take-off, 750m ISA+18, MTOW, grass	450 m	≤500 m	-
Min. TORA for landing, 750m ISA+18, MTOW, grass	345 m	≤500 m	-
Cruise speed	60 m/s	≥50 m/s	-
Max. cruise altitude	4900 m	≥3700 m	-

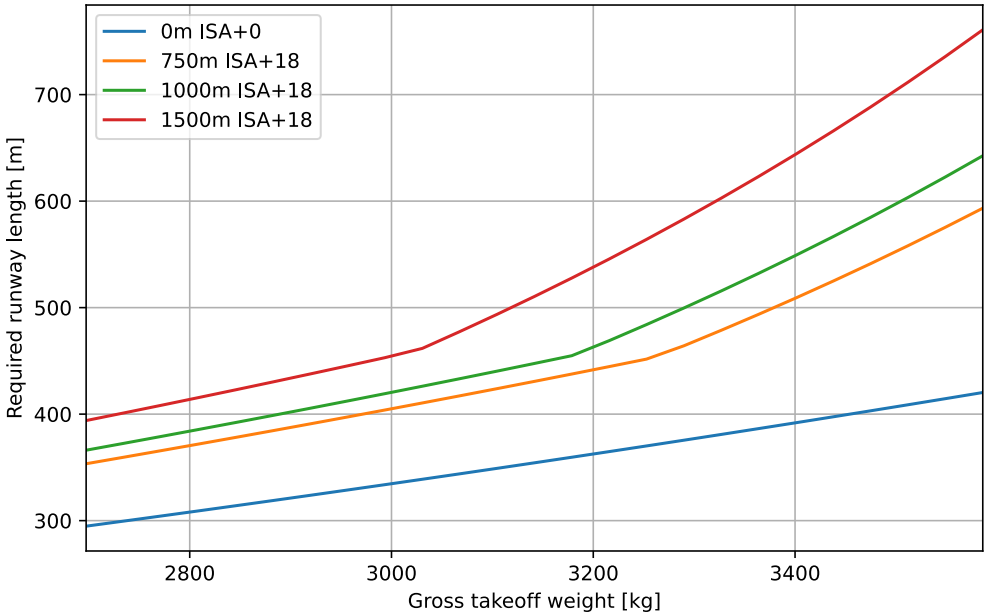

Figure 14.1: Required runway length for varying gross take-off weight (ranging from operational empty weight to maximum take-off weight) for different altitudes. Here no slope, no wind and grass runways are assumed

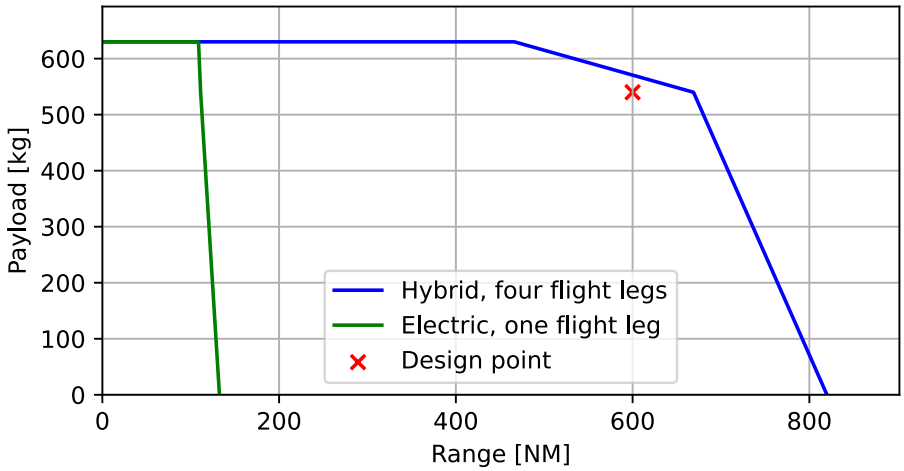

Figure 14.2: Payload-range diagram, indicating that all requirements regarding range are met by the current design. Take-offs and landings as well as mandatory reserves are included

15 | System Architecture

System architecture encompasses the design and arrangement of interconnected components that collectively define the functionality of an entire aircraft. Integral to system architecture are hardware and software block diagrams, detailed in Section 15.1 and Section 15.2, respectively. Following these, the communication flow diagram in Section 15.3 provides an overview of data exchange processes within the system. Lastly, Section 15.4 presents the data-handling diagram, highlighting how data is processed, stored, and managed across the aircraft's systems.

15.1. Hardware Block Diagram

The aircraft has many hardware components working in conjunction, and it is important to identify those components and their relationships in the design process. A hardware block diagram, like the one presented in Figure 15.1 for the HA-1 aircraft, allows for visualising this. In this diagram, the pilot is also included, as they interact with multiple parts of the hardware and are therefore an essential part of the system. For the sake of simplicity, the structures part of the hardware is not included, as it relates to every other hardware component through physical links.

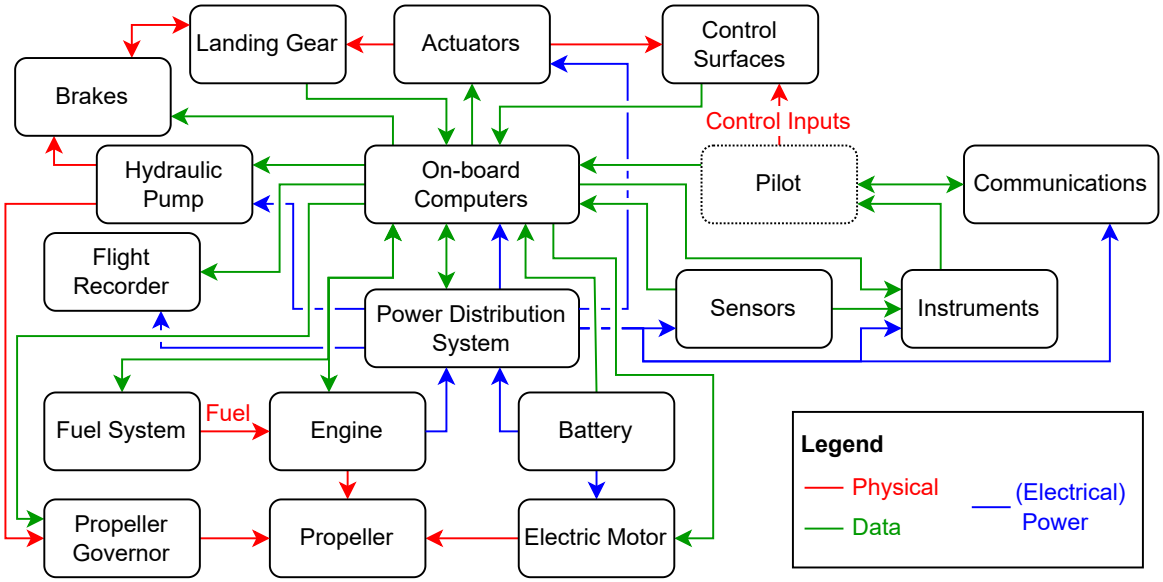

Figure 15.1: Hardware Block Diagram

15.2. Software Block Diagram

Modern aircraft like the HA-1 heavily rely on software to perform their mission, and it is thus essential to understand how this software works and how it relates to other parts of the aircraft. This can be visualised in a software block diagram, such as the one presented in Figure 15.2. It should be noted that this diagram only provides a high-level overview, and should be further expanded upon in further design phases.

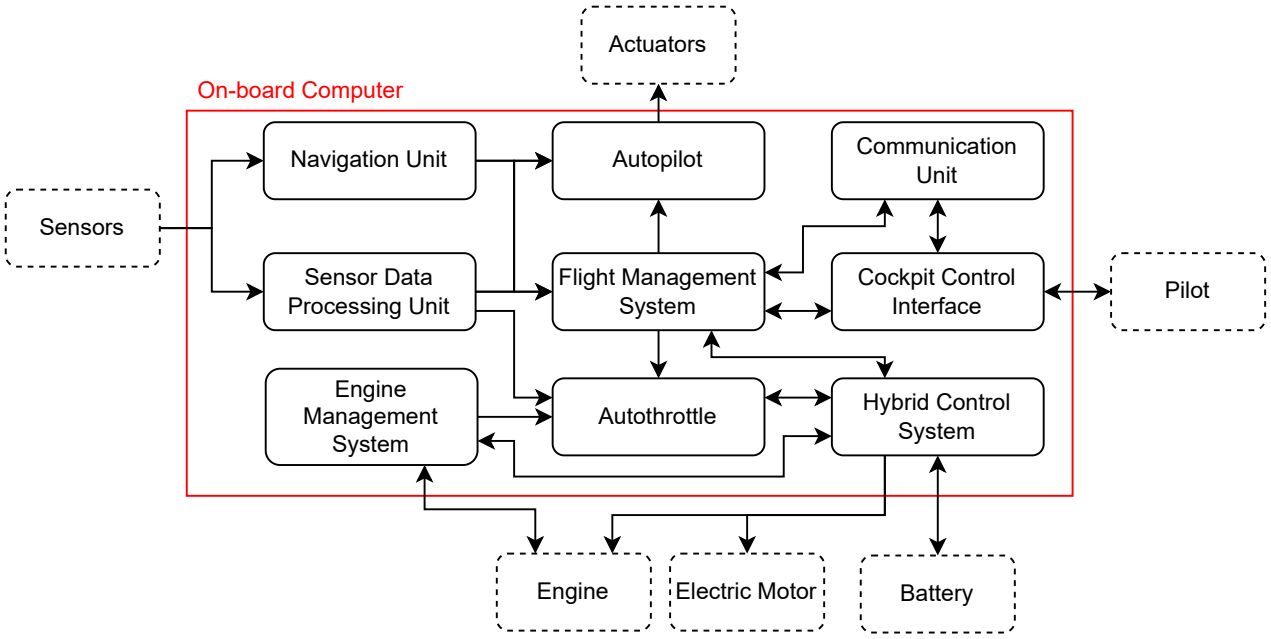

Figure 15.2: Software Block Diagram

15.3. Communication Flow Diagram

A communication flow diagram is a visual tool that illustrates how information and data are transmitted between various components within a system and its environment. Understanding the flow of data is crucial for designing an aircraft design and its maintenance. In case of system malfunctioning, engineers and technicians would be able to identify the source of failure promptly, reducing downtime and improving safety. Therefore, a communication flow diagram was constructed for HumanAir's aircraft as well and this can be found in Figure 15.3.

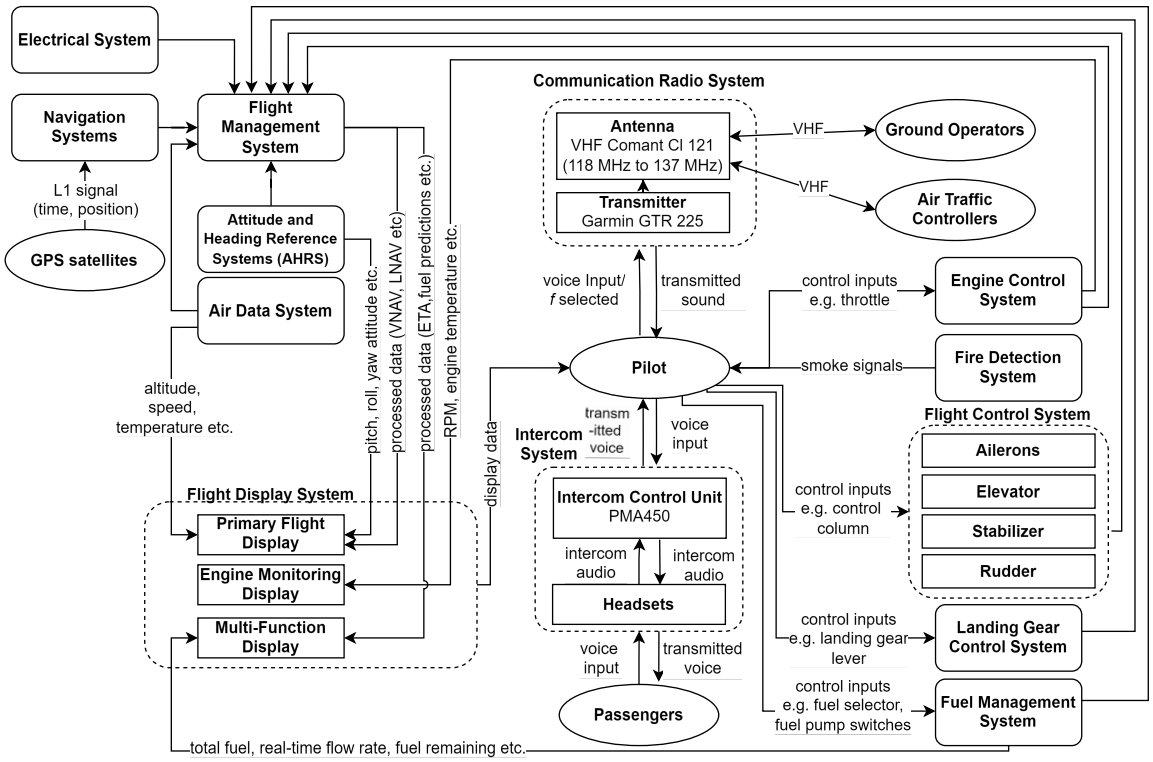

Figure 15.3: Communication Flow Diagram

The pilot provides direct inputs to various critical systems, including engine control, flight control, and landing gear control. This is typically achieved through physical controls using instruments such as throttle levers, rudder pedals, and fuel selector valves. These manual inputs are then transmitted to the respective systems, where they are processed and generate outputs. The resulting outputs are further routed to the flight management system for analysis.

The flight management system manages and stores the flight-related data. Additionally, it plans and manages the aircraft's route from departure to destination. To perform this task, the flight management system obtains data from various systems, including navigation, electrical, air data, and attitude and heading reference systems. After processing, the flight management system transmits the data to the flight display system, allowing the pilot to observe the effects in real-time.

Effective communication with ground operators and air traffic controllers is crucial for the safe operation of an aircraft. The pilot maintains communication with them via the aircraft's communication radio system, ensuring safe take-off and landing. Additionally, for clear communication with passengers, the pilot utilises the intercom system through microphones.

15.4. Data Handling Block Diagram

Data handling can be approached in two primary ways: centralised and decentralised computing architecture systems. In centralised computing systems, data management occurs at a single central position, while decentralised systems distribute data management across multiple locations. To select the optimal solution for HumanAir's aircraft, a trade-off was conducted based on five criteria outlined in Table 15.1:

Table 15.1: Trade-off Criteria and Justification for Computing Architecture Systems

Criterion	Justification	Accounts for	Ranking Strategy	Weight	Weight Justification
Reliability (RLB)	Directly linked to passenger safety and it ensures that aircraft can complete flights as scheduled without any disruptions	System operates consistently and predictably.	Based on literature [67]	0.25	Essential for passenger safety and schedule adherence. Safety is always of paramount importance.
Real-time Performance (RTP)	Crucial for timely and accurate data processing, which affects precise control over navigation, communication and avionics systems to changing flight conditions	System processes and responds to data in real time.	Based on literature[(a)]	0.20	Real-time performance allows pilots to make informed decisions quickly and safely (linked to safety as well).
Security (SCT)	Protects critical flight information from unauthorised access.	Integrity and confidentiality of data.	Based on literature [67]	0.20	Ensures operational safety and data protection but is relatively less important since HumanAir is not a military aircraft
Maintenance (MTN)	Ease of maintenance is important to minimise downtime and ensure efficient updates	Ease of maintenance, updates	Based on literature[(a)]	0.20	Given that MAF operates in a remote region, easy maintenance is critical
Cost (CST)	To meet the unit and operating cost requirements (REQ-UR-08 and REQ-UR-09), the cost should be kept as low as possible	Initial and operating cost	Based on literature [67]	0.15	Compared to other criteria, which are linked to passenger safety, this is less important

With the determined criteria, the trade-off was performed in the Table 15.2 below:

[(a)] URL: `https://www.hivenet.com/post/decentralized-or-distributed-whats-the-big-difference` [accessed 17 June 2024]

Table 15.2: Trade-off for Computing Architecture System

	RLB	RTP	SCT	MTN	CST	
	0.25	0.2	0.2	0.2	0.15	**Score**
Centralised	4	4	3	5	4	4
Decentralised	3	3	4	3	3	3.2

Consequently, HumanAir's aircraft adopt a centralised computing architecture. The flight management system illustrated in Figure 15.3 features an onboard computer responsible for processing data from multiple systems under a centralised framework. To provide clarity on the data flow, a detailed data handling diagram depicting the inputs and outputs directed towards the onboard computer has been developed in Figure 15.4. Each arrow is labelled with three key details: (1) the type of data being transmitted, (2) the communication protocol used, and (3) the data volume. Different line colours indicate varying data rates.

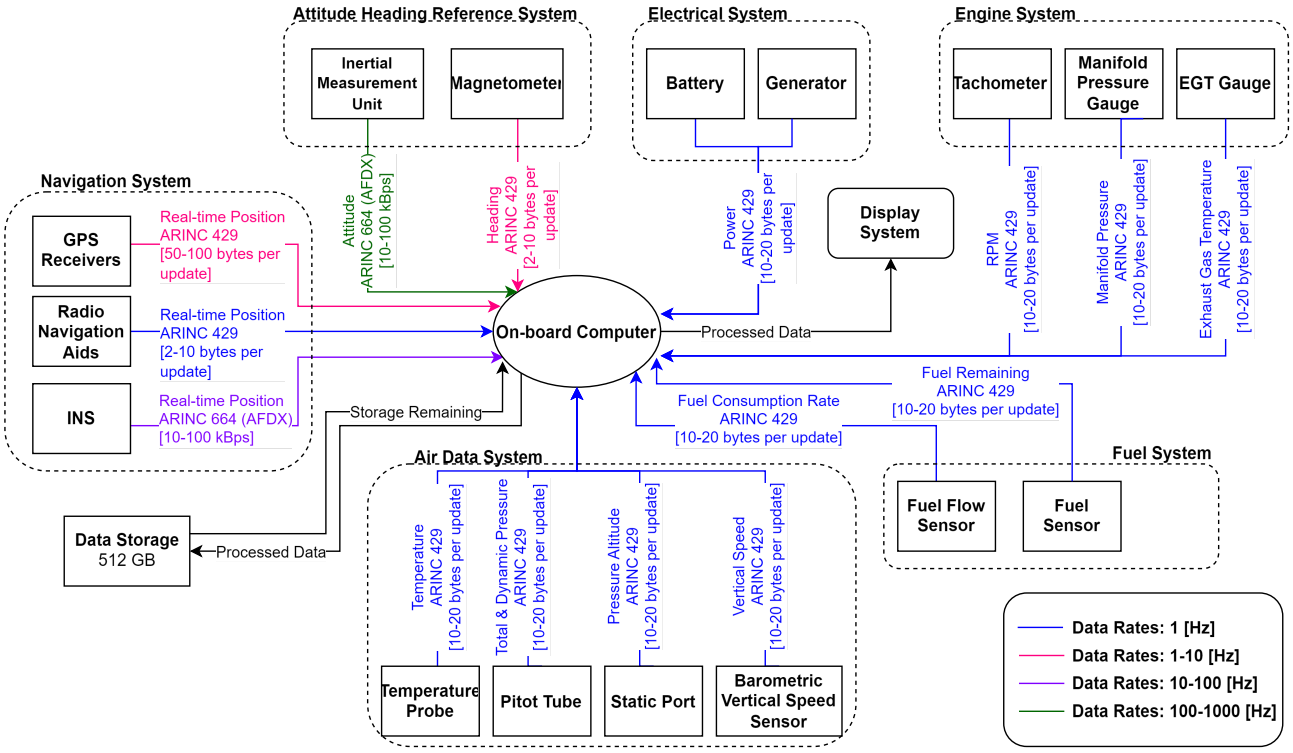

Figure 15.4: Data Handling Block Diagram

As illustrated in Figure 15.4, the onboard computer gathers data from a multitude of systems. For instance, it receives real-time position data from sensors such as the Global Positioning System (GPS), Inertial Navigation System (INS), and radio navigation aids. This information is subsequently processed by the on-board computer. Additionally, the computer utilises other data, such as the planned route and current ground speed, to calculate the estimated time of arrival and estimated time en route. Subsequently, this data is transmitted to the display system, where the pilot can access it.

In addition to its primary functions, the on-board computer is responsible for data storage. It records essential data including aircraft parameters, pilot inputs, and system status for flight monitoring, maintenance, and safety management. The data storage system receives processed data from the onboard computer. Furthermore, it communicates the remaining storage capacity to indicate when the system is nearing its maximum capacity and can no longer store additional data.

16 | Ground Operations, Logistics and Infrastructure

To minimise difficulties and costs associated with transitioning the fleet to a new type of aircraft, effort was taken to ensure ground operations remained as similar as possible to MAF's current practices. Nevertheless, given the hybrid-electric design, some departures from the original concept are inevitable. Section 16.1 describes the refuelling and recharging process as well as the associated ground infrastructure. Section 16.2 shows the most a flow chart summarising ground operations at MAF bases. All the prices presented in the following section are expressed in 2024 USD.

16.1. Refuelling and Recharging

Refuelling

Given the relative difficulty and increased expense associated with obtaining AVGAS, an engine was selected that runs on jet fuel, which is comparatively cheap and easy to acquire. In general, there is no need to alter the refuelling procedures from MAF's current operational model. However, thanks to the use of jet fuel, it is now permissible to refuel while passengers are on board should the need arise, provided appropriate safety measures are taken[(a)].

Electric power

In order to meet the requirement of achieving a 50% reduction in CO_2 emissions, a hybrid powertrain was selected. This in turn necessitates ground infrastructure to supply the required electric energy to the aircraft battery. Given MAF's bases often do not have reliable access to (green) electricity, ground power generation and storage were considered as part of the system.

Initially, wind and solar power were considered to generate the energy required. However, analysis of wind speed data at MAF's operating bases revealed that at most of the bases, there was insufficient wind to rely upon. At most, it could be used as a supplementary source for part of the year in a handful of locations and thus was not investigated further.

Solar insolation data on the other hand indicated that solar panels were a much more favourable option. Given a 250 kWh battery on each plane, the required energy production capability was then calculated assuming two aircraft per base, and that each aircraft would be charged twice daily. Therefore, a daily energy production capability of 1000 kWh is required. Per square metre, Arusha, Tanzania (one of MAF's Cessna 206 bases) receives an average of 5.4 kWh of solar energy per day. Assuming a solar panel efficiency of 20%, about 930 m^2 of solar panels would therefore be required to generate the required energy every day. However, a solar panel's output decreases by about 0.5% a year. Therefore, more solar panels are initially required, in order to ensure sufficient power is still being generated by the end of the 25-year lifespan of the solar panels. The required area can then be calculated by

$$\text{Total area} = \frac{\text{Base area}}{0.995^{25}} \tag{16.1}$$

where the base area is the area required to generate the required energy without factoring in degradation. Applying this equation to the 930 m^2 required in Arusha gives an initial area requirement of roughly 1050 m^2. Table 16.1 gives the daily insolation and required solar panel area (accounting for degradation) for all MAF bases from where Cessna 206s, 182s, and GippsAero GA-8 Airvans operate. It is important to note that these are all calculated for a fleet of two aircraft per location. In reality, different locations will have different fleet sizes and thus different power generation requirements.

In addition to solar panels, a battery is also required. This is because the solar panels themselves are not able to generate the required energy to charge the aircraft within an hour, per MAF's requirement.

[(a)] URL: `https://skybrary.aero/articles/refuelling-passengers-board` [accessed 17 June 2024]

Instead, the solar panels charge the ground battery throughout the day at a slower rate and then discharge quickly to charge the aircraft batteries.

Table 16.1: Average Daily Insolation and Required Solar Panel Area

Location	Average Daily Insolation [kWh/m^2]	Solar panel area required [m^2]
Arusha	5.4	1051
Kampala	5.4	1059
Nhulunbuy	6.0	946
N'djamena	5.8	974
Antananarivo	4.7	1203
Juba	5.4	1041
Dili	5.6	1019
Mount Hagen	4.7	1203

Assuming two aircraft may need to be charged simultaneously or in close succession, the battery must therefore be able to store at minimum 500 kWh of electric energy. However, it is generally inadvisable to charge a battery to 100% of its capacity and discharge it all the way to 0%. A typical maximum operational range for the state-of-charge (SOC) is 10%–95% of the maximum capacity [68]. Furthermore, batteries degrade over time, with their maximum capacity decreasing. Assuming the battery is charged to 95% and discharged to 10%, the required capacity can then be calculated using

$$\text{Required capacity} = \frac{500\ \text{[kWh]}}{0.95 - 0.1} = 588.2\ \text{kWh} \approx 600\ \text{kWh} \tag{16.2}$$

16.1.1. Cost

To ensure the cost requirement is met, it is important to factor in the cost of all components. A 1100 m^2 solar system is roughly equivalent to a 220 kW system. The price for such a system is between roughly \$250 000 and \$385 000[(b)]. For the battery, it is estimated that in 2030 grid-scale batteries will cost between \$260 and \$440 per kWh [69]. This gives a price between roughly \$150 000 and \$260 000 for a 600 kWh battery. The last major element of ground power delivery infrastructure is the charger itself. In order to charge the aircraft battery within one hour, the charging system must be able to deliver 250 kW of power. While price data for high power DC chargers is difficult to obtain, it is estimated that a Tesla Supercharger capable of delivering 250 kW costs roughly \$45 000[(c)]. Together, this gives a cost of between \$390 000 and \$735 000 for the ground battery, power generation system and two charging stations. Per aircraft, this then gives a cost range of \$195 000–370 000.

16.2. Operations Flow Diagram

Figure 16.1 shows a flow chart summarising the most important activities to be performed on the ground at the MAF base between flights. The interior of the aircraft was designed to be reconfigured between passenger seating and freight within half an hour, in compliance with requirement **HA-UR-13**.

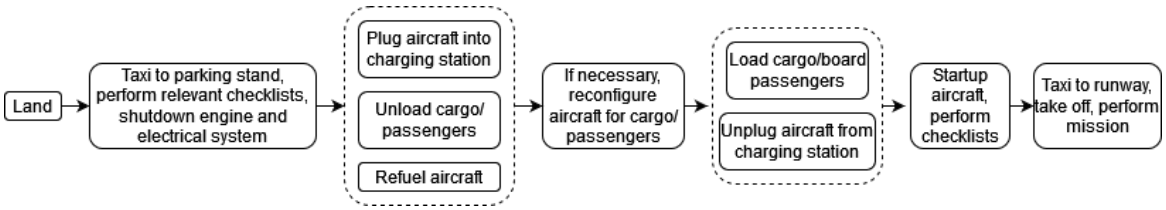

Figure 16.1: Flow Chart Showing Most Important Ground Operations

[(b)]URL: https://quotes.solarproof.com.au/system-sizes/220kw-solar-system-information-facts-figures/ [accessed 17 June 2024]

[(c)]URL: https://electrek.co/2022/04/15/tesla-cost-deploy-superchargers-revealed-one-fifth-competition/ [accessed 17 June 2024]

17 | Cost Breakdown Structure

The cost breakdown structure aims to verify the aircraft design meets MAF's requirements on unit cost and operating cost, as well as ensuring that the aircraft programme will be profitable for the manufacturer. Section 17.1 gives a breakdown of the development and manufacturing costs for the aircraft, and therefore the final unit cost. Section 17.2 analyses the overall profitability of the HumanAir programme as a whole, and finally section 17.3 compares the costs of HumanAir's concept with the Cessna 206 and 208. All the costs presented in this section are expressed in 2024 USD unless specified otherwise.

17.1. Cost Analysis

One of the initial stakeholder requirements was a unit price of US$1.5M or less (HA-UR-09). The main costs of bringing the aircraft to market are development (including engineering, testing, and building of prototypes) and manufacturing (comprising labour, raw materials, parts, and quality control). In order to estimate the total cost of the programme, Raymer's approach was used [38]. This was found to yield a more reasonable result than alternative methods, such as the one presented by Roskam [70]. It should be noted that at such an early stage in the design process, the only tools available are statistical, and that therefore are only an indication of the final programme cost and unit price. Further analysis will be needed at a future stage in the design process.

In Raymer, equations 18.1 through 18.9 are used to estimate the total development and production cost. This figure can then be divided by the total production run to obtain a unit cost. It should be noted that these equations give costs in 1986 dollars, and thus have been adjusted where appropriate to give a cost in 2024 dollars. Similarly, modern labour costs have been used instead of those suggested by Raymer [71]. Additionally, the equation for tooling cost (which mainly refers to all aspects of preparing for production) has been modified to be slightly lower, due to the assumption that the aircraft will be manufactured in cooperation with an experienced producer of similar aircraft. Table 17.1 gives an overview of total research and development, material, labour, testing (including renting of test facilities) and quality control costs for a production run of 500 aircraft. This is roughly the amount of aircraft produced in a 15-20 year production run, similar to that of comparable aircraft like the GA-8 Airvan[(a)]. Precise definitions of each item can be found on pages 507-508 of Raymer.

Table 17.1: Overall Programme Costs, as Calculated According to Raymer for a 500 Aircraft Production Run

Item	Labour hours	Cost (US$1000, FY2024)
Engineering	554 500	52 685
Tooling	363 650	11 990
Manufacturing	3 609 900	129 030
Development support	-	10 035
Flight test	-	12 660
Materials	-	180 820
Quality control	480 100	15 830
Total	-	**413 050**

Table 17.2 gives an overview of the costs of major non-airframe components that must be purchased from suppliers, i.e. the engine, propeller, electric motor, battery and avionics.

[(a)] URL: `https://aeropedia.com.au/content/gipps-aero-ga-8-airvan/` [accessed 25 June 2024]

Table 17.2: Individual Costs of Major Non-airframe Components, Per Aircraft

Item	Cost (US$1000, FY2024)	Source
Engine	232	(b),(c)
Propeller	51	(d)
Electric motor	100	(e)
Battery	70	(f)
Avionics	29	(g)
Total	**482**	-

These component costs can be added together, multiplied by the number of aircraft produced, and added to the sum of the costs in table 17.1 to obtain an estimate for the total cost of the entire programme. This figure can then be divided by the number of aircraft produced to find the aircraft unit cost. Doing so gives a total programme cost of roughly $640M and a unit cost of approximately **$1.28M**. In order to maintain profitability, it was desired to keep the unit production cost below $1.4M. The figure of $1.28M therefore gives a 9.3% margin.

Additionally, the operational cost per hour had to be calculated to make sure that the design complies with **HA-UR-08**. Using the flight data provided by MAF (also used for the CO_2 emissions reduction estimation), the hourly operating cost is estimated at $209. However, since the batteries mounted on the aircraft used can only sustain around 1000 cycles at the ideal DoD. Thus, the batteries have to be replaced every 2 years which accounts for approximately 1000-1200 flight hours. In Table 17.2 , the price of two batteries is estimated at $70 000, which results in a cost of $35 000 for one battery. Distributing this cost over 1000 hours of flight, the hourly operating cost is estimated at **$244**.

17.2. Return on Investment

Requirement **HA-UR-09** states that for MAF, the maximum unit price should not exceed $1.5M. While the unit cost for a single aircraft ($1.28M) is below this threshold, allowing for a modest profit when selling at $1.5M, this does not cover the cost of the ground infrastructure, which must be factored in for MAF.

Taking a ground infrastructure cost of $285 000 (the average of the range calculated in Chapter 16) gives a total system cost (aircraft and ground infrastructure) for MAF of $1.565M. In order to meet MAF's price requirement, it has been decided to sell the aircraft to them at a price of $1.5M (ie. a loss of $65 000 per aircraft). Assuming 20 aircraft are sold to MAF, this gives a total loss of $1.3M. Assuming a sale price of $1.5M is maintained for other customers (for whom ground infrastructure is not included, as this is a requirement specific to MAF's operations), the profit from the sale of six aircraft will compensate for the loss made on sales to MAF.

Given a total aircraft development and manufacturing cost of $640M, plus the ground infrastructure cost for 20 aircraft (20 x $285 000), the total cost is $645M. Taking a sale price of $1.5M, this means that roughly 430 aircraft will need to be sold to break even. Assuming a rate of 30 sales per year, this means the programme will break even after about 14 years, and eventually achieve a total programme profit of ca. $100M after the entire production run of 500 aircraft.

To make the outlook more favourable, the sale price for non-MAF customers could be increased to

(b) URL: https://www.avweb.com/news/500-horsepower-v-12-turbo-diesel-engine-from-germany/ [accessed 19 June 2024]

(c) URL: https://www.lawyerdb.de/Inflationrate.aspx [accessed 19 June 2024]

(d) URL: https://ottosenprop.com/products/p7636223-0152td-4hfr34c763-94lma-4 [accessed 19 June 2024]

(e) Information provided by H3X by email

(f) URL: https://about.bnef.com/blog/lithium-ion-battery-pack-prices-hit-record-low-of-139-kwh/ [accessed 19 June 2024]

(g) URL: https://www.airteam.eu/garmin-g1000-nxi [accessed 19 June 2024]

$2M. In this event, about 330 aircraft will need to be sold to break even (including the aircraft sold at a loss to MAF). This would take roughly 11 years.

17.3. HA-1 compared to Similar Aircraft

The primary customer of the HA-1, MAF, required an aircraft capable of replacing the currently operated Cessna 206 while improving several aspects such as CO_2 emissions and hourly operational unit cost. Therefore a comparison between the developed aircraft and similar aircraft including the Cessna 206 can be visualised in Table 17.3.

Table 17.3: HA-1 vs Competition

Parameter	HumanAir HA-1	Cessna 206	Cessna 208
Unit cost	$1 500 000	$550 000 – 1 200 000	$2 164 000
Operational cost / hour	$322	$650	$842
Aircraft currently flying	-	N/A in Europe Approx. 3000 in US	150 in Europe Approx. 400 in US
CO_2 reduction of the HA-1	-	23%	48%

From the table, it is clear that HA-1 performs better in almost all categories with respect to the two selected aircraft. It is worth mentioning however that the hourly cost for the Cessna 206 assumes only 200 hours of flight per year while for the other two aircraft, the cost is calculated for 600 flight hours. Thus, that price is expected to be lower than $650 per hour. However, the price can be still approximated at $400 which is around 25% more than what the HA-1 concept proposes. This will account for the difference in prices since the $300 000 paid extra will be distributed by operating the aircraft for less than 5 years.

The operating cost was calculated using the same method as described in the midterm report [12]. It also includes $29 per hour to account for the replacement of batteries every two years. It combines fuel cost as well as maintenance and overhaul, including spare parts.

In Table 5 it can also be seen that the operational cost per hour for HA-1 is higher than the previously calculated $244 per hour, and that also the CO_2 emission is reduced from 70% to around 23/48%. That is due to the fact that the ground charging station is not included in the unit cost of HA-1 for any other customers than MAF. That is done since the cost approximated for it will not be relevant for other customers since it is based on the data specific to MAF airbases - temperature profile, wind profile, surface available etc. The other customers may still be satisfied by the achieved reduction without charging with fully renewable energy or might opt for other renewable energy sources like hydropower, wind power, or nuclear power.

Given all the aspects mentioned above, the hourly cost and the emission reduction level were updated based on average European levels of 0.22 kgeCO_2/kWh by 2030 [72] and a price of 0.2847 €/kWh[(h)] (equal to $0.31/kWh) as the charging price from the conventional electrical grid. Further analysis can be performed by the customer to determine the advantage that building a new charging facility will bring to their operations.

[(h)] URL: `https://ec.europa.eu/eurostat/statistics-explained/index.php?title=Electricity_price_statistics` [accessed 14 June 2024]

18 | Sustainable Development Strategy

To ensure sustainability significantly influenced design choices and was properly integrated into the design process, a sustainable development strategy was developed. Sustainability was approached from three perspectives during the design process: economic, environmental, and social [73–75]:

1. **Environmentally sustainable design** seeks to minimise environmental impact, accounting for all emission types.
2. **Economically sustainable design** aims to minimise initial investment cost and long-term maintenance and operation costs.
3. **Socially sustainable design** focuses on ensuring the product is accessible, inclusive and beneficial to all members of society in the short and long term.

This chapter provides an overview of how these sustainability aspects were integrated into the design process and presents guidelines for future design phases.

18.1. Environmental sustainability

When estimating the environmental impact of the design, it was important to account for all emissions over the entire product's lifetime. The lifetime phases with largest accompanying emissions were identified through a coarse Environmental Life Cycle Analysis (ELCA)[(a)], and the percentage of life cycle emissions per phase was estimated based on statistical data of fossil fuel-powered aircraft similar to the HA-1 [76, 77].

Emissions from the design, certification, and deployment phases were found to be negligible, given conventional design choices [76, 77]. Since no unconventional design choices were made for the HA-1, no special attention was allocated to analysing emissions during these phases.

Emissions during the manufacturing phase include all emissions embodied within the aircraft components [78]. This ranged from 20% of life cycle emissions for the smallest aircraft, to under 1% for large commercial ones [76, 77, 79–81]. If the HA-1 would be fossil-fuel powered, emissions produced during the manufacturing phase (which include material embodied emissions, manufacturing process emissions, and energy usage and generation [81, 82]) would account for around 5% of life cycle emissions[76]. Since conventional materials were selected for both internal and exterior aircraft components of the HA-1, no significant increase in airframe manufacturing emissions was expected.

However, the HA-1 is hybrid-electric in nature. Hence the manufacturing of the battery adds additional manufacturing emissions not considered by the statistical data used. According to a comparison between electric and regular vehicles, the manufacturing emissions are a factor 1.6 higher [(b)]. Similar or even lower factors are expected for the HA-1, especially with the advancement in battery technology and the HA-1's late entry to market, allowing for embodied battery emissions to decrease. Using this multiplication factor for the HA-1, only about 8% of the HA-1 total LCA emissions would originate from manufacturing.

Emissions during the operations phase accounted for ca. 80 % of aircraft life-cycle emissions [76, 77]. These can be further broken down into fuel emissions (main source, around 89% of operation emissions for a Cessna 172N) and other emissions, mostly related to maintenance [80]. It was thus this phase which was most critical to achieve the desired emission reduction. It is for this reason, that the HA-1 has been equipped with a hybrid-electric system, which significantly reduced emissions in this stage.

End-of-Life (EOL) phase emissions gained importance with the hybrid-electric system. Proper battery disposal is essential to prevent toxic waste. Special EOL considerations were developed for the battery, which are presented, together with total aircraft EOL considerations in Section 18.5.

[(a)] URL: `https://www.sciencedirect.com/topics/earth-and-planetary-sciences/life-cycle-analysis` [accessed 2 May 2024]

[(b)] URL: `https://www.transportenvironment.org/articles/how-clean-are-electric-cars` [accessed 19 May 2024]

In general, the HumanAir initiative aimed to develop an aircraft design with 50% lower CO_2 emissions as compared to the Cessna 206, per average mission., and achieved this goal, although only after a number of operational years. This is because current battery technology forced slightly too much of the engine power to be supplied by the ICE. However, as battery technology improves, the aircraft reliability on fossil fuel power will decrease, and on average 50% was achieved. For a more detailed explanation, please refer to Section 18.4.

Note that, following the principle of reducing CO_2 emissions by half as compared to the Cessna 206, all other HA-1 emissions from fossil fuel combustion would also be halved, thus also mitigating most additional major environmental pollutants other than CO_2. However, with the introduction of the battery, additional sources of toxic waste were introduced, most notably thermal runaway. To protect passengers, the batteries shall be encapsulated in a fire retardant casing equipped with a ventilation system that would redirect toxic lithium gasses into the atmosphere. Despite this, overall emissions from battery failure are expected to be lower than those from continuous fossil fuel use, given the low probability of such events and frequent battery replacements.

The following sustainable design philosophies should continue to be applied in future design stages:

- **Material Selection and Manufacturing Process**: Prioritize materials with lower environmental impact and implement sustainable manufacturing techniques.
- **Energy Efficiency and Alternative Propulsion**: Explore and invest in propulsion systems with lower emissions, and optimize aircraft efficiency to reduce energy consumption.
- **End-of-Life Considerations**: Design components for easy disassembly and recycling, and establish partnerships with recycling facilities to reclaim valuable materials from retired aircraft.

18.2. Economic sustainability

A common challenge with sustainable solutions is their higher cost compared to traditional options. This was one reason why sustainable fuels like hydrogen and ethanol were not feasible for this design.

To avoid imposing significant costs on MAF, the unit cost of the aircraft was kept below US$1.5 million, with operational costs at US$244, meeting MAF's budget requirements. While the Cessna 206 had a lower unit cost, its higher operational costs of US$322 would ultimately make it more expensive than the HA-1.

Future economic sustainability strategies include:

- **Cost Estimation and Reduction**: Continuously monitor and reduce costs throughout the development process without compromising sustainability goals.
- **Market Diversification and Collaboration Opportunities**: Explore new markets beyond humanitarian missions, such as commuter and cargo services, and investigate potential collaborations with existing players.

18.3. Social Sustainability

The HumanAir project is primarily dedicated to supporting current MAF operations, which are fundamentally humanitarian in nature[(c)]. By focusing on aiding communities in remote areas, the project inherently contributes to societal welfare and is thus inclusive. In order to allow MAF to continue the critical work they do, and allow continuation of the current social sustainability MAF provides, they have been offered a reduction in the unit price of the HA-1 aircraft compared to the private market, keeping the unit cost of the aircraft at 1.5 million.

The following preliminary social sustainability strategies shall still be kept in mind in the future:

- **Community Engagement**: Engage with local communities and stakeholders to understand their needs and preferences regarding air transportation services.
- **Accessibility**: Design the aircraft to accommodate passengers with disabilities and special needs.

[(c)]URL: `https://mafint.org/what-we-do/quality-safety` [accessed 3 May 2024]

18.4. CO_2 Emissions Calculator

In order to achieve the desired 50% reduction in CO_2 emissions, it is important to be able to estimate the CO_2 emissions of the aircraft design. Though this aircraft design is capable of flying over 600 NM, most of MAF's missions are shorter. With a hybrid-electric aircraft, the battery can be used for a large portion of the flight at short distances, significantly reducing emissions. Furthermore, the lower cruise speed compared to current operations will influence both fuel and maintenance emissions.

A more detailed CO_2 emissions calculator was thus created, taking all these factors into account. First, MAF provided the distribution of lengths of individual flight legs. However, they generally cannot refuel or recharge at remote bases, so each mission consists of multiple legs before recharge/refuel. MAF thus also provided some statistical data (minimum, maximum, average, and median) regarding the length of missions before refuelling for some of their aircraft. The first dataset suggested a log-normal distribution of flight lengths, so log-normal distributions were fit to the aircraft individual data, and an average overall distribution was created, presented in Figure 18.1. With this profile, combined with design cruise speed, estimated battery capacity and cruise power, it was possible to determine the (weighted average of) fuel emissions per mission for a given aircraft design.

The emissions due to maintenance must still be considered, however. With a lower cruise speed, missions are longer, and thus the maintenance emissions per mission are higher. This is not a linear scale, though, as some maintenance is related to flight cycles rather than flight time. To obtain an estimate, it was assumed that maintenance emissions scale linearly with maintenance cost, and statistical data on maintenance cost per flight hour depending on flight time was used (see Figure 18.2). The graph was scaled to match the maintenance costs of a Cessna 206, and it was assumed that the maintenance costs (and therefore emissions) for HumanAir would follow the same distribution as for the Cessna. With this data (and the design cruise speed), it was thus possible to estimate maintenance emissions per mission for the aircraft design.

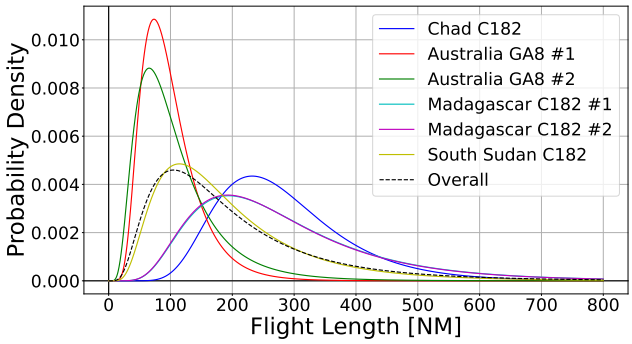

Figure 18.1: Modelled Distribution of MAF Mission Lengths[(d)], with Averaged Overall Distribution Overlaid

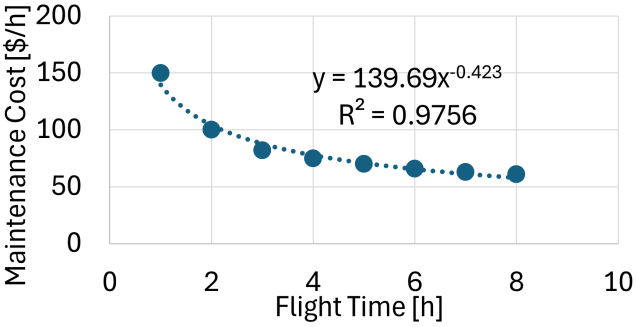

Figure 18.2: Dependence of Maintenance Cost Per Flight Hour on Flight Time[(e)]

Finally, combining fuel and maintenance emissions data, total emissions per return mission can be estimated. With current battery technology (energy density around 350 Wh/kg [83]), the emissions reduction only amounts to 37%. Battery technology has been rapidly developing, however, and it is expected that in around 10 years, energy density could reach 685 Wh/kg [84], allowing for an emission reduction of 70%. Lyent is a company that already started mass production of high energy density Lithium-Sulfur energy cells that vary between 300 and 600 Wh/kg[(f)]. Additionally, Airbus already developed and flown a battery-powered aeroplane for 11 days using batteries that have a specific energy density of 350 Wh/kg which were developed by Sion Power [(g)]. The goal of programs such as the ESS-1K Workshop funded by the US government is to reach in the next 10 years an energy

[(d)] Data provided directly by MAF.
[(e)] URL: `https://www.linkedin.com/pulse/understanding-airplane-maintenance-costs-tabish-khan/` [accessed 16 May 2024]
[(f)] URL: `https://lyten.com/products/lithium-sulfur-batteries/` [accessed 20 May 2024]
[(g)] URL: `https://sionpower.com/` [accessed 20 May 2024]

density of 1000 Wh/kg with a volumetric density of 1000 Wh/m^3 for batteries [(h)]. As the aircraft must be delivered within 5 years, however, this technology is unlikely to be available by then. A plan was thus devised under which the aircraft will be delivered in 5 years, with current battery technology, thus not quite meeting the emissions reduction target. Once the new battery technology is ready, the battery of the aircraft can be swapped for a new one (included in the aircraft purchase price). After some time, the higher than required reduction will compensate for the additional initial emissions, thus reaching the overall target. A plot of when the target will be met depending on when better technology is available is presented in Figure 18.3. If better batteries are, as expected, available in 10 years' time, the 50% emissions reduction target will be met in 2039 and far exceeded afterwards.

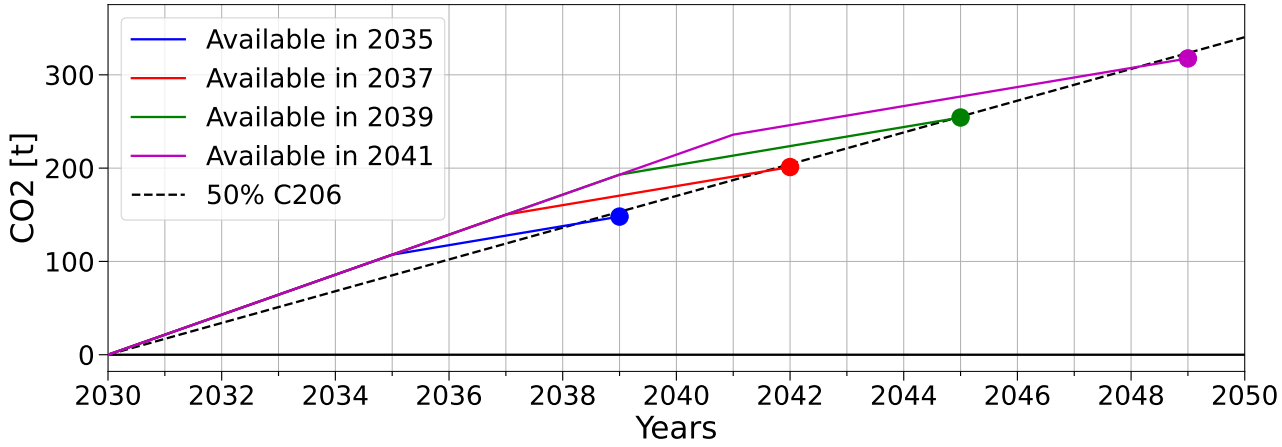

Figure 18.3: Plot of Overall CO_2 Emissions Depending on Date of Improved Battery Introduction

It is important to mention that the new battery technology is expected to have a higher volumetric density than the currently, available batteries. Thus, some considerations must be implemented in the design procedure of the aircraft. The weight of the new batteries must be kept constant with respect to the old batteries that will be eventually replaced. This ensures the stability and controllability of the aircraft will not be affected and no additional structural consideration needs to be taken into account. Additionally, the design must encompass the largest volume out of the two possibilities such that no additional space is required at any point in the lifetime of the aircraft. Finally, the batteries need to be placed such that they can be easily removed and replaced. Special compartments were designed to facilitate such operations.

The solution of replacing only the batteries instead of the entire aircraft is more economically sustainable for two particular reasons. Firstly, the price of a battery would not exceed more than $35000. Since the aircraft will depreciate after a couple of years with more than $35000 it is not profitable to try and sell the aircraft to recover the cost of a brand new aircraft when only the batteries can be swapped. Additionally, all the batteries - both current and future technology - must be replaced every two years. Therefore the replacement of new battery technology can be made during one of the planned battery swaps that are required regardless of the presence of the new technology on the market.

18.5. Aircraft End of Life Considerations

A very important part of the aircraft's lifetime is the actions taken at EOL. Depending on these actions, the environmental impact of this phase can be quite significant. The most environmentally hazardous component of the aircraft, by far, is the battery. Other components are primarily metal and will not release large quantities of toxins upon decomposition. Hence, a detailed EOL analysis will be performed for the battery in Section 18.5.1. For the remaining aircraft components, only a generalized

[(h)]URL: `https://theaircurrent.com/technology/path-to-1000-wh-kg-battery-development/` [accessed 20 May 2024]

description of EOL procedures will be provided, as this largely depends on the policy of the third-party organisation that ensures EOL of the aircraft.

18.5.1. Battery EOL

As mentioned in Section 18.4, the battery will eventually have to be decommissioned and replaced. When assessing EOL characteristics of the old battery, the first consideration would be to determine when EOL of the battery occurs. For safety reasons, it was decided to replace the battery after it's rated 1000 charging cycles [84], which translates into two years of operation per battery.

The second consideration is the process of removing the battery from the aircraft. In order to ease this process, the aircraft's internal design was adapted. To facilitate this, the aircraft's internal design was adapted. For the forward battery position, illustrated in Figure 18.4, a removable compartment was incorporated into the floor directly above the battery, located below the pilot and first passenger row seats. The seats are designed to be removable as well. For the aft battery, a removable section is included in the most aft wall of the internal cabin. This design eliminates the need for cutouts in the fuselage and nosecone structure, thereby saving significant structural weight.

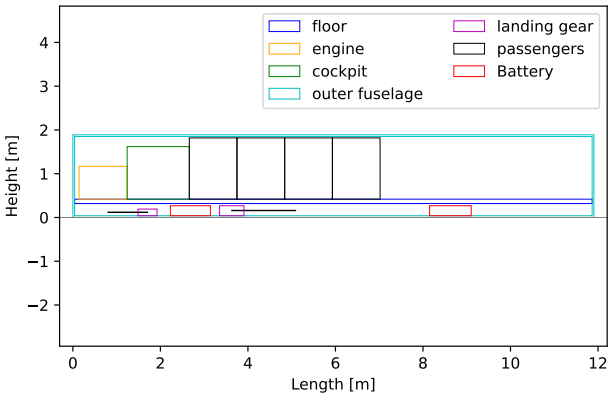

Figure 18.4: Fuselage Side View

The most important consideration regards what to do with the batteries once they are retrieved. There are several options: reuse, recycle, or dispose. Disposal is not an option due to its adverse environmental effects. Reusing the batteries is possible but requires frequent maintenance checks as the batteries would have exceeded their rated cycles, increasing the risk of failure, which could be catastrophic for larger battery packs. For recycling the batteries, three methods exist:

Pyrometallurgy uses heat to convert the metal oxides present in the used batteries into metals or metal compounds. In this process, all carbon-based compounds are burned, and the valuable metals like Co, Ni, and Mn end up in an alloy, while other components like the electrolyte, steel, aluminium, and lithium are lost as slag or off-gas [85, 86].

Hydrometallurgy employs acid solutions to exploit the high solubility of transition metals (e.g., Co, Ni, Mn, and Fe) and lithium in acid. Most commonly, substances like H_2SO_4 and H_2O_2 are used. Recovering the electrolytes is also possible but requires more complex procedures [85, 86].

Direct recycling aims to restore the cathode material without decomposing the battery into its constituent elements. The recovered materials can be refurbished or directly reused in new battery packs [85, 86].

Neither method is perfect, each having its pros and cons in terms of cost, percentage of minerals retrieved, and environmental impact. Hydrometallurgy, while not the most environmentally friendly, is the most widely used and economically feasible technique, yielding high mineral extraction percentages [87] at an average cost of 3 to 8 US$ per kg of battery, depending on the facility and country of origin [(i)]. Hence, this methodology is suggested for the HA-1. Note that, after recycling, the retrieved minerals are not returned to MAF. Direct recycling is the most environmentally friendly method as it avoids incineration and toxic acid reactions [85–87]. However, it requires manual labour, making it significantly more expensive than automated hydrometallurgy and pyrometallurgy. For a list of potential battery recycling facilities, one can refer to the paper by Zachary et al. [86].

[(i)] URL: `https://www.automotivemanufacturingsolutions.com/ev-battery-production/ev-battery-recycling-cost-and-components/41287.article` [accessed 19 May 2024]

18.5.2. Airframe EOL

After the batteries have been removed, the majority of aircraft components still remain and can be separated into two categories: (1) components that can be refurbished and (2) components that have actually reached their End-Of-Life (EOL) and need to be recycled [88].

Refurbished items may include aeroplane seats, cockpit electrical instruments, landing gear, and other high-value parts. These components are typically removed from the decommissioned aircraft, inspected, and repaired[(j)] [89]. When the components are planned to be reused as aircraft components, additional repairs and safety checks will be necessary to meet the required safety and performance standards[(k)] [89].

Components to be recycled vary widely in nature but can be categorized into three main categories: ferrous metals, non-ferrous metals, and plastics [89]. The initial challenge, however, is to separate these components from each other, as they occur all over the aircraft. After stripping the aircraft of all refurbishable components, the aircraft will be prepped to be fed into a hammer mill, which shreds the aircraft parts into pieces [88]. Using sieves, magnets, and eddy current separation, the resulting scrap is then separated into the aforementioned categories [89], which can then be further recycled.

An important consideration lies in this recycling process. For the non-ferrous scrap pile, for example, a large variety of aluminium and titanium alloys may be present, which are both very popular metals within the aircraft and automotive industry[(l)] [89]. Furthermore, the separation process is not perfect, so a number of impurities may still be present in the recycled material [89]. Hence, when the scrap material is remelted together, the end product will be a different alloy which combines all the alloys fed into it, along with their accompanying constituents and impurities. As a result, the material is likely not reusable by any client that requires a specific alloy. Research is being conducted, however, that takes advantage of the different refraction mechanisms of different types of alloys to also separate the alloys. Example mechanisms used are X-ray fluorescence or laser-induced breakdown spectroscopy [90]. Nevertheless, the mixed aluminium can still be used in industries with more relaxed requirements for their materials. Especially since recycled metals are significantly less expensive, energy-intensive and environmentally polluting to obtain, as illustrated in Figure 18.5 [89].

Recyclable materials	Potential recovery (kg/year)	Actual recovery (kg/year)	Scrap recycling process/kg		New raw material production process/kg	
			Energy consumption (MJ)	CO_2 emission (kg)	Energy consumption (MJ)	CO_2 emission (kg)
Al alloy	1.1×10^7	2.2×10^6	2.4	0.29	47	3.83
Steel	1.5×10^6	3.1×10^5	/	/	/	/
Non-ferrous metals (except Al)	7.4×10^5	1.5×10^5	/	0.44	/	1.25
Composite material	2.2×10^5	4.3×10^4	33	2	234	12
Other	1.9×10^7	3.8×10^6	/	/	/	/

Figure 18.5: Cost and environmental impact of recycling materials vs new material production [89]

Regarding the HA-1, a distinguishing feature is the uniform use of Aluminum alloy 6061-T6 throughout the aircraft. While this might sound promising for recycling purposes, making separation using innovative methods redundant, the aircraft will very likely be scrapped together with other automotive or aeronautical vehicles simply because it is cheaper. Furthermore, the hammer mill will always contain some form of impurity remaining from previous recycling operations. Hence, reuse of the material of the HA-1 for aerospace use will not be possible without thorough further refinement and inspection.

[(j)] URL: `https://aircraft.airbus.com/en/newsroom/news/2022-11-end-of-life-reusing-recycling-rethinking` [accessed 25 June 2024]

[(k)] URL: `https://aircraft.airbus.com/en/newsroom/news/2022-11-end-of-life-reusing-recycling-rethinking` [accessed 25 June 2024]

[(l)] URL: `https://www.addere.com/materials/titanium/titanium-in-the-automotive-industry/` [accessed 24 June 2024]

19 | Risk Assessment

As the HumanAir project is still in its very early stages, the proposed solution can only be worked out up until a certain point. As there is no physical product yet, a lot of uncertainties remain for the detailed design, manufacturing, certification, distribution, operating and end-of-life phases of the project. To ensure these risks are accounted for before they happen, Section 19.1 works out a risk map in which proper mitigation strategies and contingency plans are worked out to reduce the magnitude of the risks. After that, Section 19.2 establishes if the current proposed falls within the planned contingencies.

19.1. Risk analysis

During the previous design stage, a lot of technical risks on the project have already been defined [12]. These were mostly related to the risk of the failure of components, or to unexpected events that have an impact on the aircraft's performance. However, while designing the aircraft in more detail, multiple choices were made that bring a significant risk. Not only can these influence the technical performance of the part, but they can have a greater impact which might influence the overall feasibility of the HumanAir project. Table 19.1 provides an overview of these risks. Also, an appropriate mitigation strategy and contingency plan are discussed.

Table 19.1: Pre-Mitigation Risk Analysis. L = Likelihood, C = Consequence, R = Risk

ID	Description	L	C	R	Impact	Strategy	
						Mitigation	Contingency Plan
PR-POW-01	Current battery technology not good enough to meet CO_2 requirement.	0.9	0.9	0.81	The project will not meet the user requirement on CO_2 emissions.	**Reduce:** Look at battery technology available at the time of production.	When new battery technology is available, a more efficient battery will be installed within the unit cost.
PR-POW-02	Delivery date for new battery technology is not met.	0.5	0.7	0.35	The project will take longer to meet the user requirement on CO_2 emissions.	**Reduce:** Look for multiple companies that may be able to provide the new technology.	Increase the lifespan of the aircraft to still obtain the required CO_2 reduction within the lifetime.
PR-POW-03	Targets for solar power not met.	0.3	0.5	0.15	Not enough green energy available to charge up the battery.	**Reduce:** Include a safety margin for the number of solar panels to be installed.	Use the power from the local power grid.
PR-POW-04	Propeller efficiency is lower than estimated.	0.3	0.7	0.21	Increase in CO_2 emissions as more power is required.	**Remove:** Obtain data from the propeller manufacturer on the propeller efficiency and incorporate this in the design.	Develop our own custom propeller instead of buying an available one.
PR-POW-05	Battery power deteriorates over time.	0.9	0.7	0.63	The project might not meet the user requirement on CO_2 emissions.	**Reduce:** Implement adequate charging and cooling. Reduce: Implement detailed battery monitoring.	Replace the battery when the battery life has been reached.

PR-DES-01	Zero-lift drag targets not obtained in windtunnel test.	0.5	0.7	0.35	Increase in CO_2 emissions as more power is required.	**Reduce:** Perform multiple windtunnel tests throughout the designing stage to be able to incorporate results in the design. **Reduce:** Validate the CFD results with windtunnel data to increase CFD accuracy.	Allocate more resources to wing design, as this provides the most drag.
PR-DES-02	A performance-impacting mistake is discovered in the design process.	0.9	0.7	0.63	The product might not operate according to the user requirements or not operate at all. New design iteration required, delaying the project.	**Reduce:** Implement proper verification and validation on design tools. **Reduce:** Implement standardised design procedures. **Reduce:** Regular project stagegates at which the design will be judged by external experts.	Perform another design iteration.
PR-DES-03	MTOW is higher than estimated.	0.7	0.9	0.63	Snowball-effect will increase the weight of all components.	**Reduce:** Use safety margins and contingencies during the design process.	Perform class-III weight estimation to increase accuracy and perform new design iteration if needed.
PR-DES-04	Failing to meet CS23 requirements.	0.5	0.5	0.25	Delay in delivery of product.	**Reduce:** Keep close contact with the certification authorities during the design phase.	Implement design feedback from EASA.
PR-FIN-01	Aircraft costs are higher than estimated.	0.7	0.7	0.49	More sells needed to obtain the break-even point.	**Reduce:** Design a business plan for more aircraft than needed to meet the break-even point.	Move manufacturing to different countries with cheaper manufacturing costs.
PR-FIN-02	Competitor brings a competitive aircraft to the market.	0.7	0.5	0.35	Less interest in the HumanAir HA-1.	**Transfer:** Cooperate with existing companies to develop and produce the aircraft.	Elongate design phase to outperform the competition.
PR-FIN-03	No manufacturer wants to pick up the HumainAir programme.	0.5	0.9	0.45	Production costs will increase significantly since HumanAir will need to produce the aircraft in-house.	**Reduce:** Include the external manufacturers from the design phase already to ensure interest in the product.	Set up own manufacturing location and accept reduction in profit.
PR-FIN-04	Part suppliers go out of business.	0.3	0.5	0.15	Delays in delivery of product.	**Reduce:** Keep close contact with all involved manufacturers. **Reduce:** Work with multiple part suppliers.	Contact one of the other manufacturers.
PR-FIN-05	Amount of sold aircraft target not met.	0.7	0.9	0.63	The project will make a loss.	**Reduce:** Attract multiple customers instead of only one. **Transfer:** Attract investors and shareholders that will partly carry the risk. **Reduce:** Apply contingencies on the target sell number.	Increase aircraft unit cost

PR-DEL-01	Delays in manufacturing due to various reasons.	0.7	0.5	0.35	Delays in delivery of product.	**Reduce:** Work with existing experienced manufacturers. **Reduce:** Spread manufacturing work over multiple manufacturers. **Reduce:** Keep a stock of parts so that parts are always available.	Contact more suppliers and manufacturers to reduce product backlog.
PR-DEL-02	Delays in certification due to various reasons.	0.7	0.5	0.35	Delays in delivery of product.	**Reduce:** Contact airworthiness authorities early on in design phase to quickly discover non-compliance	Continue manufacturing to the extent possible. Inform customers about possible delays.
PR-DEL-03	Delays in product shipping due to various reasons.	0.7	0.5	0.35	Delays in delivery of product.	**Reduce:** Keep close contact with local authorities to monitor the situation in the region.	Inform customers about possible delays.
PR-MIS-01	MAF starts flying longer compared to the analysed average mission profile.	0.1	0.7	0.07	Increase in CO_2 emissions.	**Accept:** The aircraft will be designed for their current mission profile and any deviances are at their own responsibility.	N/A
PR-RIS-01	Failure to identify a risk.	0.7	0.7	0.49	Unexpected change in the project for which no plan has been thought out.	**Reduce:** Assign a dedicated experienced project risk manager.	Reflect on mistakes in risk assessment and determine mitigation strategy.
PR-LDG-01	Retractable landing gear concept does not comply with low maintenance targets.	0.5	0.9	0.45	Retractable landing gear cannot be used. Therefore drag targets not met.	**Reduce:** Use/develop a low-maintenance retraction mechanism.	Design aerodynamic fairing for the fixed landing gear and perform new design iteration. Accept changes to CO_2 reduction.
PR-LDG-02	Pilots may not know how to operate retractable landing gear.	0.7	0.7	0.49	Pilots cannot operate the new aircraft.	**Remove:** Provide training to all pilots who will operate the new aircraft.	Install manuals in the aircraft for reference during flight.
PR-EOL-01	Customer does not want to invest in proper EOL procedures.	0.5	0.3	0.15	Sustainability targets will not be met.	**Reduce:** Design easy to follow end-of-life procedures that can be implemented by customer.**Transfer:** Make customer responsible for end-of-life.	HumanAir will recycle the battery to ensure proper end of life of the hardest component to properly recycle.
PR-REQ-01	Change in user or stakeholder requirements	0.3	0.7	0.21	Current design might not comply with requirements anymore.	**Reduce:** Keep close contact with all stakeholders to identify changes early on.	Perform new design iteration.
PR-LIF-01	Aircraft does not reach projected lifetime	0.5	0.7	0.35	Aircraft is less attractive to potential customers.	**Reduce:** Perform detailed analysis of aircraft systems lifetime. **Reduce:** Supply customers with detailed documentation on aircraft maintenance.	Update maintenance procedures.

PR-PRO-01	Engine manufacturer goes out of business.	0.3	0.7	0.21	No engine is available to power the aircraft that meets the requirements.	**Reduce:** Contact engine supplier early on in the design and place order as an investment.	Certify an existing diesel engine for use in aircraft.
PR-SEC-01	The solar panel site may be vulnerable to security breaches.	0.5	0.5	0.25	Damaged or stolen solar panels, limiting the power produced.	**Reduce:** Install fencing around the solar panel site. **Reduce:** Only have solar panels at MAF bases, where security is already established.	Replace stolen or broken solar panels and inform local authorities supported by camera evidence.

After applying the mitigation strategy for every risk, the likelihood and consequences of each of them may change. Therefore, the values are re-evaluated and presented in Table 19.2. This table also highlights the residual risks, which are the risks that remain after implementing the mitigation strategies. Additionally, it lists the responsible members for each risk.

Table 19.2: Post-mitigation Risk Analysis. L = Likelihood, C = Consequence, R = Risk

ID	L	C	R	Residual Risk	Responsible
PR-POW-01	0.5	0.9	0.45	The new battery technology takes longer to arrive than estimated.	Design department.
PR-POW-02	0.5	0.5	0.25	Longer lifetime needed to make CO_2 targets.	Design department.
PR-POW-03	0.3	0.3	0.09	The project will take longer to meet the CO_2 reduction targets.	Design department.
PR-POW-04	0.1	0.7	0.07	Delays in design as a new design iteration may be needed.	Design department.
PR-POW-05	0.5	0.3	0.15	Increased cost and maintenance time.	Design department.
PR-DES-01	0.3	0.5	0.15	Delays in design as a new design iteration may be needed.	Design department.
PR-DES-02	0.3	0.7	0.21	Delays in design as a new design iteration may be needed.	Design department.
PR-DES-03	0.7	0.3	0.21	Delays in design as a new design iteration may be needed.	Design department.
PR-DES-04	0.3	0.5	0.15	Product requires significant changes.	Design department.
PR-FIN-01	0.7	0.3	0.21	Reduction in profit made by the HumanAir program.	Financial department.
PR-FIN-02	0.1	0.3	0.03	Delayed development time hurts business case.	Financial department.
PR-FIN-03	0.3	0.9	0.27	Increase in unit cost	Financial department.
PR-FIN-04	0.3	0.3	0.09	No new part supplies can be found	Financial department.
PR-FIN-05	0.7	0.3	0.21	Investors and shareholders may pose extra constraints on the project.	Financial department.
PR-DEL-01	0.3	0.5	0.15	Delayed delivery of product due to unmitigated manufacturing faults.	Production department.
PR-DEL-02	0.3	0.5	0.15	Product requires significant changes or delay of delivery.	Certification department.
PR-DEL-03	0.3	0.3	0.09	Customers receive their aircraft later than expected.	Distribution subcontractors.
PR-MIS-01	0.1	0.7	0.07	Unchanged	MAF
PR-RIS-01	0.3	0.7	0.21	Unexpected change in the project for which no plan has been thought out.	Risk manager.
PR-LDG-01	0.3	0.9	0.27	Unchanged	Design department.
PR-LDG-02	0.1	0.7	0.07	N/A	Training department.
PR-EOL-01	0.3	0.3	0.09	Sustainability targets will not be met.	Maintenance department.
PR-REQ-01	0.3	0.5	0.15	Stakeholders change their mind on the requirements.	Relationship manager.
PR-LIF-01	0.3	0.5	0.15	Users do not adequately maintain their aircraft.	Maintenance department.
PR-PRO-01	0.1	0.7	0.07	Engine manufacturing runs into issues.	Design department.
PR-SEC-01	0.1	0.5	0.05	Increased costs due to replacement of panels.	Maintenance department.

A risk map can be created using the assessed values of consequence and frequency from the previous tables. A risk map is a visualisation tool that highlights risks requiring careful attention. The map uses consequence and likelihood as its axes, with different colours indicating the severity of risks. The risk map for risks before mitigation is presented in Table 19.3, and the map for risks after mitigation can be found in Table 19.4.

Table 19.3: Pre-mitigation Risk Map

	Very Low RIsk	Low Risk	Medium Risk	High Risk	Very High Risk
	Risk Assessment				
Consequence: Catastrophic (=0.9)	PR-MIS-01	PR-POW-04, PR-REQ-01, RP-PRO-01	PR-FIN-03, PR-LDG-01	PR-DES-03, PR-FIN-05	PR-POW-01
Consequence: Critical (=0.7)			PR-POW-02, PR-DES-01, PR-LIF-01	PR-FIN-01, PR-RIS-01, PR-LDG-02	PR-POW-05, PR-DES-02
Consequence: Marginal (=0.5)		PR-POW-03, PR-FIN-04	PR-DES-04, PR-DEL-03, PR-SEC-01	PR-FIN-02, PR-DEL-01, PR-DEL-02	
Consequence: Minimal (=0.3)			PR-EOL-01		
Consequence: Negligible (=0.1)					
	Very Unlikely (=0.1)	Unlikely (=0.3)	Probable (=0.5)	Very Probable (=0.7)	Frequent (=0.9)
	Likelihood				

Table 19.4: Post-mitigation Risk Map

	Very Low RIsk	Low Risk	Medium Risk	High Risk	Very High Risk
	Risk Assessment				
Consequence: Catastrophic (=0.9)	PR-POW-04, PR-MIS-01, RP-PRO-01, PR-LDG-02	PR-FIN-03, PR-LDG-01 PR-DES-02, PR-RIS-01	PR-POW-01		
Consequence: Critical (=0.7)					
Consequence: Marginal (=0.5)	PR-SEC-01	PR-DES-01, R-DES-04, PR-DEL-01, PR-DEL-01, PR-REQ-01, PR-LIF-01	PR-POW-02	PR-DES-03, PR-FIN-01, PR-FIN-05	
Consequence: Minimal (=0.3)	PR-FIN-02	PR-POW-03, PR-FIN-04, PR-DEL-03, PR-EOL-02	PR-POW-05		
Consequence: Negligible (=0.1)					
	Very Unlikely (=0.1)	Unlikely (=0.3)	Probable (=0.5)	Very Probable (=0.7)	Frequent (=0.9)
	Likelihood				

Comparing Table 19.3 and Table 19.4, it is evident that most risks have shifted to low or very low-risk regions. However, even after applying the mitigation strategy, PR-POW-01 remains a high risk, as the consequence of the battery technology not being available might lead to the project not meeting the emission reduction targets and therefore not meeting the user requirements. However, the potential advantages are deemed to outweigh the risk here. As HumanAir is entering a market where such big emission reductions have never been achieved, it is deemed necessary to take the risk in pursuit of innovation.

Finally, some risks remain in the “high” category. These risks should be closely monitored throughout the remainder of the project.

19.2. Technical Resource Budget

The technical resource budgets are used to make sure important resources relevant to the design process are properly attributed [91]. In the current phase of the design process of the aircraft, the most important resources are the weight of the aircraft and the power used by the subsystems. These resources will be relevant in the further design processes where specific components will have to be selected based on the established budgets.

Using the weight estimation method described in Chapter 8, the weight distribution by each subsystem was calculated and the complete sets of results is tabulated in Table 8.2.A summary of the main weight groups is provided below:

Table 19.5: Weight Budget

Weight component [N]	Value
MTOW	35192
OEW	26471
Fixed equipment weight	3960
Structures weight	8990
Powerplant weight	5490
Payload	6922
Fuel weight	2782
Battery weight	7079

The power budget was also calculated based on the Electrical Block Diagram presented in Section 12.6. The main power sources are the battery system mounted on the aircraft and the IC engine. In addition to these two systems, power is required to power the avionics that run at 28V DC and 60A in total [(a)]. Thus, their maximum power consumption is rated at around 1680W which represents only **0.45%** of the maximum power that can be provided by the IC engine alone and **1.08%** of the maximum power that can be deployed by the battery system. Therefore, the power consumed for avionics can be considered negligible with the implementation of the parallel system architecture from Figure 12.4.

A power breakdown can be constructed based on the primary systems identified. The results can be visualised in Table 19.6.

Table 19.6: Power Budget[(b)]

Power [W]	Lower Bound Value	Upper Bound Value
Primary Flight Display	50	100
Multi-Function Display	100	200
Communication Radios	10	30
Navigation Radio	10	30
Transponder	10	20
Autopilot	10	50
Automatic dependent surveillance–broadcast	10	20
Weather radar	100	200
Intercom system	5	10
Hydraulic pumps	1000	2000
Landing gear electric motor driven system	500	1500
Power required propeller take-off	373000	
Power required propeller cruise	133000	
Power available IC engine	373000	
Power available motor	380000	
Power margin take-off	50.0%	49.6%
Power margin cruise with batteries alone	32.6%	32.5%

As can be seen, the critical case for the power budget is defined by the cruise operation while only using the batteries. Even though the engine is able to be run in parallel with the batteries to power the instruments, that will impact negatively the emission. Therefore, the decision was made to move on with not additional power from the engine when batteries are engaged during the cruise.

The cost breakdown structure is presented in Chapter 17. The margin in cost such that a relevant profit margin is still attained is set at 9.3%. This value will be used as the contingency applied for the cost in the TPM which is explained in detail in Section 19.3.

[(a)] URL: `https://www.cfinotebook.net/notebook/operation-of-aircraft-systems/electrical` [accessed 19 June 2024]

[(b)] URL:`http://www.aeroelectric.com/Reference_Docs/Cessna/cessna-poh/C208_675HP_1998_POH_Cessna-Caravan-updated-to-2004.pdf` [accessed 19 June 2024]

19.3. Technical Performance Measurement

The Technical Performance Measurement (TPM) deals with relevant parameters to the design process that can determine the success or the failure of the project [91]. Firstly, the most important resource parameters need to be identified. This can be deducted from the top-level user requirements and the project objective statement and are the following:

- **CO_2 Emissions** - The main objective of the project is to decrease the operational CO_2 by 50% compared to a Cessna 206 as mentioned by **HA-UR-006**. Thus, the relative importance is evaluated at **30**%.
- **Cost** - The sustainability strategy proposed doesn't limit only towards CO_2 emissions but also towards the financial aspects of the mission. The aircraft is going to be purchased and operated by MAF, a humanitarian organisation, funded by donors. Thus, judging by the two top-level user requirements regarding the unit cost **HA-UR-009** and the operational cost **HA-UR-008**. Thus, the relative importance is evaluated at **25**%.
- **Range** - The range is given as a top-level requirement **HA-UR-001** relevant to humanitarian operations. Thus, the relative importance is evaluated at **10**%.
- **MTOW** - The maximum take-off weight was chosen as a parameter since it encompasses OEW, payload mass, and fuel mass. Payload is defined by a top-level requirement **HA-UR-002** which can determine the success or failure of the mission. Thus, the relative importance is evaluated at **10**%.
- **Take-off length** - The take-off length is given as a top-level requirement **HA-UR-003** relevant to humanitarian operations. Thus, the relative importance is evaluated at **10**%.
- **Implementation Time** - The implementation time plays a crucial role in the development of the aircraft design.
- **Power/Thrust** - The power generated by the aircraft is a relevant parameter in the sizing of the propulsion system. However, since the parameter is not set as a top-level requirement, its relative importance is evaluated at **5**%.

The pre-planned contingencies were not changed with respect to the ones presented in [12]. The current values had to be updated based on the technical resource budgets and the risk identified. A 12% contingency was used for the weight budget which is directly related to the performance parameters: range, emissions, take-off length. The power contingency based on Table 19.6 was found to be 32.6% for the most constraining case, while the cost contingency was set at only 9.3%. The newly obtained values are tabulated in Table 19.7.

Table 19.7: Updated Contingencies

	Emissions	**Range**	**MTOW**	**Cost**	**Take-off length**	**Time**	**Power**
Planning	50	50	50	50	50	35	50
Conceptual Design	25	25	30	30	25	25	22
Preliminary Design	15	21	21	20	21	15	15
Current values	12	12	12	9.3	12	10	14.3
Detailed Design	2	12	12	15	12	10	10
Manufacturing	0	10	10	10	10	10	10
Flight Test	0	5	5	3	5	5	5
Production	0	0	0	0	0	0	0
Relative importance	**30**	**10**	**10**	**25**	**10**	**10**	**5**

The TPM values for all the parameters for each phase can be determined by multiplying the relative importance of each parameter with its contingency. The result can be visualised in Figure 19.1.

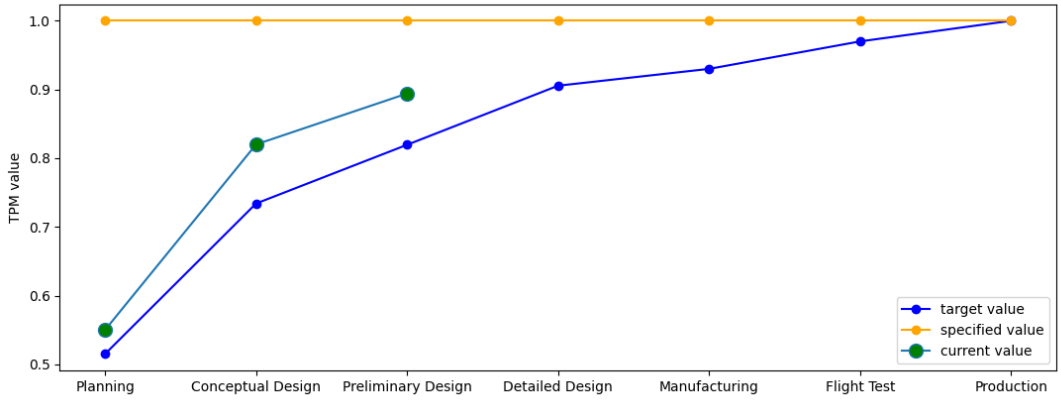

Figure 19.1: Technical Performance Measurement Graph

The current value lies between the target and specified values. Thus, so far the resources are allocated in a proper way. There is enough margin left with respect to the specified value which decreases the risk associated with the development process in the remaining phases.

20 | Design Tool Description

With all design adapting parameters identified, their interdependency can be modelled and integrated into a dedicated design tool designed, verified and validated by the project team. This chapter includes the description of the tool in Section 20.1. With all aircraft design procedures outlined, the aircraft specifications could be iterated and a final preliminary design was found. Section 20.2 includes a sensitivity analysis of the tool in order to increase confidence in the final work and analyse which parameters could be sensitive if unforeseen circumstances appear in terms of changing design margins.

20.1. Script Description

The script has multiple parts where iterations and convergence are made to find all of the parameters necessary for the design with the procedures defined in the subsystem chapter earlier discussed. The main loop has 4 main options: **Generate**, **Class 1 Weight Estimation**, **Class 2 Weight Estimation** and **Fuselage Sizing**. One shall first run all of them when the design tool is opened for the first time with later having the option to run them separately. All of the calculated parameters are saved in the file 'design.json' which is divided into different sections such as Aerodynamics, Stability, Performance etc. The main loop with the four options isis represented in Section 20.1. The loops that are used and included while running the 'main.py' file are shown in a more detailed way with capital letters from A up to G. The flowchart has also a legend in the right part of the figure to have a better idea of which block represents what. A red-coloured block means that the parameter is an output, whereas a green-coloured block means that the parameter is an input given by the user based on some specifications of the mission and overall requirements.

Three situations can occur in the code: *Optimum*, *Yes/No* and *Convergence*. Yes/No referees call for user input. A plot or value will be shown. Based on the requirements of the mission and the engineering judgment, the user can choose to type 'y' so that the script can continue or type 'n' for which a new set of values or plots will be shown to be further interpreted. Optimum gets a limit set by the requirements of the user and loops through the specific part of the code until it gets the optimum value within the limit set. When it has been reached, the tool will continue in the direction of the arrow that exits the block and does not go to an input. Lastly, the convergence block, represented by a pink colour, goes through a loop until the last found value and the new value fall within a 2% difference or lower. If convergence is met, the software will continue by going against the arrows that enter the block and will not follow the arrows that exit that respective block.

Besides the main loop represented by capital letters from A to G, the program has more capabilities which are not part of a loop or are not integrated into the main loop because they are not dependent on always updating the values.

The extra options are the brake checking, calculating the wind-gust diagrams, getting the battery optimisation deployment, calculating an optimisation to get the design of the wingbox, getting the loading diagrams from which the x_{cg} excursion can be seen, making a fatigue analysis, making a flutter analysis and plot the power loading diagrams to see exactly which design point was found for which the W/S and W/P values were taken.

The wingbox design consists of an optimisation for which the objective is to sustain the loads and decrease the weight such as the factor of safety being close to the value of 1 along the span of the wing. The aerodynamic forces and coefficients are simulated in XLFR5 and then imported in the same file with the optimisation tool. As the number of discrete points is limited, interpolation was used to get a better refinement of forces applied to the wing's structure.

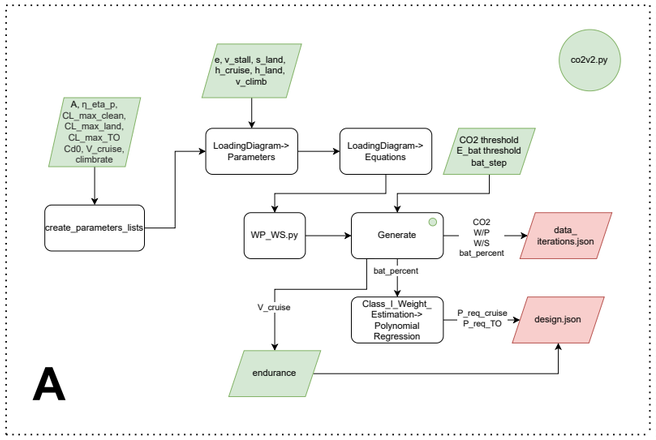

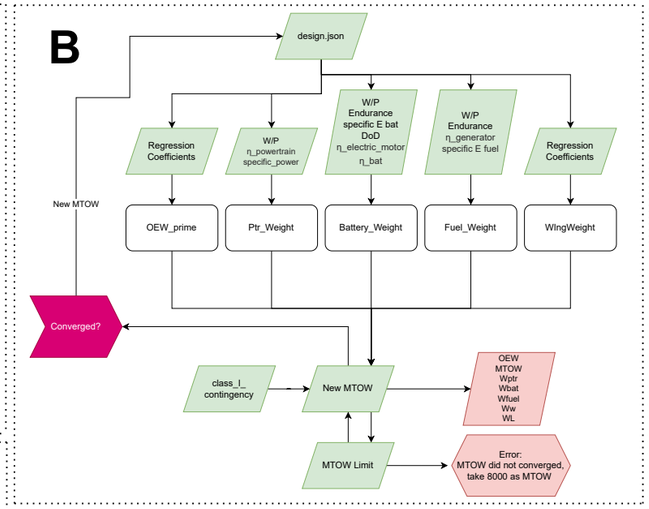

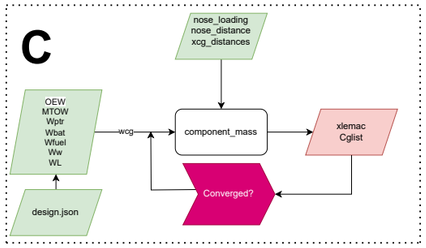

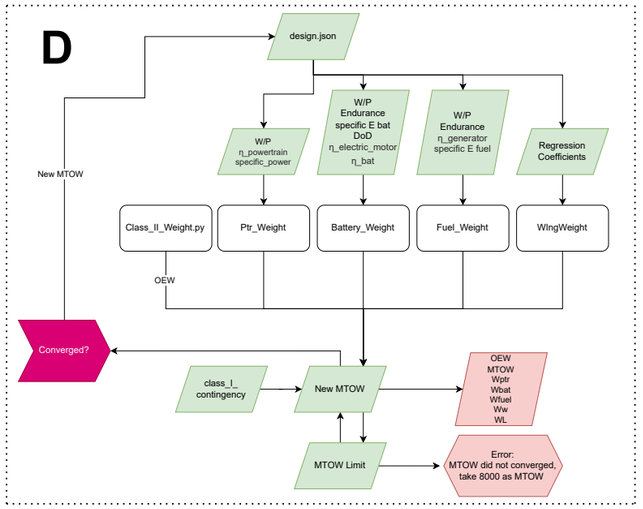

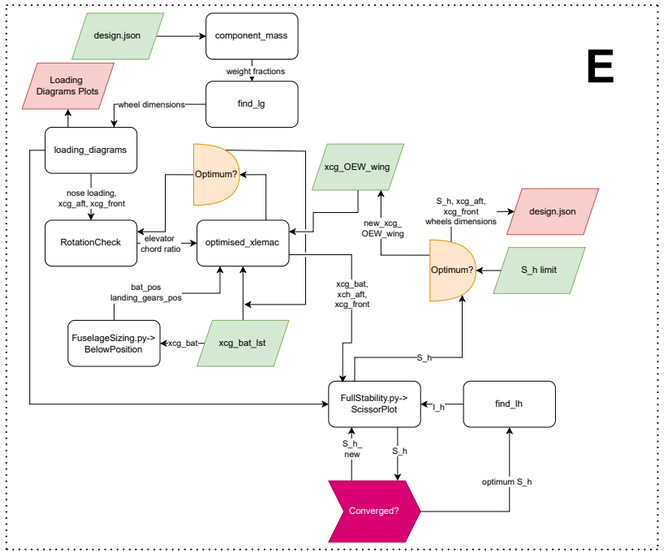

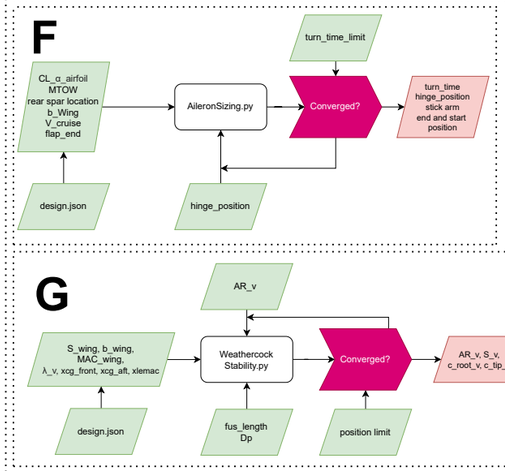

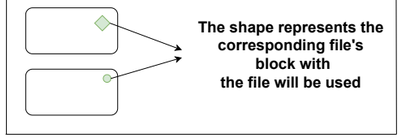

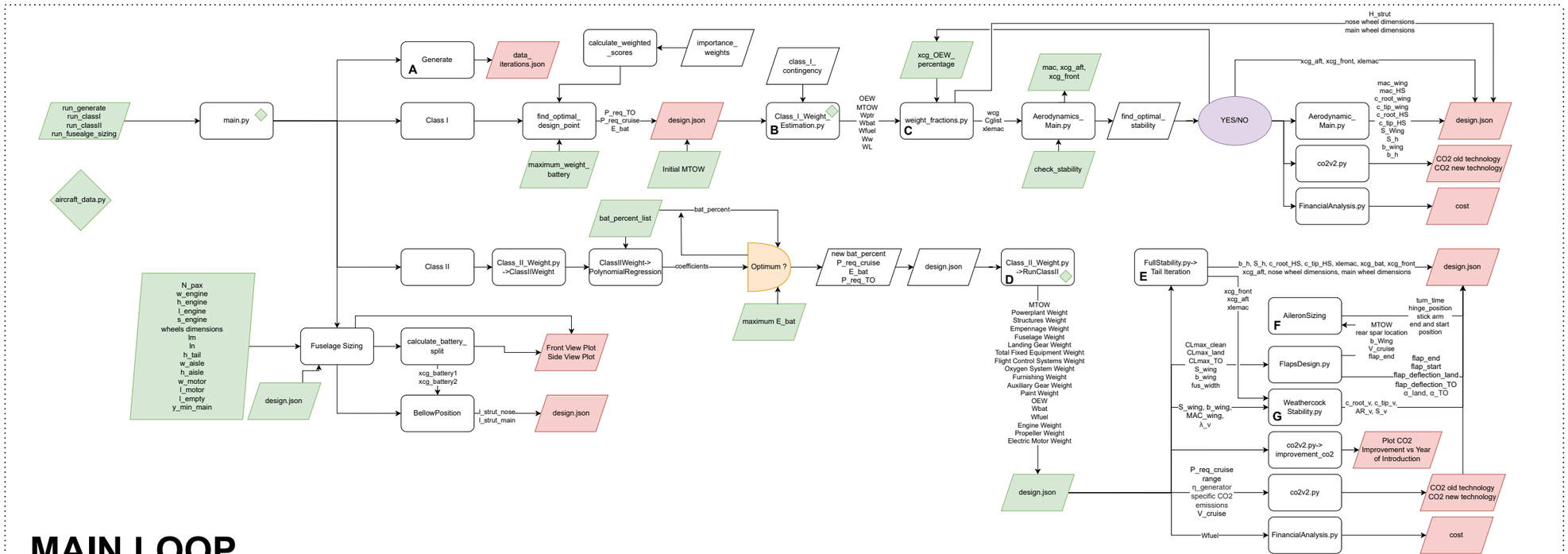

Figure 20.1: Software Flowchart

20.2. Sensitivity Analysis

Sensitivity analysis aims to verify whether slight changes in model inputs yield realistic variations within the script output. Also, the analysis will check if the parameters found are still within the design margins and if a converged point can be found. Due to the immense number of parameters that can be changed and influence the general loops, a simplification was made by identifying the most crucial steps in which if one value changes, the 'snowball effect' will critically damage the convergence procedure. Most of the parameters for the different subsystems are influenced by the maximum take-off weight (MTOW) which is lastly calculated during the class 2 weight estimation. Thus, each component weight was varied by -10% up to +20% to observe the relative difference in MTOW. The upper limit was taken to have a higher magnitude than the lower magnitude as it applies a conservative process. Increasing the weight is not a wanted option. The contingencies and the risks take care of a big change. Thus, the variation in percentages chosen is a reasonable one. As mentioned before in Section 8.2, the components are as follows: Wing, Empennage, Fuselage, Landing Gear, Powerplant System, Flight Control System, Hydraulics, Instruments, Electrical System, Air Conditioning, Oxygen System, Furnishing, Auxiliary Gear Equipment, Paint, Fuel and Battery. Also, the total structural weight and the total fixed equipment weight were plotted to observe a more general view of the main groups of components. A visual representation of the results can be seen in Figure 20.2.

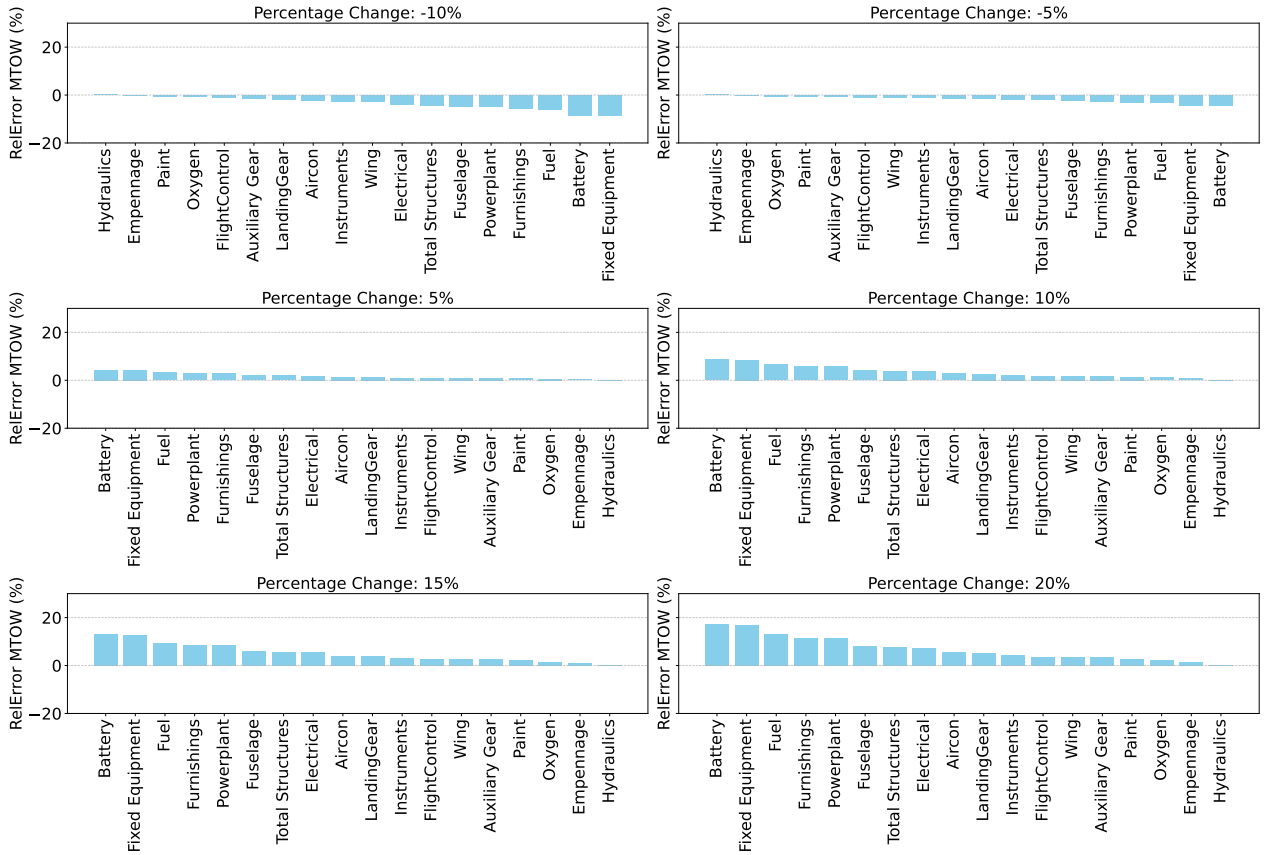

Figure 20.2: Sensitivity Analysis on the Class 2 Weight Estimation Loop of the Script

The battery, fuel, fixed equipment and powerplant have the biggest influence on the MTOW. An interesting finding is that the fixed equipment group has a more than expected impact on the weight of the aircraft, especially for the -10% variation. The value is still reasonable as it includes most of the components listed which are approximately 12% of the MTOW. In the other cases, the battery has the biggest relative error its weight is changed which is expected as it is one of the heaviest components of the aircraft. The limiting case which is still acceptable is for the 15% change because the increase in the battery weight leads to an increase of the MTWO up to approximately 40000 N which is the limit of the class 2 weight estimation presented in Section 8.2. Thus, the upper limit is +15%.

The design margins are an important aspect of the project because they reflect whether the requirements are met or not. Hence, the CO_2 reduction is analysed as a relationship to the MTOW. Stability was one of the most complicated loops in the script so it shall be analysed as well. The direct link is between the MTOW and the surface area of the horizontal stabilizer. The percentages increased by 5% magnitude for the lower limit as a more detailed change can be analysed. The new percentages chosen are between ±15%. The results can be seen in Figure 20.3.

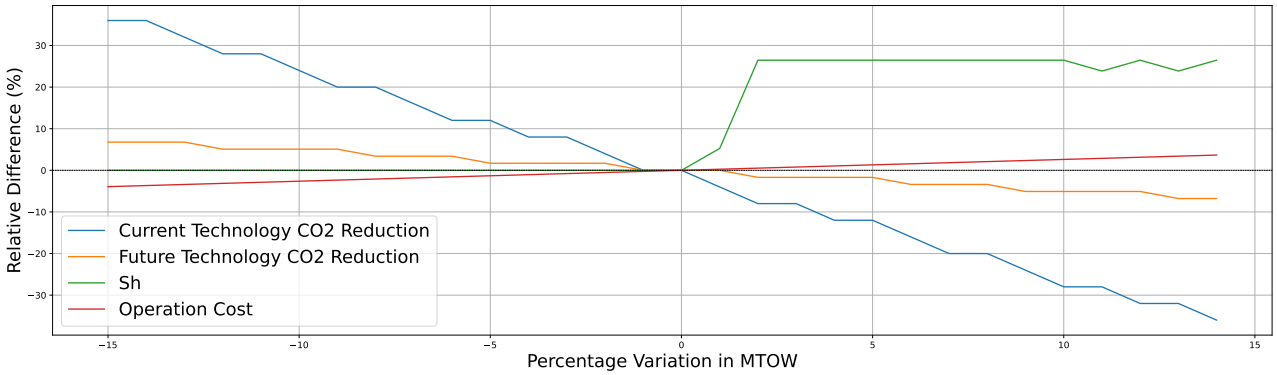

Figure 20.3: Top Level Sensitivity Analysis by Varying MTOW, showing a negative effect of an increase in MTOW on all plotted parameters.

The CO_2 reduction was anticipated to be changed proportionally with the variation in MTOW as they are strongly related. Even with those changes, the overall reduction can be reached by 50% by introducing the new battery technology. Operational cost is almost not affected which is a good thing as it shows that it is not sensitive and will always be within the design margins required by the requirements. The area of the horizontal stabilizer has a sudden increase up to 20% after the variance in MTOW is a positive one. The phenomenon is produced by the fact that the convergence loop for stability requires a new point on the scissor plot. The behaviour of the curve starts to stabilise. A sudden increase could be expected if a drastic increase in the weight of the aircraft occurs.

It can be concluded that the design is not sensitive up to a reasonable margin which is still within the design margins. The analysis was made for the most important low-level loop and the most important top-level parameters which cover the most sensitive parameters of the design tool.

After conducting the sensitivity analysis, a profound comprehension was gained regarding how the important aspects of the software are impacted by the MTOW. On the other hand, to increase confidence in the design integrity, a broader analysis shall be performed during the next phase of the design process.

21 | RAMS Analysis

Over its operational lifetime, the HA-1 will eventually encounter failure of at least one of its components. Depending on the component, the impact of this failure on the functioning of the system can vary widely. To ensure customer safety and satisfaction, it is important to understand the potential impact of failures, their likelihood, the estimated downtime resulting from these failures, and how to mitigate them through maintenance. Reliability, Availability, Maintainability and Safety (RAMS) analysis aims to provide exactly this.

During RAMS analysis, all possible system failures and the components causing them are first identified. Then, for each critical component, its RAMS characteristics are analyzed. Finally, all component characteristics are aggregated to achieve the overall aircraft RAMS characteristics.

When analyzing component RAMS characteristics, each aspect of the RAMS analysis aims to evaluate the following [92]:

Safety: Evaluates the impact of a component failure on passengers, including the associated downtime and costs to ensure the aircraft is safe to fly again after replacing the failed component.

Reliability: Evaluates the likelihood of no failure events occurring.

Availability: Combines downtime estimates from the safety analysis and the results from the reliability analysis to estimate the percentage of its operational lifetime a system, consisting of multiple components that can fail individually, is available for use.

Maintenance: Uses all results from the safety and reliability analyses to identify mitigation measures for critical component failure, aiming to maximize passenger safety, and minimize downtime and costs.

21.1. Fault Tree Analysis

As mentioned in the chapter introduction, to perform a RAMS analysis for the HA-1, it is first necessary to identify what failures can occur. This can be done through various techniques, the most common of which is Fault Tree Analysis (FTA). FTA takes a top-down approach, starting with system failure effects (the top events), such as an in-flight aircraft shut-down, and determining what components are responsible for these failures.

For the HA-1, aircraft failure is defined as the inability to meet the functions specified by the functional analysis performed in Section 4.2. This report will only focus on assessing critical system failures, as visible in Figure 21.1.

Clearly, many components can cause aircraft failure. Hence, providing a detailed RAMS analysis for each would be beyond the scope of this report. Therefore, an example RAMS analysis will be performed only for the aircraft gearbox. The RAMS characteristics of other components can be obtained through similar analysis as presented.

21.2. Safety

Safety analysis aims to evaluate the impact of a component failure on passengers, including the associated downtime and costs to ensure the aircraft is safe to fly again after replacing the failed component. Since the gearbox only aims at transferring the engine torque to the shaft, the most catastrophic consequence of gearbox failure is total loss of internal combustion engine (ICE) thrust [93]. Since the components of the gearbox are safely contained within the engine cowling, which is designed to contain any gearbox projectiles that might occur, no projectile danger exists for the passengers. Depending on the nature of the failure, the engine would either experience sudden high torque resistance from the shaft and stall, or experience no resistance at all, and rotate the engine shaft freely. Both scenarios would have no detrimental effects on the rest of the aircraft [93], assuming an emergency landing can be performed.

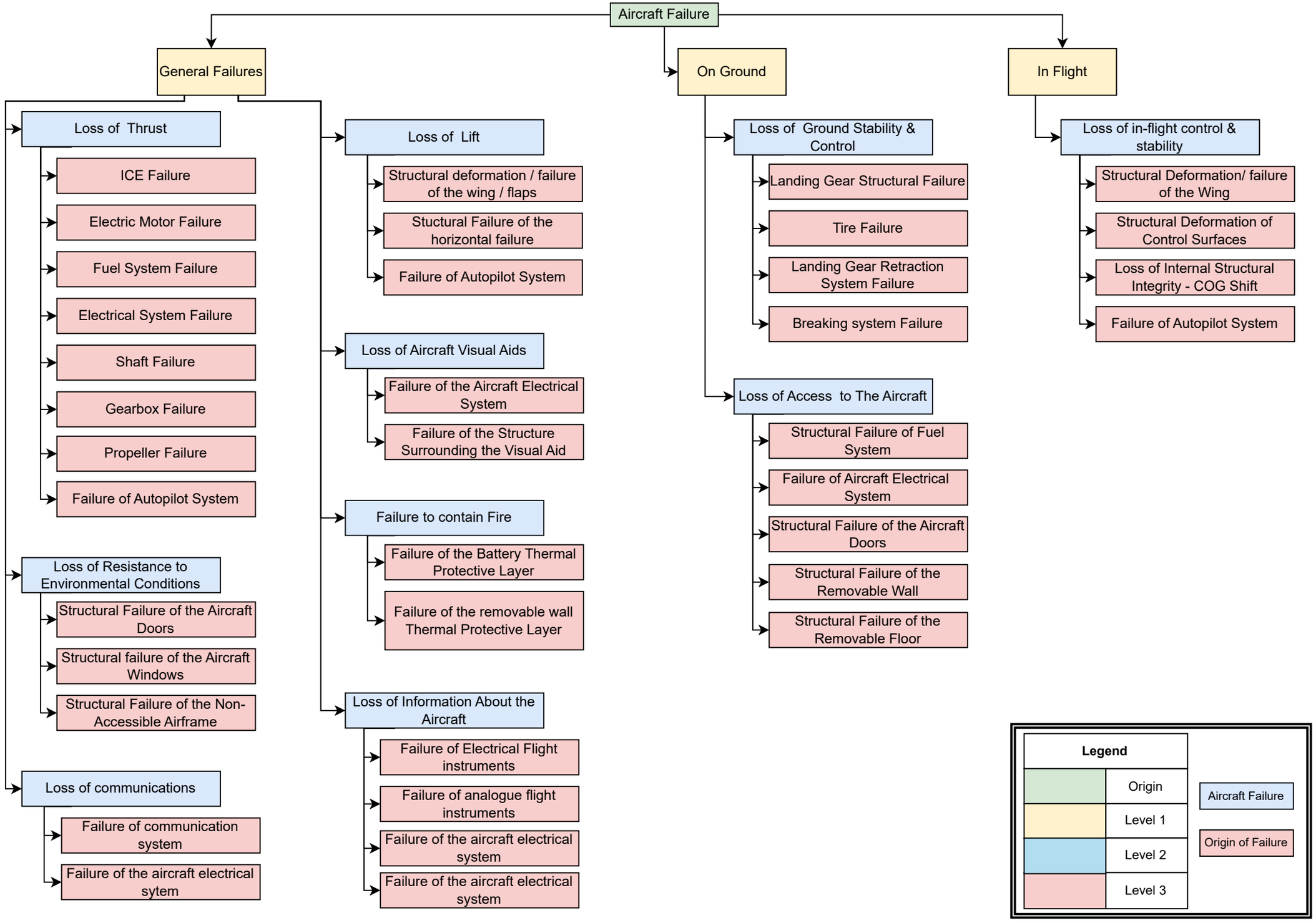

Figure 21.1: Fault Tree

Since the selected engine includes an integrated gearbox, it is not feasible to replace the entire unit; instead, individual parts will need to be replaced. Consequently, while the nature of the failure will influence the downtime and cost, the process will always involve purchasing and replacing specific components. The only variables will be the type and quantity of components that need to be replaced.

The maximum possible downtime resulting from any component failure is the sum of component shipping time, maintenance duration, and the duration of final system testing. The maximum possible cost of repair is given by the sum of component cost, and mechanics wages.

Of course, if components are already in stock, no downtime or cost due to shipping is present. Furthermore, the cost of post-replacement inspection is comparatively small, hence it is left out of the equation.

Estimating actual values for each of these elements is challenging, as the exact gearbox components for the RED A03-003 ICE are unknown. Typically, gearbox overhauls take one or more weeks and cost between 500 to several thousand USD[(a)], depending on the severity of the problem and the gearbox manufacturer.

The results of the safety analysis will differ for other aircraft components. For analyzing those, the following methodology is advised: (1) Identify the potential failures and their effects on passengers and aircraft safety. (2) Determine the associated downtime and costs for ensuring the aircraft is safe to fly again. Use either experience or statistical data from comparable aircraft for this. (3) Evaluate the impact on the overall aircraft operation and performance.

21.3. Reliability

For assessing the reliability of systems, Kissling and Stangl [94] proposed a methodology based on reliability distribution function analysis. A reliability distribution function is a type of probability distribution function that provides the *un*likelihood of an event (the probability of no failure occurring) for a specific value of a probability variable (in this case is the service life of the component) [94]. It can be obtained by taking 1 minus the probability of failure of the component for each value of the probability variable.

First, it is necessary to identify the reliability distribution function for each type of system component, which can vary in type and distribution parameters (e.g. shape and scale parameter for the Weibull distribution). For mechanical systems, Bertsche recommends the use of a three-parameter Weibull distribution, but other distributions may be appropriate depending on their prediction accuracy [95].

Next, the failure modes of the system are analyzed, with the goal of determining which components run in parallel and which in series. Parallel components have redundancy, meaning that their failure does not result in the failure of the total system. Series components, on the other hand, ensure total system failure upon their malfunctioning.

The user must then select a service life that is satisfactory for them. Based on the individual reliability distribution functions, each component will yield a corresponding reliability for that service life. The total system reliability distribution function can be created by first condensing all parallel components into a single element, representing the total reliability of the redundant subsystem, and then selecting the lowest reliability among the series components.

To compute the total reliability of a parallel subsystem, the reliability of each component must be converted back into its failure rate, which is 1 minus its reliability. The failure rates of all components are then multiplied together, and the result is subtracted from 1.

For their example calculation of a simplified three-axis gearbox, whose reliability curves are shown in Figure 21.2, it is evident that, for a service life of 10×10^4 h, the gears are the least reliable component

[(a)] URL: `https://bookmygarage.com/blog/how-much-does-gearbox-repair-cost-uk/` [accessed 19 May 2024]

and will thus drive the reliability of the gearbox system. Similar results are expected for the RED A03-003 ICE gearbox, as it uses similar components.

The results of the reliability analysis will differ for other aircraft components. For analyzing those, the following methodology is advised:

- Identify the relevant subsystem components.
- Determine the appropriate reliability distribution function parameters for each component.
- Analyze the system configuration to determine which components are in parallel and which are in series.
- select a satisfactory subsystem service life and find all component reliability values for this service life.
- Condense the parallel components into single elements to represent the total reliability of redundant systems.
- Calculate the system reliability by combining the reliabilities of the series components.

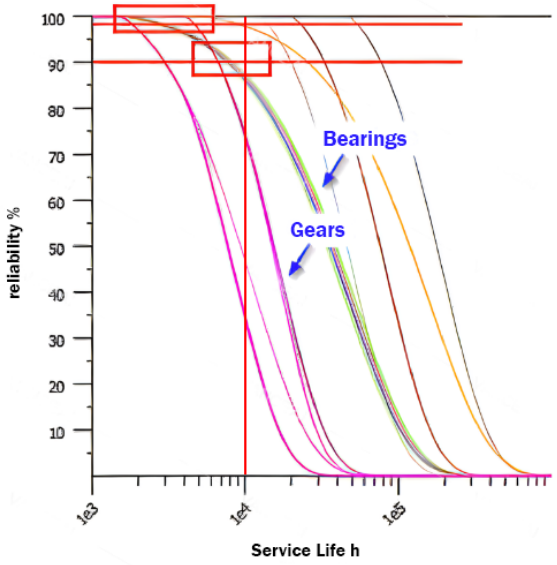

Figure 21.2: Gearbox Component Reliability Functions [94]

21.4. Availability

The system availability measures the percentage of its operational lifetime during which the aircraft is actually available for use, accounting for downtime due to failure events. To calculate this, the downtime estimates from the safety analysis and the results from the reliability analysis are combined. Since availability is more of a system-level analysis, this introduction will be general and not focused specifically on the gearbox.

Each subsystem's reliability estimate and resulting downtime will be taken into account. A linear time scale will be initialized, representing the service life passed. At each time step (= one hour assuming the service life is given in hours), a random value between 0 and 1 will be generated for all components. This value is then compared to each component's reliability value at the service life. If the generated value is higher than the component's reliability (expressed as a decimal), it indicates a component failure.

When a component fails, the necessary maintenance time for that failure is added to the service life, plus the time required for regular engine overhaul. It is assumed that all other components are fixed during this overhaul period. After maintenance, the system's service life continues, but evaluation of the reliability starts back from 0.

21.5. Maintainability

Based on the reliability and safety analysis, the necessary information is available to properly identify critical components in terms of passenger safety, downtime, and cost, thereby guiding inspection and maintenance activities. The reliability analysis highlights which subsystems pose the greatest risks, while the safety analysis is able to identify the effect of subsystem failure and corresponding costs. It is then up to the manufacturer to trade-off between the three metrics that they find most important: passenger safety, cost or downtime, and allocate maintenance and inspection activities to the subsystems with the highest impact on the selected category.

Additionally, the aircraft should be designed to mitigate any detrimental effects of the critical subsystem failure, potentially enforcing new subsystem design/selection. This approach ensures the safe and efficient operation of the aircraft, aligning with the manufacturer's preferences.

22 | Verification & Validation

This chapter covers the verification and validation procedures for the system and the tools used throughout the design process up to the end of the preliminary design phase. V&V ensures that high confidence is obtained and that the tools created can be generalised to a more general set of parameters such that a change in the design will not make the tools invalid. System V&V will be discussed in Section 22.1 where suggestions and recommendations are shown on how the system will comply with the requirements and mission definition. Section 22.2 presents the procedures for the tools used in the design such that high confidence can be achieved.

22.1. System V&V

Verification and Validation of the system are important as they give confidence that the product designed can provide the desired performance. A brief overview of how V&V can be made during various stages of the design are summarised in the following list:

- **Pre-design stage:** Analytic modelling; Wind tunnel testing to verify and validate the analytic models used
- **Design iteration stage:** Repeated aeroelastic calculations to verify constraints on or optimise the aeroelastic properties of the configuration
- **Frozen design stage:** Tests of structurally scaled models and comparison with analytic structural models; Wind tunnel tests with aeroelastically scaled models to verify analytical aerodynamic models and coupling
- **Prototype stage:** Ground vibration and flexibility tests to provide final validation of structural models; Analytical calculations to prepare for flight testing; Flight-test program

22.2. Tool V&V

Besides V&V of the system, one more important aspect that needs to be considered is the tools V&V. Assuring high confidence that the tools can be used for multiple cases is crucial to reproducibility and possible future changes in the design margins. The tools helped the project team to get a final conceptual design and gave a high confidence in the results. Note however that due to time constraints verification and validation still need to be carried out on the flight performance analysis code. However as mentioned in Chapter 14 the results of this specific tool correspond well with the initial estimations, and this can be considered a form of verification in itself.

22.2.1. Script Design Tool

Verification

Verification of the developed design tools involves ensuring that the outcomes of the numerical model align with those of the intended theoretical models. This was achieved by using unit tests. They check the functioning of individual or multiple modules. The unit tests are run via the Python pytest package and automatically use a GitHub pipeline every time a new commit is made to the codebase. This method ensures rapid problem identification in case of a faulty commit. The pipeline also helped to keep track of the total code coverage and to see which files were not tested yet. The unit tests are summarised in Table 22.1. Two categories of unit tests were performed: a visual inspection, and an examination of whether the expected output is correct, as well as its type and shape. The coverage of the code by the unit tests was also analysed, with the metrics presented in Table 22.2.

Table 22.1: Unit tests for the modules tested of the Python tool. The number of tests per file and the confidence/accuracy achieved are also presented. Functions coloured in green passed the tests, while those in red failed it initially. In such cases, the modifications are explained.

File	No.Tests	Explanation	Confidence/ Accuracy
AileronSizing.py	6	Checks if the formulas are correctly written, checks if the output has the right shape and expected magnitude	Rtol: 1e-3
BrakingCheck.py	1	Checks if the formulas are correctly written, checks if both cases work	100%
Class_II_Weight.py	25	Checks if the formulas are correctly written and adapted, and checks if the convergence loop works; *Modification:* Contingency was applied twice and removed from one place; battery weight now contains the right efficiencies	Rtol: 1e-1
Class_I_Weight.py	8	Checks if the formulas are correctly written, checks if the output shape is correct and in the right order	Rtol: 1e-3
Equations.py	8	Checks if the formulas are correctly written; *Modification:* temperature offset was added	Rtol: 1e-4
FlapsDesign.py	2	Checks if the formulas are correctly written, checks if the surface of the flaps is possible	Rtol: 1e-9
FlowParameters.py	3	Checks if the magnitude of the numbers are correct and if they match hand calculations	Rtol: 1e-2
FuselageSizing.py	22	Visual check for placement, checks if the positions are well set up, checks if the battery packages fit within the fuselage length, checks if the landing gear has the option to fold backward	Rtol: 1e-2
LoadDistributions.py	12	Checks if the txt files are correctly read, checks if some edges cases don't give an error	Rtol: 1e-1
LongitudinalStability.py	4	Visual check, checks if the formulas are correctly written	Rtol: 1e-2
PlanformDesign.py	8	Visual check, checks if the formulas are correctly written	Rtol: 1e-3
WP_WS.py	2	Visual check, checks if the convergence works	Rtol: 1e-2
WeathercockStability.py	1	Checks if the formulas are correctly written, checks if the rudder has space	99%
aerodynamic_isa.py	4	Checks if the formula are correctly written, checks if the numbers match hand calculations	Rtol: 1e0
co2v2.py	3	Checks if the files are called well, checks if the flight distribution file is consistent, checks if a simple case is correctly calculated; *Modification:* one file was not updated with the new fuel weight and fixed that	Rtol: 1e-1
conceptual_co2.py	6	Checks if the files are called well, checks if the flight distribution file is consistent, checks if a simple case is correctly calculated	Rtol: 1e-1
conceptual_financial_analysis.py	1	Checks if the right values for the parameters are inputted, checks if the numbers match other documents	95%
design_values.py	1	Checks if the loading factors respect the formulas and if the edge cases are correctly handled	Rtol: 1e-2
get_flight_distribution.py	1	Checks if the distribution has the right parameters	Rtol: 1e-9
gust_diagram.py	1	Checks if loading factors are well plotted	99%
loading_diagram.py	4	Visual inspection, checks if the different velocities match the plot and the file	Rtol: 1e-2
optimisation.py	14	Checks if the formula are correctly written, checks if the aerodynamic coefficients are called correctly and checks for edge cases	Rtol: 1e0
unit_conversions.py	12	Checks if the numbers match hand calculations	Rtol: 1e-2
weight_fractions.py	3	Visual inspection, checks if the xcg excursion is well calculated	Rtol: 1e-2

Table 22.2: Code Coverage of the Unit Tests. Excludes flight performance analysis code

Case	Statements	Missed	Coverage
Including main.py	2321	343	**85%**
Excluding main.py	1969	144	**93%**

Validation

For the validation of the software tool, the database from Roskam Part 5 was used [18]. It contains a single propeller engine and twin propeller engine aircraft with their respective main specifications and component weights. The procedure to get the MTOW and compare it with the one from the book was to set the battery percentage to 0%. Furthermore, the main aspects such as the wing surfaces were taken from literature and inputted in the software [18]. The results are shown as a boxplot in Figure 22.1.

Although the script was updated for a hybrid design, the class 2 weight estimation can be used for a fully conventional aircraft as the median of the relative error has a value of 6.7%. In the figure, the lines correspond to one standard deviation(STD) and two standard deviations of the distribution are plotted. The limiting values of 2 STDs are between -1% and 14%. It gives an interval of 15%. Compared to the 12% used for the contingency at this design phase, there is a 3% difference. It comes from the uncertainties of converting the script to a conventional case. Besides the validation of the class 2 weight estimation, several validation procedures have to be met in order to increase the confidence of the script in being a general tool for hybrid aircraft. As the resources of the project are limited and the design is not yet in its detailed phase, it will be impossible to get real data for validation. The full conventional aircraft cannot be used for the validation of the other parts of the script as they are mainly focused by including batteries. Thus, it will be left for further development. The following procedures are strongly recommended as they were identified throughout the design time:

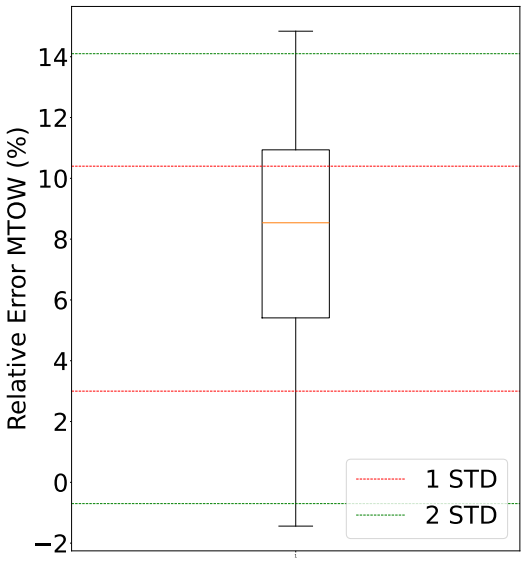

Figure 22.1: Boxplot showing relative error between the actual reference aircraft MTOW and that estimated by the Class II weight estimation loop. A median error of 6.7% and a 2 STD between 15% and -1%.

- Calculate the CO_2 emissions and compare to the CO_2 calculator of the software
- Calculate the actual power required and compare it to the one used in the software
- Calculate the wing loading with a test setup and compare the critical stresses to the ones obtained from the software
- Measure the performance of the aircraft during a flight test and compare it to the values obtained from the software(e.g. turn rate)
- Measure the weight of components of the aircraft and compare them to the ones outputted from the class 2 weight estimation and check if they go over or below the target

22.2.2. CFD Model

To verify the correct working of the CFD model, verification methods as suggested by the CFD-I course will be applied [96]. These include checking if the model converges correctly, checking if the solution is dependent on the mesh size and finally, checking the influence of a different turbulence model on the solution.

Convergence Analysis

In the convergence analysis, it is checked whether the model converges enough. After consultation with one of the coaches, it was advised to converge to at least 3 orders of magnitude lower than the initial value. Figure 22.2 provides insight into the residuals for the CFD model used.

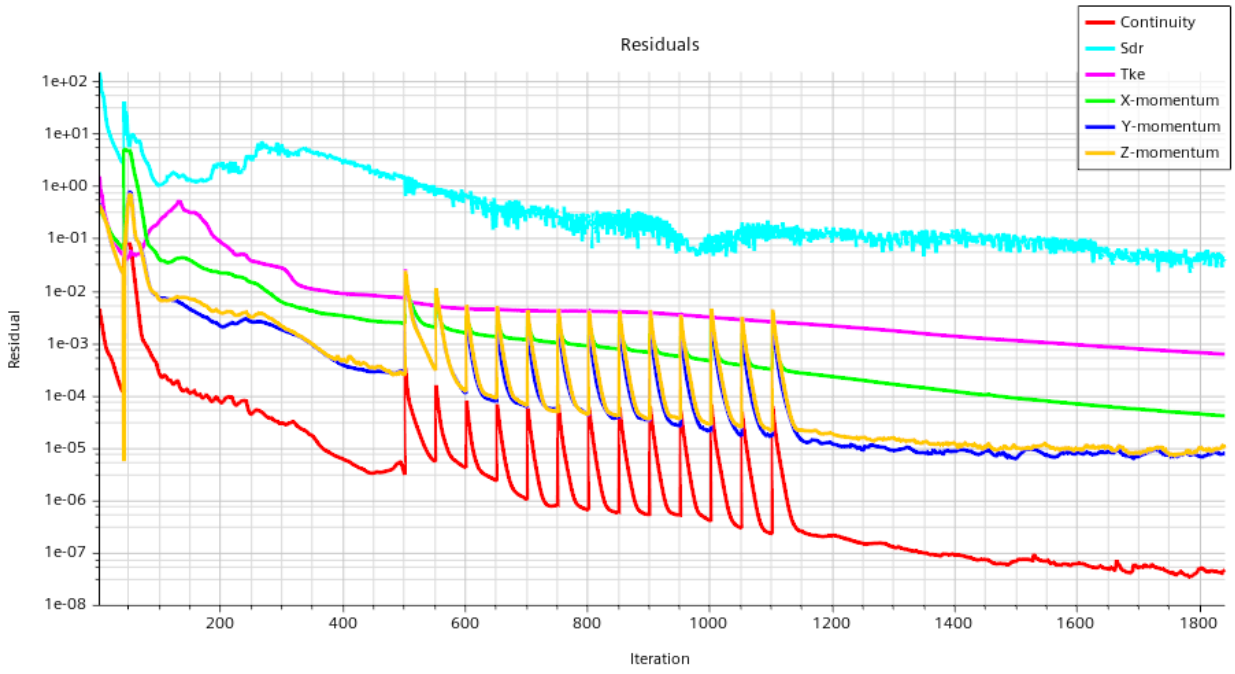

Figure 22.2: Residuals for the Model Used in the Aerodynamic Development of the HumanAir HA-1

Here, multiple parameters are monitored while iterating the solution to visualise convergence. One can observe that all variables indeed converge to three orders of magnitude lower than their initial values. Therefore, this verification is passed.

Mesh Sensitivity Analysis

To investigate the sensitivity of the model to the mesh size, the solution is plotted for different amounts of cells used in the model, as seen in Figure 22.3. It is clear from the figure that increasing the mesh size does not have a significant impact on the model anymore after 2 500 000 cells are used. Even before that, there is only a difference of around 1% in the solutions. This indicates that the mesh is sufficiently accurate, and therefore also this verification is passed.

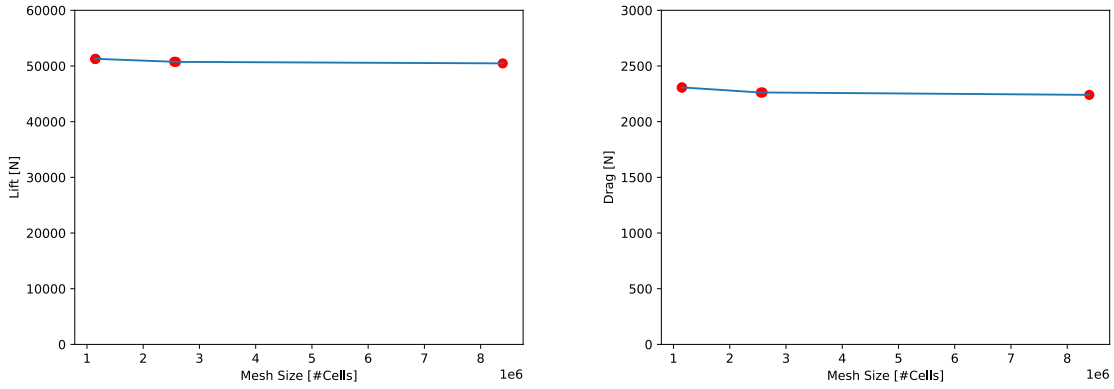

(a) Lift vs Mesh Size

(b) Drag vs Mesh Size

Figure 22.3: Solutions Plotted for Different Mesh Sizes. The very shallow slope of the line indicates the mesh has converged to a solution.

Turbulence Model

For the final verification step, different turbulence models are implemented. If the model is accurate enough, these should not provide inherently different results. For this, three turbulence models are compared: the $\kappa - \omega$ model, the $\kappa - \epsilon$ model and the Spalart-Allmaras model [(a)]. The results are shown in Table 22.3.

Table 22.3: Influence of Different Turbulence Models on the CFD Solution.

Turbulence Model	Deviation from average, Lift	Difference from average, Drag
$\kappa - \omega$	+0.23%	-0.54%
$\kappa - \epsilon$	+0.84%	+1.02%
Spalart-Allmaras	-0.14%	-0.49%

As the table shows, all models vary only marginally from the average solution. Therefore, also this verification is passed.

CFD Validation

It is hard to properly validate the CFD model, as there is no access to a wind tunnel to compare with test data. To however gain some insight into the correctness of the model, it is compared to existing flight test data on landing gear drag. Two different models have been tested for this: one where the landing gear is retracted and one where it is extended. Flight test data on general aviation aircraft from Nicolai and Carichner [65] shows that the C_{D0} added by the landing gear is in the region between 0.006-0.011. Looking at the CFD data obtained, one can observe a C_{D0} of 0.0161 for the clean configuration and a C_{D0} of 0.0261 for the configuration with extended landing gear. This is a ΔC_{D0} of 0.01, complying with the flight test data. Therefore, this validation is passed.

[(a)] URL: `https://turbmodels.larc.nasa.gov/spalart.html` [accessed 25 June 2024]

23 | Future Outlook

This chapter outlines the future steps necessary for the continuous development of the aircraft. It begins with the production plan, detailed in Section 23.1. Following this, the project design and development logic, where future steps that need to be taken are defined is described in Section 23.2. Finally, the timeline of the tasks to be performed is explained in Section 23.3.

23.1. Production Plan

A production plan is crucial for aircraft manufacturers to optimise resource utilisation, maintain efficient inventory levels, and reduce delays and downtime. To create an effective plan, understanding the supply chain is crucial to identify the overall manufacturing procedure. An aircraft supply chain consists of various stakeholders. These include suppliers, original equipment manufacturers (OEMs), customers and maintenance repair and overhauls (MROs). Interconnection between these stakeholders is illustrated in Figure 23.1.

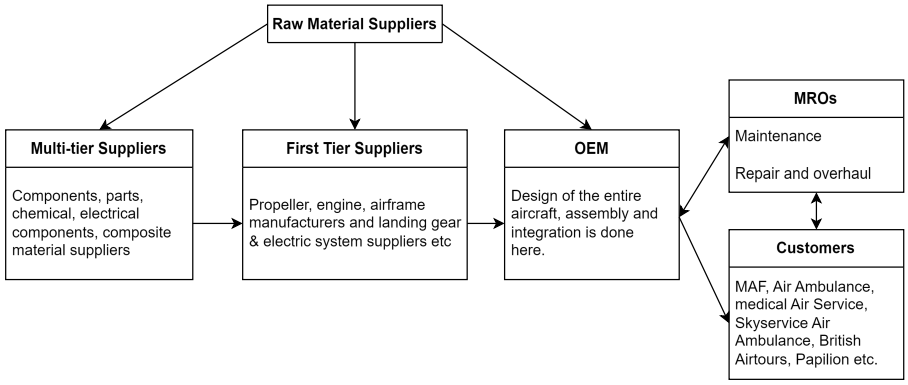

Figure 23.1: Aircraft Supply Chain Structure [97]

Multi-tier suppliers produce motors or hydraulic pumps using the consumable parts provided by raw material suppliers. First-tier suppliers then receive the parts to create aircraft sub-assemblies and systems such as engines or landing gears. OEMs such as Boeing and Textron Aviation receive them and they integrate all these components to create the final assembled product [97]. HumanAir is positioned as an OEM, responsible for the aircraft's design. To meet the market entry within five years requirement, the actual assembly and integration would be done by already existing companies such as Textron Aviation through collaboration. The overall manufacturing procedure is detailed in Figure 23.2.

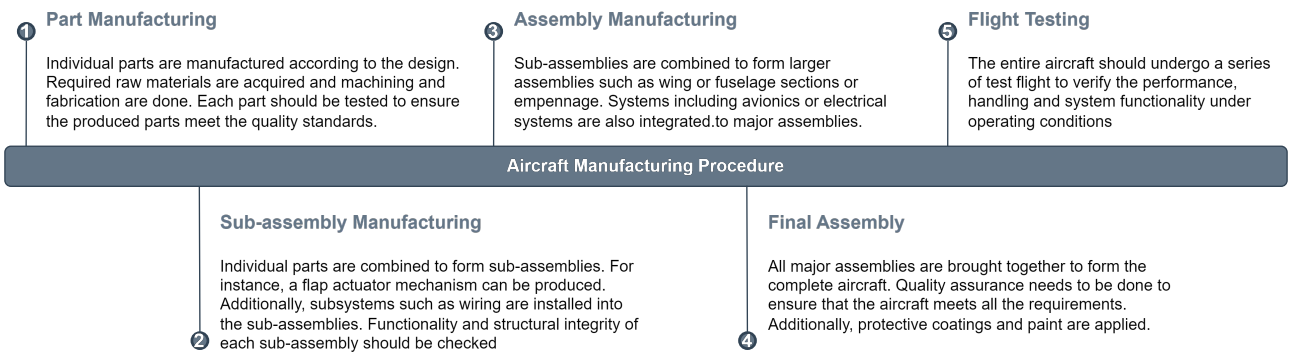

Figure 23.2: Manufacturing Procedure

Quality control is important in aircraft manufacturing because even a small defect, such as a crack in a component, can lead to serious accidents and the loss of lives. Therefore, quality control has to be done seriously to ensure passenger safety and prevent catastrophic failure. To guarantee the quality of aircraft, quality control is implemented across multiple stages, from design to the actual manufacturing phase. In the design phase, regular reviews and audits are done to ensure that the design meets safety, performance and regulatory standards. In the manufacturing phase, incoming materials or components are inspected before use, and dimensional inspections, functional testing, and non-destructive testing methods such as hardness testing, radiography, thermography, or ultrasonic testing are employed to detect any defects without damaging components. Final checks are also performed after the integration of components.

Stock inventory control will be managed using a combination of Just-In-Time (JIT) and Just-In Case (JIC) principles. JIT strategy aims at reducing waste and improving efficiency and thus, a business receives parts from suppliers just in time before production. This approach will be applied to critical and high-value components such as landing gears or engines. By minimising the time high-value components spend in inventory, the risk of deterioration or damage is reduced, ensuring the highest quality. Additionally, this not only reduces the costs of storage but also decreases the opportunity cost of stock-holding. This cost advantage is particularly beneficial since newly established businesses, often face limited capital. By effectively managing capital, HumanAir would increase the chances of survival within the market and potentially decrease the unit cost of aircraft, thus enhancing cost competitiveness.

Businesses that utilise JIC methods hold a high level of stocks to reduce the risk of stock-out. This would be applied to consumables such as fasteners or adhesives. To manage these stocks efficiently, min-max inventory control principles would be implemented to calculate desired stock levels for these items. Before reaching the minimum level, the item shall be reordered and thus, continuous monitoring of inventory levels is necessary. To facilitate effective monitoring, stock control charts would be created enabling stock managers to determine the most optimal order time and quantity. By employing this approach, HumanAir can partially mitigate the risk of potential production delays.

23.2. Project Design and Development Logic

Many more steps are required to after the end of the DSE to take this initial design to an operational aircraft, and beyond. Figure 23.3 presents the project design and development logic, where these future steps are defined, by identifying various future phases and breaking them down into sub-tasks as needed. Furthermore, the logical flow between these steps is also presented. At this stage, it is most important to identify the future phases to finalise the design, so the majority of the logic diagram is devoted to this. The manufacturing and end-of-life phases are not expanded in the diagram, but are instead discussed in Sections 23.1 and 18.5 respectively.

23.3. Post-DSE Gantt Chart

While the future project phases and their relationships have been identified, it is also important to determine the timeline of these tasks, in order to meet the 5-year deadline to market. This is done by means of a Gantt chart, presented in Figure 23.4. This chart also allows for parallel tasks to be easily identified and shows dependencies with arrows. It should be noted that while the operations phase was included for completeness, its duration is not determined as it will depend on the operator.

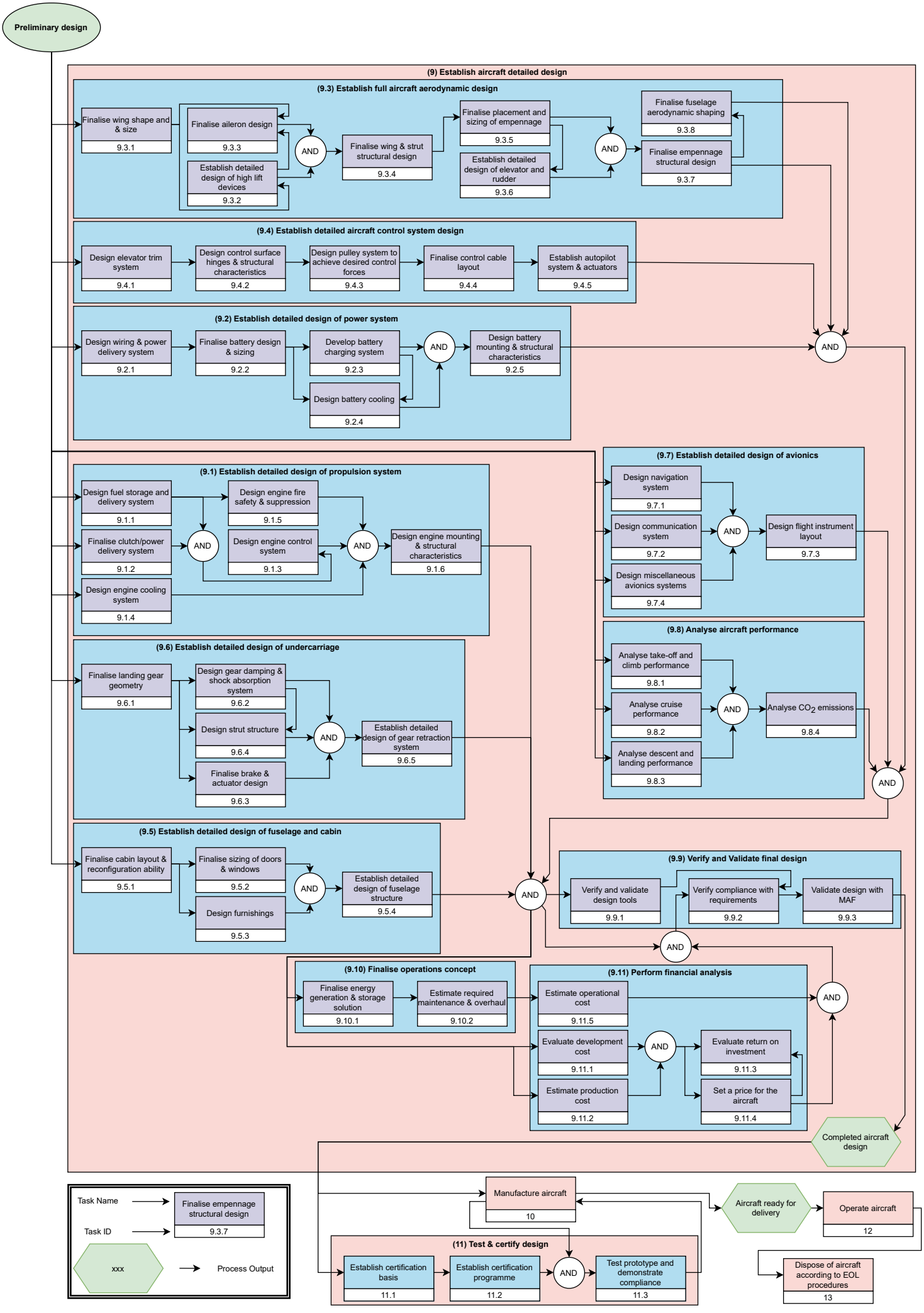

Figure 22.3: Project design & development logic

ID	WBS	Task Name
1	1	Project Planning
2	2	Mission Analysis
3	3	Conceptual Design
4	4	Revise Conceptual Design
5	5	Preliminary Design
6	6	Project Continuity Planning
7	MS.1	Preliminary Aircraft Design
8	8	Final Reports and Presentations
9	**9**	**Establish aircraft detailed design**
10	**9.1**	**Establish detailed design of propulsion system**
11	9.1.1	Design fuel storage and delivery system
12	9.1.2	Finalise clutch/power delivery system
13	9.1.3	Design engine control system
14	9.1.4	Design engine cooling system
15	9.1.5	Design engine fire safety & suppression
16	9.1.6	Design engine mounting & structural characteristics
17	**9.2**	**Establish detailed design of power system**
18	9.2.1	Design wiring & power delivery system
19	9.2.2	Finalise battery design & sizing
20	9.2.3	Develop battery charging system
21	9.2.4	Design battery cooling
22	9.2.5	Design battery mounting & structural characteristics
23	**9.3**	**Establish full aircraft aerodynamic design**
24	9.3.1	Finalise wing shape and size
25	9.3.2	Establish detailed design of high lift devices
26	9.3.3	Finalise aileron design
27	9.3.4	Finalise wing & strut structural design
28	9.3.5	Finalise placement and sizing of empennage
29	9.3.6	Establish detailed design of elevator and rudder
30	9.3.7	Finalise empennage structural design
31	9.3.8	Finalise fuselage aerodynamic shaping
32	**9.4**	**Establish detailed aircraft control system design**
33	9.4.1	Design elevator trim system
34	9.4.2	Design control surface hinges & structural characteristics
35	9.4.3	Design pulley system to achieve desired control forces
36	9.4.4	Finalise control cable layout
37	9.4.5	Establish autopilot system & actuators
38	**9.5**	**Establish detailed design of fuselage and cabin**
39	9.5.1	Finalise cabin layout & reconfiguration ability
40	9.5.2	Finalise sizing of doors & windows
41	9.5.3	Design furnishings
42	9.5.4	Establish detailed design of fuselage structure
43	**9.6**	**Establish detailed design of undercarriage**
44	9.6.1	Finalise landing gear geometry
45	9.6.2	Design gear damping & shock absorption system
46	9.6.3	Finalise brake & actuator design
47	9.6.4	Design strut structure
48	9.6.5	Establish detailed design of gear retraction system
49	**9.7**	**Establish detailed design of avionics**
50	9.7.1	Design navigation system
51	9.7.2	Design communication system
52	9.7.3	Design flight instrument layout
53	9.7.4	Design miscellaneous avionics systems
54	**9.8**	**Analyse aircraft performance**
55	9.8.1	Analyse take-off and climb performance
56	9.8.2	Analyse cruise performance
57	9.8.3	Analyse descent and landing performance
58	9.8.4	Analyse CO2 emissions
59	**9.9**	**Verify and Validate Final Design**
60	9.9.1	Verify and validate design tools
61	9.9.2	Verify compliance with requirements
62	9.9.3	Validate design with MAF
63	**9.10**	**Finalise Operations Concept**
64	9.10.1	Finalise energy generation & storage solution
65	9.10.2	Estimate required maintenance & overhaul
66	**9.11**	**Perform financial analysis**
67	9.11.1	Evaluate development cost
68	9.11.2	Estimate production cost
69	9.11.3	Evaluate return on investment
70	9.11.4	Set a price for the aircraft
71	9.11.5	Estimate operational cost
72	9.MS.1	Completed Aircraft Design
73	10	Manufacture Aircraft
74	**11**	**Test & Certify Aircraft**
75	11.1	Establish certification basis
76	11.2	Establish certification programme
77	11.3	Test prototype and demonstrate compliance
78	MS.2	Aircraft Ready for Delivery
79	12	Operate Aircraft
80	13	Dispose of aircraft according to EOL procedures

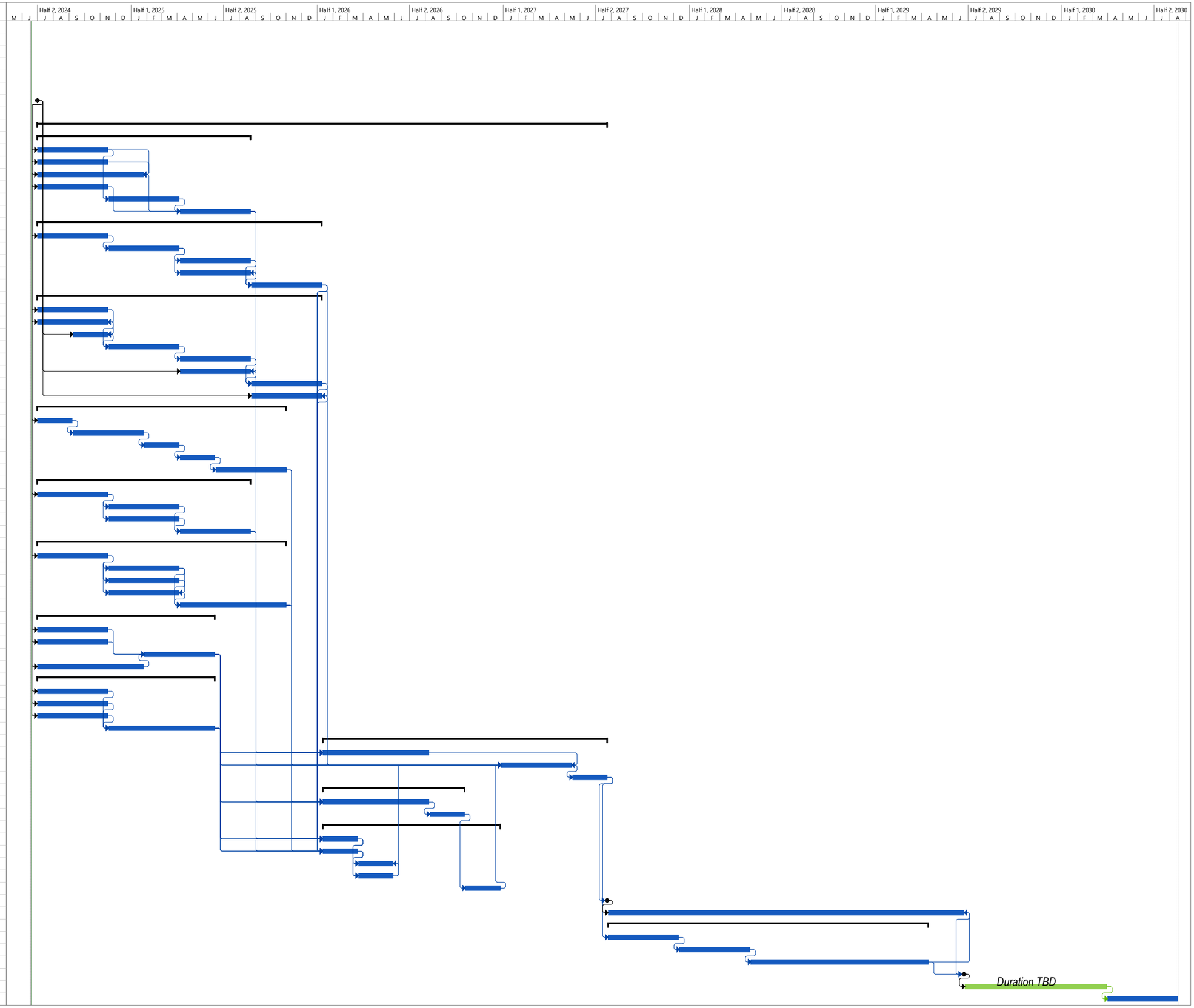

Figure 23.4: Post-DSE Gantt Chart

24 | Conclusion

This report aimed to provide a complete overview of all activities conducted by the HumanAir project team to arrive at a final design proposal. To achieve this, a set of requirements was used to constrain the design space, after which subsystems were designed and sized to arrive at the final design proposal seen in Figure 24.1: the HumanAir HA-1. This hybrid conventional aircraft manages to reduce emissions by 50% compared to the Cessna 206, while also providing a lower operating cost.

Figure 24.1: The HumanAir HA-1

An important note regarding the design is that the 50% reduction will not be met on initial deployment. After a certain amount of time, the current battery will be swapped out for one with a higher efficiency. This however depends on when the new technology is available.

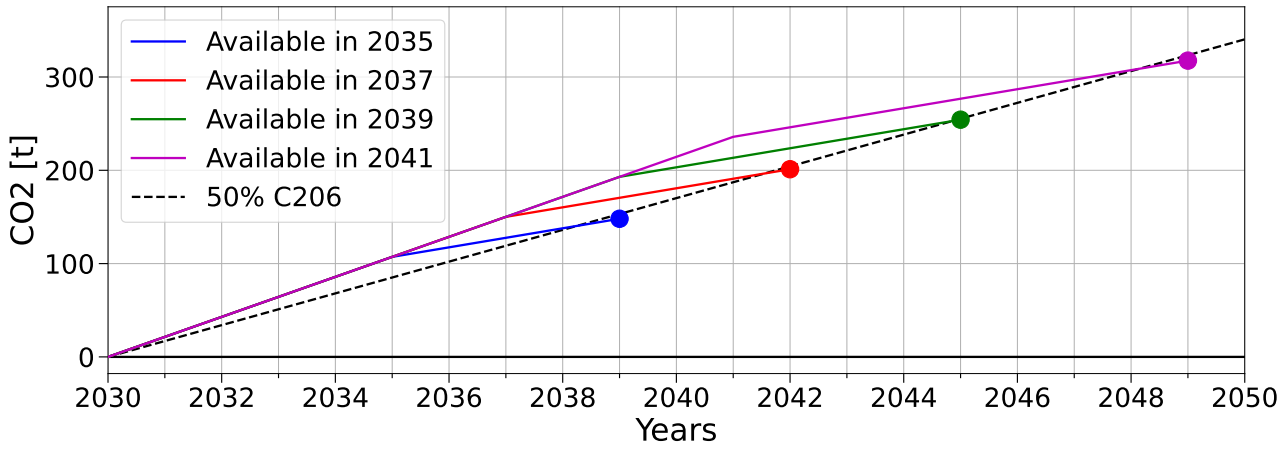

Figure 24.2: Plot of Overall CO_2 Emissions Depending on Date of Improved Battery Introduction

If the new battery technology arrives in 10 years, the emission target will be met in 2039 and far exceeded afterwards. Hence, HumanAir believes that the proposed solution will prove to be competitive in the already crowded general aviation market.

However, some recommendations on the further proceedings of the project can be made. The main consideration here is that the project is incomplete. In the limited time frame of the Design Synthesis Excercise, HumanAir has made an effort to provide a design which is as complete as possible within the limits of the available resources. Therefore, this report and the work performed should be seen as a starting point for further detailed analysis. During this detailed design, one should pay attention to

four specific points. First of all, while some preliminary verification and validation have been performed, the coverage of verification methods and the sensitivity analysis have been restricted due to time constraints. Next to this, no real-life evaluations have been performed, limiting the validation broadness. When continuing this project, one should put more time and resources into these V&V practices to confirm the findings presented in this report, especially for the flight performance analysis.

Secondly, the wing strut should be worked out in more detail. Due to limited time, no Finite Element Modelling or real-life evaluations could be performed to inform a sizing process. Two concepts have been proposed, but there is no quantitative analysis on these yet. This should be a priority during further developments of this project.

Additionally, the landing gear retraction mechanism has to be worked out in more detail, including the precise mechanics and bay doors, to properly estimate the cost, reliability, and maintenance required. Due to limited time, only one mechanism was investigated at an early stage in the design. But now that drag targets are easily met, the possibility of the landing gear being positioned in fuselage side pods behind the wing strut should be investigated. If this proves to be a feasible option it would drastically simplify the gear retraction, improving its reliability and maintainability.

Then, an estimate should be made on the cost of the ground infrastructure in case it would be placed in Europe or the United States. These two regions provide a large market for people who might be interested in the HA-1. However, currently, the ground infrastructure cost has only been worked out for the primary customer, Mission Aviation Fellowship, who is mainly active in Africa. In case Western customers might be interested in acquiring the same ground infrastructure, this should be worked out in more detail.

Finally, as mentioned before, the success of the project rests on the availability of a new battery technology. While companies advertise these to be available in 10 years, it should be closely monitored and the battery producers should be actively involved in the development of the HumanAir HA-1.

Bibliography

[1] Bakker, H. and de Kleijn, J., *Management of Engineering Projects - People are key*, NAP, 2014.

[2] Gao, Z., Lin, P.-N., Chakraborty, A., Sells, B. E., Briceno, S. I., Crossley, W. A., and Mavris, D. N., "Challenges and Opportunities: A Strategic General Aviation Exploratory Analysis for 2030," *2018 AIAA Aerospace Sciences Meeting*, American Institute of Aeronautics and Astronautics, Kissimmee, Florida, Jan 2018, p. 2009, doi:10.2514/6.2018-2009.

[3] Global Insight Services, "General Aviation Market Analysis and Forecast to 2033," Industry Rep. GIS25732, GIS, Lewes, Delaware, March 2024.

[4] UNHAS, *United Nations Humanitarian Air Service (UNHAS) Annual Review 2021*, World Food Programme, May 2022.

[5] General Aviation Manufacturers Association, *2019 Databook*, GAMA, 2019.

[6] Cirrus Aircraft, "2022 SR20," July 2022.

[7] Cirrus Aircraft, "2024 SR Series G7 / SR20," April 2024.

[8] Piper Aircraft, "M350," March 2024.

[9] Piper Aircraft, "Archer LX," March 2024.

[10] Jackson, S., *Systems Engineering for Commercial Aircraft*, Ashgate, Aldershot, England, 1997.

[11] Moir, I. and Seabridge, A., *Design and Development of Aircraft Systems*, Wiley, 1st ed., Nov. 2012.

[12] DSE Group 15, "HumanAir: Midterm Report," May 2024.

[13] DSE Group 15, "HumanAir: Baseline Report," May 2024.

[14] MAF Kenya, "Operations Manual Part A, Section 8.1.6 Determination of Quantities of Fuel and Oil Carried," Oct. 2022, Internal document.

[15] European Union Aviation Safety Agency, "Easy Access Rules for Normal, Utility, Aerobatic and Commuter Category Aeroplanes (CS-23) (Amendment 4)," Certification Specifications, EASA, June 2018.

[16] European Union Aviation Safety Agency, "CS-23 Amendment 6 and AMC & GM to CS-23 Issue 4," Certification Specifications, EASA, March 2023.

[17] Taylor and John, W., *Jane's All the World's Aircraft*, Marston & Co Ltd., Sampson, London, 1962.

[18] Roskam, J., *Part V: Component Weight Estimation*, No. 5 in Airplane Design, Design, Analysis and Research Corporation, Lawrence, Kansas, 2nd ed., 1999.

[19] Oliviero, F., "Aircraft Aerodynamic Analysis – Estimation of Lift & Drag," Oct. 2022.

[20] Zienkiewicz, O., Taylor, R., and Nithiarasu, P., "Chapter 8 - Turbulent Flows," *The Finite Element Method for Fluid Dynamics (Seventh Edition)*, edited by O. Zienkiewicz, R. Taylor, and P. Nithiarasu, Butterworth-Heinemann, Oxford, seventh edition ed., 2014, pp. 283–308.

[21] Nita, M. and Scholz, D., "Estimating the Oswald Efficiency factor from basic aircraft geometrical parameters," *Deutscher Luft- und Raumfahrtkongress 2012*, Hamburg, Germany, Dec. 2012.

[22] Biber, K., "Estimating Propeller Slipstream Drag on Airplane Performance," *Journal of Aircraft*, Vol. 48, No. 6, Nov. 2011, pp. 2172–2174, doi:10.2514/1.C031458.

[23] Bijl, H. and Timmer, N., "Introduction to Aerospace Engineering, Lecture 7 & 8," .

[24] Proesmans, P. and Vos, R., "Airplane Design Optimization for Minimal Global Warming Impact," *Journal of Aircraft*, Vol. 59, No. 5, June 2022, doi:10.2514/1.C036529.

[25] Group D, "Drag Polar Estimation using Cessna-206H," April 2018.

[26] Munoz, M. A. P., *Study and deisgn of a monocoque wing structure with composite materials*, Bachelor's thesis, Universitat Politecnica De Catalunya, June 2016.

[27] Turnbull, A., "The typical general aviation aircraft," Tech. Rep. CR-1999-209550, NASA, 1999.

[28] Mouritz, A. P., *Introduction to Aerospace Materials*, AIAA education series, Woodhead Publishing, Cambridge, UK, 2012.

[29] Ashby, M. F., Shercliff, H., and Cebon, D., *Materials: Engineering, Science, Processing and Design*, Butterworth-Heinemann, 2018.

[30] Misciagna, D. T. and Landi, D. J., “Integrated Ceramic Composite Firewall,” *SAE Technical Paper*, Oct. 2005, pp. 2005–01–3430, doi:10.4271/2005-01-3430.
[31] Organization, I. C. A., “Technical Instructions for the Safe Transport of Dangerous Goods by Air,” 2015.
[32] Hibbeler, R., *Engineering Mechanics: Statics*, Pearson Benelux, 2022.
[33] Megson, T., *Aircraft Structures for Engineering Students*, Elsevier, 2022.
[34] Christine Unger, “BENDING INSTEAD OF SNAPPING,” 2020.
[35] Bruhn, E., *Analysis and Design of Flight Vehicle Structures*, Tri-State Offset Company, Indiana, 1973.
[36] Howard D. Curtis, *Fundamentals of Aircraft Structural Analysis*, Richard d Irwin, 1996.
[37] Roskam, J., *Part III: Layout Design of Cockpit, Fuselage, Wing and Empennage: Cutaways and Inboard Profiles*, No. 3 in Airplane Design, Design, Analysis and Research Corporation, Lawrence, Kansas, 6th ed., 2018.
[38] Raymer, D. P., *Aircraft Design: A Conceptual Approach*, American Institute of Aeronautics and Astronautics, Inc., Reston, Virginia, 6th ed., 2018.
[39] Jenkinson, L. R., Simpkin, P., and Rhodes, D., *Civil Jet Aircraft Design*, AIAA education series, Arnold London, UK, Reston, VA, 1999.
[40] Schijve, J., editor, *Fatigue of Structures and Materials*, Springer Netherlands, Dordrecht, 2009.
[41] Rice, R. C., Jackson, J. L., Bakuckas, J., and Thompson, S., “Metallic Materials Properties Development and Standardization (MMPDS).” Tech. Rep. PB2003106632, Battelle Memorial Inst., Columbus, Ohio, 2003.
[42] Hulshoff, S. J., “AE4930 Aeroelasticity,” 2022.
[43] Schmidt, R. K., *The design of aircraft landing gear*, SAE International, Warrendale, Pennsylvania, USA, 2020.
[44] Li, W., *More Electric Landing Gear Actuation Study*, Master’s thesis, Cranfield University, Cranfield, UK, Jan. 2009.
[45] Oliviero, F., “Analysis of requirements and design principles for lateral/directional control and stability,” April 2024.
[46] Oliviero, F., “Requirement Analysis and Design Principles for A/C Stability and Control (Part I),” April 2024.
[47] Oliviero, F., “Requirement Analysis and Design principles for A/C Stability & Control (Part 2),” April 2024.
[48] Roskam, J., *Part VI: Preliminary Calculation of Aerodynamic, Thrust and Power Characteristics*, No. 6 in Airplane Design, Design, Analysis and Research Corporation, Lawrence, Kansas, 2nd ed., 1990.
[49] Al-Shamma, O., Ali, R., and Hasan, H., “An instructive algorithm for aircraft elevator sizing to be used in preliminary aircraft design software,” *Istrazivanja i projektovanja za privredu*, Vol. 15, No. 4, 2017, pp. 489–494, doi:10.5937/jaes15-14829.
[50] Xu, X., Zhao, J., Zhao, J., Shi, K., Dong, P., Wang, S., Liu, Y., Guo, W., and Liu, X., “Comparative study on fuel saving potential of series-parallel hybrid transmission and series hybrid transmission,” *Energy Conversion and Management*, Vol. 252, Jan. 2022, pp. 114970, doi:10.1016/j.enconman.2021.114970.
[51] Katrasnik, T., Trenc, F., and Opresnik, S. R., “Analysis of Energy Conversion Efficiency in Parallel and Series Hybrid Powertrains,” *IEEE Transactions on Vehicular Technology*, Vol. 56, No. 6, Nov. 2007, pp. 3649–3659, doi:10.1109/TVT.2007.901033.
[52] Formsprag Clutch, “Overrunning, Backstopping, Indexing Clutches,” May 2023.
[53] European Union Aviation Safety Agency, “Type-Certificate Data Sheet for RED A03 Series Engines,” Type Certificate EASA E.150, European Union Aviation Safety Agency, June 2022.
[54] Continental Aerospace Technologies, “CD-300 Jet-A Engine Series,” 2023.
[55] H3X Technologies, “HPDM-350 Datasheet,” Feb. 2024.
[56] European Union Aviation Safety Agency, “Type-Certificate Data Sheet for 4HFR34C(- - -) Series Propellers,” Type Certificate EASA IM.P.192, European Union Aviation Safety Agency, May 2024.

[57] European Union Aviation Safety Agency, “Type-Certificate Data Sheet for HC-B3T Series Propellers,” Type Certificate EASA IM.P.126, European Union Aviation Safety Agency, April 2021.

[58] Roskam, J., *Part IV: Layout Design of Landing Gear and Systems*, No. 4 in Airplane Design, Design, Analysis and Research Corporation, Lawrence, Kansas, 8th ed., 2018.

[59] A-21 Aircraft Noise Measure Noise Aviation Emission Modeling, “Prediction Procedure for Near-Field and Far-Field Propeller Noise,” .

[60] Moshkov, P. A., “Empirical metod of predicting Aviation Piston Engine noise,” *VESTNIK of Samara University. Aerospace and Mechanical Engineering*, Vol. 15, No. 2, Jul 2016, pp. 152–161, doi:10.18287/2412-7329-2016-15-2-152-161.

[61] Smith, M. H., “A Prediction Procedure for Propeller Aircraft Flyover Noise Based on Empirical Data,” *SAE Transactions*, Vol. 90, 1981, pp. 2114–2124.

[62] Gudmundsson, S., *General Aviation Aircraft Design*, Butterworth-Heinemann, Oxford, 2014.

[63] Ruijgrok, G. J. J., *Elements of Airplane Performance*, Delftse Universitaire Pers, 1996.

[64] Harloff, G., “Light Sport and General Aviation Airplane Comparison and Harloff Performance Factor,” Jan. 2014.

[65] Nicolai, L. M. and Carichner, G. E., *Fundamentals of Aircraft and Airship Design*, AIAA educational series, American Institute of Aeronautics and Astronautics, Reston, VA, 2010.

[66] Roskam, J., *Part I: Preliminary Sizing of Airplanes*, No. 1 in Airplane Design, Design, Analysis and Research Corporation, Lawrence, Kansas, 2nd ed., 1997.

[67] Xi, Z., “The comparison of decentralized and centralized structure of network communication in different application fields,” *2019 International Conference on Management Science and Industrial Economy (MSIE 2019)*, Atlantis Press, 2020, pp. 50–54.

[68] Wu, Y., Liu, Z., Liu, J., Xiao, H., Liu, R., and Zhang, L., “Optimal battery capacity of grid-connected PV-battery systems considering battery degradation,” *Renewable Energy*, Vol. 181, Jan. 2022, pp. 10–23, doi:10.1016/j.renene.2021.09.036.

[69] Cole, W. and Karmakar, A., “Cost Projections for Utility-Scale Battery Storage: 2023 Update,” 2023.

[70] Roskam, J., *Part VIII: Airplane Cost Estimation: Design, Development, Manufacturing and Operating*, No. 8 in Airplane Design, Design, Analysis and Research Corporation, Lawrence, Kansas, 5th ed., 2018.

[71] Federal Aviation Administration, “Economic Values for Evaluation of FAA Investment and Regulatory Decisions–Section 7: Labor cost factors,” `https://www.faa.gov/sites/faa.gov/files/regulations_policies/policy_guidance/benefit_cost/econ-value-section-7-labor-cost-factors.pdf`.

[72] Lutsey, N., “Transition to a global zero-emission vehicle fleet: A collaborative agenda for governments,” *International Council on Clean Transportation*, Nov 2021.

[73] Purvis, B., Mao, Y., and Robinson, D., “Three pillars of sustainability: in search of conceptual origins,” *Sustainability Science*, Vol. 14, No. 3, May 2019, pp. 681–695, doi:10.1007/s11625-018-0627-5.

[74] Hansmann, R., Mieg, H. A., and Frischknecht, P., “Principal sustainability components: empirical analysis of synergies between the three pillars of sustainability,” *International Journal of Sustainable Development & World Ecology*, Vol. 19, No. 5, Oct. 2012, pp. 451–459, doi:10.1080/13504509.2012.696220.

[75] Boussemart, J.-P., Leleu, H., Shen, Z., and Valdmanis, V., “Performance analysis for three pillars of sustainability,” *Journal of Productivity Analysis*, Vol. 53, No. 3, June 2020, pp. 305–320, doi:10.1007/s11123-020-00575-9.

[76] Nguyen, D. D., Kale, U., and Wangai, A. W., “Total Life Cycle Cost and Emission of Electric, Hybrid-Electric Aircraft,” *32nd Congress of the International Congress of the Aeronautical Sciences*, Shanghai, China, Sep 2021, p. 0635.

[77] Arvidsson, R., Nordelöf, A., and Brynolf, S., “Life cycle assessment of a two-seater all-electric aircraft,” *The International Journal of Life Cycle Assessment*, Vol. 29, Feb. 2024, pp. 240–254, doi:10.1007/s11367-023-02244-z.

[78] Veeramanikandan, R., Nithish, S., Sivaraj, G., and Vinodh, S., “Life cycle assessment of an aircraft component: a case study,” *International Journal of Industrial and Systems Engineering*, Vol. 27, No. 4, 2017, pp. 485, doi:10.1504/IJISE.2017.087835.

[79] Johanning, A. and Scholz, D., “Conceptual Aircraft Design based on Life Cycle Assessment,” *29th Congress of the International Council of the Aeronautical Sciences (ICAS 2014)*, Springer Berlin Heidelberg, Berlin, Germany, 2014, pp. 4755–4766.

[80] Jordão, T. C., “Life Cycle Assessment oriented to climate change mitigation by aviation,” *Proceedings of the 15th International Conference on Environmental Economy, Policy and International Environmental Relations*, Prague, Czech Republic, Nov 2013.

[81] Lewis, T., *A Life Cycle Assessment of the Passenger Air Transport System Using Three Flight Scenarios*, Master’s thesis, Institutt for energi-og prosessteknikk, 2013.

[82] Brocal, F., González, C., Reniers, G., Cozzani, V., and Sebastián, M., “Risk Management of Hazardous Materials in Manufacturing Processes: Links and Transitional Spaces between Occupational Accidents and Major Accidents,” *Materials*, Vol. 11, No. 10, Oct 2018, pp. 1915, doi:10.3390/ma11101915.

[83] NASA, “Electrified Aircraft Propulsion Flight Project Battery Industry Day,” Nov. 2020.

[84] Kondori, A., Esmaeilirad, M., Harzandi, A. M., Amine, R., Saray, M. T., Yu, L., Liu, T., Wen, J., Shan, N., Wang, H.-H., Ngo, A. T., Redfern, P. C., Johnson, C. S., Amine, K., Shahbazian-Yassar, R., Curtiss, L. A., and Asadi, M., “A room temperature rechargeable Li2O-based lithium-air battery enabled by a solid electrolyte,” *Science*, Vol. 379, No. 6631, Feb. 2023, pp. 499–505, doi:10.1126/science.abq1347.

[85] Beaudet, A., Larouche, F., Amouzegar, K., Bouchard, P., and Zaghib, K., “Key Challenges and Opportunities for Recycling Electric Vehicle Battery Materials,” *Sustainability*, Vol. 12, No. 14, 2020, doi:10.3390/su12145837.

[86] Baum, Z. J., Bird, R. E., Yu, X., and Ma, J., “Lithium-Ion Battery Recycling ─ Overview of Techniques and Trends,” *ACS Energy Lett.*, Vol. 7, No. 2, feb 2022, pp. 712–719.

[87] Islam, M. T. and Iyer-Raniga, U., “Lithium-Ion Battery Recycling in the Circular Economy: A Review,” *Recycling*, Vol. 7, No. 3, May 2022, pp. 33, doi:10.3390/recycling7030033.

[88] Asmatulu, E., Overcash, M., and Twomey, J., “Recycling of Aircraft: State of the Art in 2011,” *Journal of Industrial Engineering*, Vol. 2013, No. 1, 2013, pp. 960581, doi:https://doi.org/10.1155/2013/960581.

[89] Zhao, D., Guo, Z., and Xue, J., “Research on Scrap Recycling of Retired Civil Aircraft,” *IOP Conference Series: Earth and Environmental Science*, Vol. 657, No. 1, feb 2021, pp. 012062, doi:10.1088/1755-1315/657/1/012062.

[90] Capuzzi, S. and Timelli, G., “Preparation and Melting of Scrap in Aluminum Recycling: A Review,” *Metals - Open Access Metallurgy Journal*, Vol. 8, 04 2018, pp. 249, doi:10.3390/met8040249.

[91] Hamann, R. and van Tooren, M., *AE3-S01 Systems Engineering & Technical Management Techniques Part I Lecture Notes*, Delft University of Technology, Sept. 2006.

[92] Hamann, R. and van Tooren, M., *AE3-S01 Systems Engineering & Technical Management Techniques Part II Lecture Notes*, Delft University of Technology, Jan. 2006.

[93] Mba, D., Place, S., Rashid, H., and Keong, R. L., “Helicopter Main Gearbox Loss of Oil Performance Optimization - HELMGOP,” Tech. Rep. EASA.2011.C23, European Union Aviation Safety Agency, Cranfield, UK, Nov. 2012.

[94] Kissling, U. and Stangl, M., “Documentation of Gearbox Reliability — an Upcoming Demand,” Tech. rep., Power Transmission Engineering, Munich, June 2019.

[95] Bertsche, B., *Reliability in Automotive and Mechanical Engineering*, Springer, Berlin, 2008.

[96] Hickel, S., “Verification & Validation, CFD for Aerospace Engineers,” 2022.

[97] Ghadge, A., Karantoni, G., Chaudhuri, A., and Srinivasan, A., “Impact of additive manufacturing on aircraft supply chain performance: A system dynamics approach,” *Journal of Manufacturing Technology Management*, Vol. 29, No. 5, May 2018, pp. 846–865, doi:10.1108/JMTM-07-2017-0143.